UNIVERSITY OF CALIFORNIA,
IRVINE

Innovative Approaches to NMR Instrumentation Design to Support Characterization of Complex Biomolecular Assemblies

DISSERTATION

submitted in partial satisfaction of the requirements
for the degree of

DOCTOR OF PHILOSOPHY

in Chemistry

by

Jessica Irene Kelz

Dissertation Committee:
Professor Rachel W. Martin, Chair
Professor Athan J. Shaka
Professor Thomas L. Poulos

2023

DEDICATION

To

My mom, Irene, and first mentor, Dr. Mark Hildebrand.

You gave me a forever within the numbered days, and I'm eternally grateful.
– John Green (The Fault in Our Stars)

with humble perspective

Life is a gradual series of revelations
That occur over a period of time
It's not some carefully crafted story
It's a mess, and we're all going to die.
Crazy-Ex Girlfriend

and bountiful blessings

To laugh often and much;
To win the respect of intelligent people and
the affection of children;
To earn the approbation of honest critics and endure
the betrayal of false friends;
To appreciate beauty;
To find the best in others;
To give of one's self;
To leave the world a bit better, whether by a healthy child,
a garden patch, or a redeemed social condition;
To have played and laughed with enthusiasm and
sung with exultation;
To know even one life has breathed easier because you
have lived -
This is to have succeeded.
Ralph Waldo Emerson

in the past, present, and future.

Water is to me, I confess, a phenomenon which continually awakens new feelings of wonder as often as I view it.
Michael Faraday

TABLE OF CONTENTS

LIST OF FIGURES

LIST OF TABLES

Page

ACKNOWLEDGEMENTS

The gratitude I feel in my heart would require a thesis of its own. I hope that this abridged version can capture some of the love I have for each of you.

Wyeth, you have been a wonderful partner in every aspect of our lives, and I don't thank you enough. Thank you for choosing me; for continuing to choose me; for the beautiful life we are building together. "I don't know who we'll become / I am unfinished, I've got so much left to learn / But I'd like the company through every twist and turn / If to change is what you need / You can change right next to me / When you're high, I'll take the lows / You can ebb and I can flow / I believe that when it's done / We're gonna see that it was better / That we grew up together" (Ben Platt, Grow As We Go).

Rosalind, you have changed my entire world in the best ways; thank you for being my greatest teacher, and for your patience in knowing I am trying my best. I hope that you will feel confident enough to live your dreams and know that my love and support are unconditional. My other wish for you is that your life will be filled with friendship and mentorship from many others who love you sincerely too. There is nothing I am more proud of or that means more to me than being your mom.

To my mom, Irene, thank you for advocating for me when I was a high school student. That one act set in motion so many things that have enabled me to accomplish this goal. Beyond that your love and support set the foundation for growth and resilience. I hope that I can take what I have learned from you to be the best mom I can be. I miss you tremendously and wish I could give you one more hug.

To my dad, Jim, thank you for being supportive of me as a young woman who never wanted to be defined by my gender. Thank you for modeling integrity and service throughout your life. Also thank you for all of the support and for being a wonderful Pop-Pop to Rosalind, that means the world to me.

To my brother, Justin, ya dingus! It's pretty neat that we both got to attend each other's defenses. I'm proud of all you have accomplished. For your health.

Rachel, thank you for being the most LEGitimate advisor and mentor. It has been a transformative seven years in so many ways and you helped me navigate it all. Thank you for supporting me completely both in and out of the lab and for being someone that I admire both in and out of the lab. Thank you for entrusting me with the plants and showing me that I am capable of so much more than mass murder. Also thank you for allowing me to be curious and become involved in so many projects. I hope to maintain that shared genuine curiosity that inspired me to pursue science as a career. Lastly, always remember to use leg responsibly (or not).

Tom, thank you for becoming a mentor early in my graduate experience. Thank you for making space for NMR and not teasing me too much about our daughter's name being

partially inspired by a crystallographer. Thank you for being a role model in life and science. I look forward to more conversations over the coming years.

A.J., you are a legend in our community for both your academic successes and personality. Thank you for taking the time to talk rigorously about scientific principles and philosophy during preparation for advancement to candidacy. I appreciate how special it is to have both learned something new and laughed in every conversation with you. Also thank you for cultivating an amazing rose garden.

Doug, thank you for also supporting me since the early days of graduate school. After watching you navigate several very challenging events as Chair, I am incredibly grateful to know that I will be able to learn a tremendous amount from you about both science and leadership. I am excited to work with you and look forward to all that lies ahead.

Melanie, thank you for your support over the years here at UCI, both professionally and personally. It means a tremendous amount to me that you went out of your way to make me feel less lonely during two huge life events: grieving the loss of my mother and relative isolation during maternity leave. Thank you also for helping to pave the way for working mothers in this career.

Kieron, we couldn't have asked for a better introduction to UCI. It is tough to learn new math after turning 30 but you made that possible. I plan to carry forward aspects of your teaching philosophy into my career. From the beginning Paul and I have appreciated your sense of humor, but we are thankful to add our appreciation for your guidance and willingness to talk with us sincerely about many aspects of life. We are thankful to have been among those invited to wonderful dinner celebrations at your home and hope to continue to keep in contact.

Don, I am glad I passed the test and accepted the PBR during visitations. Thank you for introducing us to so many other wonderful people in the veteran community here on campus. Prior to that I'm not sure that either of us realized how important that would be to our transition and success. I can genuinely say some of Wyeth and I's fondest memories from here will be times we spent with you.

Jenny Y., thank you for being a wonderful mentor to Wyeth and supportive of the challenges that come from a two-body problem. Holiday parties at your home are among some of our favorite memories.

Lori, thank you for helping me with my NSF GRFP application and for your continued support during my time here at UCI. Also thank you for helping us to find the absolute best daycare for Rosalind, which has helped me to feel more comfortable continuing work and to finish my PhD.

Mark S., thank you for sharing your knowledge with me. I never would have thought I'd be machining as part of my PhD. I have a tremendous amount of respect for your talents and patience in teaching your craft.

Renée, thank you for your leadership in the chemistry department in improving the educational experience for students. It was a pleasure to work with and learn from you.

Bri, your courses in public speaking and inclusive teaching are brilliant. You've left a lasting impression on my career and I cannot endorse what you are doing enough.

Danny, I don't think there is a cooler, kinder dude on campus. I have learned so much from you and DTEI during my time at UCI. I am incredibly grateful to have been a pedagogical fellow in the wonderful program you have helped build and refine; a true gem at UCI that makes me so incredibly thankful to have come here. You have made such an impact while remaining incredibly humble. I hope to make it to a show one of these days! Until then, rock on!

Adelí and Jane, thank you for helping to make our transition to UCI as student veterans so welcoming. You are both wonderful people who care deeply about others and have made a significant impact through your work. Thank you for inviting me to participate in several events and helping us to remain connected to the veteran community.

I have had the pleasure of working with a few wonderful therapists: Dr. Ylena Shayne, Dr. Megan Benton, and Dr. Anthony Mascola. They have helped me process grief, navigate the transition into parenthood, and provided me with tools and insight in order to be a better version of myself.

A special thanks to Cynthia, Morgan, and Jenny D. from the chemistry department front office who made my life easier at several times and were always people I could count on. You often don't get as much recognition as you deserve, but I hope you know the impact you are making has immense value.

Lee, I think you were the first person that I met with a doctorate and were an exceptional chemistry teacher. Thank you for making the fundamentals accessible such that I had the confidence to pursue chemistry as a major in college. I have done my best to share that knowledge with others and hope to continue to throughout my career.

Mark H., I am tremendously grateful to have had you as my first mentor and to have had that relationship with you for 15 years (my entire adult life before he passed). While other PIs intended to only have me clean glassware as a high-school student, you allowed me to run experiments and cultivating the joy of being in a laboratory (spending many Saturdays working side-by-side). Your honest but compassionate perspective was instrumental to my non-linear path to success. You were an incredibly kind person and well-respected scientist. It is hard to lose someone that had so much impact on achieving my dreams and was such a positive force in my life. I miss you.

Clare, I'm not sure I would have made it through the chemistry major without you. You helped guide me both personally and professionally at several critical points. I am incredibly grateful to have stayed in contact and to have had your mentorship and friendship for almost 20 (gasp) years.

Amy, what a small world coming to find out that you know Rachel from graduate school! Thank you for taking so much of your time to talk with me about career preparation and work-life balance. I look forward to continuing to talk with you.

Sriram, I am so thankful to have been allowed the opportunity to work in your lab at NIH. It was an incredible experience where I met many other wonderful people and scientists. I am very thankful to have kept in touch and do intend to visit UBC someday!

Tommi, thank you for helping me prepare graduate school application materials and for being someone that I can continue to come to if I have questions. It has been exciting to see what you are doing in your career and to watch Eleanor grow up!

Skip, I feel lucky to have been in your class at UCSD and for you to have invited me to volunteer in your lab. You have been pivotal to both Wyeth and I's success in graduate school. I am inspired by your dedication to service and outreach, both in the research you do and extracurriculars you organize. Thank you for engaging in so many honest and insightful conversations with us about academia.

Stephen, thank you for being a wonderful mentor and for showing me patience as I transitioned back into a lab setting. Your organization is something I will probably always aspire to and work ethic is unparalleled.

Steve, I am so thankful to have gotten to know you through the cysteine protease survey activity. It was an absolute pleasure to visit you at Fisk University. Your support has undoubtedly helped me to achieve goals that I honestly felt were unreachable. I hope that we will have more opportunities to work together in the future!

Xander, thank you for the opportunity to collaborate with and visit your lab. I have thoroughly enjoyed and am inspired by conversations with you about the future of NMR.

Per, thank you for volunteering to work with me on the PTFE printing projects. It is an exciting and transformative technology that I hope 3M continues to develop.

Kevin, I learned a tremendous amount from you and can't thank you enough for your kind, dedicated and exacting support in helping us troubleshoot and repair our systems.

Bronte…*sorries in Canadian*, Professor Charette, I am so incredibly happy for and proud of you. Couldn't imagine having survived this experience without you. Cheers to many more years of friendship ahead. Namaste.

Amanda, thanks for bringing Delco to UCI…I mean it. I'm thankful for all of the Bachelor and game nights, and for the Glu-10 league. Looking forward to a visit to McGillin's together someday. Fly Eagles, fly! You're a wonderful colleague.

Melvin and Juana, I feel so incredibly lucky to have become friends with you through graduate school. From Friendsgivings to fourth of Julys, taco trucks to late night Starbucks runs, classes to Ballet Folklorico, and so, so many things in between. I mean,

y’all brought homemade soup when I was sick. You’re the real-life MVPs and Rosalind is blessed to have you as her Tío and Tía. I promise we will make it to Colorado!

Alec, thanks for being a friend we can talk to and laugh with about anything. But mostly thanks for always bringing the ice cream sandwiches to fourth of July celebrations.

Zach, thank you for being an inspiration as a PF and education entrepreneur! I am so proud of all you have accomplished and try to brag about you and d-Orbital Games as much as possible. Santiago Canyon College is lucky to have you. Looking forward to our little ones playing together in the near future!

Brian, a fellow ChaMPion! Thank you for all of the support over the years, especially in the beginning surviving all of the classes. I hope your dreams continue to come true!

Hannah S. I’m super thankful that you became roommates with Amanda because I’m glad that I’ve gotten to know you (and Frankie of course!).

Olga, Arturo, Tiffany, Alex, and Micah, thanks for being such wonderful neighbors. You’ve really helped it feel like home over the past few years and I hope that we will continue to be friends beyond UCI.

Brooke, Hannah P., and Rakia, thank you for helping with my transition into motherhood and for being a community of friends who not only understand how difficult it is to complete a PhD, but also how challenging it is being a new mom! Brooke, thank you also for being so kind to arrange a gift when my mom passed. I’m not sure I ever formally thanked you but it was very touching and meant a lot to me. Hannah, what a crazy small world that I know your aunt-in-law! Rakia, thank you for helping me maintain sanity during the newborn days especially, for encouraging me to overcome some of the initial anxiety and get out of the house, and for all the kindness you have shown in handing down many useful baby items to us.

Robert, thank you firstly for your incredible patience. It has been a great experience working with you on the ChaMP opportunity award collaboration.

To the Food Court West Panda Express, the fortunes that kept me going at times.

I can only think of one thing to say to my dearest friend Honica. You are the light of my life. You are the light. I love you, and don’t forget the turmeric.

Traci, thank you for genuinely supporting me no matter what…through all of life’s ups and downs. I hope I’ve been able to be that friend to you too.

Ray, thanks for being one of our very best friends no matter what direction life takes us. It is neat that we will all be UCI alumni someday. Zot, zot, zot!

Karla, I still can’t believe it took Ray so long to introduce you to us. He will never live it down. You are a wonderful person and I’m so thankful to have you as a friend.

Irv, you helped us keep our long-term goals on track and to have one less thing to worry about. That peace of mind and the security you are helping us build for our family is priceless. You are a wonderful person, role model, and friend.

Alfonza, thank you for trusting me to tutor your daughter and for sending one of the most meaningful gifts I've ever received. I hope there is enough electrical engineering in these pages to make you proud.

Kate and Ryan, thank you for continuing to include us in your lives and being some of our best friends despite distance. We look forward to many more adventures together.

Domarin, thank you for being a role model and friend. So many of the conversations we've had have brought much needed clarity and perspective when I needed it most.

Melody Childcare team, thank you for all the love you have shown Rosalind and our family. Your support made this possible.

Ed who worked at the Dunkin Donuts on Jeffrey Road in the winter of 2017. You are the reason I passed thermodynamics, and your generosity will not be forgotten.

Members of the lab past and present that I have worked with, thank you for putting up with me. Although we didn't solve all of the world's problems downstairs, I'm pretty sure we made progress on making it a better place through all of our conversations that ended on a completely different topic than where we started. The Corona Public Library outreach event couldn't have happened without you. RIP 'Mater. *Leg emoji*

Sofiya, Allison, Elliott, Alexandra, and Desire, I hope you learned as much from me as I learned from you. Thank you for the opportunity to be your mentor, and for the enthusiasm you showed for research. You made it fun and working with you was a highlight of my time here.

To all of my other friends and mentors not directly mentioned here: Thank you for being the reason that I find myself taken by surprise by moments of overwhelming, tear inducing sense of joy and gratitude for my life.

I thank Elsevier and Allen Press for permission to include copyrighted text and graphics as parts of Chapters 1, 2, 4, and 5 of my thesis/dissertation from the previously published works[1–4]. This work was supported by NIH grant 2R01EY021514-06 and NSF grant CHE-1308231 to R.W.M. J.I.K. acknowledges support from NIH grant T32 GM108561 and NSF GRFP DGE-1321846. Any opinions, findings, and conclusions or recommendations expressed in this material are those of the author(s) and do not necessarily reflect the views of the National Science Foundation. The authors would like to thank the Computer Simulation Technology, GmbH for providing CST Microwave Studio that has been instrumental in this work.

And last but not least to Dr. Steve Brule for all the important life lessons.

GO NAVY, BEAT ARMY!

VITA

Jessica Irene Kelz

2008	B.S. in Chemistry, United States Naval Academy, Annapolis, MD
2008-14	Surface Warfare Officer, United States Navy
2014-16	Project Management Consultant, Booz Allen Hamilton, San Diego, CA
2016-17	Teaching Assistant, Department of Chemistry, University of California, Irvine
2023	M.S. in Chemistry, University of California, Irvine
2023	Ph.D. in Chemistry, *emphasis in Chemical and Materials Physics*, University of California, Irvine

FIELD OF STUDY

Nuclear Magnetic Resonance Instrument Design and Fabrication for Applications in Structural Biology

PUBLICATIONS

Jessica I. Kelz, Jose Uribe, Matty Resakh, Gemma R. Takahashi, Wyeth S. Gibson, Renée Link, Kate McKnelly, Rachel W. Martin. **2023**. Developing and Implementing a Specifications Grading System in an Upper- Division Undergraduate Chemical Biology Course, The Biophysicist, 4(1) 11-29.

Jessica I. Kelz*, Gemma R. Takahashi*, Fatemeh Safizadeh, Vesta Farahmand, Marquise G. Crosby, Jose L. Uribe, Suhn H. Kim, Marc A. Sprague-Piercy, Elizabeth M. Diessner, Brenna Norton-Baker, Steven M. Damo, Rachel W. Martin, and Pavan Kadandale. **2022**. Active learning module for protein structure analysis using novel enzymes, The Biophysicist, 3(1) 49-63.

Jessica I. Kelz, Jose Uribe, Rachel W. Martin. **2021**. Reimagining magnetic resonance instrumentation using open maker tools and hardware as protocol, Journal of Magnetic Resonance Open, 6-7.

Jessica I. Kelz, John E. Kelly, Rachel W. Martin. **2019**. 3D-printed dissolvable inserts for efficient and customizable fabrication of NMR transceiver coils, Journal of Magnetic Resonance, 305, 89-92.

Rachel W. Martin, John E. Kelly, Jessica I. Kelz. **2019**. Advances in instrumentation and methodology for solid-state NMR of biological assemblies, Journal of Structural Biology, 206, 73-89.

Kelsey A. Collier, Suvrajit Sengupta, Catalina A. Espinosa, John E. Kelly, Jessica I. Kelz, Rachel W. Martin. **2017**. Design and construction of a quadruple-resonance MAS NMR probe for investigation of extensively deuterated biomolecules, Journal of Magnetic Resonance, 285, 8-17.

Mark Hildebrand, Evelyn York, Jessica I. Kelz, Aubrey K. Davis, Luciano G. Frigeri, David P. Allison and Mitchel J. Doktycz. **2006**. Nanoscale control of silica morphology and three-dimensional structure during diatom cell wall formation, Journal of Materials Research, 21(10), 2689-2698.

FELLOWSHIPS, AWARDS, AND RECOGNITION

UC President's Postdoctoral Fellowship 2023-2024

UC Irvine Graduate Division Fletcher Jones Fellowship, 2022 ($25,000)

American Chemical Society Graduate Student and Postdoctoral Scholars Recognition Program national award for Leadership in Mentoring, 2022

Graduate Division Completion Fellowship (tuition for one quarter and $7,500 stipend), Fall 2022

UC Irvine Chemistry Department, Jacqueline Smitrovich Prize, 2022 ($750)

UC Irvine Chemistry Department, Contributions to The Chemistry Department Teaching Program by a Teaching Assistant - Upper Division, 2022 ($150)

Chemistry Department Fellowship, funded fall quarter 2021 to support co-designing the implementation of specifications grading in an upper-division undergraduate course

Selected as UC Irvine finalist to apply for the Philanthropic Educational Organization (P.E.O.) Scholar Award, 2020

UCI Pedagogical Fellowship, 2020 ($2,000)

Inaugural Chemical and Materials Physics (ChaMP) Opportunity Award, 2019 ($10,000 toward a collaboration project between two labs in the program and $2,000 for travel)

National Association of Veterans' Program Administrators (NAVPA) Student Scholarship, 2019 ($500)

UC Irvine Graduate Division Brython Davis Fellowship, 2019 ($6,000)

National Science Foundation Graduate Research Fellow (NSF GRFP), July 2018 – June 2021 ($138,000)

ORAL PRESENTATIONS

“Fabrication and Testing of Solenoids Optimized from System-Defined Constraints”, Experimental Nuclear Magnetic Resonance Conference, Pacific Grove, CA, April 2023

“Advancing Career-Oriented Skills for Chemical Biology Students Using Specifications Grading”, Biophysical Society Conference, San Diego, CA, February 2023 Recipient of student travel stipend

Teaching Experiment Academy (TEA) Summit 2022 April 28-29, Virtual, Faculty Innovation Showcase “Implementation of Specifications Grading in Upper-Division Chemical Biology Course” Only graduate student speaker out of thirty-six presentations

“Reimagining the NMR Maker Space”, invited talk for a virtual journal club at Helmholtz Institute, Mainz Germany, October 2021

“Creating A Generalizable Approach to Achieve Optimized Field Profiles in ssNMR RF Transceivers”, Experimental Nuclear Magnetic Resonance Conference, Baltimore, MD, March 2020 Recipient of student travel stipend

“Ventures in Parameter Space of Variable-Pitch Solenoids”, Southern California Users of Magnets (SCUM) meeting, UC San Diego, December 2019 Only graduate student speaker out of thirteen talks

“Getting Wrapped Up in the Small Stuff: Exploring Coil RF Homogeneity Through Design and Fabrication” round table discussion at Alpine Conference on Magnetic Resonance in Solids, Chamonix, France, September 2019 Recipient of student travel stipend

“From Simulation to Fabrication: Making the Ideal RF Transceiver” lightning talk at annual UCI ChaMP poster session, April 2019

“Dissolvable Inserts for Achieving Performance Enhanced Resonators” online to the International Society of Magnetic Resonance (ISMAR) Executive Committee, October 2018

“Switching Things Up: NMR for Studies on Protein-Membrane Dynamics” UC Irvine, Irvine, CA, May 2018

“3D Imaging of Melanoma Cell Lines Using Dual-Beam Scanning Electron Microscopy” United States Naval Academy, Annapolis, MD, May 2008

POSTER PRESENTATIONS

“Resonance Assignments Toward Solution-State NMR Structure Determination of Novel Box Jellyfish Protein”, Biophysical Society Annual Meeting, San Francisco, CA February 2022 Recipient of student travel stipend

“Accessible Method to Achieve Optimized or Intricate Wire Transceiver Coil Designs”, Practical Applications of Nuclear Magnetic Resonance in Industry Conference (PANIC), Nashville, TN, October 2021 Recipient of student travel stipend

“Remixing the Nuclear Magnetic Resonance Builder Paradigm” Experimental Nuclear Magnetic Resonance Conference, Virtual, March 2021

“Creating A Generalizable Approach to Achieve Optimized Field Profiles in ssNMR RF Transceivers”, Experimental Nuclear Magnetic Resonance Conference, Baltimore, MD, March 2020 Recipient of student travel stipend

“Breaking Down Digestion in the Carnivorous Plant Drosera capensis Through Modeling and Experimentation” outreach event featuring undergraduate student research at San Diego Carnivorous Plant Society meeting, July 2019

“Optimizations in Solid-State NMR Probes Utilizing 3D Printing” Experimental Nuclear Magnetic Resonance Conference, Pacific Grove, CA Recipient of student travel stipend Also presented at annual UCI ChaMP poster session, April 2019

“Design of a Triple-Resonance Switched Angle Spinning ssNMR Probe for Studies on Protein-Membrane Dynamics” Rocky Mountain Conference on Magnetic Resonance, Snowbird, UT, July 2018 Recipient of Jack E. Crow student travel stipend

“Solid-state NMR Probe Development and Characterization of Gamma S Crystallin as a Lens-Like Hydrogel” Biomolecular NMR Winter School, Stowe, VT, January 2018

“3D Imaging of Melanoma Cell Lines Using Dual-Beam Scanning Electron Microscopy” United States Naval Academy, Annapolis, MD, April 2008

ABSTRACT OF THE DISSERTATION

Innovative Approaches to NMR Instrumentation Design to Support Characterization of Complex Biomolecular Assemblies

by

Jessica Irene Kelz

Doctor of Philosophy in Chemistry

University of California, Irvine, 2023

Professor Rachel W. Martin, Chair

Advances in technology and analytical instruments are driving factors in scientific progress, particularly in the area of nuclear magnetic resonance. However, these developments have often not been easily accessible, creating a barrier to collaborative and broadly impactful use, especially in structural biology. My research has focused on innovative approaches to NMR instrumentation design to support characterization of complex biomolecular assemblies such as crystallin hydrogels that form the eye lens or membrane-associating antimicrobial peptides identified from the carnivorous plant Drosera capensis. My work has explored applications of additive manufacturing, which has emerged as a technology that rivals and occasionally surpasses conventional fabrication methods, to the NMR instrumentation design process in terms of design achievability, relative ease of use, availability, and material library. Interest in modifying both purpose-built and commercial probes led to the development of a creative, efficient, and accessible method for NMR transceiver coil fabrication using removable 3D-printed templates. Experimental magnetic-field profiles correlated with the results of theory-driven software simulations, demonstrating the ability to fabricate verifiably unique designs for a variety of experimental applications. This method not only enables coils to be made to specification, but also supports complex designs such as saddle-coils or others that are unable to be achieved by hand such as continually-variable pitch solenoids. Expanding upon this work led to creation of a generalized and completely open-source approach in support of modularity

to quickly achieve optimized solenoid transceiver designs based on system-specific or user-defined constraints. Parameter spaces defining suitable variable-pitch solenoids were plotted in an adaptable Python workspace, yielding options that predict improvements over previously published designs. The magnetic field profiles of every viable design were evaluated based on two performance-driven figures of merit in order to identify optimized designs for experimental testing and validation using a recently developed open-source and automated benchtop approach. In order to adequately maintain transceiver coil integrity in mechanically-dynamic systems 3D-printing was further leveraged in collaboration with 3M to produce the first of their kind polytetrafluoroethylene parts at dimensions previously unable to be fabricated. Implementation of this work and complimentary open-access approaches has tremendous promise to transform the field of structural biology by expanding participation of both novices and experts alike in use or development of modular components optimized for specific challenges.

Chapter 1

Shifting the Nuclear Magnetic Resonance "Builder" Paradigm

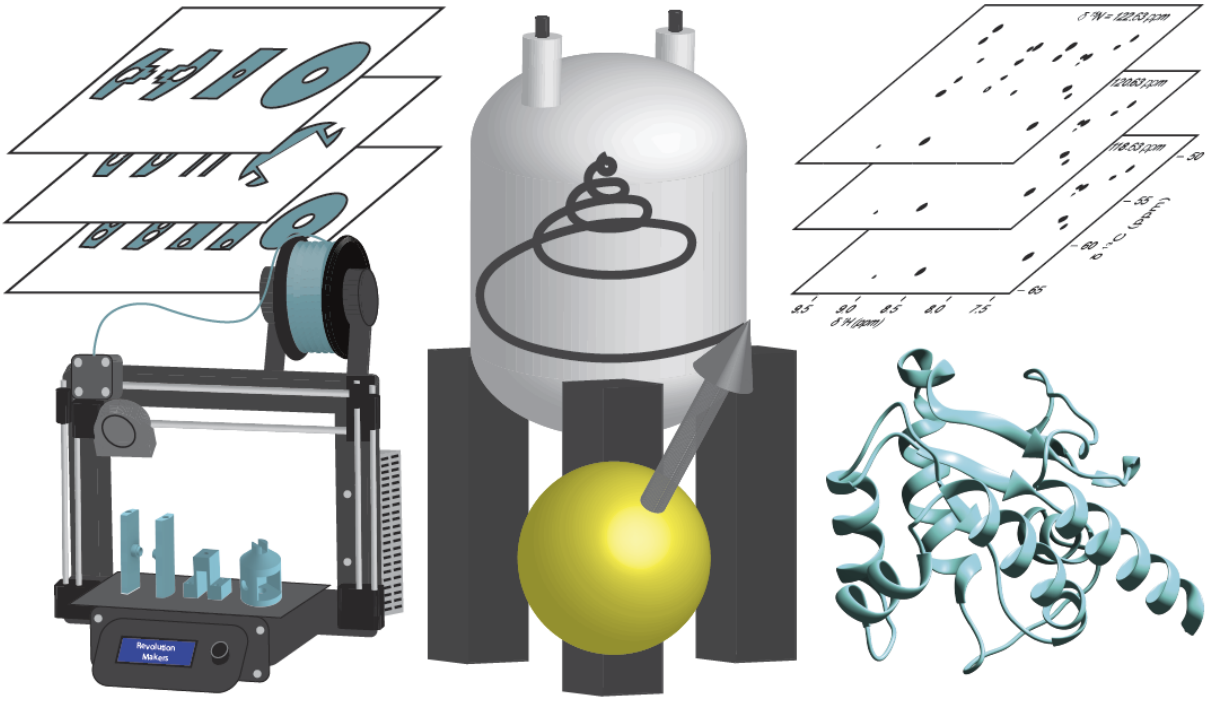

1.1 Introduction

1.1.1 Principles and relevant methods of biomolecular NMR

Spin ½ systems are commonly used in nuclear magnetic resonance (NMR) because the nuclear magnetic moment enables manipulation through magnetic fields, and relatively simple transitions between two possible states. At thermodynamic equilibrium, nuclear spins within a sample are in a random distribution of states and orientations. In an external magnetic field, nuclei with spin align to create net magnetization. This magnetization can be described classically using the gyromagnetic ratio, γ, an inherent property unique to the type of nucleus. From this, the angular frequency of precession about the external field known as the Larmor or resonance frequency, ω_0, can be defined by: $\omega_0 = -\gamma B_0$ [5].

In order to describe the full distribution of spins for a given nucleus within the sample, known as an ensemble average, superpositions of allowable states and probabilities must be determined through quantum mechanics. For a spin ½ system, the Zeeman transition energy (or splitting) between a ±½ spin state can be related to the Larmor frequency. A change in this frequency due to shielding interactions with the local environment is called the "chemical shift", one of the most important observables in an NMR experiment. The Hamiltonian for this interaction is given by the following equation: $\widehat{H}_{CS} = \underbrace{-\hbar\,\Upsilon B_0 \hat{I}_Z}_{Zeeman\ splitting}\ [1 - \underbrace{\delta_{iso} - \frac{\delta_{CSA} P_2(\cos\theta)}{2}}_{chemical\ shift}]$. P_2 is the second-order Legendre polynomial that describes the anisotropic molecular orientation dependence of the interaction. In solution this is naturally averaged through free tumbling of the molecules, but in solids this leads to spectral broadening, which can be addressed through magic-angle spinning[6].

Under sample spinning, the contribution of P_2 is dependent on the angle at which it is being spun relative to the external field. The magic angle[7,8], 54.74°, is a root of the polynomial and at sufficient spinning speeds will drive the anisotropic term to zero. Other important anisotropic interactions that are averaged through this process include homonuclear and heteronuclear dipolar couplings, which are a result of interactions between the magnetic fields created by each nucleus, and the quadrupolar coupling, in which the nuclear spins are affected by asymmetric distribution of surrounding electrons. Although anisotropic information can be used to determine orientation and dynamics, it often makes spectral peaks too broad to be easily deciphered. Therefore, MAS is used in solid-state NMR to achieve high-resolution, isotropic spectra capable of being used for structural determination.

NMR enables the study of biological assemblies under physiologically relevant conditions including amorphous and non-crystalline samples. This is an important advantage because protein conformation and functionality can be sensitively impacted by the environment. Due to the number of unique sites in biomacromolecules, it is necessary to perform multi-dimensional experiments to establish structural connectivity. Pulse sequences that apply polarization-transfer steps are the basis for multidimensional experiments. Cross polarization (CP) is a type of experiment in which magnetization is transferred between two different nuclei, I and S. In biomolecules, this is commonly used in transfers from the most sensitive nucleus, proton, to carbon or nitrogen. In magic-angle spinning (MAS) experiments this requires that the Hartmann-Hahn match condition be met such that $\omega_I \pm \omega_S = \eta\omega_R$, where ω_R is the angular frequency dictated by the MAS rate and η is ±1, ±2 corresponding to sidebands[9,10]. Proton homonuclear dipolar couplings are particularly strong in biomolecular solid-state samples due to the concentration and proximity of “neighbors”. To fully average this interaction the MAS rate must exceed the coupling linewidth, which can range from 20-100kHz.[6] Such ultra-fast MAS rates require specialized probes and reduced sample volumes, making deuteration a widely used

approach in biomolecular NMR[4] to minimize line broadening by reducing the presence of 1H dipolar couplings with relative success[11].

One of the biggest challenges in solid-state NMR is effectively using proton detection, as is routine for structure determination in solution. Many efforts have been directed toward taking advantage of the sensitivity associated with the high proton gyromagnetic ratio, while at the same time limiting the line broadening induced by the strong ^{1}H-^{1}H homonuclear dipolar coupling[12]. As is the case for many experimental methods, in practical terms, it is often possible to achieve a gain in resolution at the expense of sensitivity, or vice versa. Due to these challenges it was difficult to achieve high-resolution ^{1}H spectra of large biomolecules (MW > 20 kDa) prior to recent developments in methodology, in particular those involving fast MAS and deuterium labeling[12]. Fast and ultrafast MAS offer improved ^{1}H resolution, as linewidth is linearly dependent on the inverse MAS rate[13]; however these experiments can only be performed with small-diameter rotors and therefore reduced sample volumes. Similarly, extensive deuteration improves resolution by diminishing the number of homonuclear “neighbors” impacting each proton, resulting in less need for the high power rf decoupling that is one of the biggest contributors to sample heating[14,15]. However, these gains come at the cost of sensitivity concomitant with the reduction in proton concentration. This is usually true even for experiments with heteronuclear detection, because so many sequences begin with polarization transfer from the abundant protons to the sparse ^{13}C or ^{15}N nuclei.

Fast MAS rates (30–100 kHz) compare favorably to deuteration as a means of achieving well-resolved ^{1}H spectra in cases where sample amount is already limited to sub-milligram quantities by sample preparation constraints and loss in sensitivity would be particularly unfavorable[16]. This is particularly applicable for large proteins or those that are insoluble or otherwise difficult to express. The effectiveness of fast MAS is also dependent on the applied magnetic field

strength. Proton chemical shifts can be better resolved using fast MAS at ultra-high field than using fractional deuteration on a lower-field instrument; however, the extent to which this is true is dependent on the intrinsic heterogeneity of the protein sample. Perdeuterated, back-exchanged samples provide optimal resolution for the amide and alpha proton resonances, however in most other cases perdeuteration only provided a 10% increase in resolution compared to fast, high-field MAS spectra on fully protonated systems. It has been suggested that deuteration facilitates backbone resonance assignment, while full protonation is ideal for aliphatic side-chains and methyl resonances[17]. The effect of water concentration during crystallization of perdeuterated proteins has been shown to impact resolution and signal to noise ratios of exchangeable amide sites as well as differences in the effectiveness of different polarization transfer experiments such as CP versus INEPT[18]. These observations should be considered when determining the best approach for a given sample.

By taking advantage of all available techniques, it is expected that solid-state NMR will soon be able to characterize the full range of moderately sized proteins (10–100 kDa), through increased coherence lifetimes, more efficient cross-polarization and heteronuclear decoupling, site-specific relaxation and directly determined proton proximities and distance restraints[19]. This has been demonstrated successfully on five different proteins ranging from 5–30 kDa with different condensed states using an adapted solution- state protocol and automated computational software, MATCH, for resonance assignment[20]. The discussion of sample deuteration above focuses on its role in simplifying the proton spectra, however ^{2}H is also an excellent NMR nucleus in its own right. Methodological advances enabling optimal use of deuterium in biological systems include MAS probes capable of direct detection on ^{2}H in the context of multidimensional experiments, optimized pulse sequences, extensive or perdeuteration and recrystallization from deuterated solvent[21].

Despite being a quadrupolar (spin 1) isotope with a gyromagnetic ratio 6.5 times less sensitive than ^{1}H, ^{2}H can afford other information through its anisotropic quadrupolar interaction, providing information about bond orientation, local order, and site-specific mobility[22–25]. Using double quantum transitions reduces the vulnerability of this experiment to small variations in MAS rate and stability[26] and facilitates the use of ^{2}H as a chemical shift dimension in multidimensional experiments[27]. Another useful property is that deuterium has a much faster relaxation rate than proton, making it useful over a large kinetic range[28,29] and for dynamics studies[22,30]. Line-shapes can be analyzed to determine quantitative rate constants[31]. This coupled with its low natural abundance of 0.015% makes it ideal for site-specific studies without interference from the natural abundance background[32]. Site-specific studies can also be extended to characterize the overall mobility of macromolecules, with further potential to elucidate function. 2D $^{2}H_{DQ}$-^{13}C and 3D $^{2}H_{DQ}$-^{13}C-^{13}C correlation experiments allow assignment of sidechain spin systems[33] , representing a promising direction for future studies with recently developed instrumentation.

An important example of a solid-state NMR probe capable of utilizing deuterium signals was built for investigating the phase behavior of lipid bilayers and conformational changes in phospholipid head- groups as a function of pressure[34]. This probe required high power for broadband excitation over the entire range of the wide-line deuterium spectrum, a necessity that can be greatly reduced with the implementation of MAS in conjunction with partial motional averaging[30,35]. An auxiliary deuterium coil for decoupling in ^{2}H-labeled proteins was developed to provide the necessary decoupling power with a simple modification to existing triple-resonance ($^{1}H/^{13}C/^{15}N$) biomolecular probes without the need for another instrument[36], while a quadruple-resonance probe operating at 600 MHz proton Larmor frequency was built for multidimensional experiments including ^{2}H excitation[37]. In multidimensional experiments, the signal-to-noise was demonstrated to be comparable or slightly better when initiating excitation

through deuterium, and using Rotor Echo Short Pulse IRrAdiaTION (RESPIRATION)[32] and optimal control (OC) cross polarization pulse sequences allowed for lower rf power, better tolerance of rf inhomogeneity, and improved efficiency of magnetization transfer[38]. 2D experiments utilizing initial excitation on deuterium and hydrogen were compared, showing differences in cross peaks that can be used to identify solvent-exposed structural components or membrane interiors due to their relative ability to back-exchange[39]. The Martin lab recently developed a quadruple-resonance (^{1}H/^{13}C/^{2}H/^{15}N) probe for use at 800 MHz ^{1}H Larmor frequency. This probe includes a high-power deuterium channel for decoupling and detection of ^{2}H in deuterated biomolecular samples[40].

Traditionally, low-γ nuclei were detected indirectly through proton in order to yield higher sensitivity, as signal to noise is proportional to $\gamma 2/3$ [41]. This was speculated to be compromised by extensive deuteration; however Rienstra and Zilm independently showed that this limitation could be overcome through intermediate deuteration and reverse cross polarization (RCP) [13] and CPMAS on extensively deuterated proteins[14]. At the same time, Reif and coworkers found that fully deuterating at non-exchangable sites while back-exchanging the amide protons limits spin diffusion averaging of relaxation times, making it possible to extract order parameters from dipolar interactions and scaled quadrupolar tensor anisotropy parameters[15].

The demonstration of triple cross polarization (TCP) by simultaneous CP on ^{1}H-^{13}C and ^{2}H-^{13}C results in up to a fourfold gain in sensitivity compared to direct excitation on carbon. This method is particularly useful for systems where back-exchange is difficult or impossible, such as membrane proteins, where the protein interior is not exposed to aqueous solvent[42]. Oschkinat et al. initially used the double nucleus enhanced recoupling (DONER) pulse sequence for simultaneous irradiation of protons and deuterons, pro- viding higher sensitivity in carbon correlation spectroscopy at distances of up to 6 Å. This provided reasonable ^{1}H-^{13}C cross-

polarization efficiency even at high levels of deuteration and resulted in 3–5 times stronger peak intensities and coverage of the full aliphatic spectral range as compared to previous techniques such as PDSD and ^{1}H-DARR[43]. The effect of the fraction of deuterated sites in conjunction with the MAS rate on resolution and sensitivity has been extensively characterized[13,44,45]. Recently developed pulse sequences such as frequency-selective REDOR (FSR) support experiments on deuterated samples under fast MAS enable the measurement of long-range distances along with other structural restraints[46]. Sensitivity is of particular concern in analysis of fully deuterated systems. Smaller rotor size in conjunction with fast MAS has been shown to improve sensitivity[44], especially for multidimensional experiments requiring transfer between ^{15}N-^{13}C and ^{13}C-^{13}C [45]. A high-quality review on the structure and dynamics of perdeuterated proteins using MAS provides a more detailed reference specific to this area[47].

1.1.2 Challenging protein systems of interest

Traditionally, structures have been solved by X-ray crystallography, solution-state NMR, and more recently with cryo-electron microscopy. Solid-state NMR is a complementary approach to study proteins as mobile solids or in liquid crystal systems enabling investigation of dynamics under physiologically relevant conditions. This method is advantageous for enhancing our fundamental understanding of molecular interactions or identifying targets for chemical biology applications. The Martin lab has and continues to develop instrumentation[48–50] and experimental methods[51–54] to support the atomistic characterization of proteins such as γS-Crystallins[55–58] and a recently discovered membrane-associating plant-specific insert[59] from the carnivorous plant *Drosera capensis*[60].

Large or dynamic systems can be challenging to characterize with atomistic resolution both experimentally and in silico. This is especially true for high-concentration protein environments

that are important to cellular processes such as liquid-liquid phase separation[61,62] and diseases caused by aggregation[63,64]. Large-scale ordering is likely mediated by changes in protein-protein interactions[65], however there is a limited understanding of the nature of the many-body interactions that contribute to these phenomena.

γS-crystallins are a highly-conserved family of long-lived structural proteins that exist at uncommonly high concentrations (>300mg/mL)[66–68] in mammalian eye lenses, forming a hydrogel to focus light and support vision[66,69,70]. These proteins are long-lived making it relatively straightforward to identify and strategically target disruptions to the native short-range interactions that stabilize these proteins and are predicted to lead to loss of solubility or protein misfolding which often result in aggregates producing cataract disease; the predominant cause of blindness worldwide. Both the wild-type (WT) human γS-crystallin (PDB ID 2M3T) and the congenital cataract-associated variant, G18V (PDB ID 2M3U), have been experimentally characterized[71]. The NMR ensemble average suggests that G18V resembles the WT conformation (Figure 1.1), however peak broadening suggests slower state interconversion in the N-terminal sidechain and backbone motions predominantly near the mutation. Other conformations may exist due to steric clashes introduced by the mutation resulting in unfavorable backbone dihedral angles or solvent exposure of three cysteines (Figure 1.2) which could enable previously inaccessible intermolecular disulfide linkages[72] of exposed cysteines[55] or disruption of the interdomain interface which stabilizes the native interactions[73]. This is supported by G18V being less thermally stable[74,75] resulting in loss of solubility and aggregation[65,76–78]. Characterization of the effect of subtle changes in protein-protein interactions due to altered conformational states promises to provide valuable insight into aggregation pathways and will further inform future work to both understand how chaperone activity suppress[79–83] and post-translational modifications increase aggregation[84–86].

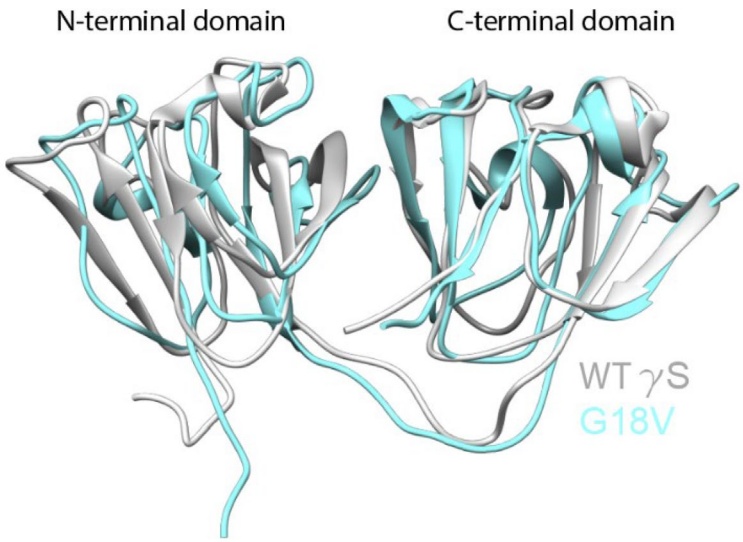

Figure 2.1: Structure of wild-type γS-crystallin (gray) and congenital cataract associated variant γS-G18V (cyan) solved by solution-state NMR[71].

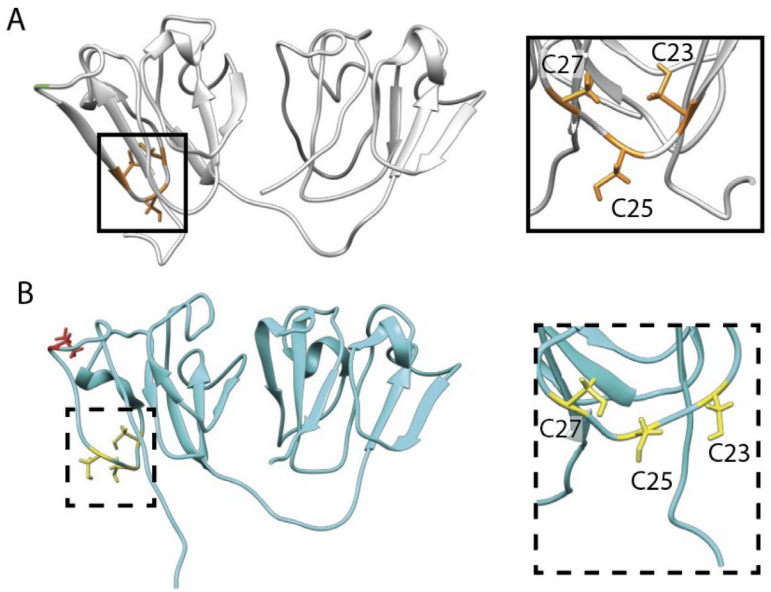

Figure 1.3: Protein structures with mutation sites and disrupted cysteine residues highlighted in A) wild-type γS-crystallin (gray), residue 18 (green), cysteines (orange) and B) G18V (cyan), residue 18 (red), cysteines (yellow).

Proteins that interact with membranes, the barriers between cells and the environment, play important roles in many biochemical processes including transport and signaling in individual

cells, as well as recognition and adhesion amongst many cells such as in immune response, cell growth, and cancer. Out of almost 170,000 structures documented in the Protein Data Bank since 1976, only 2% are membrane-associating, which is exceptionally low given that they account for one third of expressed proteins and more than 60% of drug targets. Challenges to structure determination include that they are dynamic, often unstable without the membrane and very sensitive to environment.

The Martin lab identified a plant-specific insert (PSI) from the carnivorous plant *Drosera capensis* which was hypothesized to minimize competition for nutrient resources by disrupting microorganism membranes[60]. This saposin-like protein is cleaved from an aspartic protease and the cleaved form functions independently, interacting with bacterial and fungal lipids, and has been shown to reduce growth of yeast[59]. Elucidation of the mechanism by which this protein interacts with membranes may necessitate atomistic resolution of thousands of chemical sites. Futhermore this effort promises to significantly advance the development of non-toxic pesticides and robust anti-microbials that are not susceptible to UV-degradation and function over a large range of temperatures and pH values or could also potentially serve as a tool to stabilize lipid nanodiscs for solid-state NMR characterization of other membrane proteins in the future[59].

1.1.3 Contributions to purpose-built probes

The first high-field probe capable of multidimensional experiments on biological samples, which are often lossy and generally complicate circuit design[4,87], implemented a tuning tube channel design based on transmission line theory. The benefits of this design are that it is space efficient for fitting in the smaller bore of a high-field magnet, adaptable to a wide range of frequencies, thermally stable at high RF power, and not dependent on commercially available parts.[88] This design has been used in other Martin lab probes[48–50].

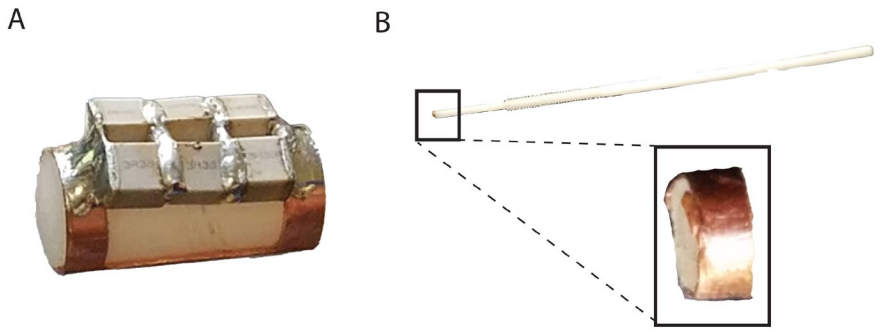

Figure 1.3: Other hand-machined pieces for testing. A) Modified-Aldermann Grant coil, B) Ball-shift homogeneity test rod and conductive ring.

The first quadruple-resonance ($^{1}H/^{2}H/^{13}C/^{15}N$) MAS probe[48] added direct detection on deuterium and will be used for structural studies because it will have the capability to perform conventional experiments to assign backbone resonances. It will also provide better resolution due to larger peak separation of the chemical shifts in the larger field (800MHz, 18.8T), which will be especially important for a high concentration sample or protein-membrane assembly. Deuterium will be beneficial for initial characterization, while allowing use of the same sample for studies in a three-channel SAS probe that is in development.

Current approaches for high molecular weight proteins include ultrafast MAS, which necessitates reduced sample size and consequently higher field strength, complicated pulse sequences that require elaborate methods development and optimization, or extensive deuteration. Also, the anisotropic interactions that are intentionally removed through MAS have valuable orientational and dynamic information can be recovered through a variety of instrumentation approaches.[89] Analysis at a second angle through Switched Angle Spinning (SAS) which spins off the magic angle during the evolution period of the pulse sequence and changes to magic angle prior to detection can provide anisotropic information such as quadrupolar interactions or scaled dipolar couplings, that can be correlated to fundamental inter and intramolecular forces to enable solving the 3D tertiary structure by measuring torsion angles

and distances[90]. In an early application, this was used to correlate broad CSA powder patterns collected in the indirect dimension to well-resolved isotropic peaks in the direct dimension.[91] SAS is also useful for orientable media such as micelles or bicelles, which are model systems for membranes. These biomacromolecules align in a predictable manner based on the angle at which they are being spun relative to the external field: at greater than magic angle, parallel with the axis of rotation; less than, perpendicular to the axis.[89] The choice of angle can be used to selectively control reintroduction of the anisotropic terms[54] and has motivated instrumentation development in this area.

Capacitive coupling was demonstrated in the first Martin lab SAS probe.[50] This contactless method allows the transceiver coil and spinning assembly to move to any angle using sets of coaxial rings of conductor (oxygen-free high conductivity copper, OFHC Cu) and dielectric (polytetrafluoroethylene, PTFE); one conductor connects to the transceiver coil and another connects to the static channel. This provides circuit integrity at any sample angle orientation. The next (^{1}H/^{13}C) SAS probe improved angle control and switching speed through pneumatic control, which had the advantage of limiting mechanical degradation by using a piston and gear mechanism to move the spinning assembly, and decreased the amount of time to perform a stable angle change to the order of ms[49]. However, this instrument was not capable of 3D structure determination. This motivated the design of a triple-resonance (^{1}H/^{2}H/^{13}C) SAS probe to provide direct detection on deuterium and the capability of performing 3D experiments, essential for structure and dynamics through both line shape and relaxation times.

This probe will enable collection of orientation and site-specific dynamics data with the same sample, possibly even the same experiment, through the angle switching and direct deuterium detection capabilities. This instrument will be used in a 500MHz (11.7T) magnet with maximum spinning speeds limited by stability during angle switching, estimated to be 5-10kHz. It is

therefore expected that deuteration will be required to improve spectral resolution, however it is useful in its own right. ^{2}H is a quadrupolar (spin 1) nucleus with inherent asymmetry in the Pake pattern that provides information on the local environment and supported by recent advances in pulse-sequences have enabled study of site-specific side-chain dynamics using deuterium as previously discussed[4], could potentially be applied to observe perturbations to the membrane as well.

Several structural components and parts of the proton channel tuning-tube assembly[88] for the SAS probe were machined by hand (Figure 1.3 A-D). In order to make the plates, pieces to enable use of the rotary wheel in the machine shop also had to be fabricated. Several of these pieces have been soldered together with a blowtorch to establish a skeleton assembly of the three-channel SAS probe as shown in Figure 1.4 E.

Figure 1.4: Hand-machined switched-angle spinning probe parts. A) Stand anchors, B) Proton-channel inductive stub and match plate, C) Top and bottom plates, D) Outer ground planes for ^{1}H / ^{2}H / ^{13}C tuning tube assemblies, E) Skeletal assembly of the SAS probe.

In working to design and fabricate parts for a new probe and modify, repair or use previous purpose-built probes, it became obvious that the conventional processes were not broadly accessible and could unintentionally limit the utility to the broader experimental community. This

was at odds with the spirit of building and innovation that had driven NMR forward and essentially made it an indispensable part of modern chemical analysis, and inspired a shift in the principal goals of instrumentation projects: to support the efficiency and creativity to improve current or develop new capabilities as well as increasing availability of these tools to those without instrumentation expertise.

1.1.4 History of collaborative instrumentation development

The early development of NMR as an ubiquitous technique for chemical analysis was marked by collaboration and communication between commercial instrument developers, academic physicists and physical chemists, and end users of the technology[92,93]. The first commercial NMR spectrometer was produced by Russell and Sigurd Varian, following very quickly after the initial discoveries of condensed matter nuclear magnetic resonance by Bloch[94] and Purcell[95], who were mostly interested in exploring the underlying physics rather than applications to chemistry. During the following years, the Varian Applications Lab, led by Jim Shoolery, played an important role in facilitating communication between instrument builders, both at Varian and in academia, and chemists who provided feedback on what kinds of advances would most impact their work. This interaction, facilitated in particular by John Roberts at Caltech[96], established the utility of NMR for studying complex organic molecules[97–99]. The magnetic resonance community has a strong tradition of instrumentation design, with an emphasis on targeted design of instruments that enable particular experimental advances. Many senior members have fond memories of experimenting with Heathkits, perusing the supplies at Radio Shack and Fry's Electronics, and chatting with far-flung amateur radio operators in a forerunner of today's online maker spaces[100]. As this early history illustrates, the magnetic resonance community is at its most vibrant and innovative when researchers with different interests and areas of expertise freely share information. Many recent

developments in NMR, notably significant advances in applications to structural biology and materials science and the concomitant push to develop expensive high-field instrumentation, have encouraged standardization and the use of commercial equipment. At the same time, increased availability of inexpensive electronic controllers and 3D printing technology present new opportunities for innovation in other NMR applications. Here we discuss some recent progress in inexpensive custom NMR instrumentation, potential new applications, and perspectives for the future.

For many decades, advances in NMR spectroscopy and to some extent medical MRI have focused on achieving high magnetic fields in order to improve both sensitivity and resolution. This is generally achieved using large, cryo-cooled superconducting magnets, causing NMR instrumentation to become so large that it generally requires a dedicated facility, whereas many other analytical instruments can be handled readily and placed on a nearby workbench in a chemistry laboratory. Furthermore, high-field NMR instruments require expensive cryogens and time-consuming maintenance. Although this technology has delivered enhanced capabilities, especially for detailed studies of biological macromolecules, for many applications low-field NMR instruments can provide a viable alternative. Low-field, benchtop NMR instruments are often found in teaching laboratories, where they can be used to demonstrate the basics of 1D and 2D NMR, relaxometry, and perform structural elucidation of simple molecules[101]. However, these instruments can also serve many functions in research labs. Low-field instruments often use permanent magnets, which present more versatility for operation under different environmental conditions and require little maintenance[102]. Low- field spectrometers can be built at impressively low cost, enabling dedicated instruments for particular chemical applications, and benefiting laboratories that otherwise would not have the means to own a traditional NMR instrument. This type of

dedicated sensor can be used to provide an uninterrupted workflow for in operando reaction monitoring, or to analyze hazardous sub- stances safely[103–105].

To take some examples from other areas of chemical instrumentation, Arduino controllers have been used as a basis for a wifi-enabled turbidity sensor that can monitor reaction progress[106], detectors for gas chromatography and gel electrophoresis[107], and a multifunctional sensor array for general chemistry laboratories[108]. In addition to their utility in teaching laboratories[109], home-built, open-source detectors can also be extremely valuable in cases where an elderly but functioning instrument relies on soft- ware that is no longer supported or requires an obsolete operating system, as in the case of a recently introduced Raspberry Pi-based detector for liquid chromatography systems[110]. Potentiostats are used for a variety of electro-chemical measurements in analytical chemistry, with research laboratories often using full-featured commercial instruments. However, low-cost, easy to assemble alternatives can be built using readily available hardware and open-source software[111,112]. These do not match high-end instruments in performance, but are suitable for undergraduate teaching labs, field measurements, and other situations where expensive instruments are not practical. Recent versions support the use of ultramicroelectrodes and are able to detect currents in the nanoampere range without additional signal amplification[113]. Inexpensive, open-source microcontrollers can be used in conjunction with 3D-printed components to create portable devices, such as a 3D-printed UV-vis spectrometer that uses a smartphone as a detector[114] and a scanning electrochemical microscope using an Arduino detector, inexpensive commercial stepper motors, and 3D-printed components[115]. In fact, the use of 3D printing in virtually all of its forms have made impacts across the field of analytical chemistry[116], not just in devices but also to improve efficiency in high-throughput optimization of enzyme immobilization and assays[117], with the option for files to be shared via the NIH 3D Print Exchange. Use of 3D printing in

chemical education showed similar rapid growth in citations over the several years leading up to 2019[118]. In magnetic resonance specifically, 3D printing has been used to develop a surface loop resonator for imaging[119], and a sample holder[120] for EPR. 3D printed components can also be used for MRI, including custom-fit head fixation for small animal studies[121] and low-cost, portable head coils for human subjects[122]. Taken together, the aforementioned works indicate significant promise for further development and creative applications of automation and 3D printing throughout magnetic resonance (MR), however here we focus on NMR instrumentation.

1.2 Additive fabrication: An accessible and adaptable approach

1.2.1 3D printing

Many instrument components are made using traditional machining methods, requiring a dedicated space containing several machines and tools such as saws, lathes and milling machines, all of which require extensive training and a safety bystander to operate. Computer numerical control (CNC) ma- chines enable limited automation of essentially the same techniques, making it possible to machine pieces that are difficult or impossible to make by hand. These processes are collectively known as subtractive manufacturing, as the part is formed by removing layers of starting material. This approach can produce pieces reproducibly and to a high degree of precision; however, it is not always accessible to users in a chemistry laboratory. Dedicated machine shops are often only available at large research universities and may not always be open for use by individual researchers. Aside from the training needed to operate the machines, designing for this workflow requires an understanding of the capabilities and limitations of this process, which

is difficult for users who do not have hands-on experience. In addition to the training time required to develop this skill set, the process is slow because parts must be made serially, so if a mistake is made or a prototype dimension is not correct, then the time must be reinvested in trying again. Although CNC machines are automated, proficient operation also generally requires several years of practice, which is impractical for students who turnover regularly or labs that are not solely dedicated to building projects. Some materials that are particularly useful can be very difficult to machine accurately at the dimensions required for the design of NMR probes and accessories. An example is polytetrafluoroethylene (PTFE) which is desirable because it has excellent electrical properties, a low coefficient of friction, low chemical reactivity, and is free of proton background. Despite these advantages, the use of PTFE has been limited because its high flexural strength often leads to bending away from cutting tools or contributes to the propensity to wobble when machining lengths of more than a few centimeters. A high coefficient of thermal expansion also leads to inadvertent and sometimes unavoidable changes in the material dimensions during the cutting process. In addition to these practical challenges, waste is inherent to subtractive manufacturing in the form of removed material, with the amount depending on dimensions of the starting material, the required workflow and experience level of the machinist.

In contrast, 3D printing is a form of additive manufacturing where layers are sequentially assembled to form the desired piece. Although this process is not free of challenges, the technique is generally more accessible than traditional machining. One similarity is that there are different styles of printers to meet a variety of needs, and while there is no “one-size-fits-all” solution, a collection of several machines is unlikely to span more than half of a typical lab benchtop. Shared 3D printers are now becoming commonplace in many engineering laboratories or other university-wide maker spaces, including at primarily undergraduate

institutions (PUIs) and liberal arts colleges. 3D printing software is generally free, meaning parts can be shared without the need to have computer-aided design (CAD) software. If it is necessary to design a new part or make modifications to an existing file, introductory versions of CAD software are also available for free, such as Tinkercad by Autodesk (San Rafael, CA). The cost of many commercially available printers with print platform areas ranging from 400 cm^2 to 800 cm^2 is also comparable to benchtop mills or lathes that are capable of making parts of similar dimensions. With regard to safety, 3D printing poses lower risk to the user for the following reasons: printers rarely have components that could cause significant physical harm to the user and the additive process does not create particulate matter that requires personal protective equipment such as glasses or respirators to be worn. By virtue of the limited risks, the technique can be self-taught through trial and error and performed independently with no need for a safety observer. Parts can often be designed with less attention to the manufacturing process, enabling complicated pieces to be made at lower cost and with a broader scope of possible features such as no-access internal channels or no-assembly interlocks. For these reasons, 3D printing is an appealing method for advances in instrumentation because it has the potential to remove barriers not only to involvement in design at any level, but also the degree to which established builders feel comfortable investing in new, high-risk, or single-application ideas.

1.2.2 Prototyping and test devices

Prototyping is essential to the design process, providing the creator with opportunities to thoroughly evaluate a concept ahead of fabrication. 3D printing is a method that can be efficiently used for low-fidelity prototyping due to its relatively rapid production capability, inexpensive material library and collaborative nature. 3D-printed prototypes can save time by

allowing the designer to quickly determine compatibility issues and problematic user interactions, enabling faster development. As a process, printing is mostly automated, allowing other work to be performed while the parts are being made. Additionally, multiple designs on the order of tens can often be made concurrently for many common probe components, speeding up prototyping efforts, especially for exploratory projects. We have used this process to redesign the spinning assembly coil platform for a cross-coil probe[40]. Measurements were taken from the existing spinning assembly in order to design a compatible coil platform. Prior to machining the final piece out of polychlorotrifluoroethylene (PCTFE) also known as Kel-F, the designed part was printed to verify dimensions and proper fit as shown in Figure 1.5A. The final part made in Kel-F took a graduate student machinist roughly three hours to machine, which is comparable to the print time on the Formlabs Form 2 stereolithography (SLA) printer using the Tough V4 resin at the high-resolution setting of 0.05 mm layer thickness. The advantage remains that if the dimensions of the prototype had been incorrect, experimenter time would not have been lost to machining an incorrect piece. Further, use of the Formlabs Draft resin which was created specifically for prototyping because it cures approximately four times faster than most other resins, could drastically reduce the total print time to only 15 minutes, however this would require a compromise of lower resolution because this material has a minimum 0.3 mm layer thickness.

Upon successfully using 3D printing to make the coil platform, we expanded to print a ball-shift assembly[123] to enable benchtop testing of RF homogeneity on a variety of coil designs. This required printing a mock spinning assembly and front-plate adapter to guide the threaded rod which are shown in Figure 1.5B and C. In total, making all of these parts out of a reasonably inexpensive and easily machinable plastic such as PEEK would cost approximately $15 and take a student machinist a day or more to make. By comparison on the Formlabs Form 2 SLA printer using the Draft resin would drastically reduce the total production time to only one hour

and cost down by an order of magnitude to $1.50. In the case of a single production the difference appears trivial; however, it would have a much more significant impact on large-scale production. 3D printing also makes custom test fixtures readily accessible to those who are not proficient at machining. At comparable resolutions, the Formlabs Draft resin is well-suited for rough, initial prototyping or parts that do not require fine details. The trade-offs in print time and resolution demonstrate the flexibility of 3D printing as a method that can be adapted for a variety of design concepts and stages.

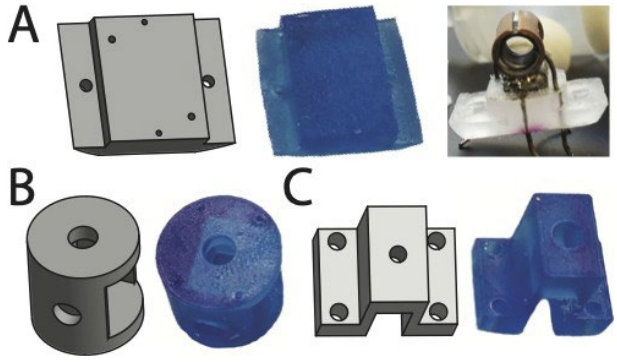

Figure 1.5: CAD drawings and corresponding 3D-printed parts made using a Formlabs Form 2 SLA printer. A) Coil platform was designed and printed to test compatibility in a commercial spinning assembly before machining the piece out of Kel-F for implementation in the probe. B) Mock spinning assembly body that allows for easily changing coils with the printed platforms for benchtop test of designs. C) Ball-shift adapter used to test RF homogeneity of coil designs. The piece can be manually threaded or completed with a heat-set threaded insert.

1.2.3 Probe components

Although concerns about proton background and dielectric loss preclude 3D printing of many probe components using readily available materials, parts that are sufficiently far from the coil and not in direct contact with key circuit components can readily be 3D printed from inexpensive materials. Examples are shown in Figure 1.6. We have applied 3D printing to make new stator legs to enable changing the spinning assembly to one configured for a different coil in a MAS probe. The legs were printed on a SLA Formlabs Form 2 with Tough V4 resin to support an

assembly that was slightly larger diameter than the original commercial version, taking roughly four hours at the highest resolution setting. The extrusion printer Ultimaker 2 was used to 3D print a more structurally robust magic-angle adjust mechanism out of polylactic acid (PLA), which would have been difficult to machine due to the small dimensions and interlocking design. 3D printing has also been used to make a pneumatic sample eject system[124] that fits onto the front of the spinning assembly body, allowing samples to be changed without removing the probe, drastically reducing the amount of time and cryogen resources required. Use of this technology has also made it feasible to relatively rapidly prototype, test and introduce a new spherical rotor design in solid-state by 3D printing suitable spinning assemblies. In addition to supporting the use of the magic-angle spinning spheres, the design of the spinning assembly has the magic-angle adjust mechanism built in, thereby optimizing this critical part of the experimental apparatus[125]. This fabrication method has also been applied to create a custom hollow spinner and tube combination for solution-state NMR. The printer was moved into a glovebox to not only improve the print quality of the nylon copolymer vessel by preventing degradation due to oxidation, but also to allow oxygen-sensitive catalysis reactions. The space in the spinner body enabled analysis of gas-phase products at the same time that NMR was used to monitor depletion of reactants[126]. This unique 3D-printed sample tube could be beneficial for potentially high-risk or high-cost experiments that may not be able to be reproduced for separate analysis or as a precursor to designs that would enable control over when reactants are added, provided that necessary solvents are compatible with the printed polymer. Inductors for LC traps to block the proton frequency on low frequency channels have been printed out of sterling silver by the company Shapeways (New York, NY) for probes at the National High Magnetic Field Laboratory. These metal printed traps were designed to have a rounded- square shape that yields better performance, but can be more difficult to achieve by hand[127].

Beyond the ideas presented here that have already been implemented, we propose that the use of 3D printing can be further expanded to make many other components for a variety of applications in NMR hardware and sample preparation. In switched-angle spinning probes the more complicated components to machine, e.g. gears and specialized spinning assemblies, should be well within the capability of most commercially available systems. If friction limits the speed or smoothness of angle changes, PTFE printing could be used a slightly higher cost, with the additional benefit of minimizing proton back ground. We also envision that chambers to encapsulate spinning assemblies could be 3D printed to convert any MAS probe into a variable-temperature (VT) probe suitable for temperature-controlled experiments. More than ever before, this approach essentially puts the limit of possibilities in the hands of the experimentalist. This has been demonstrated in the redesign of a Bruker MAS probe to change the overall experimental capability to single-crystal studies using a goniometer assembly to evaluate anisotropic interactions[128] and modular in-situ probe heads with RF coils integrated into the reaction vessel[129]. Ultimately we see this capability supporting on-demand modular probe heads, empowering users to determine the approach best suited for their analysis while providing the flexibility to implement it whenever it is needed into whatever instrument is at their disposal.

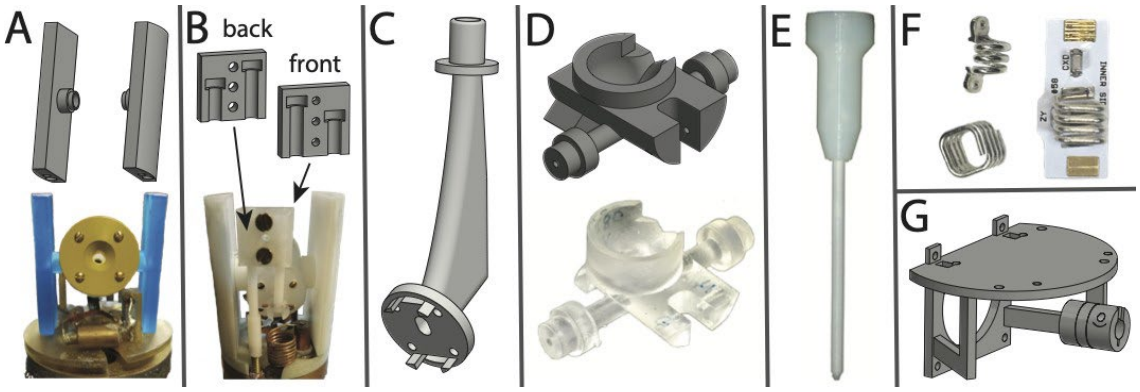

Figure 1.6: Various 3D-printed components used to adapt or improve NMR probes and sample preparation. A) Spinning assembly supports that allow a commercial probe to be modified to fit a different spinning assembly. B) Magic-angle adjust mechanism modification made to existing probe[48]. C) Sample eject adapter for DNP probe[124]. D) Spinning assembly for magic-angle spinning spheres[130]. E) Oxygen-free sample tube for liquids probe[126]. F) Squared low-frequency traps made of silver[127]. G) Single crystal goniometer design[128].

1.3 Considerations for broader applications

1.3.1 Capabilities and limitations of current 3D-printing systems

In order for 3D printing of NMR instrumentation to become broadly accessible, it will be necessary to invest in developing and disseminating protocols. Although this methodology is considerably easier and safer than traditional machining, it is not trivial and unfortunately does not produce push-button results. Firstly, there are differences in the utility of different print processes, aside from the materials that they most commonly use, which must be understood in order to maximize their utility. The two most common commercially available styles of printer have different operating principles and are therefore useful for different applications. Fused filament fabrication (FFF or extrusion) printers feed a filament through a heated nozzle, softening the material in order to deposit the layers. Many common polymers such as PLA or ABS, which are inexpensive and soluble in common solvents, are readily used with these systems. Extrusion printers with two nozzles are available, that enables support structures to be

printed out of a water-soluble material, reducing post-processing and allowing for more in- ternal features. However, these printers are generally less automated in that users have access through the printer software to adjust any of up to one hundred different print parameters, including layer thickness, cooling rate, nozzle temperature and infill density. The other common type of available 3D printers (SLA printers) use photocurable resins that have a very broad range of material properties. Options include flexible, high-temperature, castable, tough, and draft. In general, these printers are much more automated, with user control only over layer thickness and support density, size and location, making setup much easier but allowing fewer design options. Furthermore, the exact chemical composition of the resins is sometimes proprietary, making it difficult to predict solubility in common solvents or potential deleterious interaction with samples. However, because they are limited in resolution by the laser spot size rather than the nozzle diameter, SLA printers are often higher resolution and capable of smaller features than FFF systems.

Another intrinsic property of each system is the variability of materials properties in response to parameters in the print process, which can result in physical changes and may be more or less controllable. In FFF printing, it is undeniably advantageous to be able to change parameters, e.g, to increase the speed of printing for a draft part or to reduce the amount of material used for a part that does not require strength, however this can add a significant amount of complexity for novice users. For instance, ABS may experience uneven shrinking if not adequately cooled between layers, potentially causing unwanted warping. Fortunately these parameters can be calibrated and are well documented for many materials and on many systems. Fluoropolymers, which would be especially useful to applications in NMR instruments are a notable exception. To date, we are aware of only one lab that has made measurable progress in FFF printing a fluoropolymer, Kel-F, by also first developing a filament extruder capable of the high temperature requirements and devoid of metals capable of catalyzing decomposition[131]. This

may be in part because it appears that only fluorinated ethylene propylene (FEP) is commercially available as a 3D printer filament from the company Plastic2Print (Amsterdam, Netherlands), and would re- quire an engineering-grade printer with a nozzle capable of exceeding the required extrusion temperature of 260 °C, a heated build platform to pro- mote adhesion, and an enclosed chamber that is heated to prevent uneven cooling. 3M has a fluoropolymer-capable SLA printer, however they do not plan to make the system commercially available, so designs must be submitted for fabrication. While metal printing is advancing quickly as well, currently there are concerns for application to circuit components. Metals are commonly printed by either sintering layers of deposited metal powder or using 3D-printed lost wax molds. Sintering may increase resistance due to voids introduced by the layering process, oxidation, and surface roughness, which would at a minimum increase the required post-processing or at worst lead to increased risk of corona discharge. The lost wax technique is commercially available from Shapeways however the stated minimum diameter of 0.8 mm and structural support requirements mean that this may not yet be suitable for more intricate circuit components.

1.3.2 Making magnetic resonance makers: why and how

Remixing, or reusing existing knowledge in a novel way by putting together disparate pieces, is an important mode of learning and innovation. Remixing is a powerful tool for gaining proficiency: a large study of student programmers using an online community found that users who frequently remixed existing content had a larger coding vocabulary than those who did not, even after controlling for the number of projects, and that exposure to coding concepts via remixing promotes their retention[132]. The effectiveness of remixing as a learning strategy has also been documented among software engineers[133,134]. In the magnetic resonance community, the most familiar example of remixing is the vast proliferation of pulse sequences for achieving

different experimental results. Developing a new pulse sequence is rarely a matter of writing the entire sequence from scratch: in most cases, existing modules can be selected and strung together to generate the desired signals. Although developers of MR instrumentation are likewise inspired by each others' efforts, remixing is much more difficult in this domain because of the need to fabricate physical objects, a process that requires a great deal of specialized training and is subject to the availability of specific machining tools and idiosyncratic preferences for different methods. 3D printing and automation offer the possibility to greatly facilitate sharing of designs between laboratories as well as enabling remote collaboration, especially on projects that require building physical objects.

The main barriers to the use of 3D printing for casual users are lack of experience with 3D modeling software and poor 3D visualization skills in general. Many first-time or casual users rely heavily on 3D printing facility staff, whose level of expertise is highly variable. Established, subscription-model maker spaces often have expert staff, a large community of experienced users, and culture of collab- oration. On the other hand, facilities associated with public libraries and schools often have operators whose primary expertise is in information technology, library science, or teaching. Hudson et al. interviewed novice users at facilities of the latter type, and found that many first-time users struggled with drawing appropriate 3D models or appropriately customizing models downloaded from online sources, and had access to uneven levels of support from the staff[135]. Another variable is the quality of instructions for putting together complex assemblies. The current state of the art in such methods include sophisticated AR viewers that require custom hardware and software[136,137]. However, standard video is also effective[138], particularly if filmed from a first-person perspective[139]. 2D perspective drawings were found to be equally effective as 3D computer models in terms of accuracy and time to complete the task, as long as they are presented as action diagrams with arrows showing the motion of components as opposed to static structures[140].

Users' proficiency in using 3D modeling tools also affects their ability to remix and adapt existing designs. Compared to pulse sequence programming or other software development, facilitating remixing is more difficult in a context that re- quires building 3D objects, which must necessarily have an offline component. Platforms such as Thingiverse have attempted to lower the barriers to customizing existing designs by providing tools that enable users to change pre-determined parameters without having the ability to fully edit 3D models. This feature is limited to the parameters allowed by the original designer, and although it does enable novice users to customize parts that they would not able to access otherwise, it was found to be used relatively infrequently by experienced designers[141]. Furthermore, such designs were not often used as a component of remixed designs incorporating elements of two or more models[142]. Hence, a tradeoff exists between creating objects that can easily be used by a large number of casual users, and those that significantly contribute to innovation in the research community. Features that support more interactive remixing are: the inclusion of relevant dimensions for commonly available commercial products that can be enhanced with accessories (e.g. probe bodies or stators in the NMR context), compound models containing an assembly of multiple parts intended to work together, models for basic parts that can be used in a variety of contexts, and those that include de- tailed instructions for a fabrication process[141]. Another key feature enhancing uptake of both 3D models and hardware platforms is flexibility and interoperability with existing instrumentation[143]. In the magnetic resonance context, this means providing options to interface custom components with pre-existing commercial instrumentation in users' labs. User-generated and open-source hardware is highly unlikely to entirely replace commercial instrumentation in any but a tiny handful of very specialized labs, so being able to interface with the latter is critical for success. This will likely necessitate accurate measurements to be taken to ensure compatibility of printed designs in the intended instrument, which can be problematic depending on the tools available, dimension to be measured and geometry of the

part. While several steps can be taken to address this, the most broadly effective will be to account for flexibility in designs where possible[144].

In a university setting, maker spaces build engineering self-efficacy, with undergraduate students who frequently use their university's maker space reporting lower anxiety and greater motivation for engineering-related tasks[145]. Being embedded in a maker community enhances both performance and learning compared to working alone[146]. In a purely online context, productive collaboration among users distributed over large distances and in different time zones is facilitated by having a friendly, open community with a low entry barrier. This was found to be promoted most effectively by using a text-based, asynchronous communication platform, as this eliminates the need for users to coordinate meetings at particular times. Social interaction is valuable for establishing relationships and building trust among users, which is also enhanced if at least some of the community members have met offline[147]. This can be accomplished via short in-person workshops introducing the technology and encouraging collaborative discussion of user projects[143], an activity that could be performed at an educational venue such as the NMR Winter School or at a brief pre-conference workshop. Given that many of the issues reported by novice makers are related to poor 3D modeling skills, it would make sense for the first educational efforts to focus on teaching these skills and providing a strong foundation that can be adapted to the users' specific needs, which vary with both the project details and the equipment available at the users' home institutions. The free software community offers an instructive example of a distributed, collaborative effort that regularly produces professional-quality tools that can be used and improved by essentially anyone.

Taken together, these results suggest that aspiring magnetic resonance makers would do well to foster a collaborative community of expert makers, by making use of their institution's maker

spaces where available, and/or by pooling 3D modeling and printing expertise and resources with other like-minded experimental chemistry or physics groups.

1.4 Conclusion

Bringing together automation, additive manufacturing, and modularity, we can envision the development of new methods to replace otherwise tedious, labor- intensive, or unnecessarily defined as skilled tasks required in NMR instrument design or experimental applications. This changes the paradigm of magnetic resonance instrument development to one of hardware as protocol, where ease of fabrication is included as an explicit design consideration to be optimized along with performance and robustness. When strategically applied, automation can reduce time commitment and improve reproducibility by limiting human-introduced error. Alongside conventional machining, 3D printing can make the fabrication of well-curated designs more accessible, while also making the creation of new designs less restrictive and more efficient. Broad adoption of these techniques in the field of magnetic resonance will allow ideas to be shared and collaborated on much more extensively, strengthening the community through increased implementation of different perspectives and expertise in instrumentation. Renewing our commitment to innovation by embracing readily remixed concepts, the central tenet of our maker space, will lead to more generalizable approaches to achieve optimized designs and increase new experimental capabilities to the benefit of all. All relevant CAD files are provided in Appendix A.

Chapter 2

Accessible templates to achieve intricate radiofrequency transceiver designs

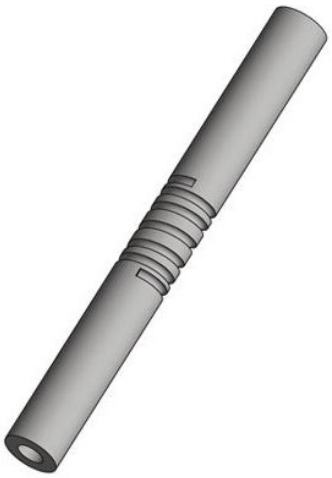

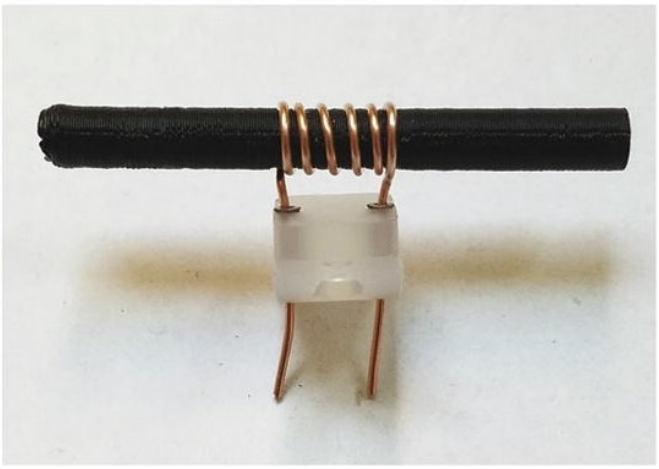

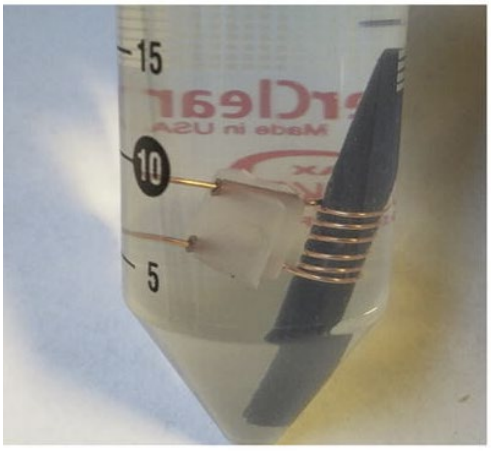

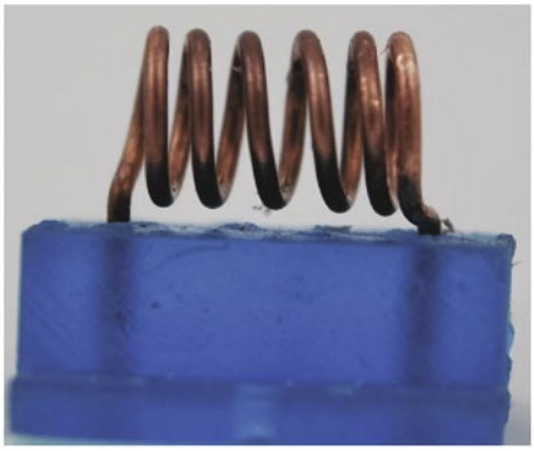

2.1 Introduction

Additive fabrication, or 3D printing, promises to minimize material waste and reduce the manufacturing cost of constructing intricate pieces in a variety of settings[148]. This technology has been used to produce key parts of magic angle spinning (MAS) NMR probes, including sample exchangers[124] and stators for a spherical rotor system[125]. So far, the use of 3D printing technology to produce NMR coils and coil forms has been limited by the available materials. Available insulators are typically organic polymers or resins that produce significant proton background signals and behave as lossy dielectric materials, making them poor choices for pieces that will be in direct contact with the transceiver coil. Here we present a method for reproducibly fabricating NMR coils with particular dimensions using 3D-printed dissolvable inserts, using solenoids with different dimensions as a proof of concept.

Solenoids are arguably the best-characterized axial resonators and have been used extensively in MAS probes. They are frequently used in solid-state NMR due to their large filling factor, scalability, ease of fabrication, ability to be multiply tuned[149] and reasonable SNR[150]. Another advantage is that solenoids generate strong B_1 fields even when oriented at the magic angle. In theory, an infinitely long solenoid has perfect RF homogeneity. However, in practice solenoids with axial lengths, diameters and number of turns appropriate for use in MAS probes fall short of the optimal geometry. The generated B field along the cylinder axis drops off significantly toward the coil ends, limiting the homogeneous region to 50% or less of the available volume in many probes[151]. Several variable-pitch solenoids with decreased spacing between turns toward the ends, expanding to a maximum at the center, have been proposed to improve homogeneity and thereby increase the readily usable sample volume.

One of the first to be introduced used a modified Biot-Savart formula to vary the pitch within experimentally justifiable limits for an eight-turn coil, followed by integration to determine the magnetic field profile[152]. Another group determined the windings required to achieve a square field profile represented by an equiripple function at high frequencies[153]. Although the dimensions and frequencies differ significantly from the coils designed for this study, the authors suggest that the equiripple function has the advantage of flexibility in design. A ribbon coil of varying width has also shown improvement to radial homogeneity for higher frequencies by minimizing gaps[154]. Improvements in solenoid RF homogeneity have been augmented by computational[155] and theory-driven simulation approaches[149,156,157]. Here we demonstrate the construction of solenoid coils with particular dimensions, using a CAD program to design a precisely specified coil and its corresponding template. The template is then 3D printed using a dissolvable material and dissolved away in appropriate solvent after the coil is wound. This procedure was validated by comparing experimental (bench-top) and simulated B_1 field homogeneity for a constant pitch and three different variable-pitch solenoids. The primary objective of this communication is to introduce a coil fabrication method that is fast, reproducible, and allows NMR coils to be easily fabricated once an acceptable design is established.

2.2 Materials and Methods

2.2.1 Coil designs

Four coils were designed with dimensions suitable for use in a standard solid-state NMR probe with a 3.2 mm rotor. Coils were drawn in Inventor Professional 2017 using 0.6 mm diameter (22-gauge) copper wire, each having six turns and an inner diameter of 3.8 mm.

2.2.2 Coil fabrication technique

The coils described above were built using 3D-printed polymer forms referred to herein as dissolvable inserts for achieving performance enhanced resonators (DIAPERs). The coil forms were designed in Inventor with the radius of the 22-gauge wire cut from a cylinder of diameter 4.1mm using pitch and turn parameters listed in Table 2.1. In preparation for 3D printing, the cylinder was made hollow to reduce waste and expedite the removal process by increasing surface area accessible to solvent. Files were exported in STL format, compatible with Cura 3D printing software which was required for printing on the LulzBot TAZ 6 and FlashForge Creator Pro. CAD drawings and STL files are available upon request. All inserts were printed within one hour at 0.2 mm resolution using IC3D 3 mm acrylonitrile butadiene styrene (ABS) filament. Each of the four coils were hand wrapped on the template. ABS dissolves in acetone at room temperature, making extraction of the coils possible with minimal risk of deformation. DIAPERs were removed by soaking in approximately 20 mL of acetone in a 50 mL conical centrifuge tube stored upright overnight. Residual ABS was removed by direct application of acetone using a paintbrush. The inductance of each coil was determined by finding the slope of a curve defined by capacitance vs. frequency and is provided in Table 2.1. Six standard American Technical Ceramics Corp. chip capacitors were used ranging from 3.3 pF to 12 pF.

2.2.3 Experimental homogeneity measurements

To evaluate spatial homogeneity of the B_1 field along the rotor axis, ball-shift assays[158] were performed in triplicate for each coil. Ball-shift assays were executed by moving a conductive ring along the rotor axis in discrete steps defined by the thread pitch, and measuring the resonance frequency shift[123]. The experimental apparatus used a 1.9 mm outer diameter, 0.3 mm thick, and 0.8 mm long copper ring on the end of a 4–40 threaded rod with an observable linear

increment of 0.6 mm. A modified Varian HXY probe was tuned to 200 MHz with a minimum S_{11} of 40 dB. Shifts in the resonance frequency were recorded by observing the response on an Agilent Technologies ENA Series Network Analyzer after moving the conductor one increment at a time until a distance comparable to the rotor length had been achieved, roughly 24 turns. This process was repeated three times to ensure reproducibility with the resulting field profile generated from the aver- age of each point normalized to the maximum frequency shift of each trial. Error was calculated by determining the standard deviation and dividing it by the square root of the number of repetitions for each axial position. Results were plotted in Wolfram Mathematica version 11.

2.2.4 B field modeling

High-frequency electromagnetic simulations were performed using Computer Simulation Technology Microwave Studio (CST MWS). Coils were imported using the IPT file format generated by Inventor. The coil material was set to the CST library value for pure copper. A discrete port was connected to one lead and defined to have 50 X resistance, consistent with the desired impedance of our NMR probe. A tuning capacitor was defined as a lumped element attached in parallel to the port and alternate lead. The capacitance value was determined using RLC circuit theory, $f = 1/\sqrt{LC}$, in order to tune to 200 MHz. The excitation duration was approximately 150 ns based on a frequency range defined as 10 MHz around 200 MHz. Boundary conditions were defined as open add space, and background was defined as normal. Based on an estimated maximum fillable length of 15.2 mm, a line was defined along the rotor axis and centered with respect to the coil length and diameter. After running each time-domain simulation, the 1D magnetic field profile at 200 MHz was evaluated along the axial curve. Unless otherwise specified, the default mesh is used to determine the step size, however this was adjusted to match the experimental increment of 0.6 mm by using Template Based

Post Processing. The results were exported as a.txt file, normalized, and plotted in Wolfram Mathematica version 11.

2.3 Results and discussion

Traditionally, constant pitch solenoids are made either freehand or by wrapping two wires around a cylinder, where the wire to be removed uniformly establishes the distance between turns on the remaining coil. For this study the uniform pitch was chosen to be slightly larger than double the wire diameter so that it would produce a coil of comparable axial length to the model variable-pitch coil[48]. These coils were designed to have six turns, as this typically yields an inductance suitable for our desired frequency range[87]. Previous experimental observations indicated that the smallest allowable distance between turns without being significantly prone to arcing is roughly 0.8 mm, especially at high power. Therefore, this was established as the tightest pitch in the adjusted designs for this study. The stretched variable-pitch coil was developed as a modification of the work of Idziak et al.[152], adjusted to the conserved coil parameters stated in the methods section. We chose it to test changes in number of turns between otherwise similarly dimensioned coils and the limitations of gap size between windings, whereas the differences between the other variable-pitch coils are quite subtle. The model variable-pitch coil changes the revolutions per pitch in addition to the pitch itself[48]. To control for changing the revolutions, a ratio-pitch coil was designed with comparable inter-turn spacing by increasing the pitch per one revolution based on ratios defined by the smallest pitch. In this study, the designs include one constant pitch and three different variable-pitch coils, shown in Fig. 2.1. Detailed information for each design is provided in Table 1.1.

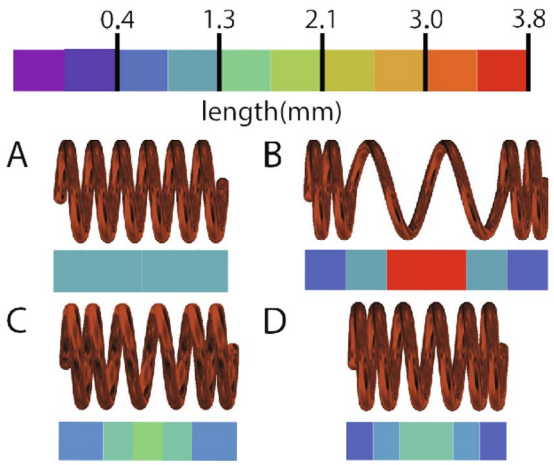

Figure 2.4:The color scale is a graphical representation of pitch. Bars below coils show the magnitude and revolutions of pitch for each design: A) constant, B) "ideal", C) model D) ratio.

Among other factors, RF homogeneity in NMR resonators sensitively depends on symmetry, which is often the most difficult characteristic to achieve in hand-made fabrication. Relatively small deviations can negatively impact RF homogeneity. Therefore, performance enhancements achieved through variable-pitch coils requires readily implementable optimization of spacing between turns. DIAPERs provide a more reproducible approach that does not require extensive expertise in coil fabrication. The complete process is shown in Figure 2.2. Using this procedure, four verifiably different coils were created within two days, with cost of manufacture totaling under 10 dollars.

Development of this method was motivated by interest in extending the utility of 3D printing for improvements in NMR instrumentation. The problem chosen for proof of concept is the comparison of variable-pitch solenoids with different dimensions with respect to RF homogeneity. Theory-driven modeling software, CST MWS, was utilized to rationalize the experimental approach through comparison to simulated results for the same coils. Figure 2.3 shows experimental and modeled data for each of the four coil designs. The homogeneous region in this study is defined at 90% of the normalized field magnitude.

Table 2.1: Design specifications for each of the four coils in this study. Turns are numbered outside to inside and are symmetric about the center. All pitch dimensions are for one revolution, with the exception of turn 1 pitch on the model coil which is 1.5 revolutions. Inductance was experimentally determined after coil recovery to determine necessary capacitance for simulated tuning in the modeling software.

Coil	Turn 1 Pitch	Tune 2 Pitch	Turn 3 Pitch	Axial Length	Inductance
Constant	1.3mm	1.3mm	1.3mm	8.6mm	72.1nH
Stretched	0.8mm	1.3mm	3.8mm	12.3mm	66.0nH
Model	1.0mm	1.5mm	1.8mm	8.5mm	72.5nH
Ratio	0.8mm	1.1mm	1.5mm	7.5mm	70.3nH

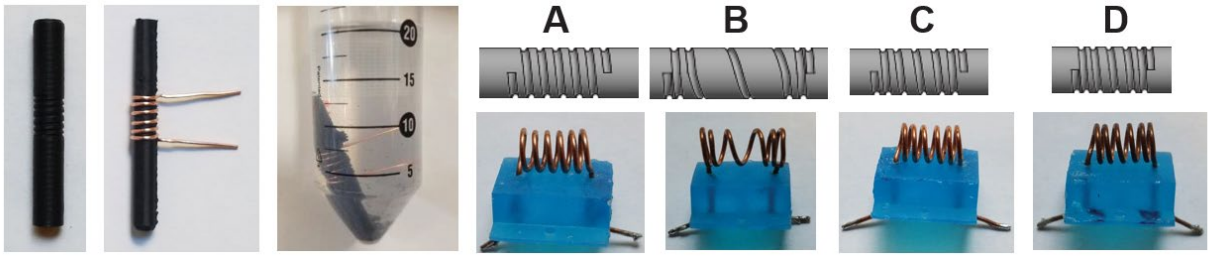

Figure 5.2: Shown is a 3D printed DIAPER made from ABS. Copper wire is wrapped around the template to form the coil. This assembly is soaked in acetone for several hours until the polymer is partially dissolved. CAD designs for the forms and recovered coils are shown from left to right: A) constant, B) "ideal", C) model D) ratio.

Two of the three variable-pitch designs show improvements over constant pitch, however the stretched variable-pitch design yielded a negligible homogeneous range. It was expected that lessening the number of turns, directly increasing gap size, would yield significant field fluctuations[154], providing a dramatically different profile to test the methods of analysis. The findings demonstrate that dimensions must be considered comprehensively and that variable pitch alone does not inevitably extend the homogeneous region. Based on the measurements performed here, the model variable pitch is effectively indistinguishable from the ratio variable pitch. It would be possible to improve the resolution of this measurement by using a finer thread pitch on the ball shift apparatus, or by using the NMR signal to map the homogeneity[123,149,159,160]. However, based on the CST results, the improvement to the length of the axial homogeneous region of the model variable pitch over the ratio pitch is only about 4%, which is likely to be negligible for most practical NMR applications. Use of the model variable-pitch design shows an

improvement of 4.0 μL or 40% based on experimental measurements over constant pitch. The coils were designed to have nearly identical axial length; therefore, improvements can be directly associated with changes in pitch.

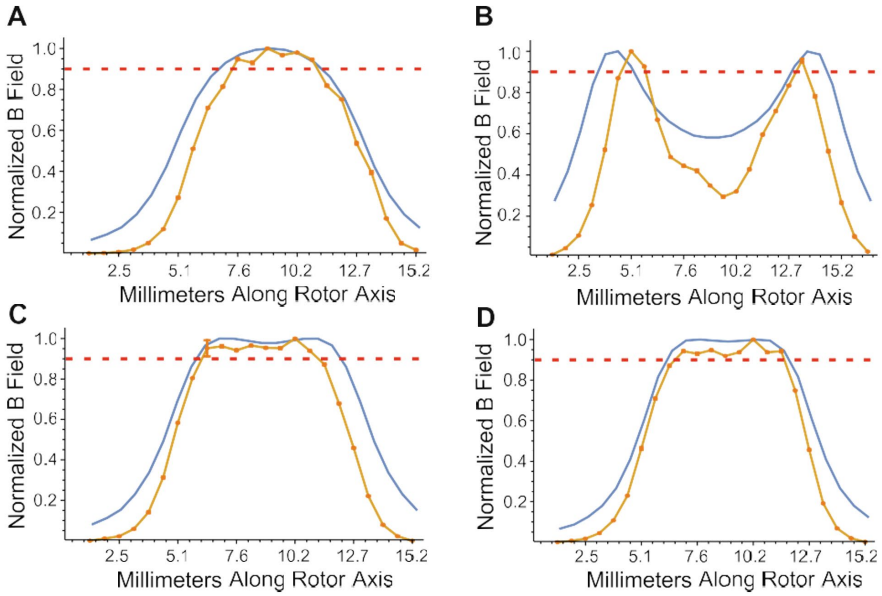

Figure 2.6: Experimental and modeled B-field homogeneity for each coil: A) constant, B) "ideal", C) model D) ratio. Averaged experimental data performed in triplicate, including error bars, are depicted in orange. The field derived from CST simulation evaluated along the rotor axis is shown in blue. The red dashed line demarcates the acceptable 90% homogeneity threshold.

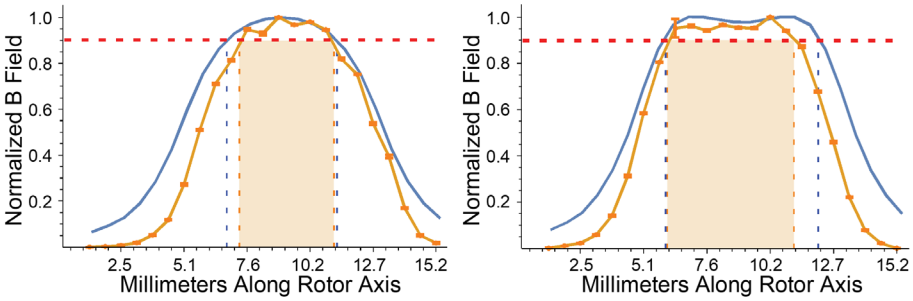

Figure 2.7: A) Constant-pitch solenoid and B) model variable-pitch solenoid homogeneity data are compared. Experimental data is shown in orange and CST simulated data is shown in blue. The homogeneous region is defined where the field is above the red dashed line with experimental region shaded. Orange and blue dashed lines show axial positions of intersection which can then be used to calculate viable sample volumes.

Our model variable-pitch solenoid was originally designed to fit within a Modified Alderman-Grant Coil (MAGC)[161] in a crossed-coil probe, which limited the available axial length to 8.9 mm.

If the solenoid were to be used in a single-coil design, this length could be extended to increase the viable sample volume further. Analyzing the percentage of homogeneous region to the total axial length of the coil along the rotor axis showed a 15% improvement with the model variable pitch over constant pitch. A common commercially available Revolution NMR 3.2 mm rotor that accommodates both desirable sample volume and spinning speed can hold 22.0 μL. Based on the designs in this study, constant pitch could utilize 45% of this volume, while the model variable pitch extends this to 63%. At a minimum this offers additional flexibility in optimizing experiments. From all aspects this is a significant performance enhancement, especially for NMR experiments where sensitivity is generally a concern that can be partially mitigated by probing larger sample volumes.

2.4 Enhancing reproducibility and expanding resonator designs

2.4.1 Testing reproducibility

The initial application of 3D-printed templates for transceiver coil fabrication[1] demonstrated the ability to create different designs that were experimentally verified to be consistent with field profiles generated using simulation software. Although this was sufficient as a proof of concept, in order to motivate acceptance by and utility for a broader user base, we tested the efficiency and reproducibility of transceiver coils made: 1) using DIAPERs for several replicates by the same moderately experienced student user, 2) using DIAPERs for single attempts by multiple novice students with minimal instruction and 3) using the traditional handmade method on a drill bit by the moderately experienced student with a DIAPER reference and faculty member with no reference. In the first study, a builder with roughly three years of experience wrapped all of the coils in order to evaluate reproducibility of a single person. Five DIAPERs designed to fabricate

a variable-pitch solenoid[48] were printed on a Lulzbot Taz 6 using ABS filament. In total the five coils took 20 minutes to wrap. The DIAPERs were individually soaked in acetone overnight to recover the coils for testing.

Table 2.2: Coil inductances measured for five coils using DIAPER templates made by the same student, a handmade attempt by the student with a DIAPER reference and a handmade attempt by a faculty member with no reference.

Coil	Inductance
1	75.1nH
2	71.4nH
3	71.6nH
4	69.8nH
5	69.6nH
Handmade (ref.)	71.8nH
Handmade (no ref.)	78.5nH

Leads were cut to 12.7 mm length in an effort to control for the inductance and further verify reproducibility, which was measured by plotting the capacitance vs. frequency given in Table 2.2. Only the first coil in the set had a measured inductance outside of one standard deviation, 2.2 nH, from the average inductance, 71.5 nH, of the five coils in the study suggesting that the inductance of the coils were reproducible within tolerances acceptable for use in tunable NMR probes.

A modified commercial 800 MHz MAS probe with a 3D-printed mock spinning assembly and removable coil platform was used to perform ball-shift assays[123]. The probe was tuned to 200 MHz and resonance frequency shifts were measured on a network analyzer to evaluate axial B_1 homogeneity for each coil. To establish a control based on the coil design, the expected axial

homogeneous length defined by the normalized B_1 field being at or above 90% was evaluated using Computer Simulations Technology (CST) and determined to be 5.7 mm. The theoretical and experimental results were plotted using Wolfram Mathematica version 11 and are shown in Figure 2.5.

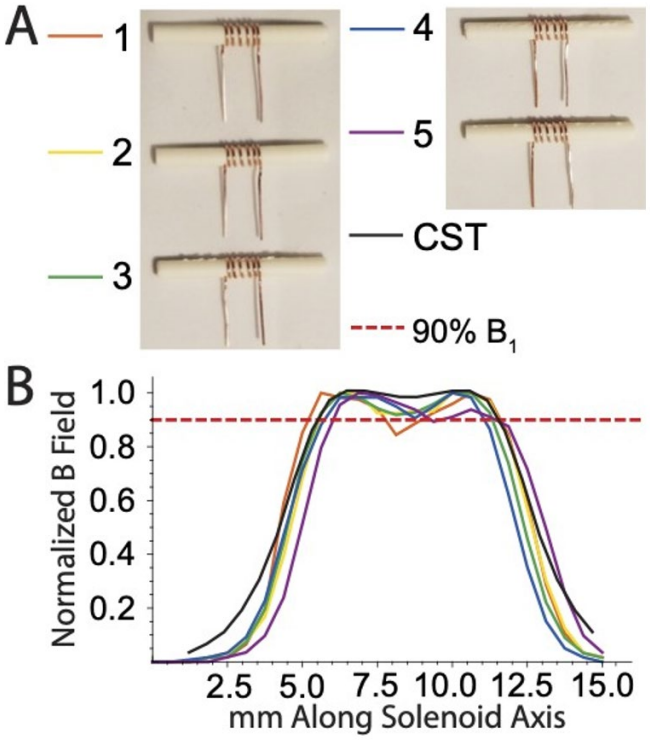

Figure 2.8: Results of individual student reproducibility study. A) Each of the five coils made using the original DIAPER template design and legend. B) Plot of the theoretical axial field profile and experimentally measured field profile for each coil.

The axial length between the first and last point where the normalized B_1 field exceeded 90% was used to evaluate and compare the homogeneous regions of the coils. Two of the five the coils, coil two and coil three, met the standard axial field homogeneity over the entire theoretically predicted length. Coil one met the overall axial length of the homogeneous region but dipped below the 90% threshold at two points. Coil four and five did not meet the expected axial length, instead falling short at 4.4 mm and 5.1 mm respectively. Although this shows that the use of the templates was only 40% reproducible, it should be noted that these replicates

were made relatively quickly, taking less time to wrap all of the coils than one by hand, and without modification to the original template design. This was also an improvement over the initial DIAPERs paper where the axial homogeneity achieved was 5.2 mm.

A comparison between the traditional handmade approach and use of a template completed the set of analyses performed. A faculty member with 20 years of experience hand-wrapped the wire around a drill bit with an extra turn and then meticulously pushed and pulled the ends to create variable pitch by eye. The moderately experienced student builder also performed the hand-wrapped method, using a DIAPER-wrapped coil as a reference rather than by eye alone. Each hand- wrapped coil took roughly 20 minutes to make, and the first attempt was tested for each user in order to ensure that comparable time was spent relative to coil production with the templates.

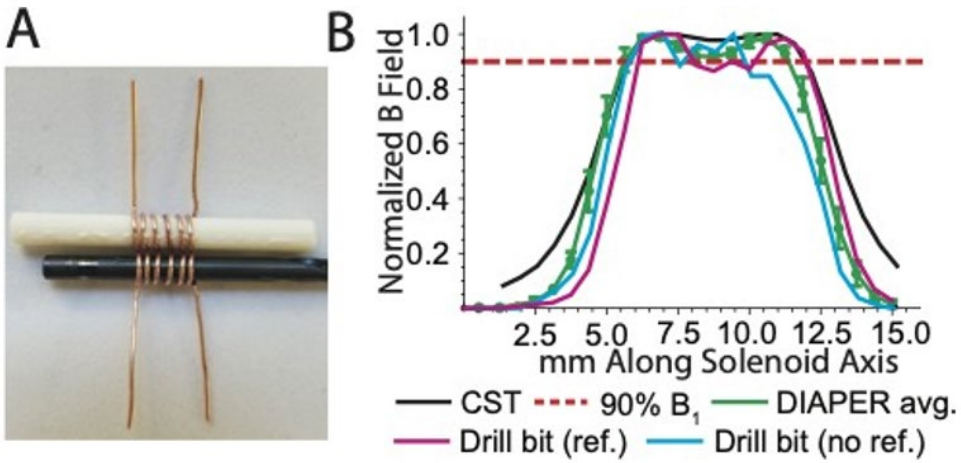

Figure 2.9: Comparison of axial homogeneity of handmade coils to those made with a template. A) Top is a coil wrapped on a DIAPER template; bottom is a handmade coil wrapped on a drill-bit and referenced to the top coil to assist achievement of the designed dimensions. B) Plot of the theoretical axial field profile, average of the single-wrapper DIAPER reproducibility test with standard deviation at each point, and experimentally measured field profiles for coils made by hand on a drill bit with and without a reference.

The average field profile of the coils from Figure 2.5 made by the moderately experienced student is shown plotted with the results measured of those made by hand shown in Figure 2.6. Based on the 90% threshold established for the original study, neither of the handmade attempts achieved homogeneity over the predicted axial length of 5.7 mm. As shown in Figure 10 the traditional method yielded less homogeneous coils than DIAPER-wrapped coils, represented as an average with standard deviation at each point, despite an expected advantage due to experience and attempt to improve on the by eye approximation using an appropriately dimensioned reference. If instead the threshold was set to the lowest measured B_1 in the homogenous region of the handmade coils, 84.8%, then the axial homogeneous regions of the handmade coil without a reference and the coil assisted by the template reference were 5.1 mm and 5.7 mm respectively. This suggests that use of the template, even if not used to wrap the coil itself, could still be beneficial to the fabrication process as a reference. Further extension of the lower threshold to previous analyses did significantly improve the success rate for coils made by a moderately experienced student using templates Figure 9B from 40% to 80% as all but one maintained over 86.5% at all points over the homogeneous region.

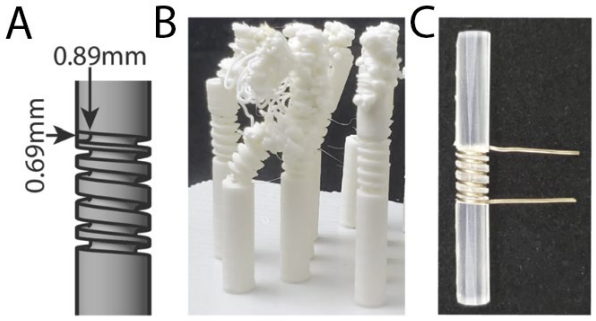

Figure 2.10: A) CAD drawing of a deeper groove DIAPER solenoid template. B) First attempts at printing the new template design with a Lulzbot Taz 6 fused-filament (FFM) printer in ABS, C) Successful print of the new template design using a Formlabs Form 3 stereolithography (SLA) printer in clear resin.

The initial effort to improve the design to support reproducibility was to increase the depth and width of the wire path groove, Figure 2.7A, in order to ensure that it was more obvious and

further prevent the wire from deviating off of the path by enabling it to fit securely within the groove. The first attempt to print this design in ABS led to a failure because the design became more “springy” such that the original print parameters programmed in the 3D printer slicer and gcode were not sufficient. In order to at least test the design in principle it was printed on a SLA printer in clear resin, Figure 2.7C, however this is not able to be dissolved as before which is discussed in more detail in the next section. Progress has been made in adjusting the print parameters to support printing the deeper DIAPER template, and it may also benefit from printing one at a time such that a reproducibility study could be performed and the technique could be truly made accessible to anyone.

Although improvements can be made to the original DIAPER design to make it even more reproducible across a broader user base, these results suggest that 3D-printed templates do offer a reliable method to attain intended performance in a transceiver coil and could better enable labs to share and achieve designs that are intricate or highly dependent on precise dimensions.

2.4.2 Other resonators

The RF transceiver is the heart of the NMR probe: the central connection to circuit components and the direct interface with the sample. Traditionally RF transceiver coils have been made by hand, necessitating a well-trained eye for symmetry and spacing between turns in addition to patient practice to achieve reproducibility. Implementation of this approach ranges from as simple as using a drill bit or other cylindrical device as a form to wrap solenoids, to purpose-built templates such as the brass jig for making a more complicated double-saddle coil[49], shown in Figure 2.8A and B, respectively. This approach has contributed to the perceived divide between “instrument builders” and other experimentalists due to the time investment needed to become

proficient at making even simple probe components, and has further instilled the idea that an extensive skill set is needed in order to participate in instrumentation development even at the level of small modifications to existing designs. This paradigm motivated the development of a method that utilizes 3D-printed templates called dissolvable inserts for achieving performance enhanced resonators (DIAPERs)[1], as shown in Figure 2.8C, to make the process more intuitive and innately controllable to achieve specific coil designs.

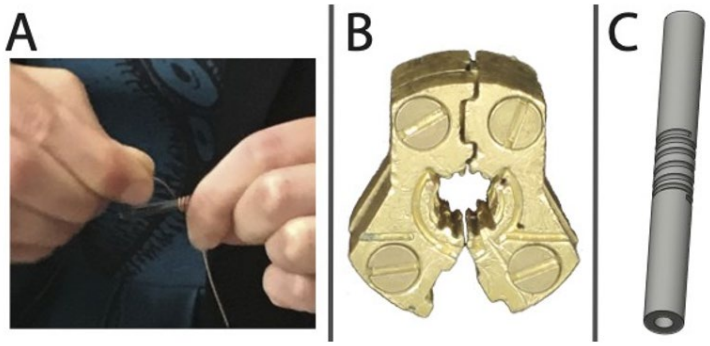

Figure 2.11: Traditional hand-made (A,B) and 3D-printing enabled (C) methods of fabricating transceiver coils are shown alongside transceivers for several applications in probes. A) Wire solenoid being wrapped on a drill bit. B) Brass template machined for wrapping a double-saddle coil. C) CAD drawing of a DIAPER template for winding a variable-pitch solenoid.

Solenoids were used as a proof-of-concept to demonstrate the utility of the 3D-printed template because in addition to being commonly used, they are relatively simple to make and easy to manipulate. Rather than free-forming the coil, the path is cut from a cylinder at a depth equal to half the wire diameter to create a guide. A common 3D print filament, acrylonitrile butadiene styrene (ABS), dissociates in acetone at room temperature within a few hours, allowing the coil to be recovered with minimal risk of deformation. We recently used dissolvable ABS templates to compare different variable-pitch solenoids to one with constant spacing. Variable-pitch solenoids demonstrate improved axial RF homogeneity of the B_1 field compared to constant-pitch because the tighter spacing between turns near the ends increases current density where it would normally drop off, thereby extending the viable sample volume in a rotor. A design used in the DIAPERs study, shown in Figure 2.9B was originally made by hand for use in a cross-coil

magic-angle spinning (MAS) probe. The 90% homogeneous region of the solenoid made by hand was reported to be 4.6 mm while the solenoid made using a DIAPER of the same design was measured to be 5.2 mm, amounting to roughly a 13% increase. We propose that other coils that have been published in the past, shown in Figure 2.9A, C and D could be made using 3D-printed templates and to a higher degree of accuracy compared to conventional means. These designs represent a range of experimental applications and outcomes. Figure 2.9A is a "tilted coil" that yields a larger magnitude B_1 field when positioned at magic angle compared to a standard solenoid. It also produces a non-zero B_1 field when aligned with B_0, enabling full range of variable-angle spinning experiments[162]. The conical coil in Figure 2.9C was used to generate B_1 field gradients to compensate for a given B_0 inhomogeneity[163]. Figure 2.9D is a double-saddle coil, a transverse resonator designed to be implemented in switched angle spinning (SAS) probes[49].

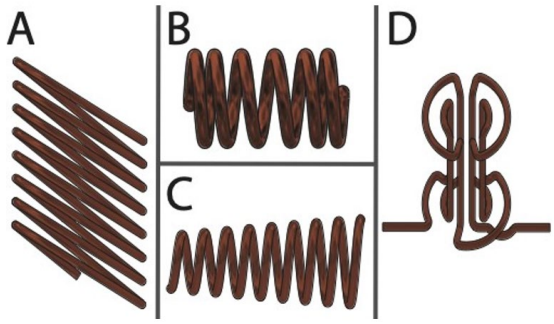

Figure 2.12: Examples of transceivers that could be fabricated using 3D-printed templates. A) Solenoid with turns tilted at 35° relative to the sample axis[162]. B) Variable-pitch solenoid used in a 3.2 mm MAS probe[48]. C) Conical coil with inner diameter starting at 5 mm and expanding by 5% at each of the eight turns[163]. D) Double-saddle coil used in a 3.2 mm SAS probe[49].

Without a standardized coil fabrication method, those who are readily able to explore new ways to control field profiles or push current limits on performance are restricted to a relatively small number of veteran builders and their students. Those experienced in instrumentation can also benefit from the ability to share designs quickly and reproducibly.

3D-printed templates also provide a more accessible method because they can reduce cost and time commitment. For example, the brass double-saddle coil template is designed to support annealing to minimize resistance introduced by work-hardening from sharp angled bends in the wire. This part took a highly experienced student machinist several days to make by hand, or alternatively having it produced by CNC machining would likely cost several hundred dollars. 3D printing could provide multiple alternatives using either extrusion or SLA printers and materials. First, an extrusion printer could be used with ABS in a similar fashion to the proof-of-concept method [20]. ABS is not a crosslinked polymer, which is the property that allows it to be extruded and dissociate relatively readily in some solvents. The glass transition temperature of ABS is 105 °C, well below 400 °C, the baseline annealing temperature of copper. This process of recrystallization to minimize internal stress is thermodynamically spontaneous, therefore annealing can be accomplished at lower temperatures by increasing the duration. Potential drawbacks are that current commercially available extrusion printers generally cannot achieve a feature size below 0.4 mm due to the size of extruder tips, calibration can be difficult and is necessary to achieve fine detail, and longer annealing is less efficient. In contrast, SLA printers are generally extremely easy to set up, have calibration parameters incorporated in printer software for compatible resins, and are able to achieve finer details because the limitation is derived from the laser spot size (currently commercially available at 0.09 mm). These printers require UV-curable resins, which result in polymers that are often highly cross-linked, making them much less soluble in common laboratory solvents.

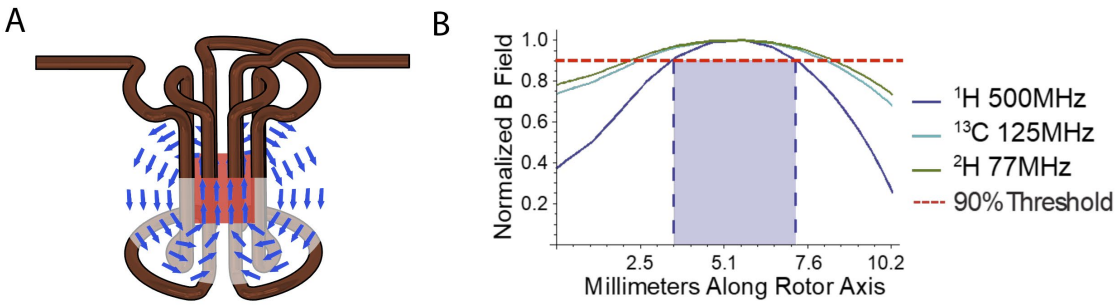

Figure 2.13: Double-saddle coil[49] A) CAD drawing with transverse magnetic field lines overlayed. B) CST modeling of overlap of magnetic field profiles at different tuning frequencies.

The double-saddle coil is a cylindrical, transverse resonator, made from sets of symmetric, axial u-shape turns shown in Figure 2.10A. This coil excels at generating B_1 fields at low frequencies, but is expected to maintain a good homogeneous region even when triply-tuned to the higher proton frequency, as shown in Figure 2.10B. The DIAPER method has been applied to a double-saddle coil template. This was originally attempted in a high temperature resin, with the motivation that it would able to withstand annealing in an inert environment to reduce resistance as a result of work hardening in the wire, in order to replace the currently used brass template to enable symmetric shaping of the coil. Many different solvents over a spectrum of several different physical properties (such as polarity and density) were used in attempts to remove the UV-cured resin (acetone, isopropyl alcohol, ethylenediaminetetraacetic acid, dichloromethane, dichloroethane, tetrahydrofuran, methyl ethyl ketone, dimethylformamide, hexane, toluene, acetonitrile, acetic acid, carbon tetrachloride, and chloroform). Dichloromethane (DCM) appeared to yield promising results, however it became apparent when used with the coil template that the material was warping / cracking rather than dissolving, which caused deformations of the coil. Formlabs resin compositions are proprietary, however we assumed that the Draft resin (which printed faster than other materials) would have the least amount of cross-linking and perhaps provide the best opportunity for success. However, none of the solvents, even piranha solution (a powerful mix of sulfuric acid and

hydrogen peroxide that can dissolve many things easily) was unable to dissolve the resin after being cured.

The Formlabs castable wax resin, which can be removed using a tube furnace or other controllable temperature oven remains a potential way forward, however it has not been fully demonstrated yet. The tube furnace available for testing had a manual temperature control which made it very difficult to achieve the temperature ramp procedure recommended to perform a controlled burn to remove the wax resin. Heating too quickly may have changed the shape of the wax and contributed to warping of the coils during the handful of attempts performed. This could potentially be overcome in the future by calibrating the furnace temperatures and automating the process with a controller.

This process offers potential promise because we hypothesize that the “burn” is actually a vaporization because it is advertised as “zero ash”. This means that the method could be performed under an inert atmosphere such as argon or nitrogen such that the surface of the coil is not oxidized which could increase resistance and negatively impact performance. We performed a “burn” under ambient atmosphere and nitrogen flow in a ventilated hood and were unable to perceive a difference in the outcome. However, if oxygen were to be used then a light acid treatment as a post-processing step should be capable of removing any surface oxidation. A potential benefit of the burn out process is that it will likely at least partially (if not fully) anneal the wire which should then reduce any resistance from work hardening.

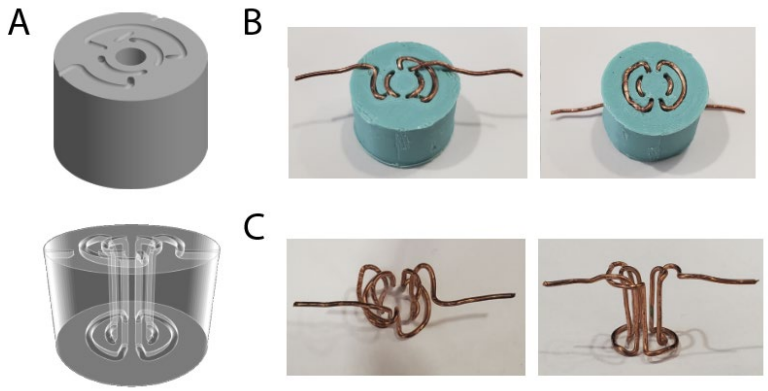

Figure 2.14: Proposed double-saddle coil DIAPER template. A) CAD drawing with internal coil path depicted. B) 22-gauge copper wire threaded into an ABS template (left – top, right – bottom). C) Recovered coil.

The current double-saddle coil DIAPER design is shown in Figure 2.11. This was printed in ABS using the Intamsys Funmat HT FFM printer. Print parameters are still being fine-tuned and currently requires a larger wire diameter path to be extruded when preparing the CAD file. To achieve this without completely redesigning the coil it also required angling the top entry and exit paths slightly so that the wire path would not self-intersect. While the result remains slightly rougher than desired and would not allow for annealing within the template, it is promising because the template only takes roughly 20 minutes to print, the cost is on the order of $0.30, and whether annealing makes an appreciable difference in the overall transceiver performance has not yet been tested.

Beyond the coil designs presented, we are also confident that 3D-printed forms can be applied to transceivers for DNP and small-tissue MRI probes. The utility of this approach is multi-faceted in that it offers the capability to optimize traditional designs as well as quickly test new ideas, it enhances the feasibility of repair even for users with limited instrumentation experience, and it broadens accessibility to more intricate geometries for general users.

2.5 Conclusions

Here we present a method for reproducibly making variable-pitch solenoids of particular dimensions using 3D-printed dissolvable inserts. This method enables accurate control of pitch, verified through observable differences in magnetic field profiles. This is advantageous because accurately constructed variable-pitch solenoids can demonstrate significant improvements to axial RF homogeneity as compared to constant-pitch designs. More broadly, 3D-printed coil templates may prove to be a viable alternative to traditional fabrication methods, offering a fast, inexpensive, reproducible, easily modifiable and scalable approach for design and construction of multiple turn coils. Future work will include testing single-use DIAPERs on the production of more complex resonators such as saddle coils or other transverse resonator designs. All relevant CAD files are provided in Appendix A.

Chapter 3

Generalized approach to optimizing solenoid transceiver designs

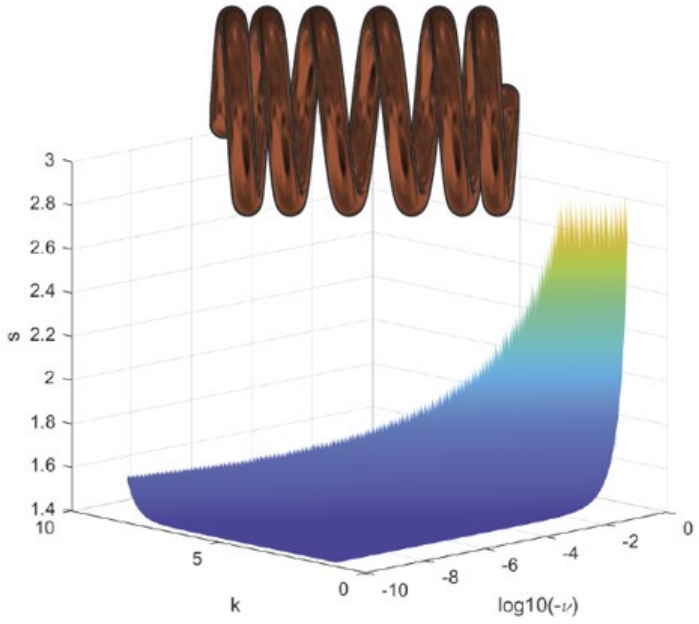

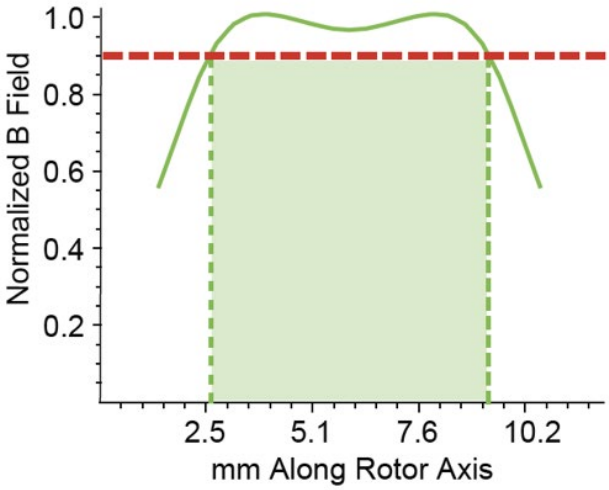

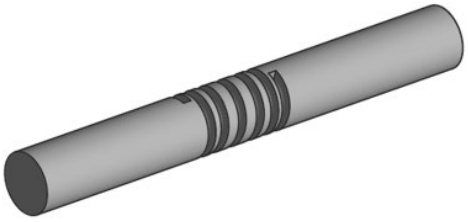

3.1 Introduction

RF homogeneity is important to NMR experiments, as the generated B_1 field is the direct interface with the sample. The dependence of ω_I and ω_S on B_1 makes it evident why RF inhomogeneity can significantly reduce magnetization transfer efficiency[149,164], thereby limiting enhancements to insensitive nuclei. However, negative effects of inhomogeneity are not limited to transfer experiments, but can also lead to reduced signal intensities during decoupling when fully packed rotors are used[165], as well as other experimental issues documented in several studies[166–168]. The impact of inhomogeneity on the signal-to-noise ratio (SNR), one of the biggest concerns in solid-state NMR, is made more significant as sample volumes are reduced to increase the MAS rate. Furthermore, lossy samples such as biological systems add other complications to the circuit design[4,87].

These concerns have been addressed through both coil design and experimental techniques. One of the simplest coil geometries, the constant-pitch solenoid, can meet the basic requirements of many solid-state NMR probes. The constant pitch solenoid, as the name implies, has a constant spacing between turns and can be wound on a cylindrical surface such as a mandrel or drill bit to meet the dimensional specifications of the probe. These coils have a low risk of electrical breakdown, and the magnitude of the maximum B_1 is largest amongst solenoids. The axial B_1 field tapers off significantly at the ends of the constant-pitch solenoid, creating an approximately parabolic magnetic field profile. The simplest way to control for RF inhomogeneity is to limit the sample to the homogeneous region of the coil using physical restrictions within the rotor. Similar effects can be achieved by shimming to create a B_0 field gradient[160] or constraining the effective sample region using tailored pulse sequences[169]. However, limiting the sample is less than ideal because it necessitates longer measurement time to achieve adequate signal and does not make use of all the available space inside the

coil. Spectroscopic techniques such as counteracting offset and phase transients[151] or CPMAS-based recoupling[151] can also be used to overcome RF inhomogeneity.

On the instrumentation side, several coil designs have been developed to address performance considerations such as field profiles, current distribution, RF conversion, and Q factor. The original Alderman-Grant coil was created as a decoupler to reduce conductive sample heating at high frequencies through lower E fields[170]. The scroll coil[171] represents an alternative effort to reduce dielectric heating by ensuring a high conversion ratio of RF power to magnetic versus electric fields. The hollow cylinder design of the loop gap resonator[172,173] generates larger current density at the ends, which compensates for decreased magnetic field strength thereby increasing the range of uniform distribution. The disadvantage of these designs is that at low frequencies[174] and for small samples[172] the Q factor is less favorable when compared to a solenoid.[175]

The constant pitch coil geometry can be described from a 3D parametric helix curve in cartesian coordinates, with the helix axis aligned to the z-axis of our coordinate system: $x(t) = r\cos(t)$, $y(t) = r\sin(t)$, $z(t) = \frac{s}{2\pi}t$. Where, r is the mean radius of the solenoid in millimeters, s is the turn-to-turn spacing, or pitch, of the solenoid in millimeters, and t is the swept angle parameter in radians defined on the interval $[-n\pi,\ n\pi]$. n is the positive integer number of turns in the solenoid. The swept angle parameter interval is chosen such that the geometric center of the coil lies at the origin of our coordinate system. While Ampere's law predicts that an infinitely long constant-pitch solenoid would have a desirable, uniform, square profile, this is not physically achievable. As an alternative approach, variable-pitch solenoid designs[1,48,152] decrease the spacing between turns at each end, thereby increasing the current density and extending the field profile to better resemble a square.

Although several probe systems have been designed with variable-pitch solenoids, very few have attempted to optimize this geometry. One of the first to be introduced used a modified Biot-Savart formula to vary the pitch within experimentally justifiable limits for an eight-turn coil, followed by integration to determine the magnetic field profile[152]. Another group determined the windings required to achieve a square field profile represented by an equiripple function at high frequencies[153]. A ribbon coil of varying width has also shown improvement to radial homogeneity for higher frequencies by minimizing gaps[154]. Optimization of solenoid RF homogeneity studies have been augmented by predictions through evaluation of performance using computational[155] and theory-driven simulation approaches[149,156,157,176].

Electromagnetic simulation software is expensive and not widely available, especially in disciplines outside of engineering, even at R1 universities. Traditional coil fabrication methods are similarly not readily accessible to those outside of instrumentation development. Templates have been machined out of Kel-F to provide structural integrity for a variable-pitch solenoid[152], and a brass tool was made to fabricate and anneal a two-turn saddle coil[49]. However, this requires expertise in machining and materials that are generally expensive or not common in the chemistry laboratory setting. Static sample holders with coil grooves have been 3D-printed[177]; however, there are potential concerns with this approach due to dielectric losses or background signal. Liquid metals have also been injected into 3D-printed coil forms[178], however due to liquid metals often being alloys which may introduce resistance or paramagnetic effects these may be not be suitable for high-frequency applications. High-frequency traps[127] have been 3D-printed in metal directly by third party companies such as Shapeways (New York, NY), however the current technology is not capable of achieving transceiver coil dimensions suitable for many high-frequency applications and other physical and electrical characteristics of the coil may be impacted depending on the metal 3D-printing process utilized. Finally, the most

accessible approach to coil fabrication is to make them by hand, however, as discussed in Chapter 2, the resulting magnetic field profile is incredibly sensitive to issues in symmetry or small changes in dimension such that it can be very challenging to accurately make more complex designs by hand.

Techniques for testing the coil homogeneity are similarly inaccessible due to being labor intensive, time consuming and challenging to perform well. The ball-shift assay[123] is an example of a conventional benchtop testing method that requires expensive equipment such as a vector network analyzer, several hand-machined parts, and has limited spatial resolution. Systematically adjusting a sample in a stator[123,167], or applying strong magnetic field gradient and acquiring a 2D nutation signal[159], are expensive in terms of utilizing magnet time that could otherwise be used for more substantive experiments. This approach is also limited in resolution.

Removable 3D-printed coil form templates and a recently developed open-source auto-ball shift assembly offer a means to overcome these barriers to both fabricate and test optimized solenoid designs. Therefore, in the spirit of making participation in instrumentation development more accessible, we present work toward creating an open-source and generalizable approach to realize and test optimized solenoid transceiver coil designs for use in solid-state NMR probes.

3.2 Materials and Methods

3.2.1 Generalized and open-source script

The script developed for this project was originally written in MATLAB in collaboration with a graduate student, Robert Marosi, in Professor Filippo Capolino's lab. The script was written to provide customizable constraints relevant to NMR probes, generate a parameter space of viable

coil designs based on exponential and gaussian modulations of pitch, display visualizations of the pitch vs. position and coil path, determine the magnetic field profile for a coil using its specific set of parameters through a Biot-Savart law calculation, and to identify optimized designs based on figures of merit; each of which will be described in more detail throughout this section. The script has since been translated into Python in order to make the method completely open-source and available and customizable for any interested user. Both scripts are provided in Appendix B.

3.2.2 Defining parameter spaces of viable designs based on user constraints

The exponential modulation was originally used to optimize a variable-pitch solenoid for a probe that allowed for a coil with an axial length of 7.6mm, inner radius of 5.2mm, eight turns and operating frequency of 270MHz[152]. This modulation was defined as follows: $z = \frac{s}{2\pi}(\varphi + v|\varphi|^k sign(\varphi))$ where z is the position along the solenoid axis, s is the maximum pitch of the coil, v is the scalar factor, and k is the exponential factor. Performance of the previously optimized design will be used as a threshold to determine if this method has merit.

The exponential modulation has three variables to parameterize. In order to test if a two-variable modulation may still yield desirable results and simply the process, we used a gaussian modulation defined by: $z = \frac{s}{2\pi}((\frac{\varphi}{2\pi})e^{\frac{-(\varphi^2)}{2c^2}}$ where z is the positions along the solenoid axis, s is the scaling factor (length) and c is the width of the gaussian.

We identified several constraints that can be manually adjusted by users of this method in order to enable optimization in the probe for which the transceiver is being designed. These user-defined constraints include: length, inner diameter, wire gauge, minimum pitch, and number of

turns. The length is limited by the axial length of the spinning assembly coil platform. The inner diameter needs to accommodate the rotor size and desired filling factor. Wire gauge is defined as the diameter of the wire being used to fabricate the solenoid. Defining minimum pitch is necessary to prevent corona discharge (arcing). The inductance of a solenoid is given by: $L = \frac{\mu_0 \times N^2 \times A}{l}$ where L is the inductance of the solenoid in henrys (H), μ_0 is the vacuum permeability, a constant ($4\pi \times 10^{-7}$H/m), N is the number of turns of wire in the solenoid, A is the cross-sectional area of the solenoid's coil (m^2), and l is the length of the solenoid's coil (m). Therefore, defining the number of turns after other physical characteristics have been defined serves as a proxy for controlling the inductance which will be important for tuning to the resonance frequencies of the specific nuclei for that probe. In the case of this study for a 3.2 mm, 800 MHz probehead, the user defined constraints were as follows: length – 8.51 mm, inner diameter 3.81 mm, wire gauge – 0.64 mm, minimum pitch – 0.76 mm, number of turns – 6 (shown in Figure 3.1A).

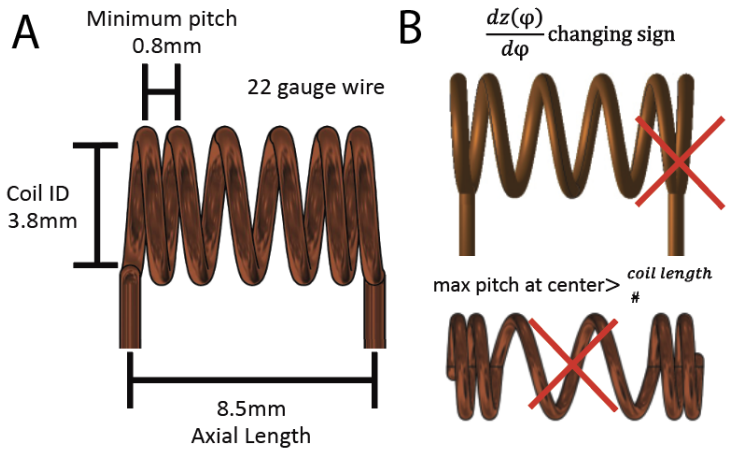

Figure 3.15: Graphic of constraints in this study. A) Constraints based on the probe used to demonstrate this approach B) Other practical constraints based on the scope of this work being focused on constant or variable-pitch solenoids.

Beyond these system-specific constraints, other practical constraints were included in order to focus the scope of this work on constant and variable-pitch solenoids that could be fabricated using a 3D-printed template[1]. Therefore, a constraint was added that prevents the differential

along the z axis from changing sign in order to exclude potential designs where the coil path turns back and those where the coil would self-intersect, which is not desirable for the probes being used. A constraint was also added to limit the center pitch from being greater than the coil length divided by half the number of turns. Although a larger gap may be preferred in some applications such as dynamic nuclear polarization (DNP), it has been previously shown to negatively affect B_1 homogeneity for standard NMR experiments[1] and may begin to resemble more of a split-solenoid design which would have different optimization criteria. These additional constraints are shown in Figure 3.1B. Using these modulations and constraints, sets of parameters yielding viable coil designs were plotted to create the parameter spaces for further analysis.

3.2.3 B_1 magnetic field modeling

Magnetic field profiles for different coil designs were calculated using both the Biot-Savart law and finite element analysis (FEA). The Biot-Savart law is a numerical integration technique that discretizes the parametric curve of the coil path and integrates the contributions from current in the wire to determine the magnetic field at a given point. It can be expressed as: $dB = \frac{\mu_0}{4\pi}\frac{I\, dl \times r}{r^3}$ where dB is the differential magnetic field vector at point P, I is the current flowing through the wire segment (dl), dl is the differential length vector of the wire segment, r is the displacement vector from the wire segment to point P, r is the distance between the wire segment and point P, μ_0 is the permeability of free space as previously defined. A MATLAB script was written to use the Biot-Savart law to calculate Bz vs z and Br vs z profiles for specified coil geometries of interest. Resulting field profiles were plotted and displayed as a figure in MATLAB and raw data was collected as .txt files.

High-frequency electromagnetic simulations using FEA were performed using Computer Simulation Technology Microwave Studio (CST MWS). Coils were imported using the IPT file format generated by Inventor. The coil material was set to the CST library value for pure copper. A discrete port was connected to one lead and defined to have 50 Ω resistance, consistent with the desired impedance of our NMR probe. A tuning capacitor was defined as a lumped element attached in parallel to the port and alternate lead. The capacitance value was determined using RLC circuit theory, $f = \frac{1}{\sqrt{LC}}$, in order to tune to 200 MHz. Boundary conditions were defined as open add space, and background was defined as normal. Based on an estimated maximum fillable length of 15.2 mm, a line was defined along the rotor axis and centered with respect to the coil length and diameter. After running each time-domain simulation, the 1D magnetic field profile at 200 MHz was evaluated along the axial curve. The default mesh was used to determine the step size. The results were exported as a.txt file, normalized, and plotted in Excel 2019.

3.2.4 Figures of merit for optimizations

Two figures of merit were developed for this study. The flatness, or uniformity, and the axial width of the Bz vs z profile in the defined homogenous region. Only B_1 values above the homogeneity threshold, set to 90% of the normalized B_1 values, were evaluated in the figures of merit in order to be comparative to previous work. To further select for optimized homogeneity, only profiles that did not exceed two threshold crossings were evaluated. In order to assess flatness, the standard deviation of the B_1 values above the threshold was calculated for each viable coil design. To assess axial width the difference in the z position (axial position) from the first threshold crossing to the last threshold crossing was calculated for each viable coil design. In this project, the coil design with optimized flatness was selected by identifying the Bz vs z profile with the minimum standard deviation over the homogeneous region. The coil design with

optimized axial length was selected by identifying the Bz vs z profile with the largest difference between threshold crossings. The coil designs meeting these criteria were selected for fabrication and experimental testing.

3.2.5 Coil fabrication with DIAPERs

Coils selected were fabricated using 3D-printed polymer forms (DIAPERs)[1]. The coil paths were designed using the parametric curve 3D sketch feature in Inventor Professional 2023 with the radius of the 22-gauge wire cut from a cylinder of diameter 4.1 mm. In preparation for 3D printing, the cylinder was made hollow to reduce waste and expedite the removal process by increasing surface area accessible to solvent. Files were exported in STL format, compatible with Cura 3D printing software which was required for printing on the Intamsys Fumat HT. CAD drawings and STL files are presented in Appendix A. All inserts were printed at 0.2 mm resolution using IC3D 3 mm acrylonitrile butadiene styrene (ABS) filament. DIAPERs were removed by soaking in approximately 20 mL of acetone in a 50 mL conical centrifuge tube stored upright overnight.

3.2.6 Benchtop testing with auto-ball shift (ABS) assembly

Fabricated coils were put into a modified commercial 800 MHz probe that was tuned to 200MHz on the carbon channel using a NanoVNA-H4 handheld vector network analyzer. The open-source auto-ball shift (ABS) assembly[179] was used to perform benchtop testing of the axial B_1 homogeneity. The ABS was attached to the probehead and the microcontroller was set to perform both full and 1/4 step runs. Using a 4-40 threaded rod this was roughly 22 and 88 steps respectively, along the coil axis to ensure the resolution was enough to capture subtle differences. In cases where the B field is much larger than the E field, the resonance frequency

shifts are directly proportional to the magnetic field amplitude at each point[34]. These values were automatically extracted and recorded. The data was normalized and field profiles were plotted in Excel 2019.

3.3 Results and discussion

3.3.1 Assumptions and limitations

Several assumptions are made within the Biot-Savart law which did not limit its utility for the systems described here, but may not be appropriate for every potential application. The thin wire approximation is a simplification often used in electromagnetism to model the behavior of a thin, infinitely long conductor or wire. This approximation is particularly useful when analyzing the magnetic fields generated by current-carrying wires and is often appropriate for solenoids. It assumes that the wire diameter is much smaller than the distance at which the magnetic field is being evaluated, that the current density is uniformly distributed across the cross-sectional area, and that the magnetic field generated has radial symmetry. These assumptions allow for straightforward analytical solutions that provide the axial magnetic field profile. In cases where these assumptions are not met, a more rigorous method such as finite element analysis may be necessary.

In the simulations performed in CST, the solenoid and tuning capacitor are treated as lumped elements, or idealized circuit components, in order to simplify the analysis. Underlying assumptions of lumped elements include: that the physical elements are small compared to the wavelength they handle, spatial properties such as capacitance and inductance are constant, they respond instantaneously to changes in voltage or current, connections are ideal, they do not propagate electromagnetic fields beyond the immediate vicinity of the element, magnetic

coupling between elements is ignored, and they are treated classically with no quantum effects. Negating these assumptions would likely necessitate modeling a more complete version of the circuit, which would add a tremendous amount of complexity and expense[176]. We posit that for the purposes of this study solenoids are not being redesigned to the extent that such an analysis would be practical, and making such a tool in an open-source format would be a tremendous undertaking.

Relatedly, another assumption is that the other circuit elements will not have a significant impact on the predicted magnetic field profiles, as they will remain constant and are accounted for through measures to control for inductance as described previously. Verifying that new coil designs do not negatively impact circuit performance through experimental testing will be described in follow-on sections and could be another way to validate that these assumptions are satisfactory. For many magnetic resonance systems these assumptions should be reasonable and appropriate.

Although this should not be prohibitive, it should be noted that 3D-printers may have different limits on resolution such that this could impact the ability to create any optimized design. This can be accounted for in the script however by adjusting the variable width_pt_stepsize in the script. The intended printer to be used to fabricate these coil templates is the Intamsys Funmat HT, which has a layer resolution of 50 microns, therefore the variable was set to be slightly larger than this threshold. There are also several third-party 3D-printing companies that may be able to perform the print for relatively low cost (on the order of tens of dollars) rather than a coil repair that could easily cost two orders of magnitude more if sent to the probe manufacturer.

3.3.2 Analysis of parameter spaces

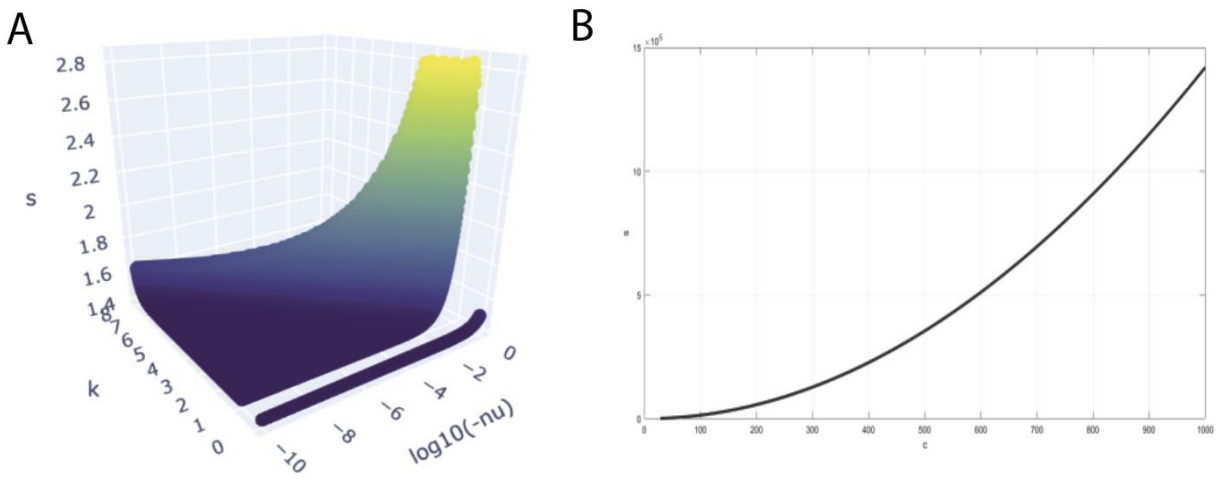

Figure 3.16: Parametric spaces based on defined constraints and A) exponential and B) gaussian modulations.

The exponential modulation yielded a 3D exponential sheet, while the gaussian modulation yielded a 2D curve as shown in Figure 3.2A,B, respectively. As expected, the gaussian modulation dramatically simplified the resulting parameter space. Although this is not an explicit constraint, the resolution of the parameter spaces can be adjusted through the variable npoints in the open-source script. In the exponential modulation parameter space depicted in Figure 3.2A, npoints was set to 500, yielding a total space of that value cubed, but only 89,000 points are plotted as valid based on the other constraints. Despite this, we continued focused most of the analysis on the exponential parameter space because this would allow for comparison to a previously published optimization[152].

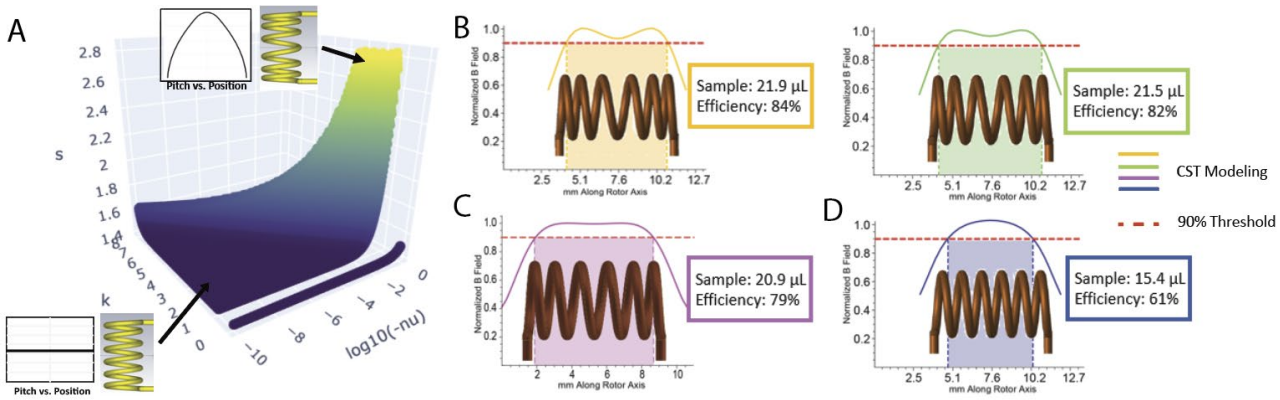

Figure 17.3: Breakdown of parameter space and simulated B fields from resulting coils. A) Top shows area with obvious variable-pitch; bottom shows area where changes are negligible. B) Results of coil parameters taken from the corresponding yellow and green areas of the parametric space which have the highest efficiency. C) Result from the lower left corner of the gaussian parametric curve which is notably flatter across the homogeneous region. D) Result showing that this method can also be used to optimize constant-pitch solenoids if desired.

Upon review of the pitch vs position plots at the extremes (s~1.4 and s~2.7) of the exponential parameter space it was found that higher values of for the maximum pitch resulted in an expected variable-pitch coil path, however lower values resulted in the modulation being so subtle that it is essentially a constant-pitch coil as shown in Figure 3.3A. This could be further constrained to select to optimize for either variable or constant pitch, however because there is merit to both designs in term of experimental outcomes and approaches, we have opted to provide both and leave that to the discretion of the user.

Selecting points from the yellow and green regions of the parametric space led to very similar predicted magnetic field profiles, shown in Figure 3.3B. The efficiency shown is defined for this evaluation as the percentage of the total axial length of the solenoid where the magnetic field is above the 90% homogeneity threshold. In each of these randomly selected samples the efficiency was quite high and by our estimations appears to at least meet if not slightly exceed the homogeneous region reported by Idziak[152] (~76%), demonstrating that this method is generalizable and useful.

The magnetic field profile shown in Figure 3.3C was the only coil design evaluated from the gaussian parametric space. While the efficiency was slightly lower than those evaluated from the exponential modulation space, it was notably more uniform (or flatter) across the entire homogeneous region. This result motivated one of the figures of merit for selecting an optimized design.

3.3.3 Evaluating open-source field modeling

Magnetic field profiles can be modeled in a handful of ways that vary in both computational and monetary expense. Computer Simulations Technology (CST) is a high-performance 3D electromagnetic (EM) analysis software that utilizes finite element analysis (FEA) in order to analyze and optimize components and systems. FEA involves discretizing a complex geometry into smaller elements and solving partial differential equations numerically to approximate the behavior of electromagnetic fields within the system, shown in Figure 3.4B. FEA is capable of handling arbitrary geometries, material properties, and boundary conditions, making it a versatile tool for simulating a wide range of electromagnetic phenomena. It provides a comprehensive view of the entire system and can capture intricate details, making it particularly useful for complex structures and situations where analytical solutions are challenging or not feasible.

Solving the Biot-Savart law along a coil path is an analytical approach specifically used to calculate the magnetic field generated by a current-carrying wire. The Biot-Savart law provides a direct mathematical expression for the magnetic field at a point due to a small segment of current. This method is particularly useful when dealing with simple geometries and configurations, such as a single wire or a loop, where analytical solutions are readily available.

However, it may become computationally intensive or impractical for more complex geometries and distributions of current, shown in Figure 3.3C.

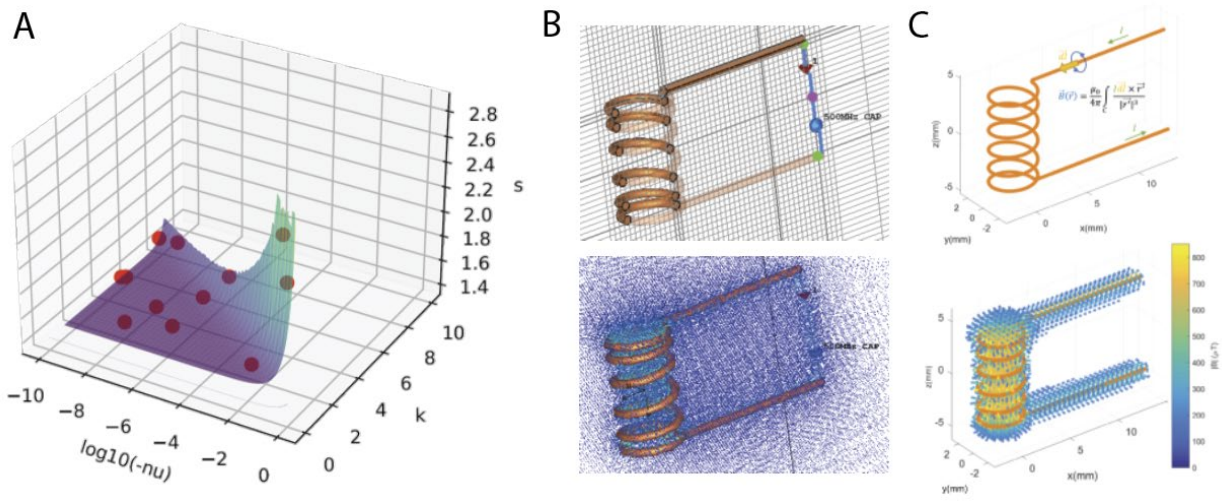

Figure 3.18: Latin hyper cube sampling of parameter space. Compare finite element analysis (CST) with Biot-Savart approximation results.

Although it may be ideal to utilize FEA because it reduces the number of assumptions and approximations, it would be unrealistic to use it to fully evaluate a minimum of several hundred coil designs as this would require several days of computational time independent of setup, which would likely be an order of magnitude more. However, in order to verify that the assumptions made by the Biot-Savart law calculations were valid, we elected to run a comparison of a subset of points. Latin hypercube sampling was used to select ten random and evenly distributed points in the parameter space, shown in Figure 3.4A. Coils based on these sets of s, k and nu values were made in Inventor Professional 2023 and exported as STP files for analysis in CST. The s, k, nu values were also manually entered into the script and Biot-Savart analysis was performed on them as well. The field axial magnetic field profiles from each were exported as text files for comparison. The maximum average difference between the value of the magnetic field profile simulated in CST compared to Biot-Savart analysis across all ten coils was 1.6%. The maximum delta found in any coil was 3.3%. Although these are statistically

significant, these values are not large enough to suggest that the previously discussed assumptions are not appropriate, and will still yield results that are likely to improve homogeneity to an extent that this approach is beneficial due to the large time savings. We also performed this analysis between the MATLAB script and the translated Python script to ensure consistency and that there were no unexpected differences. These results differed by less than one ten thousandth of a percent for all points evaluated indicating that they are essentially the same.

These results are significant because the Biot-Savart calculation is approximately 20 times faster than the corresponding CST simulation and does not require each coil to be rendered and imported as a 3D object which saves an inestimable amount of time. This makes it possible to evaluate field profiles for the entire parameter space possible on the timescale of hours to a day (on a personal laptop with a 2.6GHz CPU and six cores) versus what is estimated would take several weeks of continuous processing in CST. Further, while the optimization could theoretically be performed in CST alone, it was not straightforward to setup for geometries with more than two parameters or more than one figure of merit.

3.3.4 Choosing optimized designs for testing

Each valid set of values defined by the parameter space were evaluated using Biot-Savart. The magnetic field profiles were then analyzed based on the figures of merit in this study: minimum error and maximum width. The plots in Figure 3.5 show the results of these analyses.

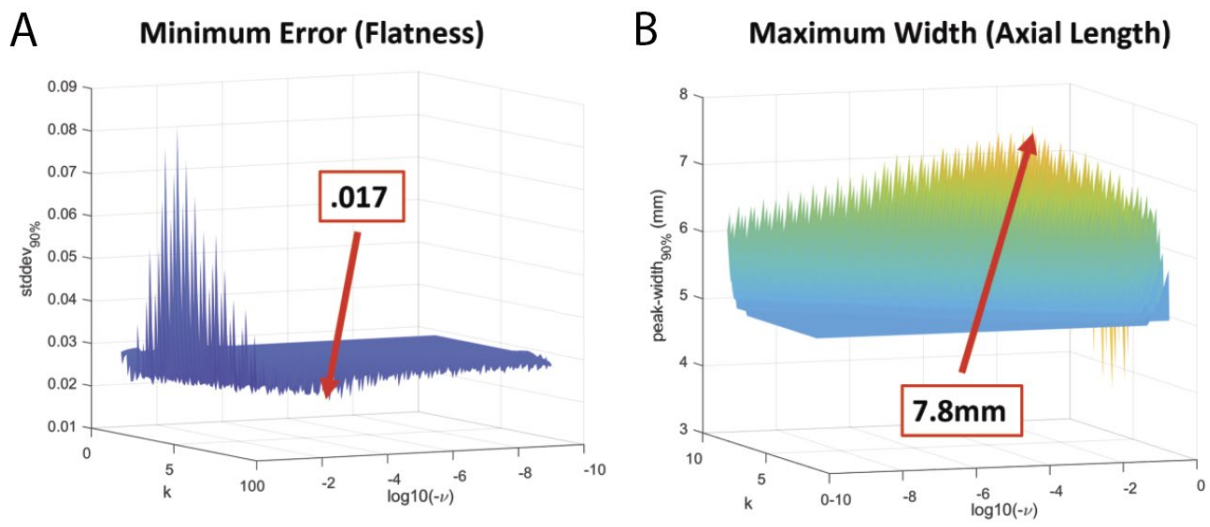

Figure 3.19: Plots of the calculated A) standard deviation (minimum error) and B) axial length (maximum width) over the homogeneous region of Bz vs. z profiles.

Simulated and experimental data presented in Figure 3.6 are for the “optimized” coil form from each plot in Figure 3.5. CST simulations were performed on these prior to the rigorous analysis of the Biot-Savart approximation. The simulated field profiles shown in blue match well with the shape of the field profiles experimentally observed using ABS in full and quarter-step modes. These were not more rigorously analyzed for agreement or the achieved optimized values because the figure of merit script required minor adjustment. During the course of this evaluation it was noted, and can be seen in Figure 3.6B that the field profile crosses the homogeneity threshold more than twice, indicating that it is not a valid parameter set. This was further verified by plotting the s, k, nu value of the point identified in Figure 3.5B and this point was not within the defined parameter space. It is expected that this discrepancy will be corrected in the near future along with the remaining work described in the next section.

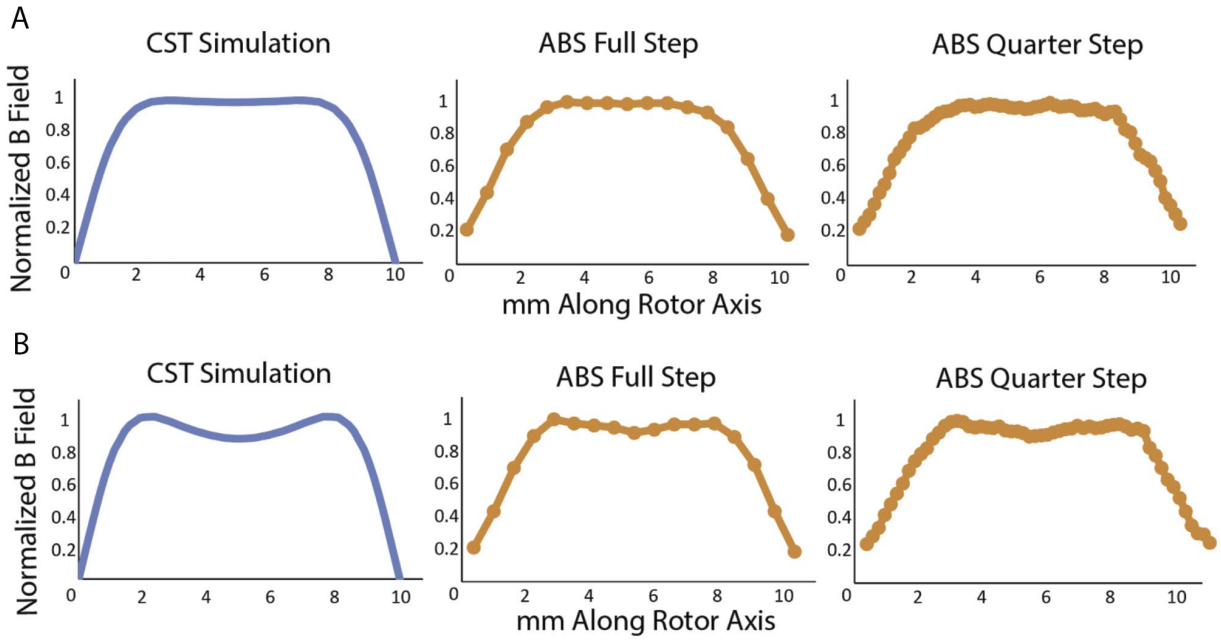

Figure 3.20: CST simulation (blue) vs auto-ball shift benchtop experimental data (orange) for variable-pitch coil forms optimized for A) flatness, B) axial length.

3.3.5 Remaining work / perspective

In the future, it would be useful to perform an NMR spin volume calculation[150] to determine if the larger magnitude of the B_1 field generated by the constant pitch solenoid may be preferrable to the variable-pitch solenoid. This will also provide a theoretical basis for observable changes in the SNR for experimental results. Benchtop testing will be performed to evaluate the probe circuit efficiency (Q factor). This is defined as: $Q = \frac{2\omega_0}{\Delta\omega}$ where Q is the quality factor, and ω_0 is the resonance frequency. Testing will be performed with the default coil in the commercial probe and optimized solenoid designs. The width of the frequency return loss at -3dB from the baseline will be measured using a Techtronix VNA for each coil and used to calculate Q. Parameter spaces will be generated using several different resolutions and used to perform all steps through the figure of merit analysis in order to determine if there is a point of diminishing return on the results of the optimized designs in each case. This can at least be used as a tool

to help an experimentalist decides if “true” optimization is required or efficiency is a better investment. Several basic NMR experiments will be performed with a constant and variable-pitch solenoid fabricated from this work. Nutation curves are a common measure of rf homogeneity and means of comparing probes by observing the intensity of the signal at 810° to that at 90°. Cross-polarization and decoupling experiments will be used to analyze any improvements to SNR[151] or artifacts[180] respectively.

3.4 Conclusions

We have demonstrated an open-source and generalizable method to optimize solenoid transceiver designs for magnetic resonance applications. This work will not only provide a tool for NMR enthusiasts to be able to keep pace with current experimental demands but findings from this project could be used to support future work by generating several high-performance resonators essential for initial populations in genetic algorithm machine learning toward intelligent development of novel coil designs. This method could expedite production of coils to meet the demands of other hardware advances such as recently developed spherical rotors[130] (to be discussed in Chapter 4) or rapidly expanding dynamic nuclear polarization (DNP)[181] applications. Radial homogeneity is also important to efficiency of ssNMR experiments, especially as faster spinning speeds lead to dispersion of the sample away from the centerline axis of the sample. This is extremely difficult to experimentally test independently, however this could also be parameterized to expand the impact of optimizations. This collaboration has the potential to contribute broadly to the field of magnetic resonance by focusing on experimentally driven objectives for transceiver performance which to this point have largely been limited by a lack of accessible, reliable fabrication methods and a generalizable approach to optimizations.

Chapter 4

Applications and future improvements

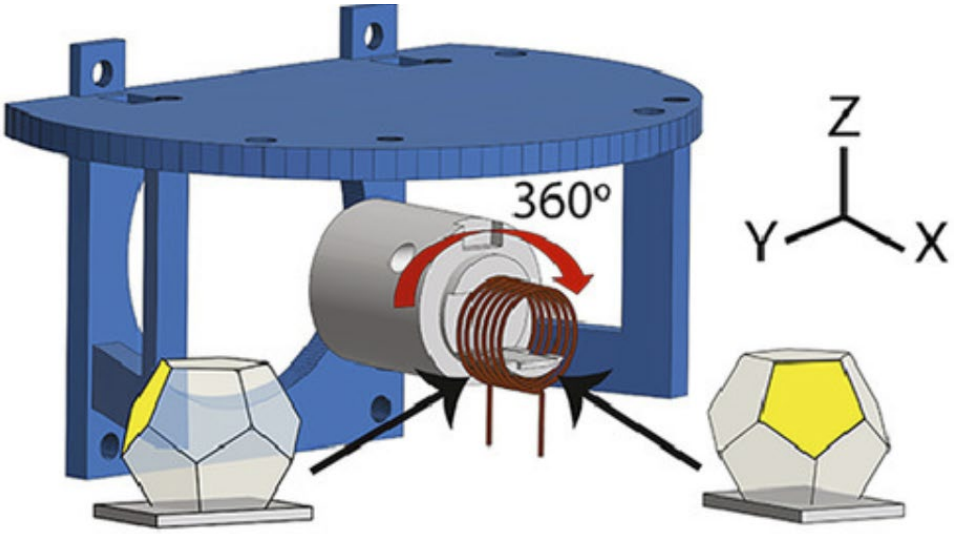

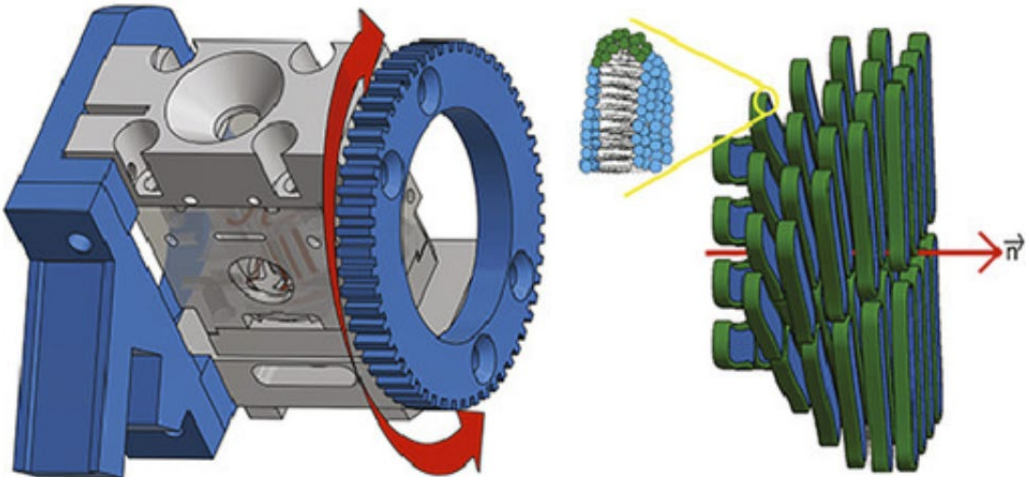

4.1 Quadruple-resonance cross-coil probe

4.1.1 Modeling of axial homogeneity with potential misalignments

Cross-coil probes are those that use two orthogonal coils, typically one axial and one transverse resonator, such that the corresponding B_1 fields are perpendicular to each other as well as the external B_0 field. As the names suggest, axial resonators produce a magnetic field parallel to the current symmetry axis and have good sensitivity. Transverse resonators generate magnetic fields that are perpendicular to the current lines, typically produce smaller electric fields at high power (low E), and have good homogeneity, especially when configured parallel to B_0[175]. Several designs have featured the transverse (or low E) resonator outside of the axial resonator[48,161,173,182] and another has the opposite configuration[156]. These can be useful in a variety of contexts, particularly for systems capable of direct detection on several resonance frequencies or when studying lossy materials that are susceptible to sample heating and degradation such as biomolecular assemblies[4].

As discussed more thoroughly in Chapters 2 and 3, RF homogeneity is important to NMR experiments, as the generated B_1 field is the direct interface with the sample. Negative effects of inhomogeneity can lead to reduced signal intensities during decoupling with fully packed rotors[9]. The simplest way to control for RF inhomogeneity is to limit the sample to the homogeneous region of the coil(s) using physical restrictions within the rotor. The overlapping homogeneous region of the two coils in the MAS probe was experimentally determined in previous work[48]. To predict and address possible changes to this overlap and evaluate the integrity of cross-coil homogeneity for potential application in a dynamic SAS probe, I modeled axial B field profiles on each of the two coils.

PTFE barriers were designed and fabricated the intent to prevent arcing (Section 4.3.2 Figure 4.15) but may also serve the function of making misalignments unlikely. Further, in a design where the coils are in close proximity to each other and the sample, even subtle misalignments may cause other issues such as inability to spin, which would necessitate correction prior to beginning an experiment anyway. However, it could be more prominent in systems where the coils are not positioned as closely together or where arc-prevention barriers are not utilized. All misalignments are referenced from the ideal starting position of the solenoid being centered in the modified-Alderman Grant. In each case the solenoid[48], is adjusted as this is most physically representative of what would happen in the actual probehead when preparing the sample for spinning. Misalignments evaluated were: vertical shift (up on z-axis by 0.006”), vertical skew (angled 3.3° toward z-axis), twist (rotated 5° along x-axis), horizontal skew (angled 5° toward y-axis) and lateral shift (forward on x-axis by 0.12”) as shown in Figure 4.1. These were prepared as CAD assemblies in Inventor Professional 2018 and exported as STEP files.

High-frequency electromagnetic simulations were performed using Computer Simulation Technology Microwave Studio (CST MWS). The coil material was set to the CST library value for pure copper; the capacitive bridge on the MAG was set to porcelain as a representative ceramic as relevant electrical properties of the chip capacitors were not available from the manufacturer. A discrete port was connected to one lead of each coil and defined to have 50Ω resistance, consistent with the desired impedance of the NMR probe. A tuning capacitor was defined as a lumped element attached in parallel to the discrete port on the alternate lead. The capacitance was determined using LC circuit theory, $f = \frac{1}{\sqrt{LC}}$, in order to tune to 800MHz for the MAG (~40nH, 0.99pF) and a representative low frequency of 200MHz on the solenoid (~72nH, 8.8pF). Each resonator was excited separately in the simulations. Based on the maximum fillable length of 15.2mm (0.6”) for a 3.2 mm rotor, a line was defined along the rotor axis. After

running each time-domain simulation, the 1D magnetic field profile was evaluated along the axial curve shown in Figure 4.1.

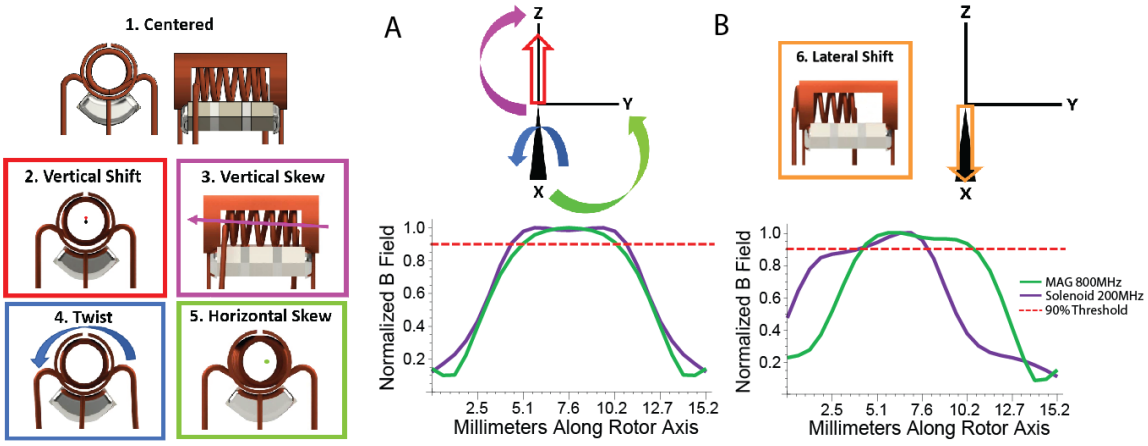

Figure 4.1: Shown is the ideal centered cross-coil alignment, 1, and several misalignments, 2-6, for the MAS probe[48]. A) CST modeled axial homogeneity for alignments 1-5, with no discernable change due to misalignment. B) CST modeled axial homogeneity for alignment 6 showing a reduction in overlap.

For most of the misalignments the axial field profiles did not change, shown in Figure 4.1A. An expected and obvious change was observed in both the axial field profiles of both the MAG and solenoid with the lateral shift shown in Figure 4.1B, however this is also the least likely misalignment to occur, particularly because the coils are secured in the X-Y plane by the coil platform.

4.1.2 Modeling of radial homogeneity with potential misalignments

Radial homogeneity is much more difficult to characterize and has only been rigorously evaluated through experiment and simulation in a handful of publications[149,183]. The biggest concern appears to be that the radial component of B_1 becomes time-dependent because the magnitude and phase of the rf is modulated with integer multiples of the magic-angle spinning frequencies. These have been found to only have minor effects on most standard NMR

experiments[183], but can negatively impact phase-encoded pulse sequences[149]. The most significant limitation in these studies is that they only evaluated a solenoid.

The same simulation setup was used as in the evaluation of the axial homogeneity, except that seven radial “slices” were added at spacings of 0.1” beginning and ending just outside of the MAG coil. The results of each data set were normalized in order to make them easily comparable to each other. As this was a preliminary evaluation, data were only taken from one time-point so findings may benefit from a more in-depth approach.

For consistency, the axial homogeneity is depicted in green for MAG and purple for solenoid just as in the axial simulation data. Results of the simulated radial B_1 field profiles for both coils are shown in Figures 4.2 and 4.3.

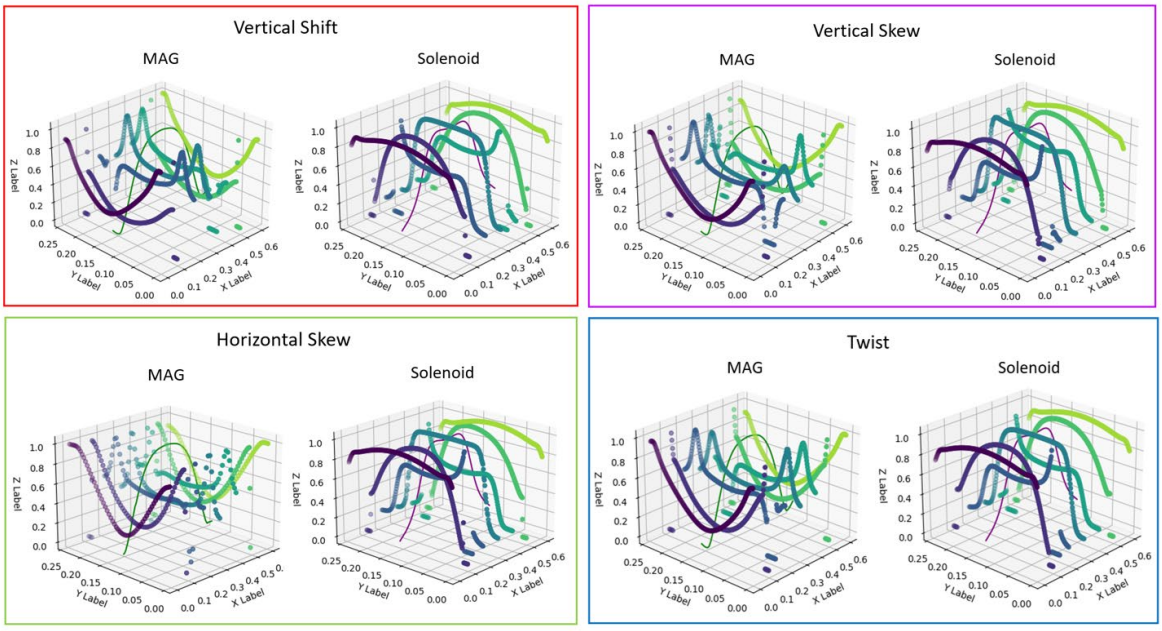

Figure 4.2: Plots of axial homogeneity for MAG (left / green) and variable-pitch solenoid (right / purple) overlayed on radial homogeneity data sets taken at values of X=0, 0.1, 0.2, 0.3, 0.4, 0.5, and 0.6” for several potential misalignments.

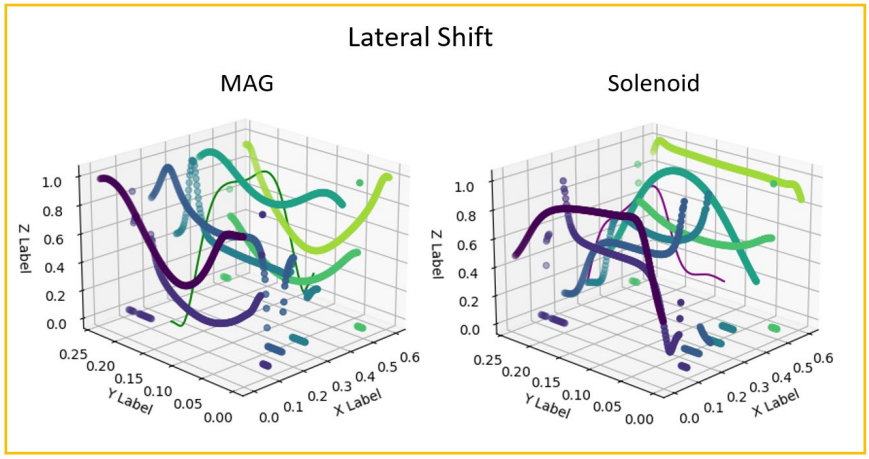

Figure 4.3: Plot of axial homogeneity for MAG (left / green) and variable-pitch solenoid (right / purple) overlayed on radial homogeneity data sets taken at values of X=0, 0.1, 0.2, 0.3, 0.4, 0.5, and 0.6" for the lateral shift misalignment.

The most obvious impact on the homogeneity in both coils is seen in the lateral shift (Figure 4.3), which is consistent with the axial homogeneity study. However, there are small but noticeable differences when visually comparing the other misalignments. Misalignments were designed to be as dramatic as possible without allowing the coils to physically touch, however there are several points in the radial distribution where the magnitude of the B_1 field unexpectedly drops to zero, which could potentially indicate areas prone to arcing. This is another avoidable and undesired effect of the misalignment that would impair performance. This could be more rigorously studied using this method in order to improve the design of cross-coil systems or barriers / inserts as discussed in section 4.3.2.

4.1.3 Redesign of cross-coil geometry

The current cross-coil design in the quadruple resonance probe[48] makes spinning consistently above 6kHz challenging due to the tight tolerances for satisfactory coil alignment around the 3.2mm rotor. This has been the biggest barrier preventing regular use of this probe to perform biomolecular NMR experiments. Although a redesign may impact the overall performance of the

probe, a proposed solution is to increase the inner diameter of both coils to better tolerate rotor instability especially early in the spin up process. Figure 4.4 shows a proposed redesign that should still fit within the current spinning assembly.

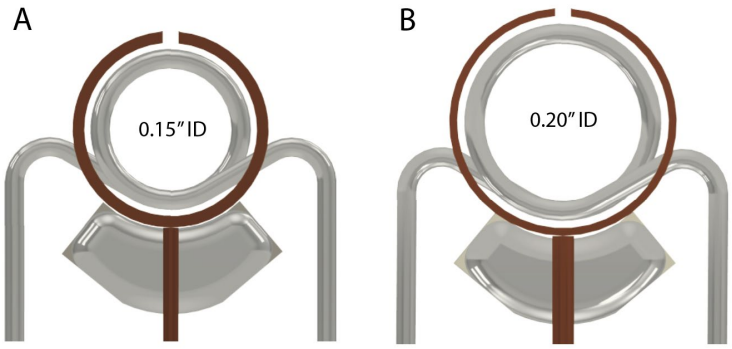

Figure 4.4: CAD drawings of the cross-coil system. A) Original, B) Proposed redesign with a larger inner diameter.

However, there are several things to consider prior to fabricated and implementing the proposed design. Overall sensitivity may decrease due to a less effective filling factor; however, this may also be able to be partially overcome by increasing the spacing between the MAG and solenoid which may permit higher transmitter power levels to be utilized without causing arcing between the coils. The homogeneity and inductance will likely also change, but these can be modeled in CST so that further adjustments can be made as necessary prior to fabrication. If the homogeneity worsens, the variable-pitch solenoid could be redesigned using the method described in Chapter 3. Modeling the inductance will help to ensure that the changes do not change it to the extent that other modifications to the channels of the probe circuit would be required in order to tune to the intended resonance frequencies. This is particularly useful for the MAG coil for which there is not a straightforward calculation to estimate the inductance. Once a satisfactory redesign is identified it can be fabricated and at least provide a modular option to support higher spinning speeds as required.

4.2 Magic-angle spinning spheres

Spinning spheres have been recently developed as an alternative to cylindrical rotors for magic-angle spinning[130]. The potential benefits of a sphere are ease of sample exchange, increasing the sample volume, a uniform sample geometry, more efficient microwave coupling in DNP applications, and improved spinning stability which may eventually enable faster spinning speeds[184]. In order to accommodate these sample rotors and DNP experiments, the Barnes lab has designed and utilized split solenoid and two-turn saddle coil resonators[185]. A split solenoid, also known as an "open-core solenoid," is typically used when it is not practical to thread a conductor or wire through the center of a closed solenoid coil. Saddle coils refer to a specific design that are characterized by their distinctive curved or U-shaped form shape resembling a saddle. They consist of two parallel conductive elements connected by curved segments at the ends, creating an opening in the center for the sample. Designing these coils to achieve optimal performance can be complex, and their effectiveness might be limited to specific applications and sample sizes. Simulations offer an effective way to probe and inform this design process. CAD files for these coils and rotors were provided by the Barnes lab to support simulations, summarized in Table 4.1, of the B_1 fields in order to inform future instrumentation design to support the use of spinning spheres.

Table 4.1: Summary of CST simulations evaluating the B_1 field homogeneity along the sample and relevant coil axis.

Rotor	System	Transceiver	Frequencies
9.5 mm sphere	MASS	Split solenoid	300 MHz, 75 MHz
9.5 mm sphere	MASS	Two-turn saddle coil	300 MHz, 75 MHz
4 mm sphere	MASS	Split solenoid	300 MHz, 75 MHz
4 mm sphere	MASS	Two-turn saddle coil	300 MHz, 75 MHz
3.2 mm cylinder	SAS	Two-turn saddle coil	300 MHz, 75 MHz

Parameters that remained consistent throughout all magic-angle spinning sphere (MASS) simulations are as follows. The rotor was static and the sample void was filled with glycerol ice. The spinning assembly was not included due to intersections with the provided coil files when aligned. Simulations were run using the time domain solver with open (add space) boundaries. All magnetic field results presented are the magnitude of the real component.

The first simulation was conducted on a split solenoid with wire diameter of 1.3 mm was designed for a 9.5 mm spherical rotor system. The provided inductance for the coil was 51 nH. The coil was tuned to a resonance frequency of 300 MHz and 75 MHz using a 5.5 pF and 88.3 pF lumped element capacitor respectively. The results at 300 MHz and 75 MHz are shown in Figure 4.5 and 4.6 respectively.

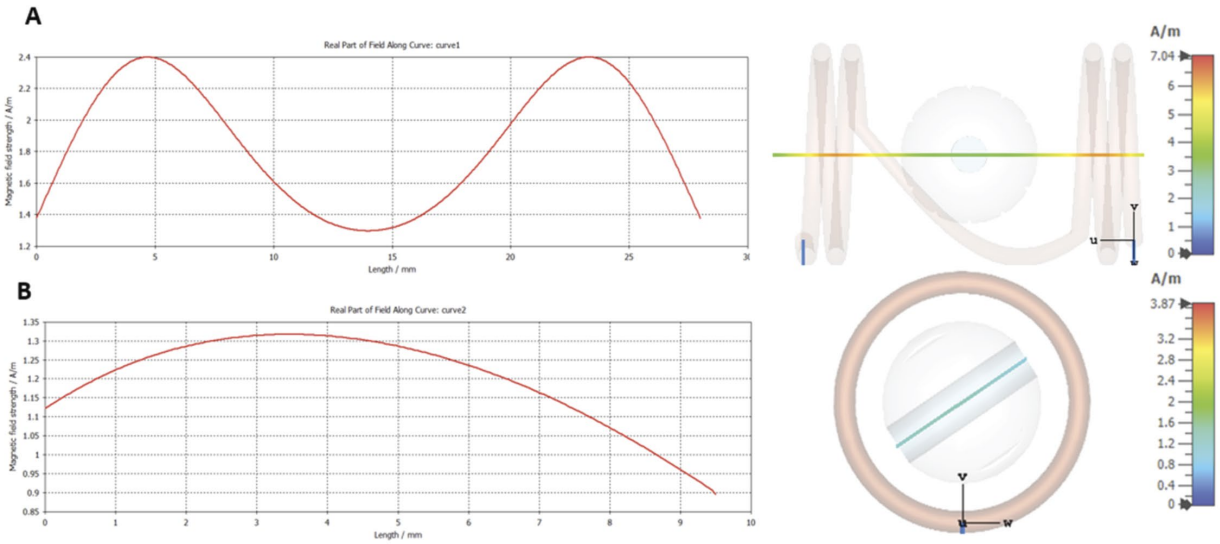

Figure 4.5: 9.5 mm split solenoid tuned to 300 MHz. A) Solenoid axis B) Sample axis.

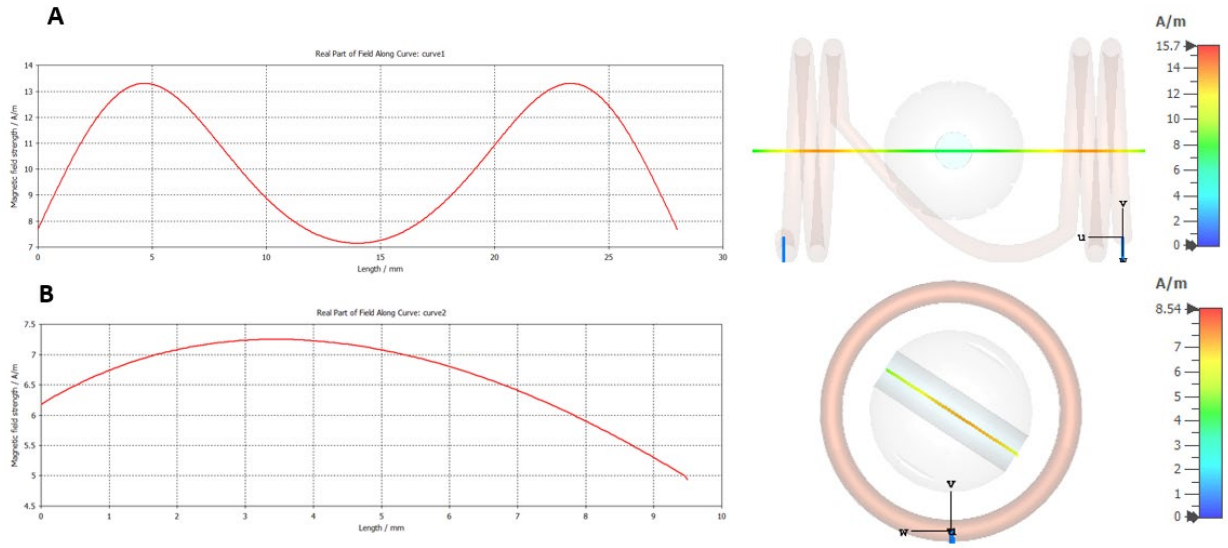

Figure 4.6: 9.5 mm split solenoid tuned to 75 MHz. A) Solenoid axis B) Sample axis.

The next simulation was conducted on a two-turn saddle coil with wire diameter of 1.3 mm designed for a 9.5 mm spherical rotor system. The provided inductance for the coil was 18 nH. The coil was tuned to a resonance frequency of 300 MHz and 75 MHz using a 15.6 pF and 250.2 pF lumped element capacitor respectively. The warning message “Some shapes of the CAD model overlap each other” was noted. A numerical simulation of such a model was still possible using the mesh type "FPBA" (Finite Integration Method with Perfect Boundary Approximation). The results at 300 MHz and 75 MHz are shown in Figure 4.7 and 4.8 respectively.

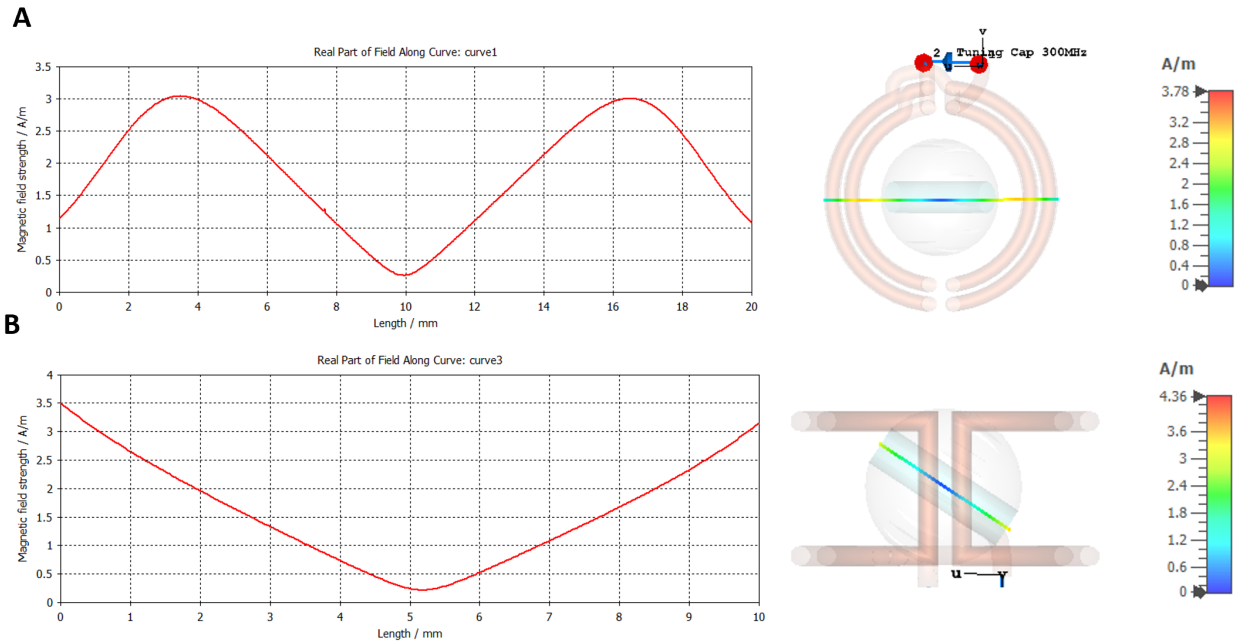

Figure 4.7 9.5 mm two-turn saddle coil tuned to 300 MHz. A) Solenoid axis B) Sample axis.

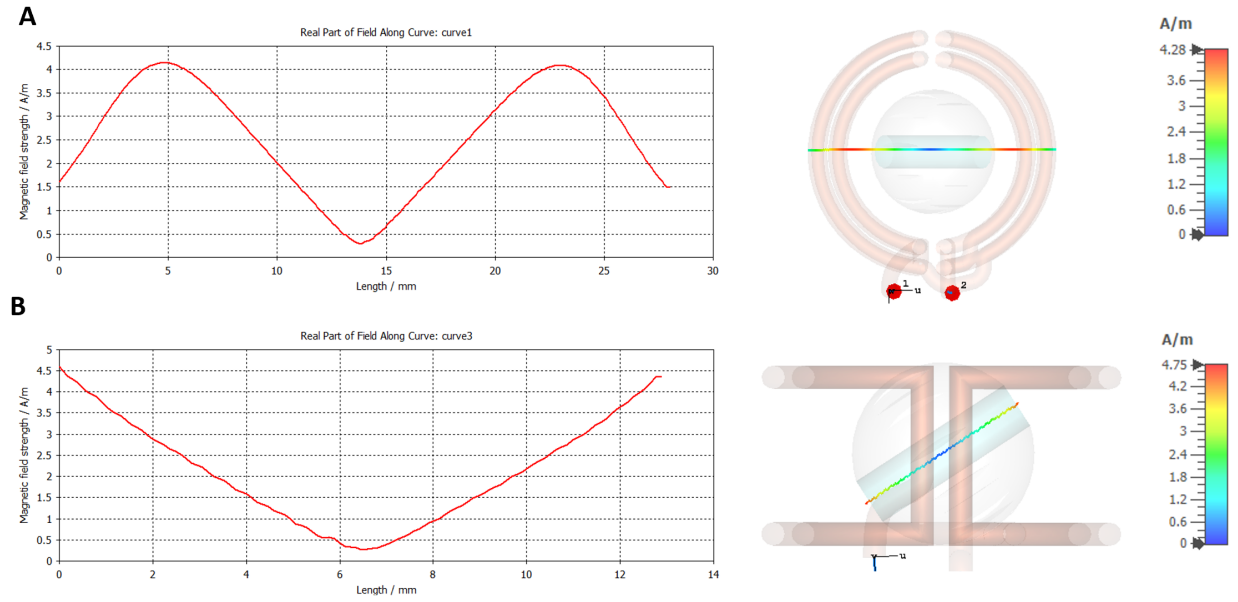

Figure 4.8: 9.5 mm two-turn saddle coil tuned to 75 MHz. A) Solenoid axis B) Sample axis.

The next simulation was conducted on a split solenoid with wire diameter designed for a 4 mm spherical rotor system. The provided inductance for the coil was 5 nH. The coil was tuned to a resonance frequency of 300 MHz and 75 MHz using a 56.3 pF and 900.6 pF lumped element

capacitor respectively. The results at 300 MHz and 75 MHz are shown in Figure 4.9 and 4.10 respectively.

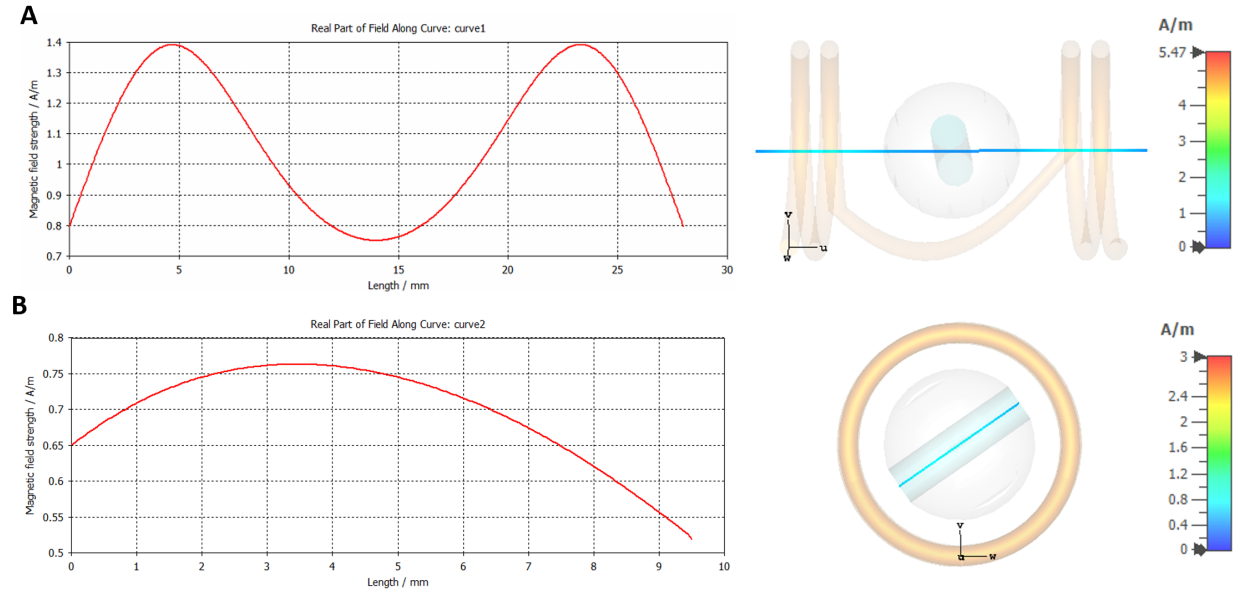

Figure 4.9: 4 mm split solenoid tuned to 300 MHz. A) Transverse axis. B) Sample Axis.

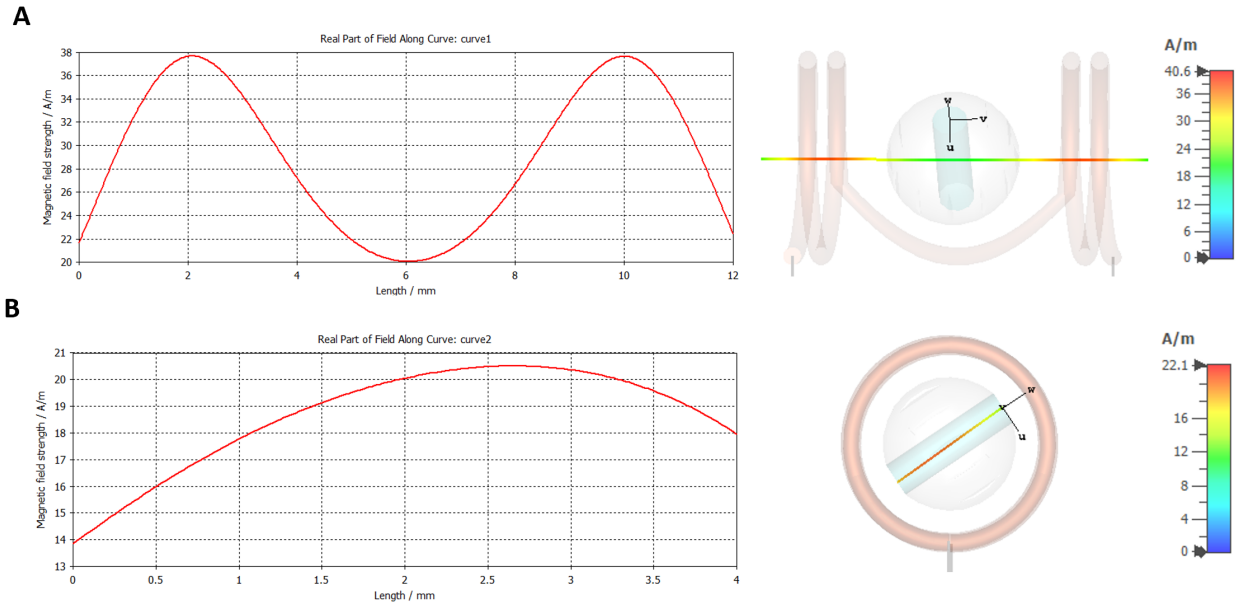

Figure 4.10: 4 mm split solenoid tuned to 75 MHz. A) Transverse axis. B) Sample Axis.

The next simulation was conducted on a split solenoid with wire diameter of 0.6 mm designed for a 4 mm spherical rotor system. The provided inductance for the coil was 2 nH. The coil was tuned to a resonance frequency of 300 MHz and 75 MHz using a 140.7 pF and 2502 pF lumped element capacitor respectively. The results at 300 MHz and 75 MHz are shown in Figure 4.11 and 4.12 respectively.

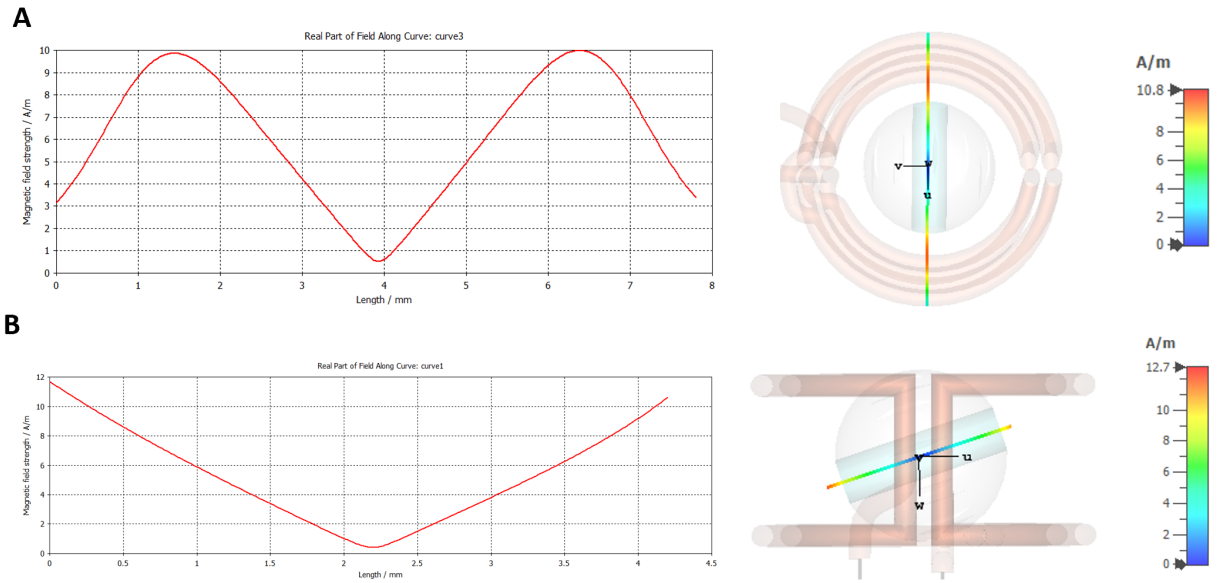

Figure 4.11: 4 mm two-turn saddle coil tuned to 300 MHz. A) Transverse axis. B) Sample Axis.

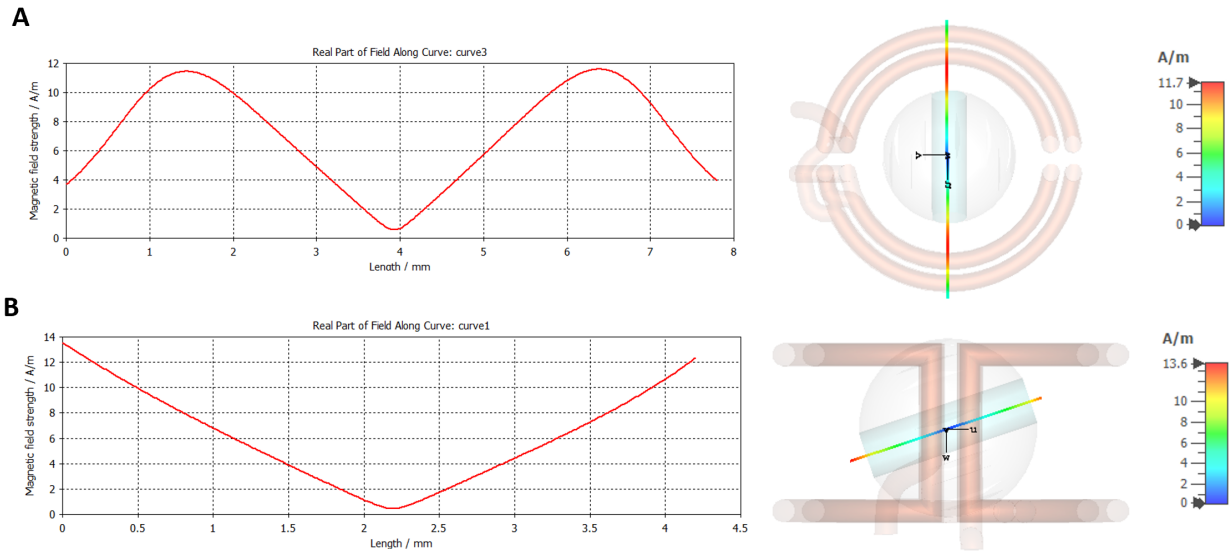

Figure 4.12: 4 mm two-turn saddle coil tuned to 300 MHz. A) Transverse axis. B) Sample Axis.

The next simulation was conducted on a two-turn saddle coil with wire diameter of 0.6mm designed for a 3.2 mm cylindrical rotor utilized in a switched-angle spinning (SAS) probe[49]. The inductance for the coil had been previously measured as 115 nH. The coil was tuned to a resonance frequency of 300 MHz and 75 MHz using a 2.4 pF and 39.2 pF lumped element capacitor respectively. The results at 300 MHz and 75 MHz are shown in Figure 4.13 and 4.14 respectively.

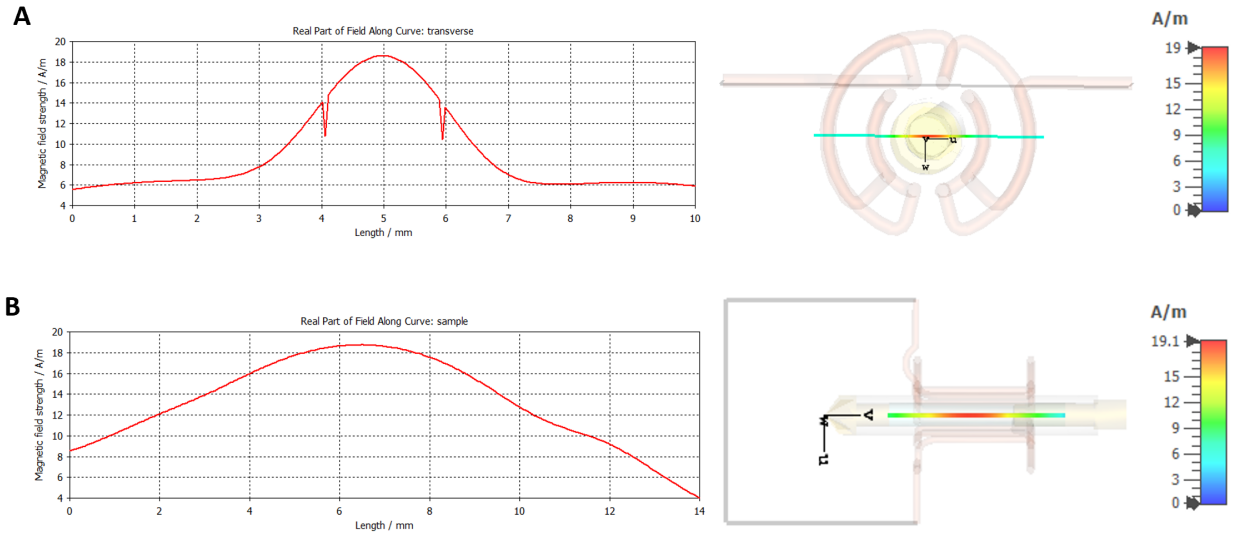

Figure 4.13: 3.2 mm two-turn saddle coil in SAS probe with cylindrical rotor tuned to 300 MHz. A) Transverse axis. B) Sample axis.

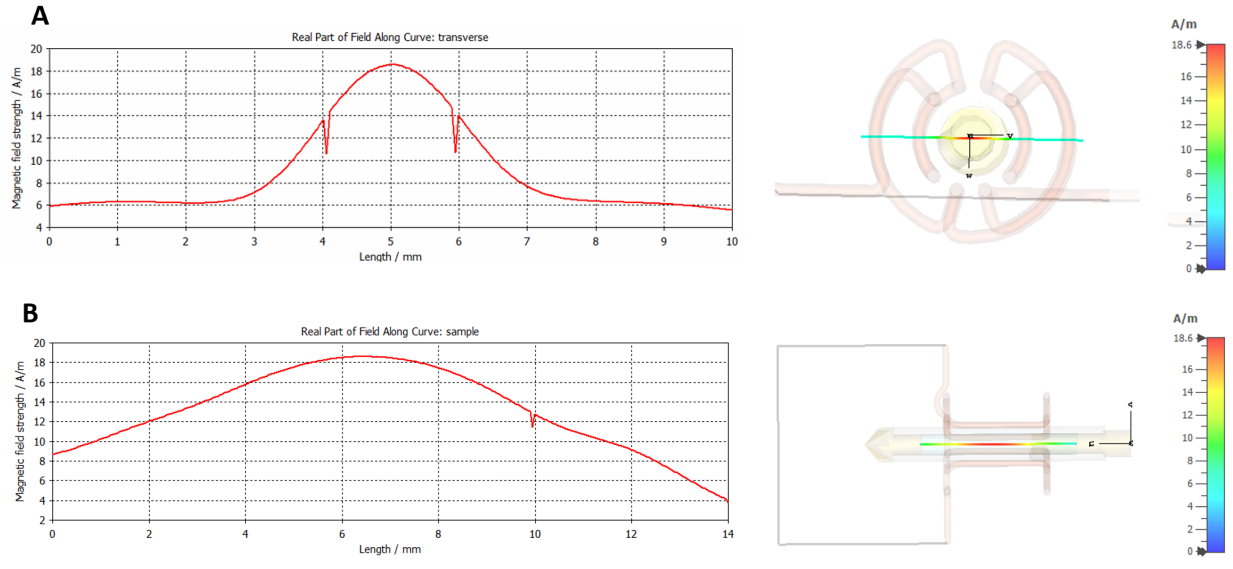

Figure 4.14: 3.2 mm two-turn saddle coil in SAS probe with cylindrical rotor tuned to 75 MHz. A) Transverse axis. B) Sample axis.

A broad observation regarding the results of all these simulations is that homogeneity appears to be more challenging when the sample and coil axis are not the same (as in the case of the MASS systems), possibly because the radial component may play a larger role. This asymmetric inhomogeneity across the sample volume was particularly pronounced in the MASS simulations with a split solenoid shown in Figures 4.5B, 4.6B, 4.9B, 4.10B. This is not generally a complication in conventional MAS or SAS systems, however those also less commonly use split solenoids, so a more thorough evaluation would be beneficial. Amongst the saddle coil simulations, the 3.2 mm MAS design had the strongest B_1 across the sample, with the magnitude peaking in the center. This is likely due to the second turn having a smaller diameter than the first. Unfortunately, a redesign of the MASS two-turn saddle may also require a redesign of the spinning assembly which currently is fully encompassed within the inner diameter of the coil.

4.3 Potential improvements from fluoropolymer additive manufacturing

4.3.1 Effect of coil platform loss tangent on efficiency

3D printing has recently been implemented in parts of the probehead that are in direct contact with the transceiver. Static sample holders with coil grooves were printed using the common 3D-print filaments polyethylene terephthalate glycol (PETG), high impact polystyrene (HIPS), polylactic acid (PLA) and polyamides (Nylon)[177]. Spinning assemblies have been 3D printed in zirconia (zirconium dioxide)[186] and acrylonitrile butadiene styrene (ABS)[187] with a minimum order of magnitude cost reduction. No deleterious background effects were observed in these studies, however the electrical properties of these materials could potentially affect the efficiency of the circuit through power losses in the material in contact with the resonator.

Polychlorotrifluoroethylene (PCTFE) is often used in spinning assemblies, including in the quadruple resonance probe[48], because it is the most easily machined fluoropolymer however it is not yet commercially available as a 3D print filament. Fluorinated ethylene propylene (FEP) has similar electronic physical properties as PCTFE but it is more difficult to machine. Fortunately, it is available as a 3D print filament from Plastic2Print (Amsterdam, Netherlands) however printing protocols have not been rigorously developed and presents unique challenges as a relatively soft material. Although there are several other fluorinated and conventional materials used for these probe parts, these will provide a reference for comparing losses in fluoropolymers and less insulating materials such as zirconia. A list of the relevant physical properties for these materials are provided in Table 4.2. Future studies might include polyoxymethylene, Delrin, or the polyimide-based resin, Vespel which have also been used in commercially manufactured spinning assemblies.

These properties were used to create new materials (PCTFE, FEP, and Zirconia) in CST to define the properties of the coil supports in the simulations. The solenoid leads were in direct contact with platform. The dissipation factor, often denoted as tan δ (tan delta), is a measure of the energy loss in a dielectric material when subjected to an alternating electric field. It is the ratio of the material's loss tangent to its dielectric constant. The dissipation factor is used to quantify the efficiency of energy conversion between electrical and thermal forms in insulating materials. The dielectric constant, also known as permittivity, is a property of a material that describes its ability to store electrical energy in an electric field. It is the ratio of the capacitance of a capacitor filled with the material to the capacitance of the same capacitor with a vacuum or air between its plates. The dielectric constant indicates how much the electric field within the material is influenced by an applied electric field. In the context of dielectric materials, ε (epsilon) often represents the dielectric constant or permittivity of the material. Electric conductivity is a

measure of how well a material can conduct an electric current. It is the reciprocal of resistivity (resistance to current flow). Materials with high conductivity allow electric charges to flow easily, while insulators have low conductivity. The dissipation factor, or loss tangent often denoted as tan δ (tan delta), is the ratio of the imaginary part of the complex permittivity (related to energy dissipation) to the real part of the complex permittivity (related to energy storage) of a material. It quantifies the amount of energy lost as heat when an alternating electric field is applied to a dielectric material.

Table 4.2: Relevant electronic material properties. Average values were taken from matweb.com Dissipative factors were evaluated at 0.001 MHz and estimated for zirconia which depends on temperature and crystal structure.

Material	**Dielectric Constant (ε)**	**Dissipation Factor (tan δ)**	**Electrical conductivity (S/m)**	**Density (kg/m^3)**
PCTFE	2.5	0.0002	1.4e-15	2100
FEP	2.1	0.0003	1.0e-18	2150
Zirconia	25	0.001	0.0005	5500
ABS	3.0	0.022	1.4e-16	1050

Despite the challenges with 3D printing fluoropolymers, PCTFE has been used to make sample cups for DNP applications[131], and FEP has been used to print rotor inserts to maintain sample humidity[187], however it is likely more development would be necessary for both in order to print to the tolerances typically required in a stator for stable spinning. If the results of this study yield significantly less power loss or a higher Q factor for solenoids in contact with the PCTFE or FEP platforms than the other more lossy materials, then it may further motivate the development of 3D printing with fluoropolymers to make high performance parts less expensive and more accessible.

4.3.2 Coil stabilizers

3D printing technology is rapidly becoming a realistic route to using materials in ways that are simply not supported by traditional machining techniques. Notably, 3M (Maplewood, MN) has

introduced small-scale 3D printed PTFE parts to consumers. Compared to protonated polymers, using PTFE for parts in close proximity to the sample significantly reduces proton background. It also has a smaller loss tangent than similar, more easily machined fluoropolymers such as PCTFE, resulting in higher efficiency. Power applied through the coil is used to measure the magnetic effectiveness[176], which can be easily compromised by arcing, so it is best practice to minimize the potential for electrical discharge in probe circuit elements. Although cross-coil designs can be used to optimize performance in aspects such as isolation and sensitivity, coils are often also in close proximity to each other in order to maximize filling factor of each, which can introduce susceptibility to corona discharge. A common preventative measure is adding a PTFE barrier that minimizes the volume of ionizable air between the coils and provides insulation due to a higher dielectric constant[87]. In our cross-coil probe, we initially used small pieces of PTFE sheet as the barrier between the outer modified Alderman-Grant resonator and inner solenoid[48] as shown in Figure 4.15. However, these were difficult to arrange and offered little benefit in terms of maintaining symmetry and coil position. To improve upon this, we designed inserts to fit as shown in Figure 6. An initial attempt was made to machine the inserts, however due to the cylindrical wall being extremely thin at 0.3 mm the part was barely salvageable. To test feasibility of 3D printing the parts instead, prototypes were made using a Formlabs Form 2 with the Tough V4 resin. Upon successful prototyping, 3D-printed PTFE parts were produced by 3M. These inserts met design specifications and were then implemented into the probe.

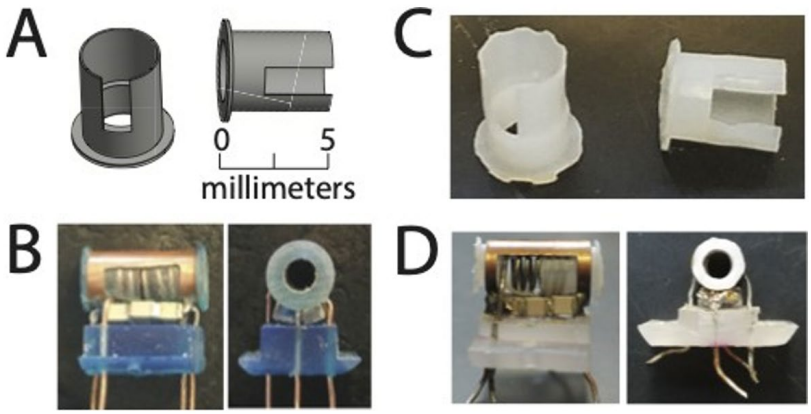

Figure 4.15: Inserts for application in a cross-coil MAS probe. A) CAD drawing of inserts to go in between a modified Alderman-Grant and variable-pitch solenoid in a cross-coil probe. B) 3D-printed pieces in a mock-up of the coil assembly to test dimensions and design ap- plication. C) 3D-printed PTFE inserts made in collaboration with 3M. D) Implementation of the 3D-printed PTFE inserts in the cross-coil MAS probe.

This methodology can also be used for coil forms that provide more structural integrity to the coil rather than just a physical barrier. One such coil support was machined out of boron nitride to support maintaining a constantly varying pitch that was impossible to make by hand[152]. In another case, a Macor form was machined to maintain the structural integrity of a double-saddle coil while it was undergoing angle changes in a switched-angle probe[49]. To further test the utility of the 3M PTFE 3D printing technology, we submitted the part shown in Figure 4.16 for manufacture. This design had previously been implemented into a SAS probe built in our lab for use with the double-saddle coil, but the dimensions made it very difficult to machine in a fluoropolymer, even by a relatively advanced graduate student machinist. Macor was chosen as the alternative, but a proton background was observed during probe testing, which was suspected to come from hydration water in the ceramic. Discussions with 3M led to a few alterations to the PTFE design, such as expanding the wire slots from the coil diameter of 0.65 mm to 0.71 mm and adding slots down the sides that had no structural significance other than to balance the print, preventing the warping experienced during initial print trials. The smallest dimension in the part is the wall that supports the top and bottom of the coil, which is 0.07 mm thick. This was successfully printed by 3M

as verified by measurements by calipers upon receipt. Implementation of this part into future generations of SAS probes should significantly reduce proton background and limit dielectric losses.

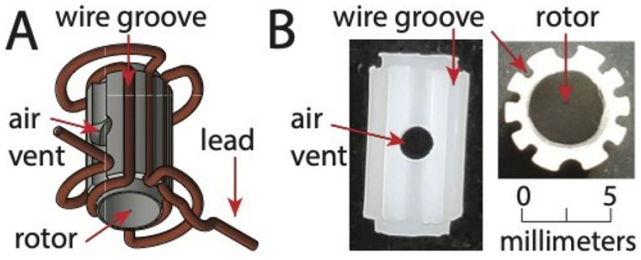

Figure 4.16: Support for double-saddle coil. A) CAD drawing showing design implementation. B) 3D-printed PTFE support made in collaboration with 3M.

4.4 Conclusions

Advances in instrumentation such as MASS are undeniably enabled by the use of additive manufacturing which will be crucial to future innovations to support new experimental capabilities. As 3D printing technology and methods improve, probe components may no longer be limited to designs that account for limitations based on available tools or machinability of materials. Particularly, development of fluoropolymer 3D printing has the potential to improve probe circuit performance and efficiency. Open-source and accessible benchtop methods such as Auto-Ball Shift described in Chapter 3 will make rigorous evaluation of radial homogeneity possible and potentially enable new optimization pathways. If homogeneity is experimentally determined to be an issue the coil alignment inserts can be designed and used to effectively prevent it. Inhomogeneity potentially caused by the coil designs currently utilized in the MASS systems will likely benefit from continued development of 3D-printed coil templates to support optimized designs of more complicated transceivers, which may also extend their utility to other systems where their use may be limited due to current challenges in fabrication. All relevant CAD files are provided in Appendix A.

Chapter 5

Implementation of Specifications Grading into an Upper-Division Chemical Biology Lecture Course

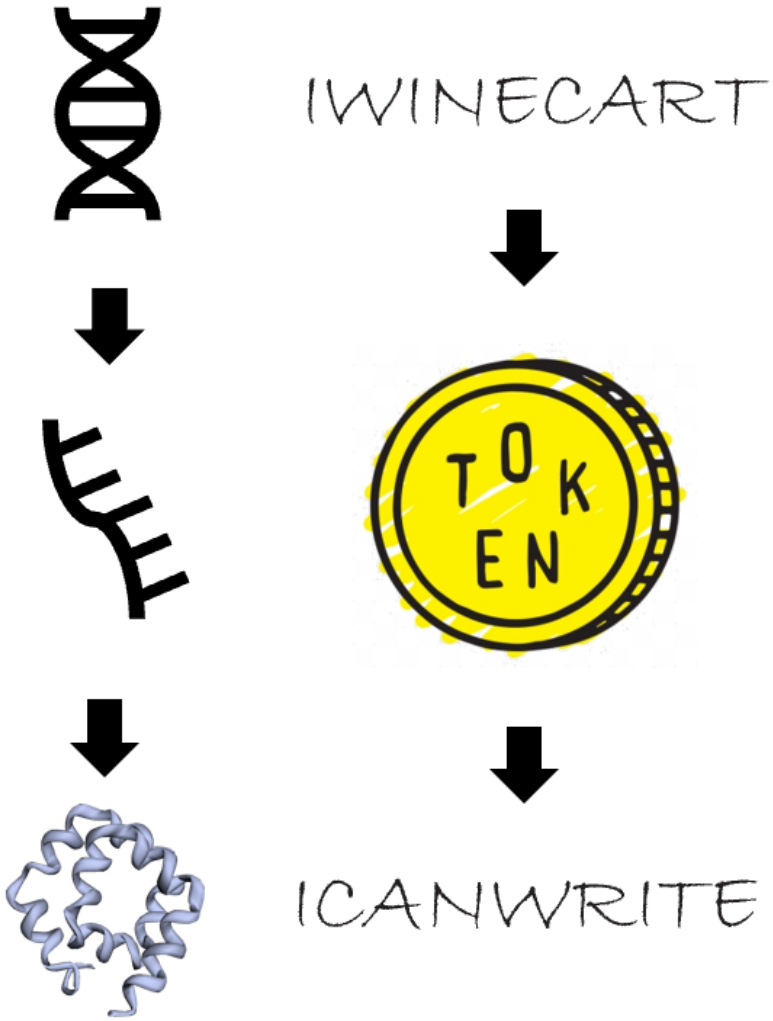

5.1 Introduction

Introduction to Chemical Biology is an upper-division course taken by third- and fourth-year undergraduates in the chemistry major at the University of California, Irvine (UCI). It is required for both the chemistry major and to meet the biochemistry requirement for the American Chemical Society (ACS) degree certification[188]. Although the student demographic primarily comprises chemistry majors, the course is also open to students from the School of Biological Sciences as an elective; typical enrollment is around 100-120 students. The course covers the fundamentals of Chemical Biology, specifically the application of chemical techniques and mechanisms to explain biological phenomena at the scale of atoms and bonds. Topics include structures and reactivity, chemical mechanisms of enzyme catalysis, chemistry of signaling, biosynthesis, and metabolic pathways. The lectures provide background information and context required to connect fundamental principles from chemistry with key concepts governing living organisms. In practice, most of the material covered relates to the Central Dogma of Molecular Biology[189], following the flow of information from DNA to RNA to protein. The logic and interpretation of experiments are heavily emphasized in this course; “How do we know?” is at least as important as “What happens?”.

Chemical biology has emerged as a recognized subdiscipline within the last several decades and bridges the gap between the molecular detail of chemistry and complex systems of biology. Despite being integral to several areas of transformative research, core competencies such as those outlined for other subdisciplines by the American Chemical Society Committee on Professional Training (ACS CPT) guidelines or seminal texts on undergraduate biology education[190] have not similarly been established for chemical biology[191]. This may be in part because the subject matter is evolving at a very rapid pace[192], making it challenging to develop

an integrated curriculum suitable for multiple majors that is appreciable by students and achievable by instructors[193]. For example, the textbook[194] utilized for this course is less than a decade old at present (a short timescale for many STEM subjects), however since the textbook was published in 2013 the genome editing method CRISPR-Cas9[195,196] was developed and subsequently awarded a Nobel Prize, single-molecule benchtop nucleic acid sequencing[197,198] has become commercially available at a price point allowing mass use and mRNA vaccines[199] have been developed for commercial use. This flood of new information is potentially made even more problematic by the "tyranny of the textbook"[200], as these are often the default learning tool for undergraduate education.

Undergraduate education in such an interdisciplinary subject would benefit greatly from activities or assignments that require students to apply their knowledge to real-world research and mimic responsibilities in future careers. One such activity for upper-division students is the use of case studies that develop critical skills necessary to read literature, justify methods, analyze data, critique findings, and propose hypotheses[191]. Assignments based on peer-reviewed literature need to be well planned so as not to be too complicated or time consuming and are therefore often underutilized in the classroom despite being essential to future education and careers. Not only does addressing this issue this have the potential to ameliorate employer dissatisfaction with recently graduated science major communication skills[201] but it also serves as a means to keep the course material up to date with relevant advances in the field.

The goal of Chem 128 in its most recent iterations (2019-2022) was therefore focused on providing students with a working foundation in chemical biology concepts, techniques, and applications, particularly filtered through the lens of reading the current literature. Central to this objective is the ability to effectively interpret, analyze, and critique scientific papers in writing.

Students are assigned approximately one paper per week from relevant journals, and submit two mini-review assignments during the academic term in which they critique a paper and discuss relevant background literature. The course was taught from 2019-2021 using a traditional points-based assessment system in which the two writing assignments accounted for a total of 20% of the students' final grade. Many students had no prior experience with scientific writing or reading current literature, generating stress for the students and frustration for the instructor. The majority of review papers submitted by students did not meet the expected standards and left the instructor with the unsatisfying choice to either grade the assignment accordingly, which would lower students' grades and be unintentionally discouraging, or give artificially high grades even though the standards were not met. Neither option felt appropriate for the most comprehensive assessments of the course objectives or supportive of student learning. This disconnect motivated the implementation of a simultaneously more rigorous and flexible grading policy.

Specifications grading is a student-centered assessment method focused on demonstration of learning objectives[202]. It has been successfully used in general chemistry lecture[203,204], organic chemistry lecture[205–207], organic chemistry laboratory[208], biochemistry laboratory[209], cell biology lecture[210] and various other STEM courses[211]. Inspired by these efforts, we developed a version of this system for the winter 2022 offering of Chem 128 at UCI. Here we present, to the best of our knowledge, the first implementation of specifications grading in an upper-division chemical biology lecture. Further, we provide a reflective analysis of potential benefits and areas for improvement to future implementations based on student and instructor perceptions and offer considerations for future education research.

5.2 Scientific and pedagogical background

Proficiency in quantitative analysis is often strongly prioritized in STEM education. However, numerical assessments can be satisfactorily completed without a rigorous conceptual understanding of the material, whereas vague or out of context responses to open-ended questions or essays highlight knowledge deficits[212]. Further, memorization of equations or stand-alone facts does not support the broader goals of science education, which are enabling graduates to apply their fundamental knowledge to make predictions, explain observable outcomes of an experiment, and assess new situations. To the greatest extent possible, information learned should be demonstrated through assessments that mimic real-world use in order to extend the utility of students' knowledge and skills beyond the classroom to independent scholarship[213].

Analytical writing has been demonstrated to enhance conceptual learning, especially when used in tandem with other assignments, to engage the students with material across the cognitive spectrum[214]. Due to the nuanced understanding needed to achieve effective written communication in STEM and its importance to most career paths after graduation, students would likely benefit from pedagogical efforts to incorporate more frequent development of this critical skill[215]. Consistent practice and feedback is most advantageous[209], however written assignments tend to be among the most time-consuming types of assessments to complete and to grade, resulting in less favor amongst both students and instructors. For students, the reasons scientific writing poses a challenge are numerous and multi-faceted. Writing experience gained through other courses such as humanities does not necessarily transfer well due to the distinct organization, specialized terminology, and different audience of lab reports and critiques of peer-reviewed work[216]. More generally, students also tend to have difficulty connecting

seemingly disparate knowledge[217], which is then further complicated by simultaneously processing and incorporating new course-specific knowledge, as this is among the highest-level cognitive skills[218].

Simply incorporating more written assessments alone may still not yield the desired results without improved instruction. In order for students to learn content or writing, practice will ideally include elements such as: providing a rationale for the design of an investigation, making sense of data, crafting an argument, and refining a text in light of a critique[218]. Success in these abstract and high-order cognitive tasks is made more challenging by students' complicated relationship with feedback[219–221]. On one hand, students are eager to receive feedback and it is an essential tool for learning. Effective feedback is specific, understandable, and helpful for completing a future task such that a student is willing and able to use it[222]. On the other hand, feedback can also be unintentionally problematic if it is not presented well. Poor-quality feedback is not useful due to being too authoritative, generic, confusing, or if it is unclear how to implement it in future assignments[223]. Although the aforementioned may seem obvious, there are subtleties to successful execution. After receiving a grade, a student may have little motivation to actively engage with the feedback if assignments are viewed as modular[224] or stand-alone products, even if a similar task is assigned later in the course. This lack of incentive is further reinforced if the grade for the assignment has already been determined because students can no longer directly benefit from revision efforts[225]. This contradiction of intent on both sides can be mitigated if the student and instructor use the feedback to create a dialogue such that students are able to incorporate it into their own process of learning[222]. It has been shown that when provided with the opportunity to perform iterative, reflective refinement, student views on feedback improve due to increased literacy and appreciation for the rationale[226]. Proactive recipience, or active engagement in the feedback process[220] is one of the most important factors that increase overall performance[219].

Developing a more flexible and interactive mode of assigning grades also has compelling implications for student learning and inclusion. Traditional grading provides a static picture that is often misconstrued as aptitude, therefore minimizing the opportunity for feedback that could be beneficial to development of creative problem solving. This generally tends to increased anxiety and lower interest in learning, especially among students from minority demographics[227]. Norm-referenced grading was developed because it was believed to be less subjective[228] and is often accepted as a meaningful way to communicate between institutions[229]. However, these "standard" curves can be deceiving because they may represent a comparison of student work relative to each other[230] rather than actually conveying meaningful information about individual student understanding or retention of knowledge[231]. In fact, it has been shown that competitive environments in which students feel the need to outperform peers leads to less retention[232]. Academic performance may become motivated based on extrinsic validation more than intrinsic curiosity, which can impact self-esteem[233] and how students perceive the educational experience in relation to themselves[234]. This does a disservice to students as individuals by denying them effective opportunities to learn through reflection[235,236] as they work toward the ultimate goal of becoming self-regulated learners[237], as well as to the broader scientific community if we are complicit in accepting the loss of talented underrepresented students[238,239], for what at best amounts to tradition given the problems and misconceptions that have been identified. This is particularly important in the wake of the COVID-19 pandemic which disproportionally negatively affected students from minoritized groups[240]. The impact of the pandemic on student well-being will be unique to each individual in terms of its scope and duration[241], however it can potentially be mitigated by efforts in the classroom to improve self-efficacy, a component of well-being that has been correlated to performance. Negative trends in interpersonal communication, problem solving and grades have been reported in a recent study

about the return to in-person teaching at institutes of higher education, with a proposed solution being to modify course content and delivery[242].

Specifications grading has the potential to provide several notable benefits for both instructors and students[202]. A specifications grading system was utilized in a “Writing for Chemists” course developed at UCI with the goal of providing students frequent opportunities to engage with feedback and submit revisions[215]. This assessment method differs from the traditional points-based grading system in that students are required to demonstrate achievement of learning objectives at a satisfactory level or no credit is earned. To offset the higher stakes of removing partial credit, a key feature of this method is that instructors must provide very clear, detailed specifications for what is considered satisfactory. For instructors this can result in less time spent grading, and for students this shifts the focus from negotiating partial credit to improving understanding of course concepts in order to adequately demonstrate a learning objective[243]. Also, one of the core tenets of specifications grading is the use of tokens to return a sense of ownership over the learning experience to the students. Tokens provide opportunities for flexibility in submission deadlines and the opportunity to incorporate instructor feedback in the resubmission of revised course assessments while also maintaining a sustainable workload for instructors. To earn higher course grades students must demonstrate a mastery of more advanced or complex skills and content applied to more assignments. Requiring revisions instead of awarding partial credit, motivates students to actively understand why their previous work did not meet learning objectives which supports learning[235,236]. Students will not necessarily achieve all the possible learning outcomes, but their course grade will indicate which outcomes they have and have not achieved. Overall, this method enables instructors to adequately uphold high standards while shifting agency for the overall grade to the student[244–247] by enabling them to revisit challenging concepts or skills in a productive way.

The major goals of the specifications grading redesign of Chem 128 was to promote improvement of the writing assignment submissions such that students could adequately demonstrate application of knowledge to new situations and engagement in scientific argumentation[218], and student self-efficacy through their perceived ability to succeed in the course and confidence to effectively communicate about course concepts. These are both essential skills to advance research literacy and future career success. As we were unable to directly compare other results to previous versions of the course due to the COVID-19 pandemic, these metrics serve as a means of evaluating the effectiveness of this stand-alone implementation toward these goals.

5.3 Materials and methods

5.3.1 Course design

Specifications grading can be hybridized with points-based assessments in a partial implementation[204], however we elected to utilize a full-specifications grading option (no points component) in the most recent iteration of the course in order to simplify the assessment policy and to try to create maximum buy-in from the students. This required establishment of rules for using tokens, updates to assignment rubrics to reflect mastery criteria for meeting learning objectives, and creation of an overall grade tracker based on demonstrated proficiency across the various course assessments. The course had several formal assessments over a range of cognitive levels designed to evaluate fundamental understanding of the application of chemical techniques and mechanisms to explain biological phenomena at the scale of atoms and bonds. In previous course iterations these included: discussion section worksheets, problem sets, quizzes, midterm, final, and writing assignments. Minor changes to the grading schema included

replacing the two exams with four quizzes because it is our interpretation that high-stakes, summative exams are philosophically contradictory to the intent of specifications grading[202] and eliminating one of the five problem sets due to time constraints. Worksheets, problem sets and quizzes were designed as assessments of fundamental knowledge and skills. The writing assignments were designed as mini reviews of the protein and nucleic acid literature, requiring students to combine concepts learned in the course in order to critically analyze methods, results, and proposed future work.

5.3.2 Token Policy

In this course, students earned all tokens by completing small, course-related activities. Up to seven tokens could be earned over the duration of the quarter broken down as follows: pre-course self-efficacy survey (2), syllabus assignment (1), chemical biology meme (1), attending a relevant department seminar (1) and post-course self-efficacy survey (2); shown as activity and number of tokens earned respectively. The pre-course self-efficacy survey was due by the end of the first week of the class and the post-course survey was due by week eight of the ten-week quarter to provide time to use the earned tokens. Mandatory participation in research-related surveys is prohibited in the classroom so alternative assignments such as reading a chemistry education research publication and writing a brief (2-3 sentences) summary were also made available to students who chose not to participate in the surveys.

The Token Trade-In List provided to students through a page in the course learning management system (LMS) at the beginning of the quarter is provided in the Appendix C. This document detailed specific guidelines on how tokens could be used, which included: resubmission of research paper(s) (first paper 2 maximum, second paper 1 maximum),

resubmission of a problem set (2 maximum), revision to one quiz question (1 per quiz, maximum 4), opt to take final to replace quiz score (1 per quiz, maximum 4), not attend a discussion section (1 maximum), and late assignment submission (3 maximum per assignment, 1 token per 24 hour period, 72 hour maximum extension). Maxima that could be applied to any given assessment, a time limit of one week to complete revisions after each assignment, and a deadline to use tokens by week nine of the quarter (except for the final exam) were established as a means to mitigate student and instructor workload. Each problem set and quiz resubmission also required a student reflection on the changes made to correct mistakes or incorporate feedback. Reflections were not required for resubmission of the writing assignments.

The two teaching assistants (TAs) assigned to the course maintained a tracker of tokens earned and used for each student. Individual assignments were marked as either complete or incomplete. TAs then utilized a single, editable “Token” assignment in the LMS, the score for which would increase when tokens were earned and decrease when used in order to monitor the number of tokens each student had available. Students were required to email TAs directly with the specific need (i.e. 24-hour late submission) to request use of tokens. An external inventory was accounted for in an Excel spreadsheet accessible to both TAs which contained how students earned tokens and how they used them.

5.3.3 Rubrics

The writing assignment rubric was adapted from grading criteria used from a writing course taught by K.J.M. at Emory University and previous iterations of the chemical biology course. Updates to and expansion of the rubric made feedback both more general, as it did not require

the instructor to provide as many individual comments, and more detailed because each criterion was written to be more specific and clear. Rubric criteria encompassed skills previously observed to be problematic in student scientific writing: scientific vocabulary, concision in writing, formatting and organization, flow, conventions of scientific writing[248], proper use of literature citations, presentation of data, and avoiding plagiarism[201]. Eleven of the twenty-four criteria were designated as "core," shaded in green in Table 5.1, and were required to be met along with a cumulative total of 17 for "low pass" and 21 for "high pass" assessment. If the minimum requirements were not met, the assignment was evaluated as "needs revision". In line with the specifications grading method, criteria beyond those designated "core" were higher-order cognitive tasks such as justification of methods. If minimum criteria to achieve a passing grade were not met, the assignment was marked as "needs revision" and students were allowed the opportunity to apply a token to resubmit. Students who achieved a "low pass" were also permitted to resubmit to attempt to achieve a "high pass".

Table 5.1: Assessment Criteria for Writing Assignments

Writing Assignment Rubric Criteria	
Page Limit: Is within 1/2 page of the limit and does not exceed the maximum number of pages.	**Spelling:** Words are spelled and used correctly (contains fewer than 2 errors).
Citations: References are cited using the format of any journal. Author names or first author et al. must be included, along with title, journal, issue, page numbers or article number, and year. Papers are cited in the order they are mentioned, and figure captions include citations for the paper where the figure first appeared.	**Sections:** Paper progresses in a logical manner; providing background on the field, identifying the research question addressed by the paper, explaining the methods used to answer it, discussing the overall merit of the work in demonstrating their claims, and proposing steps for future work.
Figures: Paper contains at least one figure, with a caption. All figures are large enough to see.	**Paragraphs:** All information in each paragraph is clear, coherent, and related.
No plagiarism: Text is written in student's own words, including figure captions. Excessive similarity to another student's paper will be considered academic dishonesty, excessive similarity to published papers or online sources will be considered failure to summarize in original words and results in a	**Transitions:** Each paragraph has a clear and coherent topic sentence that ties together the section in which it resides (i.e. each topic sentence transitions logically from the prior paragraph).

revision.	
Summary: Does not include quotations, whether long blocks of text or multiple short phrases. These are not plagiarism, but they do not fulfil the requirements of the assignment.	**Technical Writing:** Student avoids overly wordy, confusing or "flowery" text. Sentences are straightforward; no run-ons.
Research Problem: Provides a clear statement of the scientific or technological research question the work addresses.	**Figures:** All figure(s) are referenced in the text to support a claim.
Background: Briefly describes the state of the field before the main paper to provide context for the current work.	**Terminology:** No errors in chemical biology terminology.
Methods: Briefly and clearly describes the experimental or theoretical methods used.	**Definitions:** Technical terms are defined, experiments not discussed in class are explained.
Discussion: Clearly explains at least one major experiment, simulation, or theoretical result from the paper. Explains the logic step by step and describes each result. Depending on the paper, more than one may be necessary to explain the take-home message.	**Methods:** Justifies the choice of which experiment(s) or simulation(s) are included.
Controls: Correctly identifies quality control metrics from the result described above. Not every paper has positive and negative controls, but all should have some type of quality control.	**Figures:** All figure(s) present in the paper are appropriate to illustrate important aspects of the main paper or background information.
Conclusions / Future Work: Student provides a reasonable next step for this line of research.	**Clarity:** Writing is clear and makes sense, without missing words, switches in tense, or other problems impacting understanding.
Grammar: The writing is grammatically correct such that it does not distract from the ideas presented (fewer than 2 unclear sentences).	**References:** 3-5 appropriate references and 0 inappropriate references are used.
High pass	All core and total ≥ 21
Low pass	All core and total ≥ 17
Needs Revision	Not all core met and /or total < 17

5.3.4 Grade criteria

Ultimately grade criteria are at the discretion of the instructor, which maintains academic freedom in applying this method. However, the general expectation in specifications grading is that students will need to demonstrate mastery of skills or concepts with higher cognitive demand and / or complete more work in order to earn higher final letter grades. We used

Bloom's taxonomy[249,250] to establish baseline skills for grade demarcations. Each question on a problem set or quiz was assigned a letter grade for the purpose of establishing performance thresholds on assignments. "C"-level questions were based on knowledge and understanding, requiring students to: define, summarize, identify, and perform simple calculations. "B"-level questions were based on application and analysis, requiring students to: make connections among different topics, apply principles to a new problem, draw structures, propose mechanisms, or deduce the correct equations to use. "A"-level questions were based on evaluation and creating, requiring students to: explain how methods were used, justify methods and controls by assessing their impact on the results, generate hypotheses and describe an experimental design to test them, or make predictions. These general descriptions were made available to the students, however the letter grade associated with each question was not released until afterwards in order to promote maximum participation in the exercises. Minima for low pass and high pass scores were consistently applied to all assignments and quizzes. To earn a low pass students were required to either satisfactorily complete all of the "C"-level questions or all but one of the "C"-level questions and at least one other question. To earn a high pass students were required to demonstrate at least all but one of the "C"-level questions and achieve at least 80% satisfactory completion of the assignment, which would necessitate demonstrated skills at both the "B" and "A"-level. If the criteria for low pass were not met then the assignment or quiz would be returned as "needs revision" and the student would be allowed to use to token to preform revisions and improve the score. The highest score achieved after allowed resubmissions was recorded.

The overall grade determination matrix for the course is presented in Table 5.2. Students earned the highest grade for which they met all of the minimum requirements. In order to achieve a "D", students were required to earn a "low pass" on all assessments and complete six discussion section worksheets. Plus and minus grades are used at UCI, so additional

distinctions were made from the base grade requirements. For plus grades students needed to complete at least one additional discussion section worksheet and earn a “high pass” on a research paper when “low pass” was required. For minus grades, students were permitted completion of one fewer discussion section worksheet and earning a “low pass” when “high pass” was required on a research paper.

Table 5.2: Overall Grade Determination Matrix

Course Components	**Criteria Required to be Met to Earn Letter Grade**		
	A	B	C
Discussion Section Worksheet	9/10 complete	8/10 complete	7/10 complete
Problem Sets	4/5 high pass 1/5 low pass	3/5 high pass 2/5 low pass	1/5 high pass 4/5 low pass
Quizzes	3/4 high pass 1/4 low pass	2/4 high pass 2/4 low pass	1/4 high pass 3/4 low pass
Nucleic Acid Research Paper	high pass	1 high pass	low pass
Protein Research Paper	high pass	1 low pass	low pass

5.3.5 Self-efficacy survey

The fourteen-question self-efficacy survey used for this course, provided in the Appendix C, was modified from a validated survey to probe student confidence in learning biology, especially as non-majors[251]. There were three assessment factors addressed by the questions: methods of chemical biology (question 1), generalization to other chemical biology/science courses and

analyzing data (questions 2-7), and application of chemical biology concepts and skills (questions 8-13). The survey questions were adapted very minimally to make the wording applicable to this course. Table 5.3 documents the changes in wording from the original survey questions (bold) to the survey used for this course (bold, italic). Question 14 was the only question we added that was not adapted from the original survey but was deemed pertinent to assessing the goals of the course. The full survey is provided in the Appendix C for further reference. The survey was made available through the UCI's instance of Qualtrics, a cloud-based platform for distributing web-based surveys. Participation was completely voluntary (an alternative assignment was provided for students who chose not to participate) and results were analyzed *en masse* to maintain anonymity.

Table 5.3: Changes to Validated Survey Questions

Original Question[251]	**Adjusted Question**	**Assessment Factor**[251]
Q1 How confident are you that you could critique an experiment described in a **biology textbook** (i.e., list the strengths and weaknesses)?	Q1 How confident are you that you could critique an experiment described in a ***journal article*** (i.e., list the strengths and weaknesses)?	Methods of chemical biology
Q2 How confident are you that you will be successful in this **biology** course?	Q2 How confident are you that you will be successful in this ***chemical biology*** course?	Generalization to other chemical biology / science courses and analyzing data
Q3 How confident are you that you will be successful in **another biology** course?	Q3 How confident are you that you will be successful in ***a molecular biology*** course?	Generalization to other chemical biology / science courses and analyzing data
Q4 How confident are you that you will be successful in an	Q4 How confident are you that you will be successful in an	Generalization to other chemical biology / science

ecology course?	***analytical chemistry*** course?	courses and analyzing data
Q7 How confident are you that you could explain something that you learned in this **biology** course to another person?	Q7 How confident are you that you could explain something that you learned in this ***chemical biology*** course to another person?	Generalization to other chemical biology / science courses and analyzing data
Q8 How confident are you that after reading an article about a **biology** experiment, you could write a summary of its main points?	Q8 How confident are you that after reading an article about a ***chemical biology*** experiment, you could write a summary of its main points?	Application of chemical biology concepts and skills
Q9 How confident are you that after reading an article about a **biology** experiment, you could explain its main ideas to another person?	Q9 How confident are you that after reading an article about a ***chemical biology*** experiment, you could explain its main ideas to another person?	Application of chemical biology concepts and skills
Q10 How confident are you that after watching a television documentary dealing with some aspect of **biology**, you could write a summary of its main points?	Q10 How confident are you that after watching a television documentary dealing with some aspect of ***chemical biology***, you could write a summary of its main points?	Application of chemical biology concepts and skills
Q11 How confident are you that after watching a television	Q11 How confident are you that after watching a television	

documentary dealing with some aspect of **biology**, you could explain its main ideas to another person?	documentary dealing with some aspect of ***chemical biology***, you could explain its main ideas to another person?	Application of chemical biology concepts and skills
Q12 How confident are you that after listening to a public lecture regarding some **biology** topic, you could write a summary of its main points?	Q12 How confident are you that after listening to a public lecture regarding some ***chemical biology*** topic, you could write a summary of its main points?	Application of chemical biology concepts and skills
Q13 How confident are you that after listening to a public lecture regarding some **biology** topic, you could explain its main ideas to another person?	Q13 How confident are you that after listening to a public lecture regarding some ***chemical biology*** topic, you could explain its main ideas to another person?	Application of chemical biology concepts and skills
N/A	***Q14 How confident are you that you could apply concepts learned in this chemical biology course to a research project?***	Application of concepts to research project (*unvalidated addition)

5.4 Results and discussion

A total of 107 students enrolled and 99 students completed the winter 2022 iteration of the course described here. We judged the use of specifications grading to be an overall success, as there were no concerning differences in overall grade distribution, the mean results of the student self-efficacy survey improved slightly, and there were substantial improvements observed on several rubric metrics between the initial submission of writing assignment 1 and writing assignment 2. This is particularly significant because it was many students' first exposure to this grading method which can initially cause anxiety[208,252] and it was the first implementation for this course which can be challenging for a variety of reasons[253]. We are encouraged by these results that other educators in biophysics may be able to adapt this framework for their own classrooms.

5.4.1 Token economy

The token system should ideally be aligned to support demonstrated mastery of course objectives without allowing students to generate an unmanageable workload for themselves or the instructors[202,254]. Providing too few tokens causes students to hoard them, preventing them from revising their work, whereas providing too many allows students to mismanage their workload by pushing everything to the end of the class, which is a suboptimal learning experience as well as producing an unrealistic amount of grading for the instructors at the end of the course. We designed our token economy similar to the system implemented in the "Writing for Chemists" course[215].

Tracking tokens not only served as a means of accounting but also allowed for analysis of the overall way students used their tokens. Out of seven total available, the average number of tokens earned and used was six and four respectively. Thirty-five out of ninety-nine students used fewer than half of the available tokens and only four used all seven. As shown in Table 5.4, the highest percentage of tokens were used on writing assignment 1 (124, 32.9%), quiz revisions (103, 27.3%), and writing assignment 2 (66, 17.5%). While exact replication of this policy is not the only means to achieve these results, as administered the token system employed adequately supported the goals of the course as it was not detrimental to student performance or instructor workload.

Table 5.4: Breakdown of Token Usage

Approved Token Use	Total Number Used	% of Total
Missed Discussion Section	13	3.5
Problem Set (Late Submission)	28	7.4
Problem Set (Revision)	22	5.8
Quiz (Revision)	103	27.3
Quiz (Full Redo)	21	5.6
Writing Assignment (Late Submissions)	28	7.4
Writing Assignment 1 – Nucleic Acid Research Paper (Revision)	96	25.5
Writing Assignment 2 – Protein Research Paper (Revision)	66	17.5
Total	377	

5.4.2 Writing assignments

Using specifications rubrics for the writing assignments in particular enables students to learn from their mistakes on this challenging and novel (for them) task in a low-stakes context. The nucleic acid mini-review paper was assigned in week 4 of the ten-week quarter and students were allowed to use tokens to resubmit up to two times. The protein mini-review paper was assigned in week 8 and students were allowed to use tokens to resubmit once due to time

constraints at the end of the quarter. Two students did not submit either assignment despite having access to tokens that could have enabled a late submission. A detailed breakdown of the criteria marked as “needs revision” for the initial submission and any resubmissions for each writing assignment is provided in Table 5.5, where criteria shaded in green and marked with an asterisk are core. Bolded red / negative values indicate more than 25% of the class did not adequately demonstrate the rubric line item. Bolded green / positive values indicate criteria with the largest amount of improvement (less frequently marked as “needs revision”) between writing assignment 1 (WA1) and writing assignment 2 (WA2). Five overall criteria comprised of four core (citations format and placement, discussion, controls, conclusions) and one other (clarity) were marked as “needs revision” for 25% or more of the class on initial submissions for both writing assignments. Criteria that showed the most improvement from the initial submission of WA1 to the initial submission of WA2 were discussion, controls and technical writing which improved by 28%, 32% and 75% respectively, indicating that learning improved between the two assignments. In total fourteen (eleven not previously mentioned) of the twenty-four criteria yielded a decrease in the frequency of “needs revision” evaluations between the initial submissions of both assignments. Criteria where students did not improve between the initial submission of writing assignments were relatively anomalous, impacting less than 10% of the students, however this information could indicate areas to be emphasized with additional practice or discussion in future iterations of the course.

Table 5.5: Writing Assignment "Needs Revision" Criteria

Criteria (*=core)	WA1	WA1 Resub	WA1 Resub 2	WA2	WA2 Resub	Dinitial WA1 and initial WA2	Dfinal WA1 Resub and final WA2 Resub
Page Limit *	4	3	0	6	3	2	0
Citations (format and placement) *	**25**	2	0	**35**	3	10	1
Figures (1 w/ caption, legible) *	14	2	1	13	0	-1	-2
No plagiarism *	1	0	1	6	0	5	0
Summary *	4	2	0	4	0	0	-2
Research Problem *	6	0	0	3	0	-3	0
Background *	18	1	0	13	0	-5	-1
Methods (describe) *	19	0	0	10	0	-9	0
Discussion *	**68**	3	0	**49**	3	**-19**	0
Controls *	**75**	12	0	**51**	7	**-24**	-5
Conclusions *	37	1	0	37	0	0	-1
Grammar	6	0	0	5	0	-1	0
Spelling	5	1	1	5	0	0	-1

Sections	2	0	0	7	0	5	0
Paragraphs	10	0	0	2	0	-8	0
Transitions	8	0	0	7	1	-1	1
Technical Writing	**32**	2	0	8	1	**-24**	-1
Figures (referenced in text)	4	2	0	7	1	3	-1
Terminology	16	1	1	18	4	2	3
Definitions	**29**	1	1	23	0	-6	-1
Methods (justify use)	9	1	0	6	1	-3	0
Figures (appropriate)	3	4	0	5	1	2	-3
Clarity	**37**	2	0	**36**	5	-1	3
References (3-5 appropriate)	8	2	0	6	0	-2	-2

For both writing assignments, most students received an overall evaluation of “needs revision” on the first submission, but achieved “high pass” by the final submission, as shown in Table 5.6. Slightly more students received a final grade of “low pass” on the second paper, likely due to only having one submission attempt and possibly other competing time requirements at the end of the quarter. The reason we do not assess this to represent declining performance is because roughly 20% of students improved the initial submission grade from writing assignment one to two, with “needs revision” dropping from 87 to 65 respectively. Students not only applied feedback to make corrections to each individual assignment, but these results indicate that

feedback from WA1 was also utilized to improve the initial submission of WA2. We interpret this finding to demonstrate that students learned new skills and knowledge throughout the revision process. Almost all students were able to achieve “high pass” on both writing assignments, and while not directly comparable to previous iterations of the course, student performance was qualitatively noted to be much more consistent and improved overall.

Table 5.6: Student Grades on Writing Assignments

Assignment	**Needs Revision**	**Low Pass**	**High Pass**
Nucleic Acid Research Paper Initial	87	0	10
Nucleic Acid Research Paper Final	0	2	95
Protein Research Paper Initial	65	0	31
Protein Research Paper Final	0	7	90

5.4.3 Grade distributions

This course was taught by the same instructor for four consecutive years beginning in winter quarter of 2019. In 2019, students’ final letter grades were determined by the total points accumulated over the duration of the course from the following assessments: quizzes and discussion problems (10%), problem sets (15%) writing assignments (20%), midterm (25%), and final exam (30%). The late policy for points-based grades permitted assignments to be accepted up to one hour late with no penalties and a 10% reduction in score for assignments received each 24-hour period beyond the original deadline. While using points-based assessments, students were not permitted to revise or resubmit work. Specifications grading was utilized in 2022 with the grade criteria and token policies previously described.

Final grade distributions for the 2019 and 2022 courses are shown in Figure 5.1. Winter 2020 and 2021 grades were omitted from the comparison because these iterations were substantially altered to accommodate remote instruction due to the COVID-19 pandemic. The 2019 points-based grade distribution was characteristically Gaussian with a mode grade of B+ (typical for an upper-division course taken primarily by majors) for a class size of 108 students. In this implementation of specifications grading, significantly more students earned A+ and A final grades, yielding a unimodal distribution across the 99 students. The net workload and expectations for the course predominantly remained unchanged. Therefore, the grade shift is representative of more students demonstrating mastery of the learning objectives, in part due to opportunities for revision. As an example of this, make-up quizzes were written to be conceptually similar but with unique questions such that answers could not be memorized and learning must be demonstrated. The general shift to higher grades is consistent with some other implementations of specifications grading in undergraduate STEM education[203,208,255]. We hypothesize that this may be in part because a student that would typically earn a “B” in a traditional points-based system is presented with the tools and awareness to achieve an “A”[203,231,256]. The grade distributions are not directly comparable to each other in terms of changes in student learning due to adjustments in the course structure and the unknowable impact of the COVID-19 pandemic. However, we have included the grades to provide a baseline for evaluating whether we provided enough opportunities for rework and in order to demonstrate this implementation did not lower students’ grades on average despite the more rigorous standards.

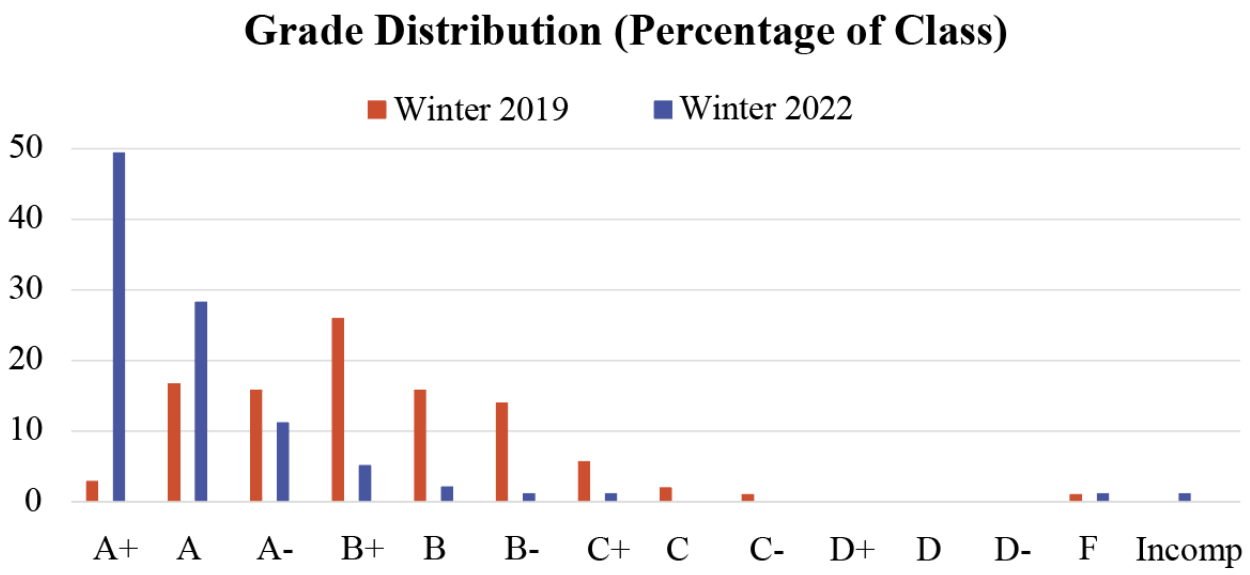

Figure 5.1: Comparison of grade distributions for two classes taught in-person by Professor Rachel Martin. Grades for winter 2019 (red) were determined using a conventional point-based system and show a relatively gaussian distribution (n=108). Grades for winter 2022 (blue) were determined using pure specifications grading criteria and resulted in a distribution that is unimodal, and shifted to a higher average grade, compared to what is typically expected (n=99). Grades for 2020 and 2021 are not shown for comparison because of differences in instruction due to COVID-19 which are outside the scope of this work.

5.4.4 Survey results

We surveyed students at the beginning and end of the course to test whether student perceptions about their ability to succeed in this or related courses improved after exposure to the more self-directed learning approach offered in specifications grading, or alternatively, if it declined due to receiving detailed, critical feedback. As determined by the token tracker, one student did not complete either survey, twenty-two students (some of whom dropped the course) only completed the first survey, and two students only completed the second survey. Sixteen students submitted two entries for one or both of the surveys, possibly by mistake, therefore we elected to include only the first response in the analysis. This was determined based on IP address alone as names were used only for awarding token credit and were

removed from the survey results prior to analysis. In total 77 sets of surveys (~78%) were used in this investigation.

Students responded to the 14 questions with a Likert-scale ranging from (1) NOT AT ALL confident to (5) TOTALLY confident[251]. Results of the pre-course (week 1) and post-course (week 8) surveys were paired for each student. The mean result was determined for the question(s) corresponding to each assessment factor for each set of survey[251,257]. Student response means for each of the three original factors as well as the question we added were assessed for statistically significant changes. We performed both paired t-tests and Wilcoxon signed-rank tests in R statistical software[258,259] to determine whether results were significant. The results of the paired t-tests for each factor are provided in Table 5.7 and distributions of the initial and final factor averages are presented in Figure 5.2. Both tests qualitatively validated that confidence in all factors increased, indicating that student self-efficacy improved over the duration of the course. The results of this survey demonstrated that specifications grading qualitatively improved student perceptions on self-efficacy to succeed in the course and communicate about related topics, especially in areas of particular focus related to the goals of the class. Extensive prior research has focused on the influence of mindset on academic performance. Our results corroborate this relationship and further suggest that academic performance influences students' mindsets[260].

Table 5.7: Comparison of Week 1 and Week 8 Responses to Survey Items

Survey Factor	Pre-Course Mean (sd)	Post-Course Mean (sd)	p-value
Methods of chemical biology	2.78 (0.80)	3.35 (0.89)	<0.001
Generalization to other chemical biology / science courses and analyzing data	3.26 (0.88)	3.51 (0.67)	0.004
Application of chemical biology concepts and skills	3.32 (0.87)	3.68 (0.76)	<0.001
Application of concepts to research project (**unvalidated addition*)	3.21 (1.04)	3.51 (1.00)	0.012

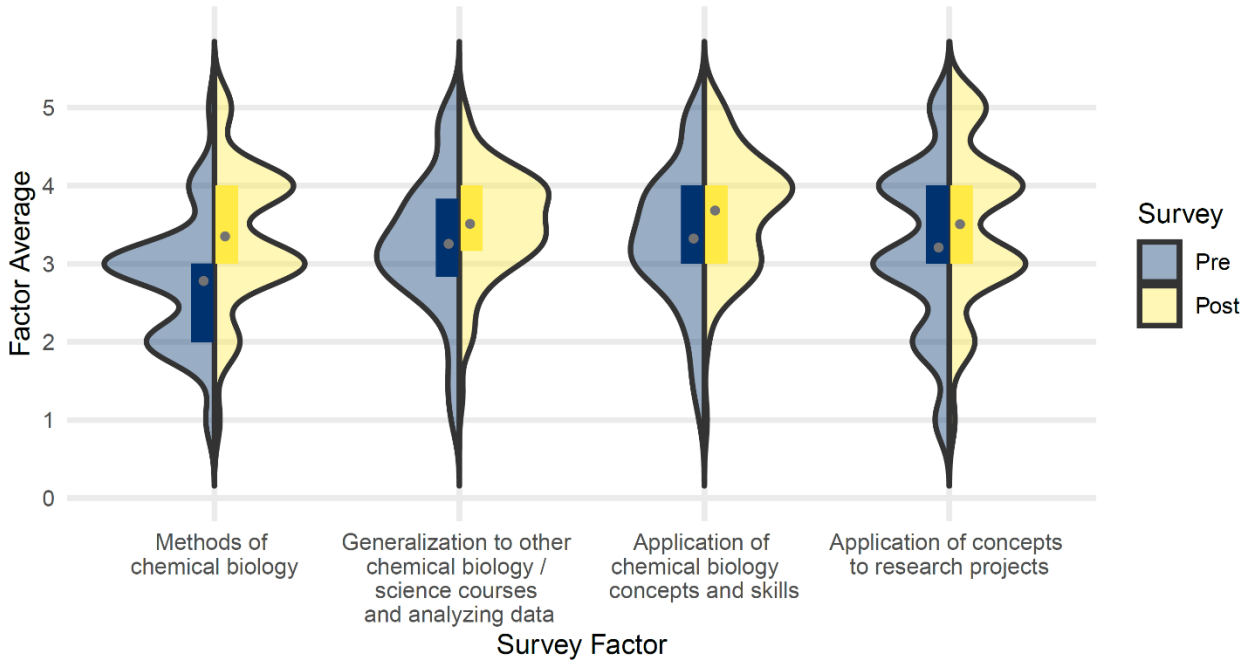

Figure 5.2: Results of student self-efficacy survey recorded in week 1 (pre-course) and week 8 (post-course) of the Winter 22 quarter (n=77). Responses range from (1) NOT AT ALL confident to (5) TOTALLY confident. Means are depicted as a gray dot within the boxed interquartile range. All assessment factors had a significant and positive change in the mean response from the initial to final survey.

Limitations of this study are mostly due to its being the first implementation of specifications grading in this course. For instance, we did not include a control group, in part because this was the first implementation of specifications grading in the course and only one section of the class was offered during that quarter. In the future it would be beneficial to perform the survey in the same manner with a version of the class with the same assessments and rubrics but taught using a traditional points-based system. We did not receive responses for both surveys from every student enrolled throughout the course, so it is possible that students who were already biased toward feeling confident answered. Further, the questions are a qualitative self-reflection which may be impacted by many factors outside of administration of this course.

5.4.5 Student perceptions

University-administered teaching evaluations were completed by 29/99 students at the end of the quarter. The free-response questions used the standard wording for teaching evaluations at UCI and therefore did not ask about specifications grading in particular. These questions are:

1. Which aspects of this class did you feel were intellectually or creatively stimulating?
2. Which aspects of this class did you feel contributed most to your learning?
3. Which aspects of this class could be improved to enhance your learning?

Here we summarize the responses to these questions that related to specifications grading aspects of the course. Comments on other course features, such as the specific topics covered, the lectures, or the discussion sections, are not included. Students' comments on specifications grading in this course were mostly positive, and many of the negative comments focused on

organizational issues related to this being the first time the grading scheme was implemented in this course.

Students liked that the course was organized around four quizzes rather than a midterm and a final. Some found it easier to stay engaged and monitor their progress with more frequent assessments. Reduced anxiety due to the lower stakes of each quiz was also mentioned. Although more frequent, low-stakes assessments are not unique to any one grading method, they are essentially required by specifications grading in order to adequately allow opportunities for rework. Students appreciated the increased transparency afforded by specifications grading, since they knew from the beginning how their grades would be determined. They also found that specifications grading made it easier to understand what to prioritize, which is important in a class where a large amount of complex material is covered. Some students appreciated completing revisions, which allowed the opportunity to learn from mistakes, and the token economy, which enabled management of revision attempts. Of the 28 respondents, 72% answered that the instructor provided opportunities to better understand material (36% strongly agree, 36% agree). These results are consistent with expected benefits of specifications for the student learning experience[202].

Students also provided suggestions for improvement, many of which focused on the materials being new and not previously tested. As an example of relatively common feedback[208,261], some students found the rubrics confusing and thought the grading scheme could be explained better. We plan to improve these materials for future use based on the students' comments. Some other requests are more difficult to implement or are inconsistent with course goals. For example, one student mentioned wanting to know which questions are "A," "B," or "C" before the assignment is turned in. We made the deliberate choice not to reveal the question classifications until after the assignment is turned in because we wanted students to make a

good-faith effort on all problems rather than only attempting the “C” or “C and B” problems. Some students wanted more time to revise the assignments, and one specifically requested an unlimited window until the end of the quarter. Although we will be more mindful of spreading out the assignments in the future, it is not realistic or desirable to offer unlimited time for revisions, both because of the instructional team’s workload, and because allowing assignments to pile up until the end of the quarter rather than revising them in a timely manner does not provide an optimal learning experience for students. Finally, one student expressed dislike for specifications grading because it is more work for the students, particularly those without substantial writing practice. However, they also acknowledged understanding our goals in implementing it and voiced that they felt it made them a better writer which is consistent with student perceptions in other writing classes utilizing specifications grading[215,262] and is consistent with the more general observation of student dissatisfaction with methods they view as unconventional regardless of improved performance[263].

5.4.6 Teaching assistant and instructor perceptions

Here we present qualitative assessments assembled from the teaching assistants and course instructor following completion of the grade submissions. From an instructional standpoint, it was expected that some challenges would arise due to this being the first implementation of specifications grading for the course and this grading scheme being new to many students. After a brief initial period of clarifying the instructions related to grading rubrics and token use, the majority of student interactions at office hours and after class meetings were focused on substantive topics related to learning objectives such as how to identify the controls in an experiment or how to draw a chemical mechanism correctly. From an instructor perspective, the best feature of specifications grading was the shift in focus from points and grades to problem-

solving and skills. It was observed that less time was dedicated to discussing grades because the overall course expectations were generally clearer, with a path to achieve a given letter grade and all assignments either satisfactory or returned as “needs revision”. This was a welcome contrast from previous versions of the same course, where most discussions were concentrated on negotiating for more partial credit and discussing how many points were lost for particular mistakes without the ability to directly correct them, making feedback frustrating for the students and the instructor. Removing the possibility of partial credit seemed to shift the conversation in a more productive direction, toward mastering the skills needed to succeed at the writing assignments or quizzes. This is not always the case with point-based systems where partial credit can contribute significantly to accumulating enough points to achieve a desired overall grade[202,243,264], or where final grades may ultimately be subject to curves or weighted adjustments in order to achieve a desired distribution. As a positive and perhaps non-intuitive outcome for instructors, grading was much more straightforward and faster even when accounting for time spent grading resubmissions. Open-ended questions were still challenging because a key or rubric cannot fully capture every possible variation of a correct answer or a formatting issue so some discernment is required. However, this would be the case in a points-based system as well, and it may be even more challenging to fairly apply partial credit, whereas if instructors are in doubt in specifications grading it is fully appropriate to mark as “needs revision” and allow informed revision. Adoption of this line of thinking can be challenging even with substantial buy-in, because teaching assistants and instructors have all been indoctrinated almost exclusively to points-based systems. During the course, one teaching assistant was concerned that the binary nature of specifications grading as either a pass or needs revision could be detrimental to student grades. Student communication with TAs and the course instructor was observed to improve, generally noted as more positive, less anxious, more eager to improve, and more focused on course concepts.

5.4.7 Considerations for future implementation

Buy-in from teaching assistants is critical to realize the benefits to both students and instructors. In this case, even though both teaching assistants (TAs) understood and supported the goals of specifications grading, they still found it difficult to grade each question in a binary manner after previous experiences with assigning partial credit. This required occasional reminders during our regular instructional team meetings to grade quickly and assign a passing score only when **all** required elements of the correct answer were present. In between these discussions, it was easy for TAs to slip back into the default mode of thinking about partial credit, which is contrary to the course goals and takes up too much of the TAs' time. The latter point is especially critical when dealing with revisions: because each assignment may be graded more than once, the workload becomes unmanageable if grades are not assigned quickly and without considering student effort or trying to rationalize partially correct answers. This was mostly a concern at the beginning of the course and became less of a problem with practice. Overall, the TAs, one of whom had taught the same course before the implementation of specifications grading, reported that the average workload for this course was about the same as for similar courses. The issues with implementation could potentially be mitigated by incorporating a brief training for TAs, especially those not or less familiar with specifications grading, before the course begins.

Based on some core criteria of the writing assignments being consistently rated as "not met" for the majority of students on initial submissions, shown in Table 5.5, it could be beneficial to break these criteria down and incorporate consistent practice into problem sets. Questions based on reading a piece of literature were included in a few problem sets but it may be beneficial to include them on all problem sets in the future. The questions also could be more clearly related to the core criteria on the writing assignment rubrics, which may then help students make the connection between the problem sets and the writing assignments. One other idea to support

improvement in this area was to provide students with examples of acceptable assignments, however the instructor determined that this was not aligned with the learning objectives. The students are presented with several exemplars of well-written, brief review papers (e.g. Nature "News and Views,") throughout the course. However, they are not provided with examples of this particular assignment because the goal is for them to analyze and discuss the assigned papers based on their own understanding rather than simply following a template. Further clarification to rubric line items based on student questions and feedback is likely to continue to be important in any future implementations of specifications grading due to the all-or-nothing credit system.

In this implementation answer keys for problem sets and quizzes were posted immediately after initial grades were released to students and reflections for resubmitted quizzes and problem sets were not required to be in a specific format. In the future, to ensure that the resubmission demonstrates learning and mastery of a learning objective we plan to require students to answer the following prompts in addition to the correct answer for each question to be reassessed:

"1. What was incorrect about the first approach or answer? Briefly explain why.
2. What changes did you make to achieve the correct answer? Briefly explain why these changes were necessary.
3. What did you learn that you will apply to problems like this in the future?"

We hope that questions will require students to actively re-engage with the course material and reassess any misunderstandings, promote long-term retention of the material.

It is expected that a handful of outliers may not meet all required criteria as presented in the grade determination matrix. It is not realistic to predict every possible scenario that could lead to this, however it is beneficial to have a strategy to mitigate this as uniformly as possible. In this course, most of the observed grading challenges arose when students did not meet all of the specifications needed to earn a low pass for the second writing assignment after one round of feedback and revision. Ideally, they would have a second opportunity to revise their work and earn a better grade; however, this was not feasible because it was too close to the end of the course. In all four cases where this happened, the students' second drafts showed significant improvement relative to the first, and they were assigned a score of low pass, enabling them to pass the course. One other student turned in a "revised" second writing assignment without having submitted the first draft; this was graded normally and earned a score of high pass. Although improving the rubrics and instructions will likely reduce the number of exceptions that have to be dealt with, it is probably impossible to eliminate them altogether and some flexibility is needed to determine grades in these cases.

The only major drawback of this implementation of specifications grading was the accumulation of grading near the end of the quarter. In particular, two rounds of revisions were allowed for the first writing assignment in order to make sure students were provided with enough feedback on their work and opportunities to correct mistakes. However, the initial submission for the first writing assignment was late enough in the quarter that the second round of revisions coincided with the initial submission of the second writing assignment, causing a bottleneck in grading. This led to excessive work for the instructor during this time, as well as a delay in students' receiving feedback. We believe this problem can be resolved with better scheduling, particularly moving the first writing assignment earlier in the quarter, even though students will not have as much background when they begin to work on it.

5.5 Conclusions

Due to the rapid pace of changes in the field of chemical biology, an upper-division undergraduate course was redesigned using specifications grading to support research literacy as demonstrated through comprehensive writing assignments. Specifications grading offers a tailorable, student-centered assessment approach that can be beneficial for both students and instructors, especially for high-complexity cognitive tasks that can benefit from iterative feedback. The grading system allowed students to resubmit work, qualitatively improving both their conceptual understanding and their written communication skills. Students overall were receptive to the changes and showed improvements in both self-efficacy and performance in areas aligned with the course learning objectives. Workload for the instructors was comparable to past versions of the course. Although this system requires some buy-in and additional efforts at clarification, it is likely to be beneficial in other interdisciplinary and dynamic areas of study.

5.6 IRB statement

This work, which is classified as exempt (research involving normal education practices in an established educational setting), was carried out in accordance with the standards established by the UC Irvine Institutional Review Board (UCI IRB protocol number 264).

References

(1) Kelz, J. I.; Kelly, J. E.; Martin, R. W. 3D-Printed Dissolvable Inserts for Reproducible Fabrication of High-Homogeneity Transceiver Coils. paper under revision.

(2) Kelz, J. I.; Uribe, J. L.; Martin, R. W. Reimagining Magnetic Resonance Instrumentation Using Open Maker Tools and Hardware as Protocol. *J. Magn. Reson. Open* **2021**, *6–7*, 100011. https://doi.org/10.1016/j.jmro.2021.100011.

(3) Kelz, J. I.; Uribe, J. L.; Rasekh, M. F.; Takahashi, G. R.; Gibson, W. S.; Link, R. D.; McKnelly, K. J.; Martin, R. W. Implementation of Specifications Grading in an Upper-Division Chemical Biology Lecture Course. *The Biophysicist* **2023**, *4* (1), 11–29. https://doi.org/10.35459/tbp.2022.000239.

(4) Martin, R. W.; Kelly, J. E.; Kelz, J. I. Advances in Instrumentation and Methodology for Solid-State NMR of Biological Assemblies. *J. Struct. Biol.* **2018**. https://doi.org/10.1016/j.jsb.2018.09.003.

(5) Levitt, M. Chapter 1 Nuclear Magnetism, Chapter 2 Magnetism. In *Spin Dynamics: Basics of Nuclear Magnetic Resonance*; John Wiley & Sons, Ltd, 2008; pp 5–38.

(6) Duer, M. J. *Introduction to Solid-State NMR Spectroscopy*; Blackwell Publishing Ltd, Oxford, 2004.

(7) Andrew, E. R.; Bradbury, A.; Eades. Nucl. Magn. Reson. Spectra Cryst. Rotated High Speed, *Nature* **1958**, *182* (4650), 1659.

(8) Lowe, I. J. Free Induction Decays Rotating Solids, *Phys. Rev. Lett.* **1959**, *2* (7), 285–287.

(9) Stejskal, E. O.; Schaefer, J.; Waugh, J. S. Magic-Angle Spinning and Polarization Transfer in Proton-Enhanced NMR. *J. Magn. Reson. 1969* **1977**, *28* (1), 105–112.

(10) Wu, X.; Zilm, K. W. Complete Spectral Editing in CPMAS NMR. *J. Magn. Reson.* **1993**, No. 102, 205–213.

(11) Opella, S. J. Structure Determination of Membrane Proteins by Nuclear Magnetic Resonance Spectroscopy. *Annu. Rev. Anal. Chem.* **2013**, *6* (1), 305–328. https://doi.org/10.1146/annurev-anchem-062012-092631.

(12) Sattler, M.; Fesik, S. W. Use of Deuterium Labeling in NMR: Overcoming a Sizeable Problem. *Structure* **1996**, *4* (11), 1245–1249.

(13) Zhou, D. H.; Graesser, D. T.; Franks, W. T.; Rienstra, C. M. Sensitivity and Resolution in Proton Solid-State NMR at Intermediate Deuteration Levels: Quantitative Linewidth Characterization and Applications to Correlation Spectroscopy. *J. Magn. Reson.* **2006**, *178* (2), 297–307. https://doi.org/10.1016/j.jmr.2005.10.008.

(14) Morcombe, C. R.; Gaponenko, V.; Byrd, R. A.; Zilm, K. W. ^{13} C CPMAS Spectroscopy of Deuterated Proteins: CP Dynamics, Line Shapes, and T_1 Relaxation. *J. Am. Chem. Soc.* **2005**, *127* (1), 397–404. https://doi.org/10.1021/ja045581x.

(15) Hologne, M.; Faelber, K.; Diehl, A.; Reif, B. Characterization of Dynamics of Perdeuterated Proteins by MAS Solid-State NMR. *J. Am. Chem. Soc.* **2005**, *127* (32), 11208–11209. https://doi.org/10.1021/ja051830l.

(16) Böckmann, A.; Ernst, M.; Meier, B. H. Spinning Proteins, the Faster, the Better? *J. Magn. Reson.* **2015**, *253*, 71–79. https://doi.org/10.1016/j.jmr.2015.01.012.

(17) Cala-De Paepe, D.; Stanek, J.; Jaudzems, K.; Tars, K.; Andreas, L. B.; Pintacuda, G. Is Protein Deuteration Beneficial for Proton Detected Solid-State NMR at and above 100

kHz Magic-Angle Spinning? *Solid State Nucl. Magn. Reson.* **2017**, *87*, 126–136. https://doi.org/10.1016/j.ssnmr.2017.07.004.
(18) Akbey, Ü.; Lange, S.; Trent Franks, W.; Linser, R.; Rehbein, K.; Diehl, A.; Van Rossum, B.-J.; Reif, B.; Oschkinat, H. Optimum Levels of Exchangeable Protons in Perdeuterated Proteins for Proton Detection in MAS Solid-State NMR Spectroscopy. *J. Biomol. NMR* **2010**, *46* (1), 67–73. https://doi.org/10.1007/s10858-009-9369-0.
(19) Andreas, L. B.; Le Marchand, T.; Jaudzems, K.; Pintacuda, G. High-Resolution Proton-Detected NMR of Proteins at Very Fast MAS. *J. Magn. Reson.* **2015**, *253*, 36–49. https://doi.org/10.1016/j.jmr.2015.01.003.
(20) Barbet-Massin, E.; Pell, A. J.; Retel, J. S.; Andreas, L. B.; Jaudzems, K.; Franks, W. T.; Nieuwkoop, A. J.; Hiller, M.; Higman, V.; Guerry, P.; Bertarello, A.; Knight, M. J.; Felletti, M.; Le Marchand, T.; Kotelovica, S.; Akopjana, I.; Tars, K.; Stoppini, M.; Bellotti, V.; Bolognesi, M.; Ricagno, S.; Chou, J. J.; Griffin, R. G.; Oschkinat, H.; Lesage, A.; Emsley, L.; Herrmann, T.; Pintacuda, G. Rapid Proton-Detected NMR Assignment for Proteins with Fast Magic Angle Spinning. *J. Am. Chem. Soc.* **2014**, *136* (35), 12489–12497. https://doi.org/10.1021/ja507382j.
(21) Reif, B. Ultra-High Resolution in MAS Solid-State NMR of Perdeuterated Proteins: Implications for Structure and Dynamics. *J. Magn. Reson.* **2012**, *216*, 1–12. https://doi.org/10.1016/j.jmr.2011.12.017.
(22) Gall, C. M.; DiVerdi, J. A.; Opella, S. J. Phenylalanine Ring Dynamics by Solid-State 2H NMR. *J. Am. Chem. Soc.* **1981**, *103*, 5039–5043.
(23) Ketchem, R.; Roux, B.; Cross, T. High-Resolution Polypeptide Structure in a Lamellar Phase Lipid Environment from Solid State NMR Derived Orientational Constraints. *Structure* **1997**, *5* (12), 1655–1669. https://doi.org/10.1016/S0969-2126(97)00312-2.
(24) Gröbner, G.; Choi, G.; Burnett, I. J.; Glaubitz, C.; Verdegem, P. J. E.; Lugtenburg, J.; Watts, A. Photoreceptor Rhodopsin: Structural and Conformational Study of Its Chromophore 11- *Cis* Retinal in Oriented Membranes by Deuterium Solid State NMR. *FEBS Lett.* **1998**, *422* (2), 201–204. https://doi.org/10.1016/S0014-5793(97)01591-3.
(25) Bechinger, B.; Weik, M. Deuterium Solid-State NMR Investigations of Exchange Labeled Oriented Purple Membranes at Different Hydration Levels. *Biophys. J.* **2003**, *85* (1), 361–369. https://doi.org/10.1016/S0006-3495(03)74480-4.
(26) Eckman, R.; MiiLLER, L.; Pines, A. DEUTERIUM DOUBLE-QUANTUM NMR WlH MAGIC ANGLE SPINNING. *Chem. Phys. Lett.* **1980**.
(27) Agarwal, V.; Faelber, K.; Schmieder, P.; Reif, B. High-Resolution Double-Quantum Deuterium Magic Angle Spinning Solid-State NMR Spectroscopy of Perdeuterated Proteins. *J. Am. Chem. Soc.* **2009**, *131* (1), 2–3. https://doi.org/10.1021/ja803620r.
(28) Hoatson, G. L.; Vold, R. L. 2H-NMR Spectroscopy of Solids and Liquid Crystals. In *Solid-State NMR III Organic Matter*; NMR Basic Principles and Progress; 1994; Vol. 32, pp 1–67.
(29) Schmidt-Rohr, K.; Spiess, H. W. *Multidimensional Solid-State NMR and Polymers*; Elsevier Science: Burlington, 2012.
(30) Hologne, M.; Chen, Z.; Reif, B. Characterization of Dynamic Processes Using Deuterium in Uniformly 2H,13C,15N Enriched Peptides by MAS Solid-State NMR. *J. Magn. Reson.* **2006**, *179* (1), 20–28. https://doi.org/10.1016/j.jmr.2005.10.014.
(31) Keniry, M. A. Solid-State Deuterium Nuclear Magnetic Resonance Spectroscopy of Proteins. *Methods Enzymol.* **1989**, *176*, 376–386.

(32) Shi, X.; Rienstra, C. M. Site-Specific Internal Motions in GB1 Protein Microcrystals Revealed by 3D ^{2}H–^{13}C–^{13}C Solid-State NMR Spectroscopy. *J. Am. Chem. Soc.* **2016**, *138* (12), 4105–4119. https://doi.org/10.1021/jacs.5b12974.
(33) Lalli, D.; Schanda, P.; Chowdhury, A.; Retel, J.; Hiller, M.; Higman, V. A.; Handel, L.; Agarwal, V.; Reif, B.; van Rossum, B.; Akbey, Ü.; Oschkinat, H. Three-Dimensional Deuterium-Carbon Correlation Experiments for High-Resolution Solid-State MAS NMR Spectroscopy of Large Proteins. *J. Biomol. NMR* **2011**, *51* (4), 477–485. https://doi.org/10.1007/s10858-011-9578-1.
(34) Bonev, B. B.; Morrow, M. R. Simple Probe for Variable Pressure Deuterium Nuclear Magnetic Resonance Studies of Soft Materials. *Rev. Sci. Instrum.* **1997**, *68* (4), 1827–1830. https://doi.org/10.1063/1.1148000.
(35) McDermott, A. E.; Creuzet, F. J.; Kolbert, A. C.; Griffin, R. G. High-Resolution Magic-Angle-Spinning NMR Spectra of Protons in Deuterated Solids. *J. Magn. Reson. 1969* **1992**, *98* (2), 408–413.
(36) Huber, M.; With, O.; Schanda, P.; Verel, R.; Ernst, M.; Meier, B. H. A Supplementary Coil for 2H Decoupling with Commercial HCN MAS Probes. *J. Magn. Reson.* **2012**, *214*, 76–80. https://doi.org/10.1016/j.jmr.2011.10.010.
(37) Akbey, Ü.; Nieuwkoop, A. J.; Wegner, S.; Voreck, A.; Kunert, B.; Bandara, P.; Engelke, F.; Nielsen, N. Chr.; Oschkinat, H. Quadruple-Resonance Magic-Angle Spinning NMR Spectroscopy of Deuterated Solid Proteins. *Angew. Chem. Int. Ed.* **2014**, *53* (9), 2438–2442. https://doi.org/10.1002/anie.201308927.
(38) Wei, D.; Akbey, Ü.; Paaske, B.; Oschkinat, H.; Reif, B.; Bjerring, M.; Nielsen, N. Chr. Optimal ^{2}H Rf Pulses and ^{2}H–^{13}C Cross-Polarization Methods for Solid-State ^{2}H MAS NMR of Perdeuterated Proteins. *J. Phys. Chem. Lett.* **2011**, *2* (11), 1289–1294. https://doi.org/10.1021/jz200511b.
(39) Akbey, Ü.; Nieuwkoop, A. J.; Wegner, S.; Voreck, A.; Kunert, B.; Bandara, P.; Engelke, F.; Nielsen, N. Chr.; Oschkinat, H. Quadruple-Resonance Magic-Angle Spinning NMR Spectroscopy of Deuterated Solid Proteins. *Angew. Chem. Int. Ed.* **2014**, *53* (9), 2438–2442. https://doi.org/10.1002/anie.201308927.
(40) Collier, K. A.; Sengupta, S.; Espinosa, C. A.; Kelly, J. E.; Kelz, J. I.; Martin, R. W. Design and Construction of a Quadruple-Resonance MAS NMR Probe for Investigation of Extensively Deuterated Biomolecules. *J. Magn. Reson.* **2017**, *285*, 8–17. https://doi.org/10.1016/j.jmr.2017.10.002.
(41) *Protein NMR Spectroscopy: Principles and Practice*, 2nd ed.; Cavanagh, J., Ed.; Academic Press: Amsterdam ; Boston, 2007.
(42) Akbey, Ü.; Camponeschi, F.; van Rossum, B.-J.; Oschkinat, H. Triple Resonance Cross-Polarization for More Sensitive 13C MAS NMR Spectroscopy of Deuterated Proteins. *ChemPhysChem* **2011**, *12* (11), 2092–2096. https://doi.org/10.1002/cphc.201100084.
(43) Akbey, Ü.; Rossum, B.-J. van; Oschkinat, H. Practical Aspects of High-Sensitivity Multidimensional 13C MAS NMR Spectroscopy of Perdeuterated Proteins. *J. Magn. Reson.* **2012**, *217*, 77–85. https://doi.org/10.1016/j.jmr.2012.02.015.
(44) Asami, S.; Szekely, K.; Schanda, P.; Meier, B. H.; Reif, B. Optimal Degree of Protonation for 1H Detection of Aliphatic Sites in Randomly Deuterated Proteins as a Function of the MAS Frequency. *J. Biomol. NMR* **2012**, *54* (2), 155–168. https://doi.org/10.1007/s10858-012-9659-9.

(45) Nieuwkoop, A. J.; Franks, W. T.; Rehbein, K.; Diehl, A.; Akbey, Ü.; Engelke, F.; Emsley, L.; Pintacuda, G.; Oschkinat, H. Sensitivity and Resolution of Proton Detected Spectra of a Deuterated Protein at 40 and 60 kHz Magic-Angle-Spinning. *J. Biomol. NMR* **2015**, *61* (2), 161–171. https://doi.org/10.1007/s10858-015-9904-0.
(46) Ghosh, M.; Rienstra, C. M. ^{1}H-Detected REDOR with Fast Magic-Angle Spinning of a Deuterated Protein. *J. Phys. Chem. B* **2017**, *121* (36), 8503–8511. https://doi.org/10.1021/acs.jpcb.7b07313.
(47) Reif, B. Deuterated Peptides and Proteins: Structure and Dynamics Studies by MAS Solid-State NMR. In *Protein NMR Techniques*; Shekhtman, A., Burz, D. S., Eds.; Humana Press: Totowa, NJ, 2012; Vol. 831, pp 279–301. https://doi.org/10.1007/978-1-61779-480-3_16.
(48) Collier, K. A.; Sengupta, S.; Espinosa, C. A.; Kelly, J. E.; Kelz, J. I.; Martin, R. W. Design and Construction of a Quadruple-Resonance MAS NMR Probe for Investigation of Extensively Deuterated Biomolecules. *J. Magn. Reson.* **2017**, *285*, 8–17. https://doi.org/10.1016/j.jmr.2017.10.002.
(49) Litvak, I. M.; Espinosa, C. A.; Shapiro, R. A.; Oldham, A. N.; Duong, V. V.; Martin, R. W. Pneumatic Switched Angle Spinning NMR Probe with Capacitively Coupled Double Saddle Coil. *J. Magn. Reson.* **2010**, *206* (2), 183–189. https://doi.org/10.1016/j.jmr.2010.07.001.
(50) Qian, C.; Pines, A.; Martin, R. W. Design and Construction of a Contactless Mobile RF Coil for Double Resonance Variable Angle Spinning NMR. *J. Magn. Reson.* **2007**, *188* (1), 183–189. https://doi.org/10.1016/j.jmr.2007.06.006.
(51) Brindley, A. J.; Martin, R. W. Effect of Divalent Cations on DMPC/DHPC Bicelle Formation and Alignment. *Langmuir* **2012**, *28* (20), 7788–7796. https://doi.org/10.1021/la300885u.
(52) Shapiro, R. A.; Brindley, A. J.; Martin, R. W. Thermal Stabilization of DMPC/DHPC Bicelles by Addition of Cholesterol Sulfate. *J. Am. Chem. Soc.* **2010**, *132* (33), 11406–11407. https://doi.org/10.1021/ja1041012.
(53) Norton-Baker, B.; Mehrabi, P.; Kwok, A. O.; Roskamp, K. W.; Rocha, M. A.; Sprague-Piercy, M. A.; von Stetten, D.; Miller, R. J. D.; Martin, R. W. Deamidation of the Human Eye Lens Protein γS-Crystallin Accelerates Oxidative Aging. *Structure* **2022**, S0969212622000831. https://doi.org/10.1016/j.str.2022.03.002.
(54) Espinosa, C. A.; Thureau, P.; Shapiro, R. A.; Litvak, I. M.; Martin, R. W. Modulation of Cross Polarization in Motionally Averaged Solids by Variable Angle Spinning NMR. *Chem. Phys. Lett.* **2011**, *508* (4–6), 314–319. https://doi.org/10.1016/j.cplett.2011.04.043.
(55) Brubaker, W. D.; Martin, R. W. 1H, 13C, and 15N Assignments of Wild-Type Human γS-Crystallin and Its Cataract-Related Variant γS-G18V. *Biomol. NMR Assign.* **2012**, *6* (1), 63–67. https://doi.org/10.1007/s12104-011-9326-1.
(56) Khago, D.; Wong, E. K.; Kingsley, C. N.; Alfredo Freites, J.; Tobias, D. J.; Martin, R. W. Increased Hydrophobic Surface Exposure in the Cataract-Related G18V Variant of Human γS-Crystallin. *Biochim. Biophys. Acta BBA - Gen. Subj.* **2016**, *1860* (1), 325–332. https://doi.org/10.1016/j.bbagen.2015.09.022.
(57) Sprague-Piercy, M. A.; Wong, E.; Roskamp, K. W.; Fakhoury, J. N.; Freites, J. A.; Tobias, D. J.; Martin, R. W. Human αB-Crystallin Discriminates between Aggregation-Prone and Function-Preserving Variants of a Client Protein. *Biochim. Biophys. Acta BBA - Gen. Subj.* **2020**, *1864* (3), 129502. https://doi.org/10.1016/j.bbagen.2019.129502.

(58) Roskamp, K. W.; Kozlyuk, N.; Sengupta, S.; Bierma, J. C.; Martin, R. W. Divalent Cations and the Divergence of *Bγ* -Crystallin Function. *Biochemistry* **2019**, *58* (45), 4505–4518. https://doi.org/10.1021/acs.biochem.9b00507.
(59) Sprague-Piercy, M. A.; Bierma, J. C.; Crosby, M. G.; Carpenter, B. P.; Takahashi, G. R.; Paulino, J.; Hung, I.; Zhang, R.; Kelly, J. E.; Kozlyuk, N.; Chen, X.; Butts, C. T.; Martin, R. W. The Droserasin 1 PSI: A Membrane-Interacting Antimicrobial Peptide from the Carnivorous Plant Drosera Capensis. *Biomolecules* **2020**, *10* (7), 1069. https://doi.org/10.3390/biom10071069.
(60) Butts, C. T.; Bierma, J. C.; Martin, R. W. Novel Proteases from the Genome of the Carnivorous Plant *Drosera Capensis* : Structural Prediction and Comparative Analysis: Novel Proteases from *Drosera Capensis*. *Proteins Struct. Funct. Bioinforma.* **2016**, *84* (10), 1517–1533. https://doi.org/10.1002/prot.25095.
(61) Wang, B.; Zhang, L.; Dai, T.; Qin, Z.; Lu, H.; Zhang, L.; Zhou, F. Liquid–Liquid Phase Separation in Human Health and Diseases. *Signal Transduct. Target. Ther.* **2021**, *6* (1), 290. https://doi.org/10.1038/s41392-021-00678-1.
(62) Babinchak, W. M.; Surewicz, W. K. Liquid–Liquid Phase Separation and Its Mechanistic Role in Pathological Protein Aggregation. *J. Mol. Biol.* **2020**, *432* (7), 1910–1925. https://doi.org/10.1016/j.jmb.2020.03.004.
(63) Chiti, F.; Dobson, C. M. Protein Misfolding, Functional Amyloid, and Human Disease. *Annu. Rev. Biochem.* **2006**, *75* (1), 333–366. https://doi.org/10.1146/annurev.biochem.75.101304.123901.
(64) Padrick, S. B.; Miranker, A. D. Islet Amyloid: Phase Partitioning and Secondary Nucleation Are Central to the Mechanism of Fibrillogenesis. *Biochemistry* **2002**, *41* (14), 4694–4703. https://doi.org/10.1021/bi0160462.
(65) Takemoto, L.; Sorensen, C. M. Protein–Protein Interactions and Lens Transparency. *Exp. Eye Res.* **2008**, *87* (6), 496–501. https://doi.org/10.1016/j.exer.2008.08.018.
(66) Croft, L. R. Developmental Changes in the Low NIolecular Weight Proteins of the Bovine Lens.
(67) Thomson, J. A.; Augusteyn, R. C. Ontogeny of Human Lens Crystallins. *Exp. Eye Res.* **1985**, *40* (3), 393–410. https://doi.org/10.1016/0014-4835(85)90152-6.
(68) Robinson, N. E.; Lampi, K. J.; Speir, J. P.; Kruppa, G.; Easterling, M.; Robinson, A. B. Quantitative Measurement of Young Human Eye Lens Crystallins by Direct Injection Fourier Transform Ion Cyclotron Resonance Mass Spectrometry. *Mol. Vis.* 8.
(69) Benedek, G. B. Theory of Transparency of the Eye. *Appl. Opt.* **1971**, *10* (3), 459. https://doi.org/10.1364/AO.10.000459.
(70) Delaye, M.; Tardieu, A. Short-Range Order of Crystallin Proteins Accounts for Eye Lens Transparency. *Nature* **1983**, *302* (5907), 415–417. https://doi.org/10.1038/302415a0.
(71) Brubaker, W. D.; Martin, R. W. 1H, 13C, and 15N Assignments of Wild-Type Human γS-Crystallin and Its Cataract-Related Variant γS-G18V. *Biomol. NMR Assign.* **2012**, *6* (1), 63–67. https://doi.org/10.1007/s12104-011-9326-1.
(72) Craghill, J.; Cronshaw, A. D.; Harding, J. J. The Identification of a Reaction Site of Glutathione Mixed-Disulphide Formation on γ S-Crystallin in Human Lens. **2004**, 6.
(73) Mills, I. A.; Flaugh, S. L.; Kosinski-Collins, M. S.; King, J. A. Folding and Stability of the Isolated Greek Key Domains of the Long-Lived Human Lens Proteins γD-Crystallin and γS-Crystallin. *Protein Sci.* **2007**, *16* (11), 2427–2444. https://doi.org/10.1110/ps.072970207.

(74) Brubaker, W. D.; Martin, R. W. 1H, 13C, and 15N Assignments of Wild-Type Human γS-Crystallin and Its Cataract-Related Variant γS-G18V. *Biomol. NMR Assign.* **2012**, *6* (1), 63–67. https://doi.org/10.1007/s12104-011-9326-1.
(75) Brubaker, W. D.; Freites, J. A.; Golchert, K. J.; Shapiro, R. A.; Morikis, V.; Tobias, D. J.; Martin, R. W. Separating Instability from Aggregation Propensity in γS-Crystallin Variants. *Biophys. J.* **2011**, *100* (2), 498–506. https://doi.org/10.1016/j.bpj.2010.12.3691.
(76) Pande, A.; Pande, J.; Asherie, N.; Lomakin, A.; Ogun, O.; King, J.; Benedek, G. B. Crystal Cataracts: Human Genetic Cataract Caused by Protein Crystallization. *Proc. Natl. Acad. Sci.* **2001**, *98* (11), 6116–6120. https://doi.org/10.1073/pnas.101124798.
(77) Evans, P.; Wyatt, K.; Wistow, G. J.; Bateman, O. A.; Wallace, B. A.; Slingsby, C. The P23T Cataract Mutation Causes Loss of Solubility of Folded γD-Crystallin. *J. Mol. Biol.* **2004**, *343* (2), 435–444. https://doi.org/10.1016/j.jmb.2004.08.050.
(78) McManus, J. J.; Lomakin, A.; Ogun, O.; Pande, A.; Basan, M.; Pande, J.; Benedek, G. B. Altered Phase Diagram Due to a Single Point Mutation in Human D-Crystallin. *Proc. Natl. Acad. Sci.* **2007**, *104* (43), 16856–16861. https://doi.org/10.1073/pnas.0707412104.
(79) Horwitz, J. A-Crystallin Can Function as a Molecular Chaperone. *Proc Natl Acad Sci USA* **1992**, 5.
(80) Tanaka, N.; Tanaka, R.; Tokuhara, M.; Kunugi, S.; Lee, Y.-F.; Hamada, D. Amyloid Fibril Formation and Chaperone-like Activity of Peptides from αA-Crystallin. *Biochemistry* **2008**, *47* (9), 2961–2967. https://doi.org/10.1021/bi701823g.
(81) Takemoto, L.; Ponce, A.; Sorensen, C. M. Age-Dependent Association of Gamma-Crystallins with Aged Alpha-Crystallins from Old Bovine Lens. *Mol. Vis.* **2008**, *14*, 970–974.
(82) Kingsley, C. N.; Brubaker, W. D.; Markovic, S.; Diehl, A.; Brindley, A. J.; Oschkinat, H.; Martin, R. W. Preferential and Specific Binding of Human αB-Crystallin to a Cataract-Related Variant of γS-Crystallin. *Structure* **2013**, *21* (12), 2221–2227. https://doi.org/10.1016/j.str.2013.09.017.
(83) Sprague-Piercy, M. A.; Rocha, M. A.; Kwok, A. O.; Martin, R. W. α-Crystallins in the Vertebrate Eye Lens: Complex Oligomers and Molecular Chaperones. *Annu. Rev. Phys. Chem.* **2021**, *72* (1), 143–163. https://doi.org/10.1146/annurev-physchem-090419-121428.
(84) Hanson, S. R. A.; Hasan, A.; Smith, D. L.; Smith, J. B. The Major in Vivo Modifications of the Human Water-Insoluble Lens Crystallins Are Disulfide Bonds, Deamidation, Methionine Oxidation and Backbone Cleavage. *Exp. Eye Res.* **2000**, *71* (2), 195–207. https://doi.org/10.1006/exer.2000.0868.
(85) Harding, J. J. Viewing Molecular Mechanisms of Ageing through a Lens. *Ageing Res. Rev.* **2002**, *1* (3), 465–479. https://doi.org/10.1016/S1568-1637(02)00012-0.
(86) Sharma, K. K.; Santhoshkumar, P. Lens Aging: Effects of Crystallins. *Biochim. Biophys. Acta BBA - Gen. Subj.* **2009**, *1790* (10), 1095–1108. https://doi.org/10.1016/j.bbagen.2009.05.008.
(87) Grant, C. V.; Wu, C. H.; Opella, S. J. Probes for High Field Solid-State NMR of Lossy Biological Samples. *J. Magn. Reson.* **2010**, *204* (2), 180–188. https://doi.org/10.1016/j.jmr.2010.03.011.
(88) Martin, R. W.; Paulson, E. K.; Zilm, K. W. Design of a Triple Resonance Magic Angle Sample Spinning Probe for High Field Solid State Nuclear Magnetic Resonance. *Rev. Sci. Instrum.* **2003**, *74* (6), 3045–3061. https://doi.org/10.1063/1.1571951.

(89) Martin, R. W.; Kelly, J. E.; Collier, K. A. Spatial Reorientation Experiments for NMR of Solids and Partially Oriented Liquids. *Prog. Nucl. Magn. Reson. Spectrosc.* **2015**, *90–91*, 92–122. https://doi.org/10.1016/j.pnmrs.2015.10.001.
(90) Martin, R. W.; Kelly, J. E.; Collier, K. A. Spatial Reorientation Experiments for NMR of Solids and Partially Oriented Liquids. *Prog. Nucl. Magn. Reson. Spectrosc.* **2015**, *90–91*, 92–122. https://doi.org/10.1016/j.pnmrs.2015.10.001.
(91) Bax, A.; Szeverenyi, N. M.; Maciel, G. E. Chemical Shift Anisotropy in Powdered Solids Studied by 2D FT NMR with Flipping of the Spinning Axis. *J. Magn. Reson. 1969* **1983**, *55* (3), 494–497.
(92) Becker, E. D. A Brief History of Nuclear Magnetic Resonance. *Anal. Chem.* **1993**, *65* (6), 205–302.
(93) Morris, G. A. Varian Associates and the Birth of Commercial NMR Spectroscopy. *J. Magn. Reson.* **2019**, *306*, 12–16. https://doi.org/10.1016/j.jmr.2019.07.039.
(94) Bloch, F. Nuclear Induction. *Phys. Rev.* **1946**, *70* (7–8), 460–474. https://doi.org/10.1103/PhysRev.70.460.
(95) Purcell, E. M.; Torrey, H. C.; Pound, R. V. Resonance Absorption by Nuclear Magnetic Moments in a Solid. *Phys. Rev.* **1946**, *69* (1–2), 37–38. https://doi.org/10.1103/PhysRev.69.37.
(96) Reinhardt, C. A Lead User of Instruments in Science: John D. Roberts and the Adaptation of Nuclear Magnetic Resonance to Organic Chemistry, 1955–1975. *Isis* **2006**, *97* (2), 205–236. https://doi.org/10.1086/504732.
(97) Lauterbur, P. C. C13 Nuclear Magnetic Resonance Spectra. *J. Chem. Phys.* **1957**, *26* (1), 217–218. https://doi.org/10.1063/1.1743253.
(98) Shoolery, J. N.; Rogers, M. T. Nuclear Magnetic Resonance Spectra of Steroids. **1958**.
(99) Anet, F. A. L.; Bourn, A. J. R. Nuclear Magnetic Resonance Spectral Assignments from Nuclear Overhauser Effects [1]. *J. Am. Chem. Soc.* **1965**, *87* (22), 5250–5251. https://doi.org/10.1021/ja00950a048.
(100) Kuznetsov, S.; Paulos, E. Rise of the Expert Amateur: DIY Projects, Communities, and Cultures. In *Proceedings of the 6th Nordic Conference on Human-Computer Interaction: Extending Boundaries*; ACM: Reykjavik Iceland, 2010; pp 295–304. https://doi.org/10.1145/1868914.1868950.
(101) Riegel, S. D.; Leskowitz, G. M. Benchtop NMR Spectrometers in Academic Teaching. *TrAC Trends Anal. Chem.* **2016**, *83*, 27–38. https://doi.org/10.1016/j.trac.2016.01.001.
(102) Song, Y.-Q.; Utsuzawa, S.; Tang, Y. Low Fields but High Impact: Ex-Situ NMR and MRI. *J. Magn. Reson.* **2019**, *306*, 109–111. https://doi.org/10.1016/j.jmr.2019.07.026.
(103) Meyer, K.; Kern, S.; Zientek, N.; Guthausen, G.; Maiwald, M. Process Control with Compact NMR. *TrAC Trends Anal. Chem.* **2016**, *83*, 39–52. https://doi.org/10.1016/j.trac.2016.03.016.
(104) Singh, K.; Blümich, B. NMR Spectroscopy with Compact Instruments. *TrAC Trends Anal. Chem.* **2016**, *83*, 12–26. https://doi.org/10.1016/j.trac.2016.02.014.
(105) Blümich, B. Introduction to Compact NMR: A Review of Methods. *TrAC Trends Anal. Chem.* **2016**, *83*, 2–11. https://doi.org/10.1016/j.trac.2015.12.012.
(106) Mercer, C.; Leech, D. Cost-Effective Wireless Microcontroller for Internet Connectivity of Open-Source Chemical Devices. *J. Chem. Educ.* **2018**, *95* (7), 1221–1225. https://doi.org/10.1021/acs.jchemed.8b00200.

(107) Grinias, J. P.; Whitfield, J. T.; Guetschow, E. D.; Kennedy, R. T. An Inexpensive, Open-Source USB Arduino Data Acquisition Device for Chemical Instrumentation. *J. Chem. Educ.* **2016**, *93* (7), 1316–1319. https://doi.org/10.1021/acs.jchemed.6b00262.
(108) Zhang, Q.; Brode, L.; Cao, T.; Thompson, J. E. Learning Laboratory Chemistry through Electronic Sensors, a Microprocessor, and Student Enabling Software: A Preliminary Demonstration. *J. Chem. Educ.* **2017**, *94* (10), 1562–1566. https://doi.org/10.1021/acs.jchemed.7b00172.
(109) Urban, P. L. Open-Source Electronics As a Technological Aid in Chemical Education. *J. Chem. Educ.* **2014**, *91* (5), 751–752. https://doi.org/10.1021/ed4009073.
(110) Foster, S. W.; Alirangues, M. J.; Naese, J. A.; Constans, E.; Grinias, J. P. A Low-Cost, Open-Source Digital Stripchart Recorder for Chromatographic Detectors Using a Raspberry Pi. *J. Chromatogr. A* **2019**, *1603*, 396–400. https://doi.org/10.1016/j.chroma.2019.03.070.
(111) Rowe, A. A.; Bonham, A. J.; White, R. J.; Zimmer, M. P.; Yadgar, R. J.; Hobza, T. M.; Honea, J. W.; Ben-Yaacov, I.; Plaxco, K. W. CheapStat: An Open-Source, "Do-It-Yourself" Potentiostat for Analytical and Educational Applications. *PLoS ONE* **2011**, *6* (9), e23783. https://doi.org/10.1371/journal.pone.0023783.
(112) Dryden, M. D. M.; Wheeler, A. R. DStat: A Versatile, Open-Source Potentiostat for Electroanalysis and Integration. *PLOS ONE* **2015**, *10* (10), e0140349. https://doi.org/10.1371/journal.pone.0140349.
(113) Glasscott, M. W.; Verber, M. D.; Hall, J. R.; Pendergast, A. D.; McKinney, C. J.; Dick, J. E. SweepStat: A Build-It-Yourself, Two-Electrode Potentiostat for Macroelectrode and Ultramicroelectrode Studies. *J. Chem. Educ.* **2020**, *97* (1), 265–270. https://doi.org/10.1021/acs.jchemed.9b00893.
(114) Grasse, E. K.; Torcasio, M. H.; Smith, A. W. Teaching UV–Vis Spectroscopy with a 3D-Printable Smartphone Spectrophotometer. *J. Chem. Educ.* **2016**, *93* (1), 146–151. https://doi.org/10.1021/acs.jchemed.5b00654.
(115) Meloni, G. N. 3D Printed and Microcontrolled: The One Hundred Dollars Scanning Electrochemical Microscope. *Anal. Chem.* **2017**, *89* (17), 8643–8649. https://doi.org/10.1021/acs.analchem.7b01764.
(116) Gross, B.; Lockwood, S. Y.; Spence, D. M. Recent Advances in Analytical Chemistry by 3D Printing. *Anal. Chem.* **2017**, *89* (1), 57–70. https://doi.org/10.1021/acs.analchem.6b04344.
(117) Spano, M. B.; Tran, B. H.; Majumdar, S.; Weiss, G. A. 3D-Printed Labware for High-Throughput Immobilization of Enzymes. *J. Org. Chem.* **2020**, *85* (13), 8480–8488. https://doi.org/10.1021/acs.joc.0c00789.
(118) Pinger, C. W.; Geiger, M. K.; Spence, D. M. Applications of 3D-Printing for Improving Chemistry Education. *J. Chem. Educ.* **2020**, *97* (1), 112–117. https://doi.org/10.1021/acs.jchemed.9b00588.
(119) Tseytlin, O.; Guggilapu, P.; Bobko, A. A.; AlAhmad, H.; Xu, X.; Epel, B.; O'Connell, R.; Hoblitzell, E. H.; Eubank, T. D.; Khramtsov, V. V.; Driesschaert, B.; Kazkaz, E.; Tseytlin, M. Modular Imaging System: Rapid Scan EPR at 800 MHz. *J. Magn. Reson.* **2019**, *305*, 94–103. https://doi.org/10.1016/j.jmr.2019.06.003.
(120) Niemöller, A.; Jakes, P.; Kayser, S.; Lin, Y.; Lehnert, W.; Granwehr, J. 3D Printed Sample Holder for In-Operando EPR Spectroscopy on High Temperature Polymer

Electrolyte Fuel Cells. *J. Magn. Reson.* **2016**, *269*, 157–161. https://doi.org/10.1016/j.jmr.2016.06.003.
(121) Herrmann, K.-H.; Gärtner, C.; Güllmar, D.; Krämer, M.; Reichenbach, J. R. 3D Printing of MRI Compatible Components: Why Every MRI Research Group Should Have a Low-Budget 3D Printer. *Med. Eng. Phys.* **2014**, *36* (10), 1373–1380. https://doi.org/10.1016/j.medengphy.2014.06.008.
(122) Sarracanie, M.; LaPierre, C. D.; Salameh, N.; Waddington, D. E. J.; Witzel, T.; Rosen, M. S. Low-Cost High-Performance MRI. *Sci. Rep.* **2015**, *5* (1). https://doi.org/10.1038/srep15177.
(123) Paulson, E. K.; Martin, R. W.; Zilm, K. W. Cross Polarization, Radio Frequency Field Homogeneity, and Circuit Balancing in High Field Solid State NMR Probes. *J. Magn. Reson.* **2004**, *171* (2), 314–323. https://doi.org/10.1016/j.jmr.2004.09.009.
(124) Barnes, A. B.; Mak-Jurkauskas, M. L.; Matsuki, Y.; Bajaj, V. S.; van der Wel, P. C. A.; DeRocher, R.; Bryant, J.; Sirigiri, J. R.; Temkin, R. J.; Lugtenburg, J.; Herzfeld, J.; Griffin, R. G. Cryogenic Sample Exchange NMR Probe for Magic Angle Spinning Dynamic Nuclear Polarization. *J. Magn. Reson.* **2009**, *198* (2), 261–270. https://doi.org/10.1016/j.jmr.2009.03.003.
(125) Chen, P.; Albert, B. J.; Gao, C.; Alaniva, N.; Price, L. E.; Scott, F. J.; Saliba, E. P.; Sesti, E. L.; Judge, P. T.; Fisher, E. W.; Barnes, A. B. Magic Angle Spinning Spheres. *Sci. Adv.* **2018**, *4* (9), eaau1540. https://doi.org/10.1126/sciadv.aau1540.
(126) Lederle, F.; Meyer, F.; Kaldun, C.; Namyslo, J. C.; Hübner, E. G. Sonogashira Coupling in 3D-Printed NMR Cuvettes: Synthesis and Properties of Arylnaphthylalkynes. *New J. Chem.* **2017**, *41* (5), 1925–1932. https://doi.org/10.1039/C6NJ03614G.
(127) Gor'kov, P. L. Construction of 1H-Detect 100kHz 1H/X/Y MAS Probe for Proteins and Small Molecules, 2019.
(128) Vinding, M. S.; Kessler, T. O.; Vosegaard, T. A Simple Low-Cost Single-Crystal NMR Setup. *J. Magn. Reson.* **2016**, *269*, 120–127. https://doi.org/10.1016/j.jmr.2016.06.004.
(129) Xie, J.; You, X.; Huang, Y.; Ni, Z.; Wang, X.; Li, X.; Yang, C.; Zhang, D.; Chen, H.; Sun, H.; Chen, Z. 3D-Printed Integrative Probeheads for Magnetic Resonance. *Nat. Commun.* **2020**, *11* (1). https://doi.org/10.1038/s41467-020-19711-y.
(130) Chen, P.; Albert, B. J.; Gao, C.; Alaniva, N.; Price, L. E.; Scott, F. J.; Saliba, E. P.; Sesti, E. L.; Judge, P. T.; Fisher, E. W.; Barnes, A. B. Magic Angle Spinning Spheres. *Sci. Adv.* **2018**, *4* (9), eaau1540. https://doi.org/10.1126/sciadv.aau1540.
(131) McGuire, K. J.; Long, E. Fabrication of 3D-Printed PCTFE Material Cups for Dynamic Nuclear Polarization Target at Cryogenic Temperatures. *ArXiv191013254 Nucl-Ex Physicsphysics* **2019**.
(132) Dasgupta, S.; Hale, W.; Monroy-Hernández, A.; Hill, B. M. Remixing as a Pathway to Computational Thinking. In *Proceedings of the 19th ACM Conference on Computer-Supported Cooperative Work & Social Computing*; ACM: San Francisco California USA, 2016; pp 1438–1449. https://doi.org/10.1145/2818048.2819984.
(133) Hartmann, B.; Doorley, S.; Klemmer, S. R. Hacking, Mashing, Gluing: Understanding Opportunistic Design. *IEEE Pervasive Comput.* **2008**, *7* (3), 46–54. https://doi.org/10.1109/MPRV.2008.54.
(134) Brandt, J.; Guo, P. J.; Lewenstein, J.; Dontcheva, M.; Klemmer, S. R. Two Studies of Opportunistic Programming: Interleaving Web Foraging, Learning, and Writing Code. **2009**.

(135) Hudson, N.; Alcock, C.; Chilana, P. K. Understanding Newcomers to 3D Printing: Motivations, Workflows, and Barriers of Casual Makers. In *Proceedings of the 2016 CHI Conference on Human Factors in Computing Systems*; ACM: San Jose California USA, 2016; pp 384–396. https://doi.org/10.1145/2858036.2858266.
(136) Baldassi, S.; Cheng, G. T.; Chan, J.; Tian, M.; Christie, T.; Short, M. T. Exploring Immersive AR Instructions for Procedural Tasks: The Role of Depth, Motion, and Volumetric Representations. In *2016 IEEE International Symposium on Mixed and Augmented Reality (ISMAR-Adjunct)*; IEEE: Merida, Yucatan, Mexico, 2016; pp 300–305. https://doi.org/10.1109/ISMAR-Adjunct.2016.0101.
(137) Blattgerste, J.; Strenge, B.; Renner, P.; Pfeiffer, T.; Essig, K. Comparing Conventional and Augmented Reality Instructions for Manual Assembly Tasks. In *Proceedings of the 10th International Conference on PErvasive Technologies Related to Assistive Environments*; ACM: Island of Rhodes Greece, 2017; pp 75–82. https://doi.org/10.1145/3056540.3056547.
(138) Kant, J. M.; Scheiter, K.; Oschatz, K. How to Sequence Video Modeling Examples and Inquiry Tasks to Foster Scientific Reasoning. *Learn. Instr.* **2017**, *52*, 46–58. https://doi.org/10.1016/j.learninstruc.2017.04.005.
(139) Fiorella, L.; Van Gog, T.; Hoogerheide, V.; Mayer, R. E. It's All a Matter of Perspective: Viewing First-Person Video Modeling Examples Promotes Learning of an Assembly Task. *J. Educ. Psychol.* **2017**, *109* (5), 653–665. https://doi.org/10.1037/edu0000161.
(140) Strobel, J.; Zimmerman, G. W. Effectiveness of Paper, VR and Stereo-VR in the Delivery of Instructions for Assembly Tasks. *Int. J. Comput. Inf. Syst. Ind. Manag. Appl.* **2011**, *3*, 578–585.
(141) Oehlberg, L.; Willett, W.; Mackay, W. E. Patterns of Physical Design Remixing in Online Maker Communities. In *Proceedings of the 33rd Annual ACM Conference on Human Factors in Computing Systems*; ACM: Seoul Republic of Korea, 2015; pp 639–648. https://doi.org/10.1145/2702123.2702175.
(142) Flath, C. M.; Friesike, S.; Wirth, M.; Thiesse, F. Copy, Transform, Combine: Exploring the Remix as a Form of Innovation. *J. Inf. Technol.* **2017**, *32* (4), 306–325. https://doi.org/10.1057/s41265-017-0043-9.
(143) Morreale, F.; Moro, G.; Chamberlain, A.; Benford, S.; McPherson, A. P. Building a Maker Community Around an Open Hardware Platform. In *Proceedings of the 2017 CHI Conference on Human Factors in Computing Systems*; ACM: Denver Colorado USA, 2017; pp 6948–6959. https://doi.org/10.1145/3025453.3026056.
(144) Kim, J.; Guo, A.; Yeh, T.; Hudson, S. E.; Mankoff, J. Understanding Uncertainty in Measurement and Accommodating Its Impact in 3D Modeling and Printing. In *Proceedings of the 2017 Conference on Designing Interactive Systems*; ACM: Edinburgh United Kingdom, 2017; pp 1067–1078. https://doi.org/10.1145/3064663.3064690.
(145) Morocz, R.; Levy, B.; Forest, C.; Nagel, R.; Newstetter, W.; Talley, K.; Linsey, J. Relating Student Participation in University Maker Spaces to Their Engineering Design Self-Efficacy. In *2016 ASEE Annual Conference & Exposition Proceedings*; ASEE Conferences: New Orleans, Louisiana, 2016; p 26070. https://doi.org/10.18260/p.26070.
(146) Kwon, B.-R.; Lee, J. What Makes a Maker: The Motivation for the Maker Movement in ICT. *Inf. Technol. Dev.* **2017**, *23* (2), 318–335. https://doi.org/10.1080/02681102.2016.1238816.

(147) Aragon, C. R.; Poon, S. S. A Tale of Two Online Communities: Fostering Collaboration and Creativity in Scientists and Children.
(148) Guo, N.; Leu, M. C. Additive Manufacturing: Technology, Applications and Research Needs. *Front Mech Eng* **2013**, *8* (3), 215–243.
(149) Tošner, Z.; Purea, A.; Struppe, J. O.; Wegner, S.; Engelke, F.; Glaser, S. J.; Reif, B. Radiofrequency Fields in MAS Solid State NMR Probes. *J. Magn. Reson.* **2017**, *284*, 20–32. https://doi.org/10.1016/j.jmr.2017.09.002.
(150) Hoult, D. I.; Richards, R. E. The Signal-to-Noise Ratio of the Nuclear Magnetic Resonance Experiment. *J. Magn. Reson. 1969* **1976**, *24* (1), 71–85.
(151) Gupta, R.; Hou, G.; Polenova, T.; Vega, A. J. RF Inhomogeneity and How It Controls CPMAS. *Solid State Nucl. Magn. Reson.* **2015**, *72*, 17–26. https://doi.org/10.1016/j.ssnmr.2015.09.005.
(152) Idziak, S.; Haeberlen, U. Design and Construction of a High Homogeneity Rf Coil for Solid-State Multiple-Pulse NMR. *J. Magn. Reson. 1969* **1982**, *50* (2), 281–288.
(153) Mark Leifer. RF Solenoid with Extended Equiripple Field Profile. *J. Magn. Reson.* **1993**, No. 105, 1–6.
(154) Privalov, A. F.; Dvinskikh, S. V.; Vieth, H.-M. Coil Design for Large-Volume High-B1Homogeneity for Solid-State NMR Applications. *J. Magn. Reson. A* **1996**, *123* (2), 157–160.
(155) Engelke, F. Electromagnetic Wave Compression and Radio Frequency Homogeneity in NMR Solenoidal Coils: Computational Approach. *Concepts Magn. Reson.* **2002**, *15* (2), 129–155. https://doi.org/10.1002/cmr.10029.
(156) Doty, F. D.; Kulkarni, J.; Turner, C.; Entzminger, G.; Bielecki, A. Using a Cross-Coil to Reduce RF Heating by an Order of Magnitude in Triple-Resonance Multinuclear MAS at High Fields. *J. Magn. Reson.* **2006**, *182* (2), 239–253. https://doi.org/10.1016/j.jmr.2006.06.031.
(157) Krahn, A.; Priller, U.; Emsley, L.; Engelke, F. Resonator with Reduced Sample Heating and Increased Homogeneity for Solid-State NMR. *J. Magn. Reson.* **2008**, *191* (1), 78–92. https://doi.org/10.1016/j.jmr.2007.12.004.
(158) Maier Jr, L. C.; Slater, J. C. Field Strength Measurements in Resonant Cavities. *J. Appl. Phys.* **1952**, *23* (1), 68–77.
(159) Odedra, S.; Wimperis, S. Imaging of the B1 Distribution and Background Signal in a MAS NMR Probehead Using Inhomogeneous B0 and B1 Fields. *J. Magn. Reson.* **2013**, *231*, 95–99. https://doi.org/10.1016/j.jmr.2013.04.002.
(160) Nagashima, H.; Trébosc, J.; Lafon, O.; Pourpoint, F.; Paluch, P.; Potrzebowski, M. J.; Amoureux, J.-P. Imaging the Spatial Distribution of Radiofrequency Field, Sample and Temperature in MAS NMR Rotor. *Solid State Nucl. Magn. Reson.* **2017**, *87*, 137–142.
(161) Grant, C. V.; Yang, Y.; Glibowicka, M.; Wu, C. H.; Park, S. H.; Deber, C. M.; Opella, S. J. A Modified Alderman–Grant Coil Makes Possible an Efficient Cross-Coil Probe for High Field Solid-State NMR of Lossy Biological Samples. *J. Magn. Reson.* **2009**, *201* (1), 87–92. https://doi.org/10.1016/j.jmr.2009.08.009.
(162) Sun, Y.; Maciel, G. E. The Tilted Coil for NMR Experiments. *J. Magn. Reson.* **1993**, No. 105, 145–150.
(163) Sakellariou, D.; Meriles, C. A.; Moulé, A.; Pines, A. Variable Rotation Composite Pulses for High Resolution Nuclear Magnetic Resonance Using Inhomogeneous Magnetic and

Radiofrequency Fields. *Chem. Phys. Lett.* **2002**, *363* (1–2), 25–33. https://doi.org/10.1016/S0009-2614(02)01116-8.
(164) Šmelko, A.; Blahut, J.; Reif, B.; Tošner, Z. Performance of the Cross-Polarization Experiment in Conditions of Radiofrequency Field Inhomogeneity and Slow to Ultrafast Magic Angle Spinning (MAS). *Magn. Reson.* **2023**, *4* (2), 199–215. https://doi.org/10.5194/mr-4-199-2023.
(165) Purusottam, R. N.; Bodenhausen, G.; Tekely, P. Sensitivity Improvement during Heteronuclear Spin Decoupling in Solid-State Nuclear Magnetic Resonance Experiments at High Spinning Frequencies and Moderate Radio-Frequency Amplitudes. *Chem. Phys. Lett.* **2014**, *614*, 220–225.
(166) Horne, D.; Kendrick, R.; Yannoni, C. Bond Length Measurements in Amorphous Solids by Nutation NMR Spectroscopy: The Role of Rf Field Homogeneity. *J. Magn. Reson. 1969* **1983**, *52* (2), 299–304.
(167) Campbell, G. C.; Galya, L. G.; Beeler, A. J.; English, A. D. Effect of Rf Inhomogeneity upon Quantitative Solid-State NMR Measurements. *J. Magn. Reson.* **1995**, 225–228.
(168) Nishimura, K.; Fu, R.; Cross, T. A. The Effect of RF Inhomogeneity on Heteronuclear Dipolar Recoupling in Solid State NMR: Practical Performance of SFAM and REDOR. *J. Magn. Reson.* **2001**, *152* (2), 227–233. https://doi.org/10.1006/jmre.2001.2410.
(169) Charmont, P.; Sakellariou, D.; Emsley, L. Sample Restriction Using Radiofrequency Field Selective Pulses in High-Resolution Solid-State NMR. *J. Magn. Reson.* **2002**, *154* (1), 136–141. https://doi.org/10.1006/jmre.2001.2467.
(170) Alderman, D. W.; Grant, D. M. An Efficient Decoupler Coil Design Which Reduces Heating in Conductive Samples in Superconducting Spectrometers. *J. Magn. Reson. 1969* **1979**, *36* (3), 447–451.
(171) Grant, C. V.; Sit, S.-L.; De Angelis, A. A.; Khuong, K. S.; Wu, C. H.; Plesniak, L. A.; Opella, S. J. An Efficient 1H/31P Double-Resonance Solid-State NMR Probe That Utilizes a Scroll Coil. *J. Magn. Reson.* **2007**, *188* (2), 279–284. https://doi.org/10.1016/j.jmr.2007.06.016.
(172) Larsen, F.; Daugaard, P.; Jakobsen, H.; Nielsen, N. Improving RF Field Homogeneity in Solid-State MAS NMR Using a Loop-Gap Resonator. *J. Magn. Reson.* **1995**, *Series A* (115), 283–286.
(173) Gor'kov, P. L.; Chekmenev, E. Y.; Li, C.; Cotten, M.; Buffy, J. J.; Traaseth, N. J.; Veglia, G.; Brey, W. W. Using Low-E Resonators to Reduce RF Heating in Biological Samples for Static Solid-State NMR up to 900MHz. *J. Magn. Reson.* **2007**, *185* (1), 77–93. https://doi.org/10.1016/j.jmr.2006.11.008.
(174) Stringer, J. A.; Bronnimann, C. E.; Mullen, C. G.; Zhou, D. H.; Stellfox, S. A.; Li, Y.; Williams, E. H.; Rienstra, C. M. Reduction of RF-Induced Sample Heating with a Scroll Coil Resonator Structure for Solid-State NMR Probes. *J. Magn. Reson.* **2005**, *173* (1), 40–48. https://doi.org/10.1016/j.jmr.2004.11.015.
(175) Mispelter, J.; Lupu, M.; Briguet, A. Chapter 8: Homogeneous Resonators. In *NMR Probeheads for Biophysical and Biomedical Experiments*; Imperial College Press, 2015; pp 467–600.
(176) Doty, F. D. Guide to Simulating Complex NMR Probe Circuits. *Concepts Magn. Reson. Part A* **2018**, *47A* (2), e21463. https://doi.org/10.1002/cmr.a.21463.

(177) Long, Z.; Ruthford, J.; Opella, S. J. 3D Printed Sample Tubes for Solid-State NMR Experiments. *J. Magn. Reson.* **2021**, *327*, 106957. https://doi.org/10.1016/j.jmr.2021.106957.
(178) Xie, J.; You, X.; Huang, Y.; Ni, Z.; Wang, X.; Li, X.; Yang, C.; Zhang, D.; Chen, H.; Sun, H.; Chen, Z. 3D-Printed Integrative Probeheads for Magnetic Resonance. *Nat. Commun.* **2020**, *11* (1), 5793. https://doi.org/10.1038/s41467-020-19711-y.
(179) Uribe, J. L.; Jimenez, M.; Kelz, J. I.; Liang, J.; Martin, R. W. Automated Test Apparatus for Bench-Testing the Magnetic Field Homogeneity of NMR Transceiver Coils. *preprint* **2023**.
(180) Vega, A. J. Controlling the Effects of Pulse Transients and RF Inhomogeneity in Phase-Modulated Multiple-Pulse Sequences for Homonuclear Decoupling in Solid-State Proton NMR. *J. Magn. Reson.* **2004**, *170* (1), 22–41. https://doi.org/10.1016/j.jmr.2004.05.017.
(181) Macor, A.; De Rijk, E.; Boero, G.; Ansermet, J.-Ph.; Alberti, S. Millimeter Waves for NMR Enhancement. In *35th International Conference on Infrared, Millimeter, and Terahertz Waves*; IEEE: Rome, Italy, 2010; pp 1–2. https://doi.org/10.1109/ICIMW.2010.5612362.
(182) McNeill, S. A.; Gor'kov, P. L.; Shetty, K.; Brey, W. W.; Long, J. R. A Low-E Magic Angle Spinning Probe for Biological Solid State NMR at 750MHz. *J. Magn. Reson.* **2009**, *197* (2), 135–144. https://doi.org/10.1016/j.jmr.2008.12.008.
(183) Aebischer, K.; Tošner, Z.; Ernst, M. Effects of Radial Radio-Frequency Field Inhomogeneity on MAS Solid-State NMR Experiments. *Magn. Reson.* **2021**, *2* (1), 523–543. https://doi.org/10.5194/mr-2-523-2021.
(184) Osborn Popp, T. M.; Däpp, A.; Gao, C.; Chen, P.-H.; Price, L. E.; Alaniva, N. H.; Barnes, A. B. Highly Stable Magic Angle Spinning Spherical Rotors. *Magn. Reson.* **2020**, *1* (1), 97–103. https://doi.org/10.5194/mr-1-97-2020.
(185) Gao, C.; Judge, P. T.; Sesti, E. L.; Price, L. E.; Alaniva, N.; Saliba, E. P.; Albert, B. J.; Soper, N. J.; Chen, P.-H.; Barnes, A. B. Four Millimeter Spherical Rotors Spinning at 28 kHz with Double-Saddle Coils for Cross Polarization NMR. *J. Magn. Reson.* **2019**, *303*, 1–6. https://doi.org/10.1016/j.jmr.2019.03.006.
(186) Banks, D.; Michael, B.; Golota, N.; Griffin, R. G. 3D-Printed Stators & Drive Caps for Magic-Angle Spinning NMR. *J. Magn. Reson.* **2022**, *335*, 107126. https://doi.org/10.1016/j.jmr.2021.107126.
(187) Xu, K.; Pecher, O.; Braun, M.; Schmedt Auf Der Günne, J. Stable Magic Angle Spinning with Low-Cost 3D-Printed Parts. *J. Magn. Reson.* **2021**, *333*, 107096. https://doi.org/10.1016/j.jmr.2021.107096.
(188) ACS guidelines and evaluation procedures for bachelor's degree programs, American Chemical Society Office of Professional Training: Washington, D.C., **2015**.
(189) Crick, F. 1970. Central dogma of molecular biology. Nature 227:561-563.
(190) *BIO2010: Transforming Undergraduate Education for Future Research Biologists*; National Academies Press: Washington, D.C., 2003; p 10497. https://doi.org/10.17226/10497.
(191) Van Dyke, A. R.; Gatazka, D. H.; Hanania, M. M. Innovations in Undergraduate Chemical Biology Education. *ACS Chem. Biol.* **2018**, *13* (1), 26–35. https://doi.org/10.1021/acschembio.7b00986.
(192) Godwin, H. A.; Davis, B. L. Teaching Undergraduates at the Interface of Chemistry and Biology: Challenges and Opportunities. *Nat. Chem. Biol.* **2005**, *1* (4), 176–179. https://doi.org/10.1038/nchembio0905-176.

(193) Begley, T. P. Chemical Biology: An Educational Challenge for Chemistry Departments. *Nat. Chem. Biol.* **2005**, *1* (5), 236–238. https://doi.org/10.1038/nchembio1005-236.
(194) Van Vranken, D. L.; Weiss, G. A. *Introduction to Bioorganic Chemistry and Chemical Biology*; Garland Science: New York, 2013.
(195) Jinek, M.; Chylinski, K.; Fonfara, I.; Hauer, M.; Doudna, J. A.; Charpentier, E. A Programmable Dual-RNA–Guided DNA Endonuclease in Adaptive Bacterial Immunity. *Science* **2012**, *337* (6096), 816–821. https://doi.org/10.1126/science.1225829.
(196) Doudna, J. A.; Charpentier, E. The New Frontier of Genome Engineering with CRISPR-Cas9. *Science* **2014**, *346* (6213), 1258096. https://doi.org/10.1126/science.1258096.
(197) Wang, Y.; Zhao, Y.; Bollas, A.; Wang, Y.; Au, K. F. Nanopore Sequencing Technology, Bioinformatics and Applications. *Nat. Biotechnol.* **2021**, *39* (11), 1348–1365. https://doi.org/10.1038/s41587-021-01108-x.
(198) Wang, Y.; Yang, Q.; Wang, Z. The Evolution of Nanopore Sequencing. *Front. Genet.* **2015**, *5*. https://doi.org/10.3389/fgene.2014.00449.
(199) Pardi, N.; Hogan, M. J.; Porter, F. W.; Weissman, D. mRNA Vaccines — a New Era in Vaccinology. *Nat. Rev. Drug Discov.* **2018**, *17* (4), 261–279. https://doi.org/10.1038/nrd.2017.243.
(200) Allen, D.; Tanner, K. Putting the Horse Back in Front of the Cart: Using Visions and Decisions about High-Quality Learning Experiences to Drive Course Design. *CBE—Life Sci. Educ.* **2007**, *6* (2), 85–89. https://doi.org/10.1187/cbe.07-03-0017.
(201) Bailey, D. N.; Markowicz, L. Chemistry and English: A New Bond. 2.
(202) Nilson, L. B.; Stanny, C. J. *Specifications Grading: Restoring Rigor, Motivating Students, and Saving Faculty Time*; Stylus Publishing: Sterling, Virginia, 2015.
(203) Hollinsed, W. C. Applying Innovations in Teaching to General Chemistry. In *ACS Symposium Series*; Kishbaugh, T. L. S., Cessna, S. G., Eds.; American Chemical Society: Washington, DC, 2018; Vol. 1301, pp 145–152. https://doi.org/10.1021/bk-2018-1301.ch009.
(204) Martin, L. J. Introducing Components of Specifications Grading to a General Chemistry I Course. In *ACS Symposium Series*; Kradtap Hartwell, S., Gupta, T., Eds.; American Chemical Society: Washington, DC, 2019; Vol. 1330, pp 105–119. https://doi.org/10.1021/bk-2019-1330.ch007.
(205) Ring, J. ConfChem Conference on Select 2016 BCCE Presentations: Specifications Grading in the Flipped Organic Classroom. *J. Chem. Educ.* **2017**, *94* (12), 2005–2006. https://doi.org/10.1021/acs.jchemed.6b01000.
(206) Houseknecht, J. B.; Bates, L. K. Transition to Remote Instruction Using Hybrid Just-in-Time Teaching, Collaborative Learning, and Specifications Grading for Organic Chemistry 2. *J. Chem. Educ.* **2020**, *97* (9), 3230–3234. https://doi.org/10.1021/acs.jchemed.0c00749.
(207) Ahlberg, L. Organic Chemistry Core Competencies: Helping Students Engage Using Specifications. 12.
(208) Howitz, W. J.; McKnelly, K. J.; Link, R. D. Developing and Implementing a Specifications Grading System in an Organic Chemistry Laboratory Course. *J. Chem. Educ.* **2021**, *98* (2), 385–394. https://doi.org/10.1021/acs.jchemed.0c00450.
(209) Ponce, M. L. S.; Moorhead, G. B. G. Developing Scientific Writing Skills in Upper Level Biochemistry Students through Extensive Practice and Feedback. *FASEB J.* **2020**, *34* (S1), 1–1. https://doi.org/10.1096/fasebj.2020.34.s1.00661.

(210) Katzman, S. D.; Hurst-Kennedy, J.; Barrera, A.; Talley, J.; Javazon, E.; Diaz, M.; Anzovino, M. E. The Effect of Specifications Grading on Students' Learning and Attitudes in an Undergraduate-Level Cell Biology Course. *J. Microbiol. Biol. Educ.* **2021**, *22* (3), e00200-21. https://doi.org/10.1128/jmbe.00200-21.
(211) Tsoi, M. Y.; Anzovino, M. E.; Erickson, A. H. L.; Forringer, E. R.; Henary, E. Variations in Implementation of Specifications Grading in STEM Courses. **2019**, 24.
(212) Nakhleh, M. B. Chemical Education Research in the Laboratory Environment: How Can Research Uncover What Students Are Learning? *J. Chem. Educ.* **1994**, *71* (3), 201. https://doi.org/10.1021/ed071p201.
(213) Larkin, J. H.; Reif, F. Analysis and Teaching of a General Skill for Studying Scientific Text. *J. Educ. Psychol.* **1976**, *68* (4), 431–440. https://doi.org/10.1037/0022-0663.68.4.431.
(214) Applebee, A. N. Writing and Reasoning. 20.
(215) McKnelly, K. J.; Morris, M. A.; Mang, S. A. Redesigning a "Writing for Chemists" Course Using Specifications Grading. *J. Chem. Educ.* **2021**, *98* (4), 1201–1207. https://doi.org/10.1021/acs.jchemed.0c00859.
(216) *Argumentation in Science Education: Perspectives from Classroom-Based Research*; Erduran, S., Aleixandre, M., Eds.; Science & technology education library; Springer: Dordrecht, 2008.
(217) Hodges, L. C. *Teaching Undergraduate Science: A Guide to Overcoming Obstacles to Student Learning*; Stylus Publishing: Sterling, Virginia, 2015.
(218) Sampson, V.; Walker, J. P. Argument-Driven Inquiry as a Way to Help Undergraduate Students Write to Learn by Learning to Write in Chemistry. *Int. J. Sci. Educ.* **2012**, *34* (10), 1443–1485. https://doi.org/10.1080/09500693.2012.667581.
(219) Winstone, N. E.; Nash, R. A.; Parker, M.; Rowntree, J. Supporting Learners' Agentic Engagement With Feedback: A Systematic Review and a Taxonomy of Recipience Processes. *Educ. Psychol.* **2017**, *52* (1), 17–37. https://doi.org/10.1080/00461520.2016.1207538.
(220) Winstone, N. E.; Nash, R. A.; Rowntree, J.; Parker, M. 'It'd Be Useful, but I Wouldn't Use It': Barriers to University Students' Feedback Seeking and Recipience. *Stud. High. Educ.* **2017**, *42* (11), 2026–2041. https://doi.org/10.1080/03075079.2015.1130032.
(221) Gibbs, G.; Simpson, C. Conditions Under Which Assessment Supports Students' Learning. 30.
(222) Price, M.; Handley, K.; Millar, J.; O'Donovan, B. Feedback : All That Effort, but What Is the Effect? *Assess. Eval. High. Educ.* **2010**, *35* (3), 277–289. https://doi.org/10.1080/02602930903541007.
(223) Jonsson, A. Facilitating Productive Use of Feedback in Higher Education. *Act. Learn. High. Educ.* **2013**, *14* (1), 63–76. https://doi.org/10.1177/1469787412467125.
(224) Price, M.; Handley, K.; Millar, J. Feedback: Focusing Attention on Engagement. *Stud. High. Educ.* **2011**, *36* (8), 879–896. https://doi.org/10.1080/03075079.2010.483513.
(225) Mann, S. J. Alternative Perspectives on the Student Experience: Alienation and Engagement. *Stud. High. Educ.* **2001**, *26* (1), 7–19. https://doi.org/10.1080/03075070020030689.
(226) Hill, J.; West, H. Improving the Student Learning Experience through Dialogic Feed-Forward Assessment. *Assess. Eval. High. Educ.* **2020**, *45* (1), 82–97. https://doi.org/10.1080/02602938.2019.1608908.

(227) Schinske, J.; Tanner, K. Teaching More by Grading Less (or Differently). *CBE—Life Sci. Educ.* **2014**, *13* (2), 159–166. https://doi.org/10.1187/cbe.cbe-14-03-0054.
(228) Guskey, T. R. Making the Grade: What Benefits Students?
(229) Schneider, J.; Hutt, E. Making the Grade: A History of the A–F Marking Scheme. *J. Curric. Stud.* **2014**, *46* (2), 201–224. https://doi.org/10.1080/00220272.2013.790480.
(230) Brookhart, S. M. *Grading*; Pearson: Upper Saddle River, NJ, 2004.
(231) Bloom, B.S. Learning for mastery. Evaluation Comment, Center for the Study of Evaluation of Instructional Programs, University of California at Los Angeles. **1968**, 1:1-11.
(232) Humphreys, B.; Johnson, R.; Johnson, D. Effects of Cooperative, Competitive, and Individualistic Learning on Students' Achievement in Science Class. *J Res Sci Teach* **1982**, *19*, 351–356.
(233) Crocker, J. The Costs of Seeking Self-Esteem. *J. Soc. Issues* **2002**, *58* (3), 597–615. https://doi.org/10.1111/1540-4560.00279.
(234) Rogers, C. *On Becoming a Person: A Therapist's View of Psychotherapy*; Constable, 2004.
(235) Jonsson, A.; Svingby, G. The Use of Scoring Rubrics: Reliability, Validity and Educational Consequences. *Educ. Res. Rev.* **2007**, *2* (2), 130–144. https://doi.org/10.1016/j.edurev.2007.05.002.
(236) Reddy, Y. M.; Andrade, H. A Review of Rubric Use in Higher Education. *Assess. Eval. High. Educ.* **2010**, *35* (4), 435–448. https://doi.org/10.1080/02602930902862859.
(237) Nicol, D. J.; Macfarlane-Dick, D. Formative Assessment and Self-regulated Learning: A Model and Seven Principles of Good Feedback Practice. *Stud. High. Educ.* **2006**, *31* (2), 199–218. https://doi.org/10.1080/03075070600572090.
(238) Seymour, E. and Hewitt, N.M., Talking about leaving: Why undergraduates leave the sciences; Westview Press, **1997**.
(239) Tobias, S. They're not dumb, they're different: Stalking the second tier; Research Corporation, **1990**.
(240) Department of Education Office for Civil Rights. Education in a Pandemic: The Disparate Impacts of COVID-19 on America's Students.
(241) Plakhotnik, M. S.; Volkova, N. V.; Jiang, C.; Yahiaoui, D.; Pheiffer, G.; McKay, K.; Newman, S.; Reißig-Thust, S. The Perceived Impact of COVID-19 on Student Well-Being and the Mediating Role of the University Support: Evidence From France, Germany, Russia, and the UK. *Front. Psychol.* **2021**, *12*, 642689. https://doi.org/10.3389/fpsyg.2021.642689.
(242) Becker, T. B.; Fenton, J. I.; Nikolai, M.; Comstock, S. S.; Swada, J. G.; Weatherspoon, L. J.; Tucker, R. M. The Impact of COVID-19 on Student Learning during the Transition from Remote to in-Person Learning: Using Mind Mapping to Identify and Address Faculty Concerns. *Adv. Physiol. Educ.* **2022**, *46* (4), 742–751. https://doi.org/10.1152/advan.00079.2022.
(243) Toledo, S.; Dubas, J. M. A Learner-Centered Grading Method Focused on Reaching Proficiency with Course Learning Outcomes. *J. Chem. Educ.* **2017**, *94* (8), 1043–1050. https://doi.org/10.1021/acs.jchemed.6b00651.
(244) Docan, T. N. Positive and Negative Incentives in the Classroom: An Analysis of Grading Systems and Student Motivation. *N 6* (2), 20.
(245) Diegelman-Parente, A. The Use of Mastery Learning With Competency-Based Grading in an Organic Chemistry Course. 10.

(246) Voorhees, R. A. Competency-Based Learning Models: A Necessary Future. *New Dir. Institutional Res.* **2001**, *2001* (110), 5–13. https://doi.org/10.1002/ir.7.
(247) Eller, E. Educational Research Quarterly. *Educ. Res. Q.* **2016**, *39*, 22.
(248) Wackerly, J. Wm. Stepwise Approach To Writing Journal-Style Lab Reports in the Organic Chemistry Course Sequence. *J. Chem. Educ.* **2018**, *95* (1), 76–83. https://doi.org/10.1021/acs.jchemed.6b00630.
(249) Airasian, P.W., Raths, J., Wittrock, M., Mayer, R.E., Pintrich, P., and Cruikshank, K.A. A taxonomy for learning, teaching, and assessing: a revision of Bloom's taxonomy of educational objectives. Addison Wesley Longman, Inc., **2001**.
(250) *Taxonomy of Educational Objectives: The Classification of Educational Goals*; Bloom, B. S., Ed.; D. McKay: New York, 1974.
(251) Baldwin, J.A., Ebert-May D., and Burns, D.J. The development of a college biology self-efficacy instrument for nonmajors. Sci. Ed. **1999**, 83:397-408.
(252) Helmke, B. Specifications Grading in an Upper-Level BME Elective Course. In *2019 ASEE Annual Conference & Exposition Proceedings*; ASEE Conferences: Tampa, Florida, 2019; p 33278. https://doi.org/10.18260/1-2--33278.
(253) Streifer, A. C.; Palmer, M. S. Is Specifications Grading Right for Me?: A Readiness Assessment to Help Instructors Decide. *Coll. Teach.* **2021**, 1–8. https://doi.org/10.1080/87567555.2021.2018396.
(254) Doll, C.; McLaughlin, T. F.; Barretto, A. The Token Economy: A Recent Review and Evaluation. *Int. J. Basic Appl. Sci.* **2013**, *02* (01), 19.
(255) Carlisle, S. Simple Specifications Grading. *PRIMUS* **2020**, *30* (8–10), 926–951. https://doi.org/10.1080/10511970.2019.1695238.
(256) Damavandi, Majid. E.; Shekari Kashani, Z. Effect of Mastery Learning Method on Performance, Attitude of the Weak Students in Chemistry. *Procedia - Soc. Behav. Sci.* **2010**, *5*, 1574–1579. https://doi.org/10.1016/j.sbspro.2010.07.327.
(257) Youngblood, J. P.; Webb, E. A.; Gin, L. E.; van Leusen, P.; Henry, J. R.; VandenBrooks, J. M.; Brownell, S. E. Anatomical Self-Efficacy of Undergraduate Students Improves during a Fully Online Biology Course with at-Home Dissections. *Adv. Physiol. Educ.* **2022**, *46* (1), 125–139. https://doi.org/10.1152/advan.00139.2021.
(258) RCoreTeam.R A Language and Environment for Statistical Computing [Online]. https://www.R-project.org/.
(259) Wickham, H.; Averick, M.; Bryan, J.; Chang, W.; McGowan, L.; François, R.; Grolemund, G.; Hayes, A.; Henry, L.; Hester, J.; Kuhn, M.; Pedersen, T.; Miller, E.; Bache, S.; Müller, K.; Ooms, J.; Robinson, D.; Seidel, D.; Spinu, V.; Takahashi, K.; Vaughan, D.; Wilke, C.; Woo, K.; Yutani, H. Welcome to the Tidyverse. *J. Open Source Softw.* **2019**, *4* (43), 1686. https://doi.org/10.21105/joss.01686.
(260) Limeri, L. B.; Carter, N. T.; Choe, J.; Harper, H. G.; Martin, H. R.; Benton, A.; Dolan, E. L. Growing a Growth Mindset: Characterizing How and Why Undergraduate Students' Mindsets Change. *Int. J. STEM Educ.* **2020**, *7* (1), 35. https://doi.org/10.1186/s40594-020-00227-2.
(261) Fernandez, T.; Martin, K.; Mangum, R.; Bell-Huff, C. Whose Grade Is It Anyway?: Transitioning Engineering Courses to an Evidence-Based Specifications Grading System. In *2020 ASEE Virtual Annual Conference Content Access Proceedings*; ASEE Conferences: Virtual On line, 2020; p 35512. https://doi.org/10.18260/1-2--35512.
(262) Mirsky, G. M. Effectiveness of Specifications Grading in Teaching Technical Writing to Computer Science Students. **2018**, 7.

(263) Deslauriers, L.; McCarty, L. S.; Miller, K.; Callaghan, K.; Kestin, G. Measuring Actual Learning versus Feeling of Learning in Response to Being Actively Engaged in the Classroom. *Proc. Natl. Acad. Sci.* **2019**, *116* (39), 19251–19257. https://doi.org/10.1073/pnas.1821936116.
(264) Blackstone, B.; Oldmixon, E. Specifications Grading in Political Science. *J. Polit. Sci. Educ.* **2019**, *15* (2), 191–205. https://doi.org/10.1080/15512169.2018.1447948.

LIST OF FIGURES IN APPENDICES

LIST OF TABLES IN APPENDICES

APPENDIX A

Computer-Assisted Design (CAD) Files

All dimensions are in inches.

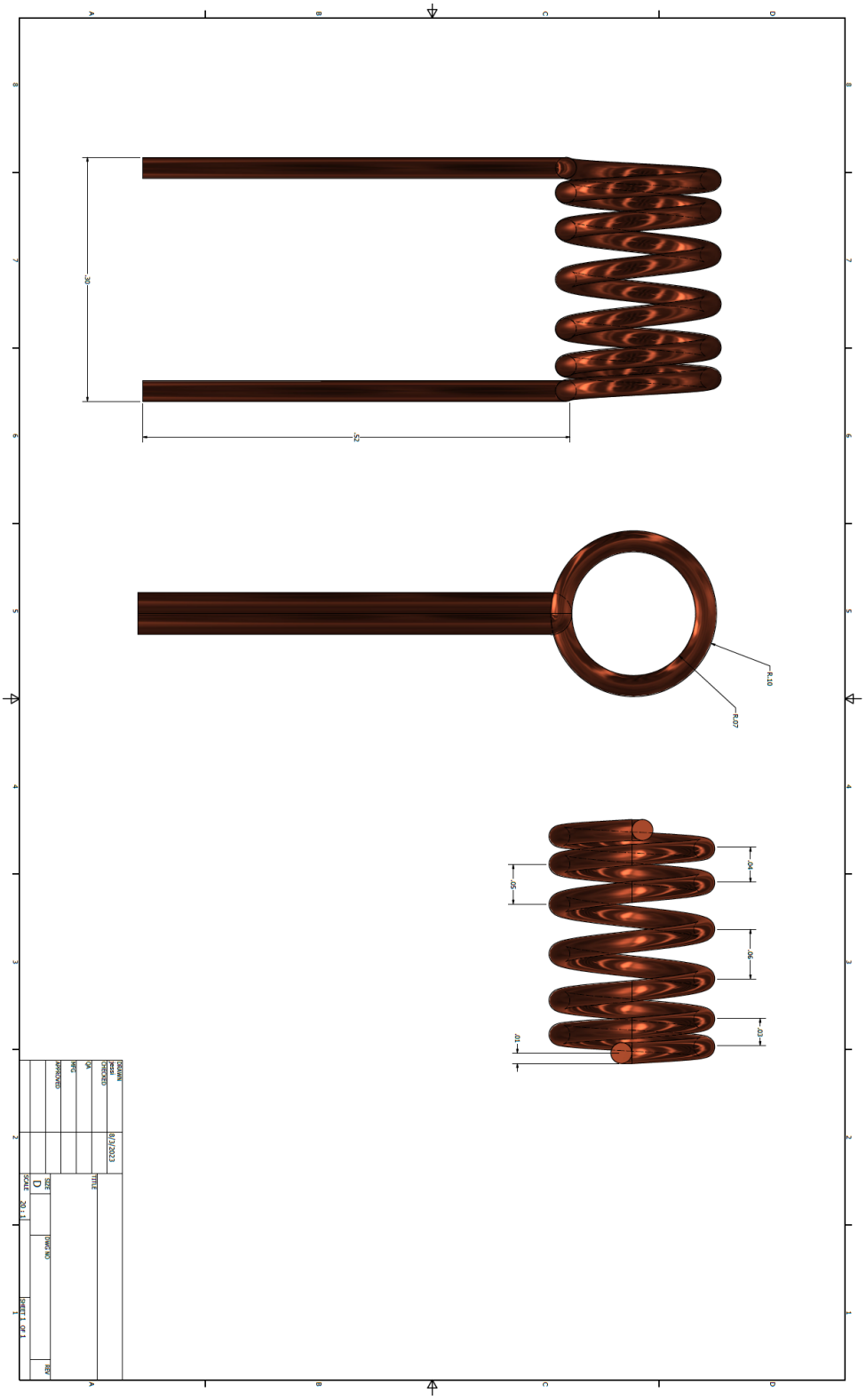

Figure A.1: 1-1.5-2 ratio variable pitch solenoid.

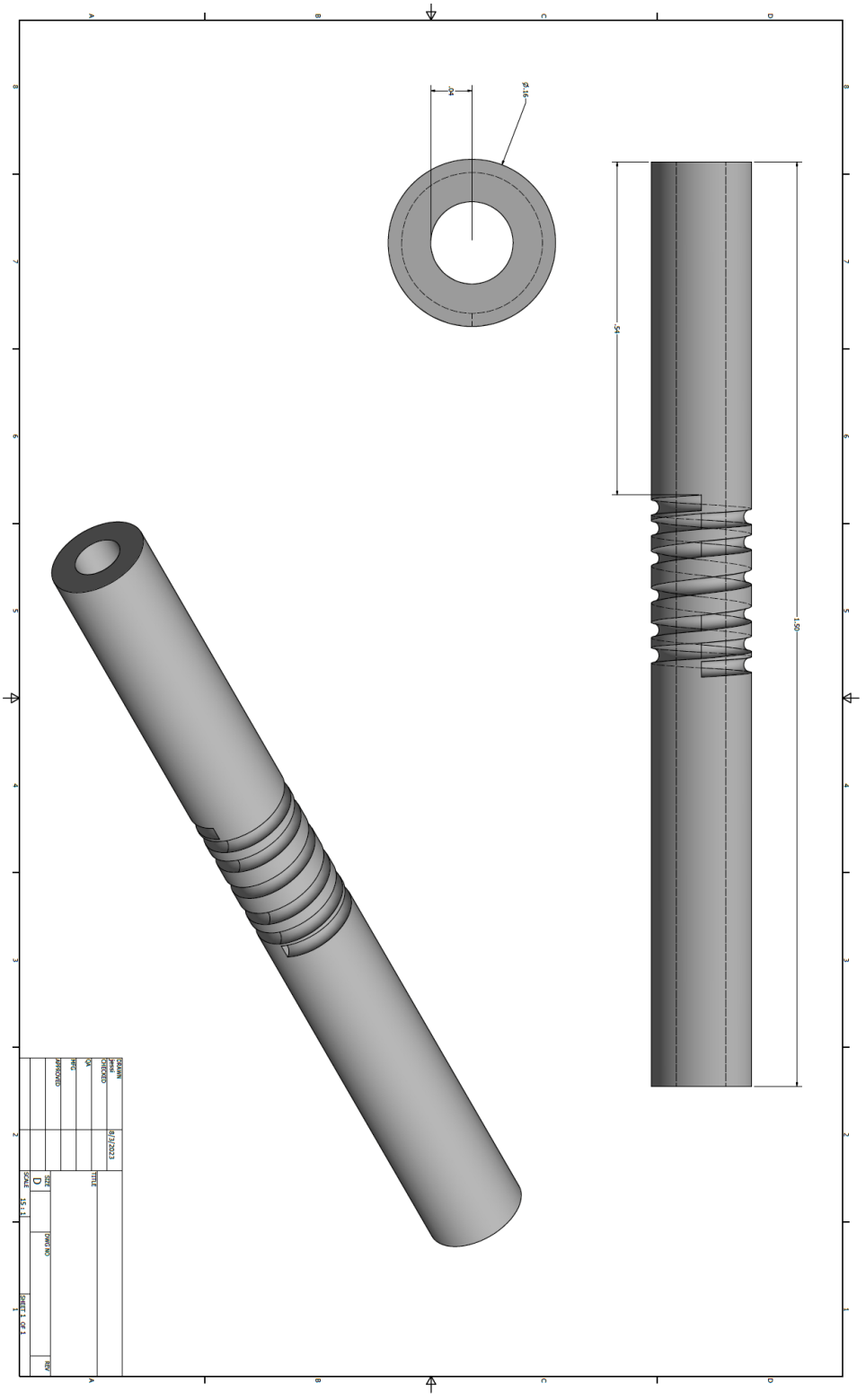

Figure A.2: 1-1.5-2 ratio variable pitch solenoid template.

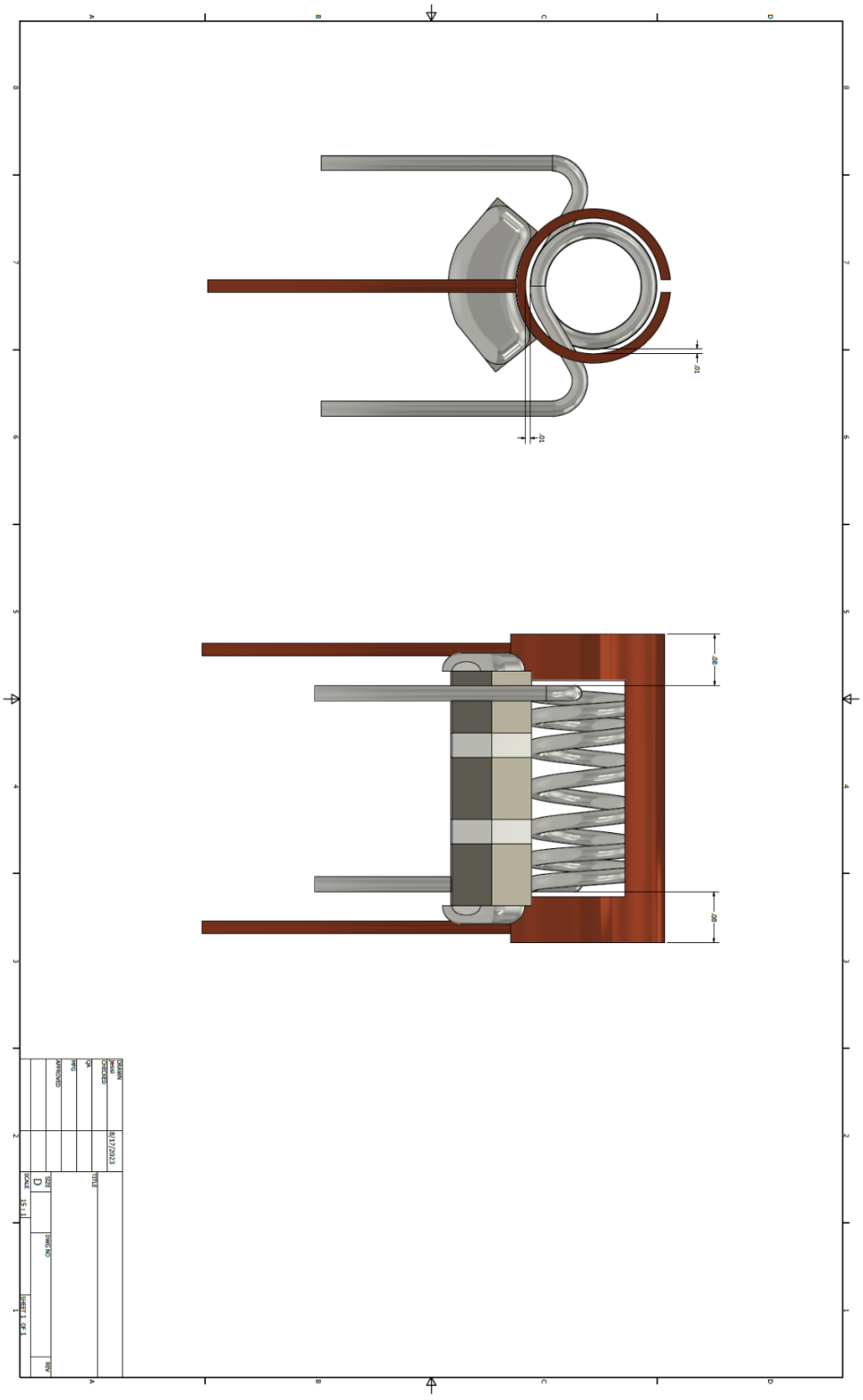

Figure A.3: Cross-coil centered.

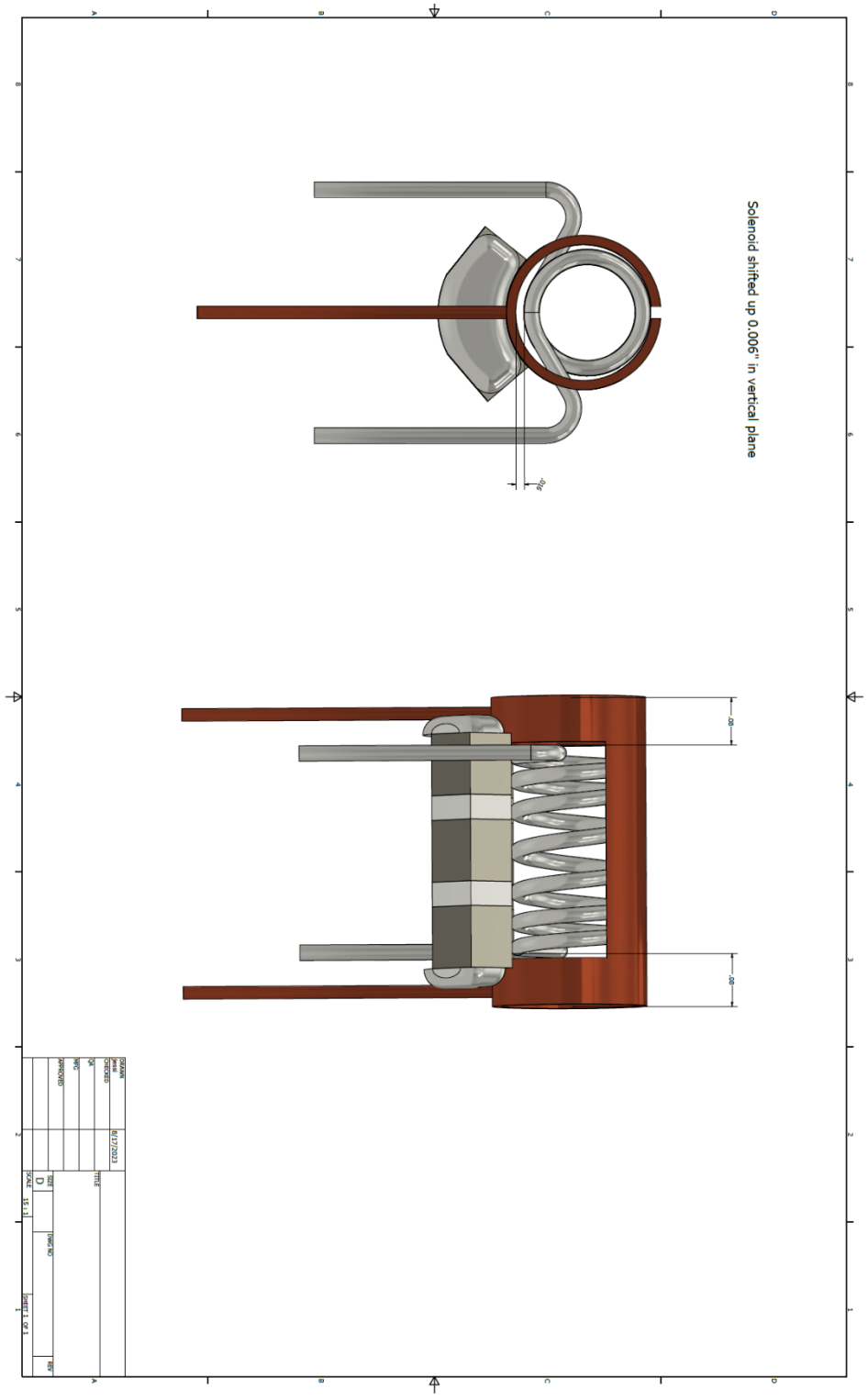

Figure A.4: Cross-coil vertical shift. Solenoid shifted 0.006” in vertical plane.

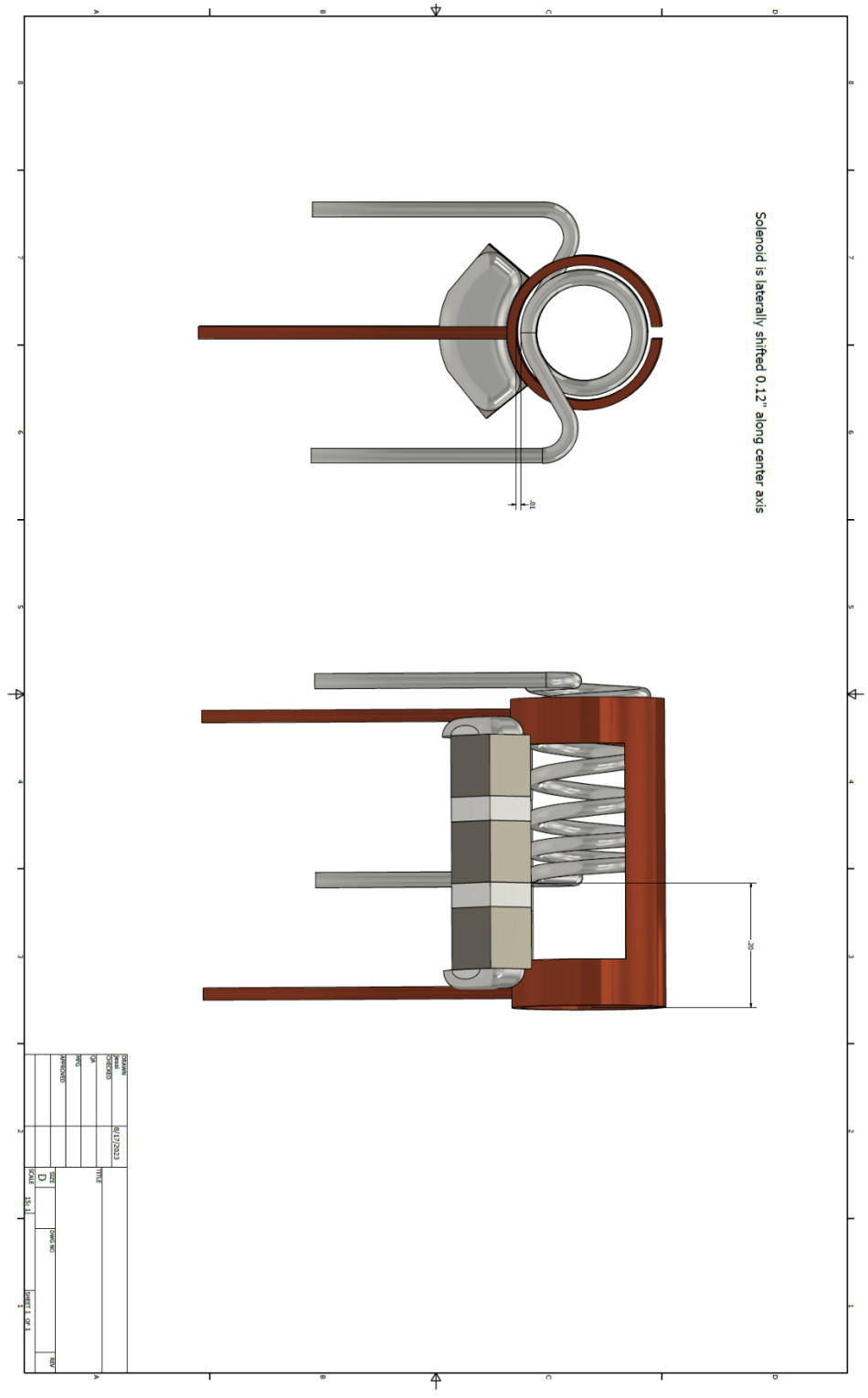

Figure A.5: Cross-coil lateral shift. Solenoid laterally shifted 0.12” along center axis.

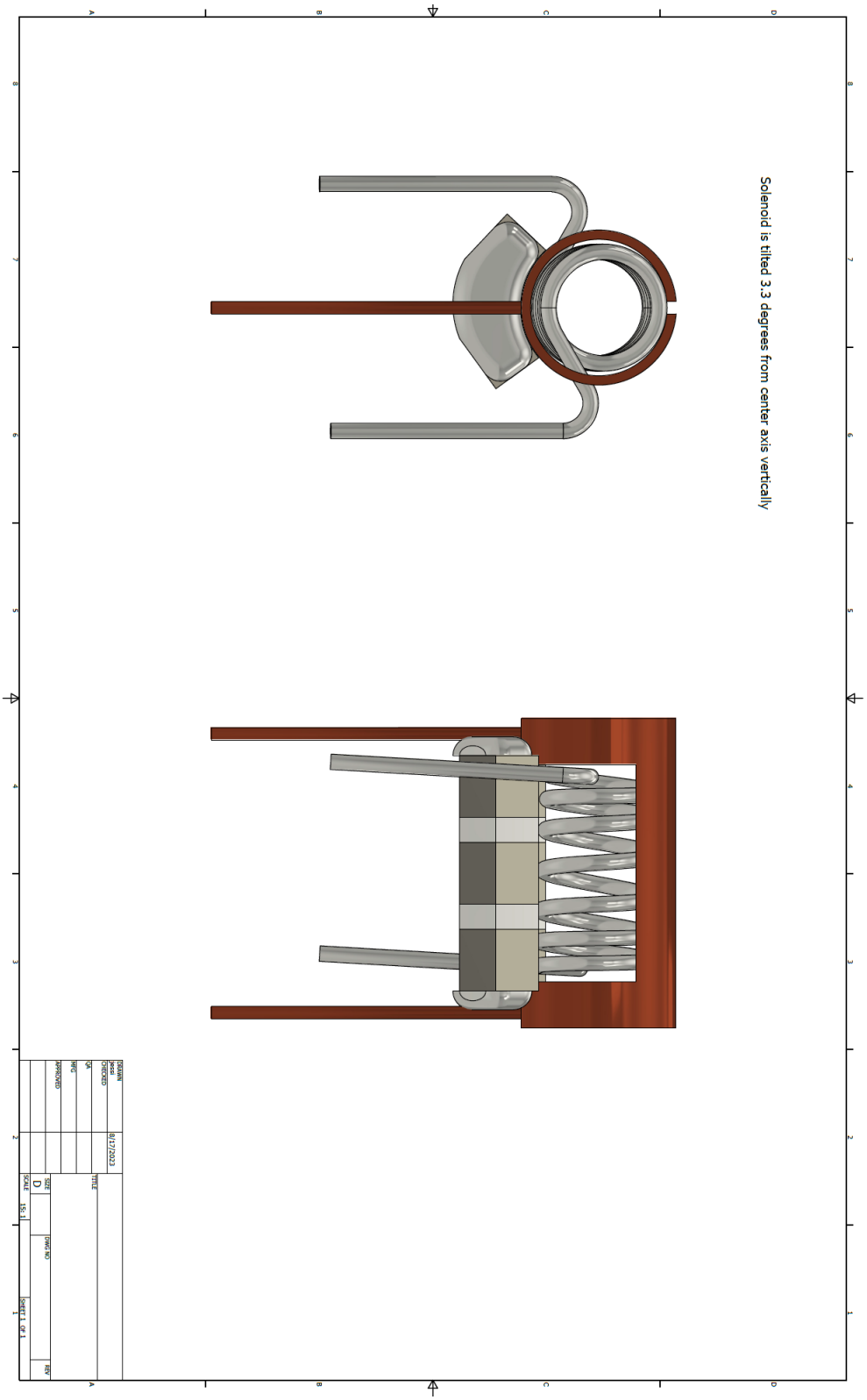

Figure A.6: Cross-coil vertical skew. Solenoid is tilted 3.3° from center axis vertically.

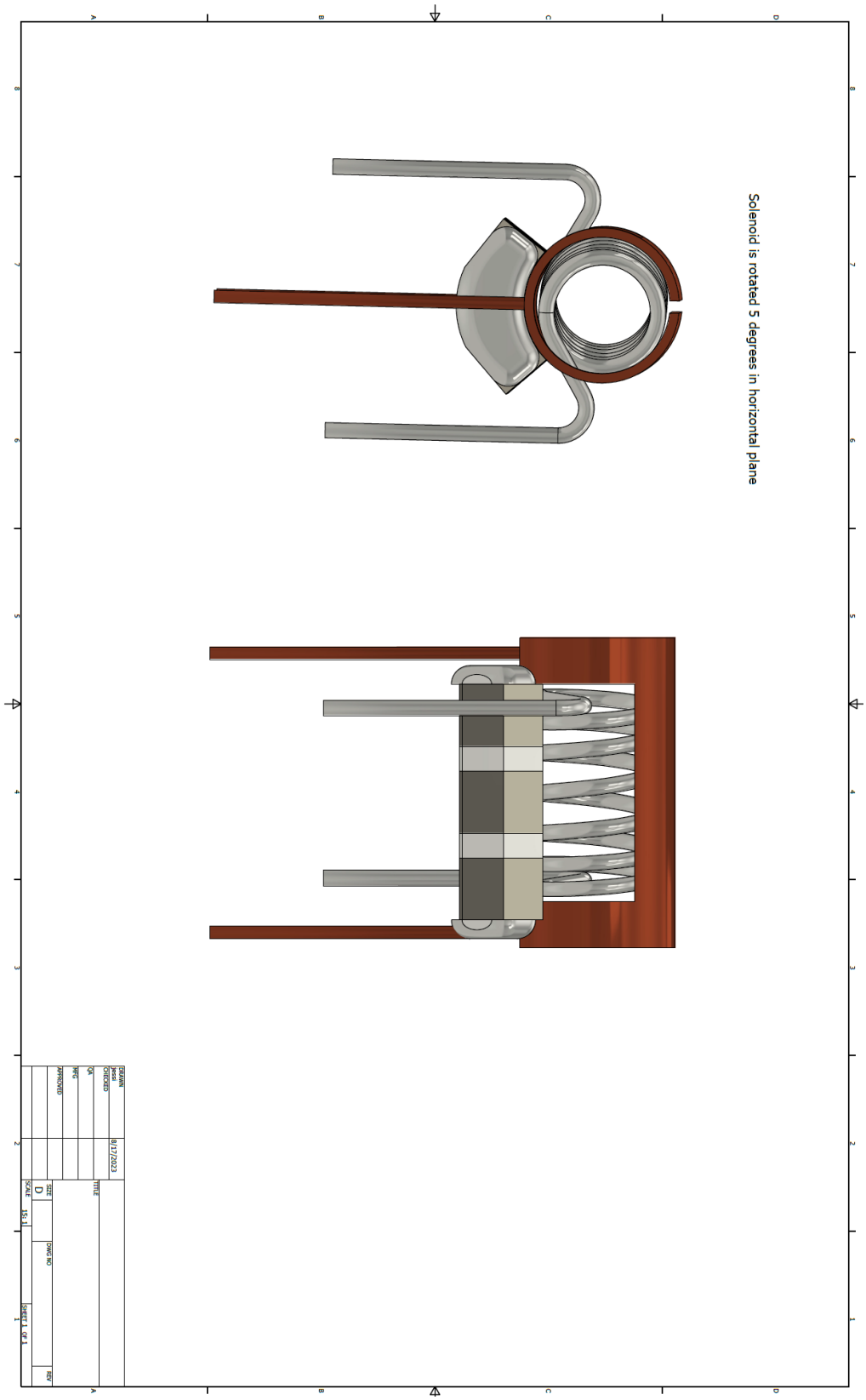

Figure A.7: Cross-coil horizontal skew. Solenoid rotated 5° in horizontal plane.

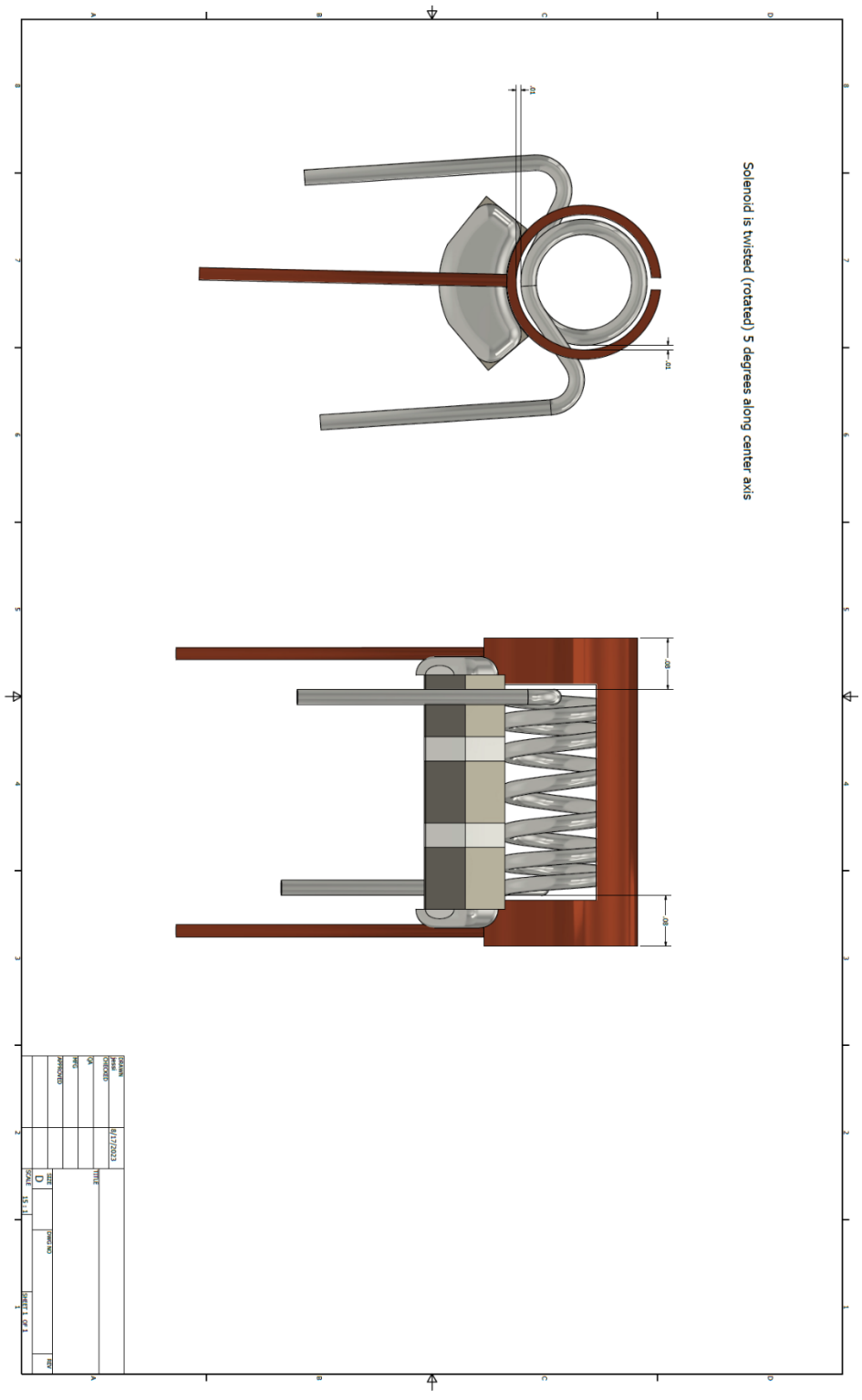

Figure A.8: Cross-coil twist. Solenoid twisted (rotated) 5° along center axis.

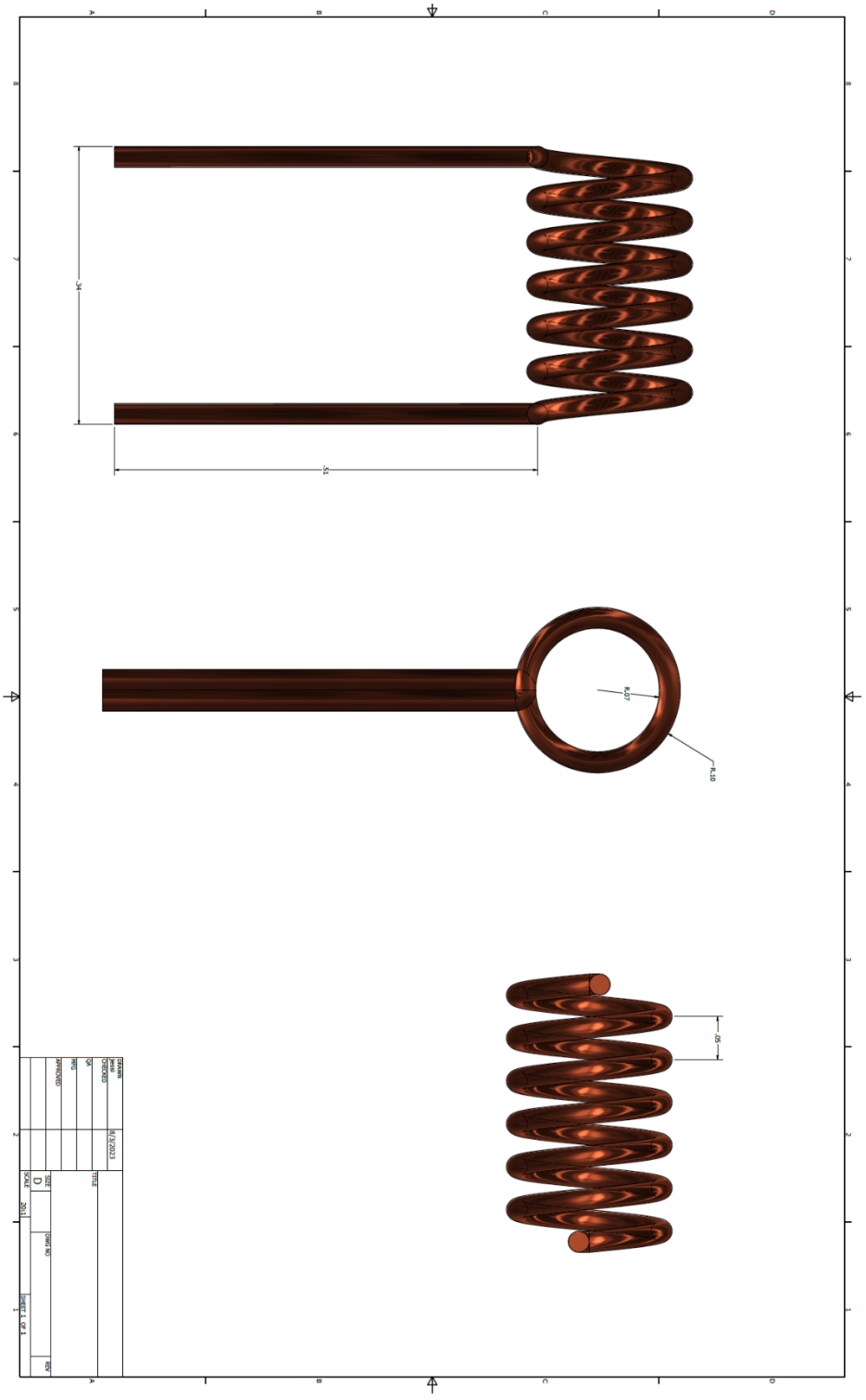

Figure A.9: Constant pitch solenoid.

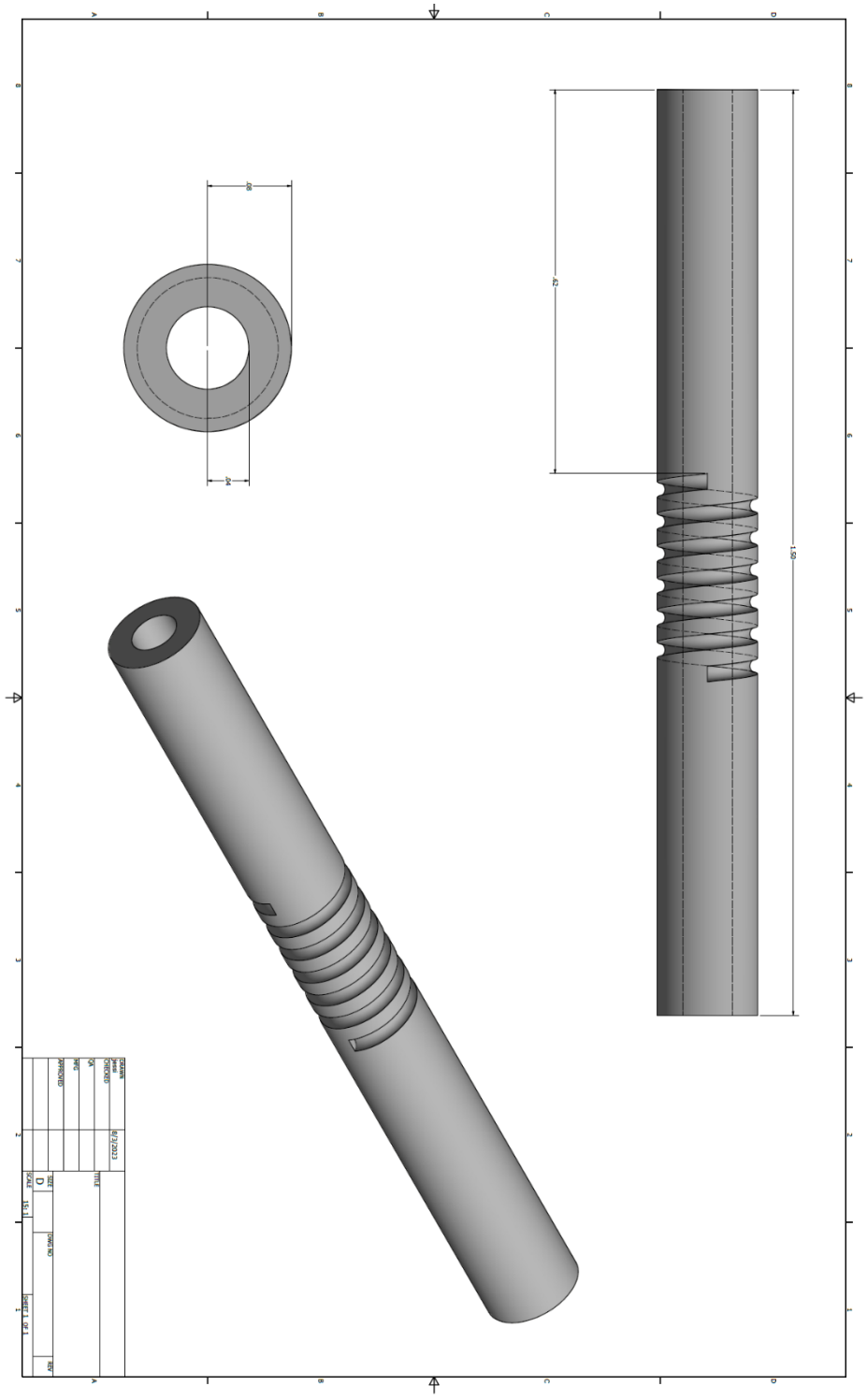

Figure A.10: Constant pitch solenoid template.

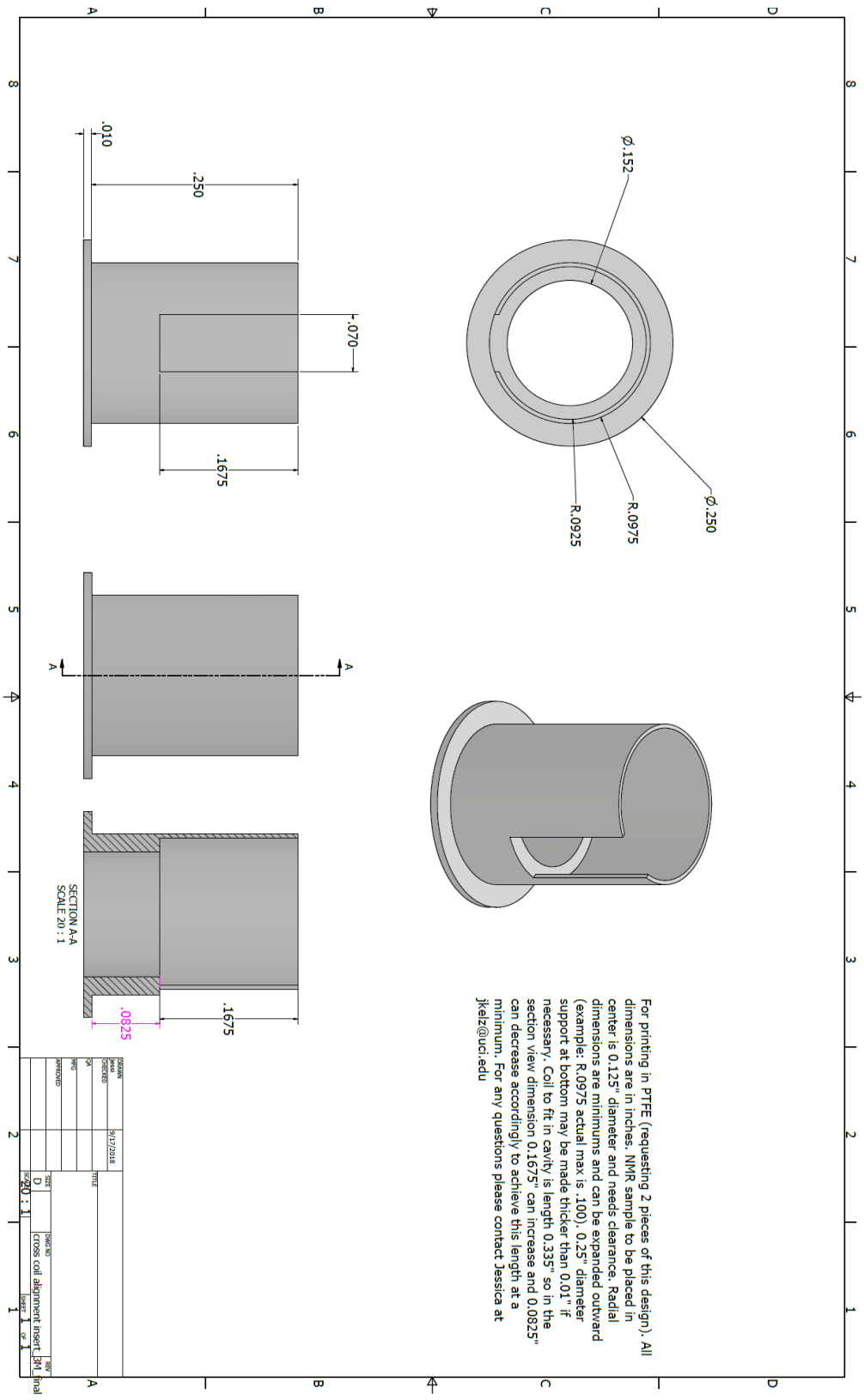

Figure A.11: Cross-coil PTFE alignment and arc-shield insert.

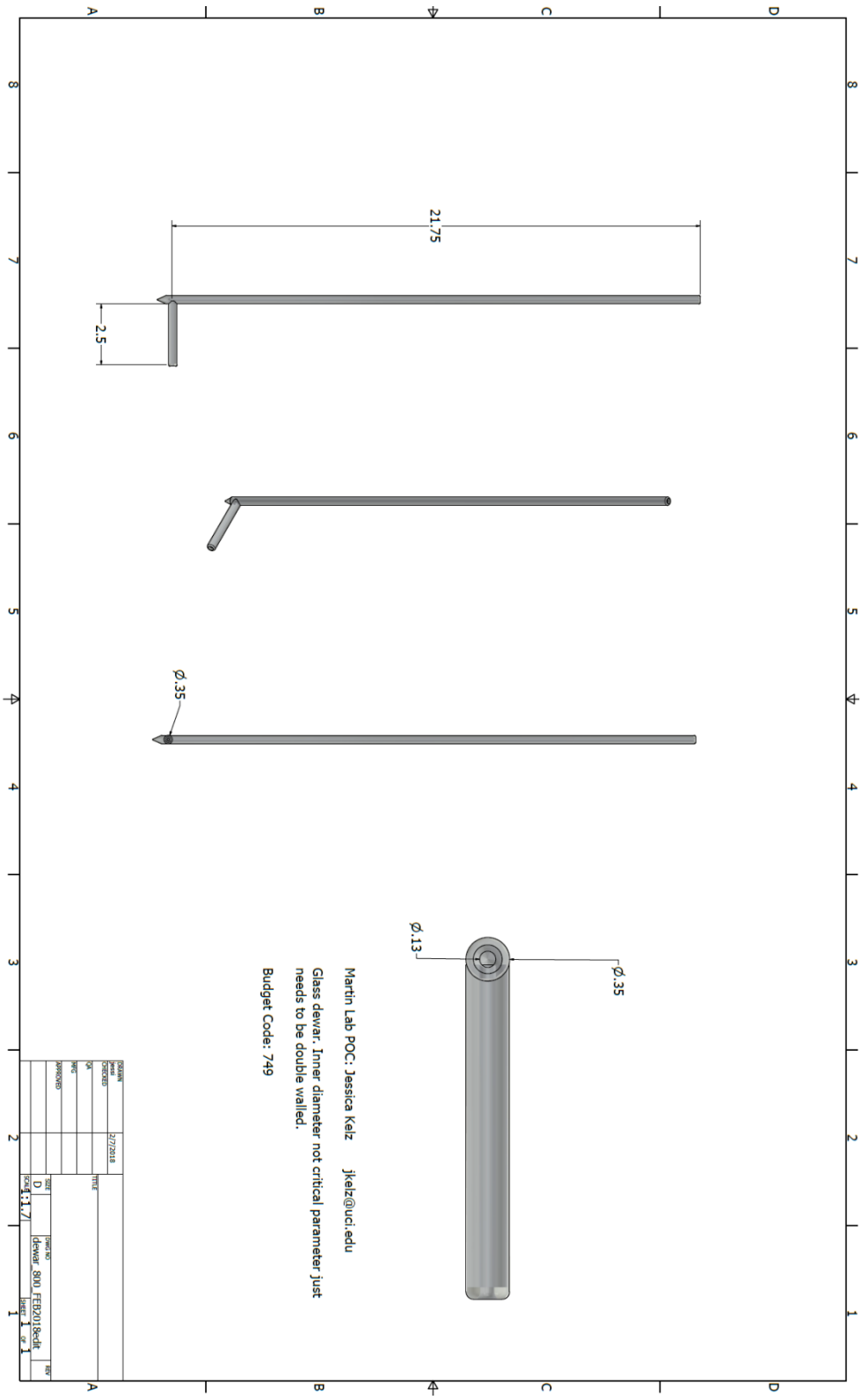

Figure A.12: 800MHz cross-coil probe dewar.

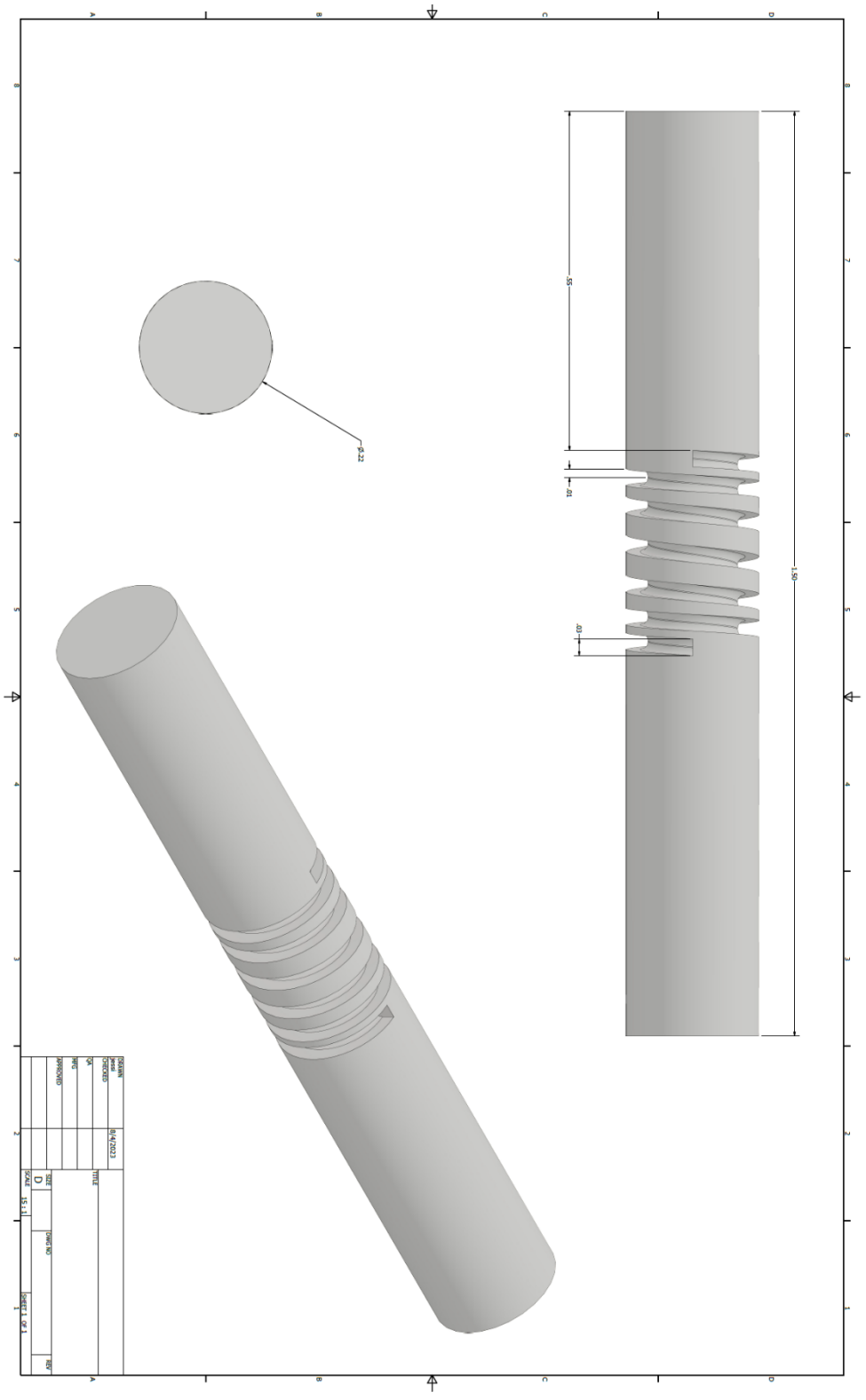

Figure A.13: Deep groove variable pitch solenoid template.

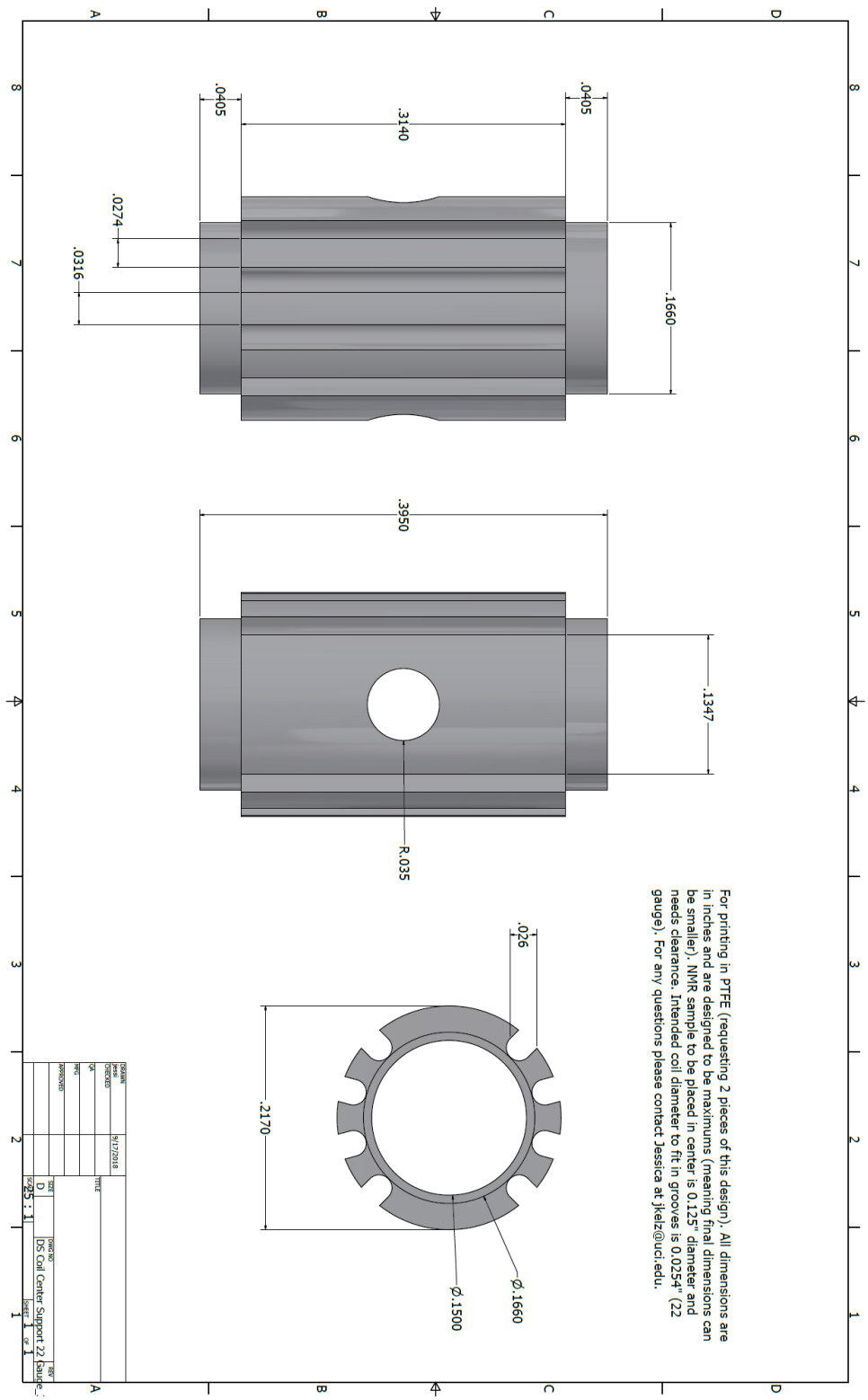

Figure A.14: Double-saddle coil PTFE stability insert.

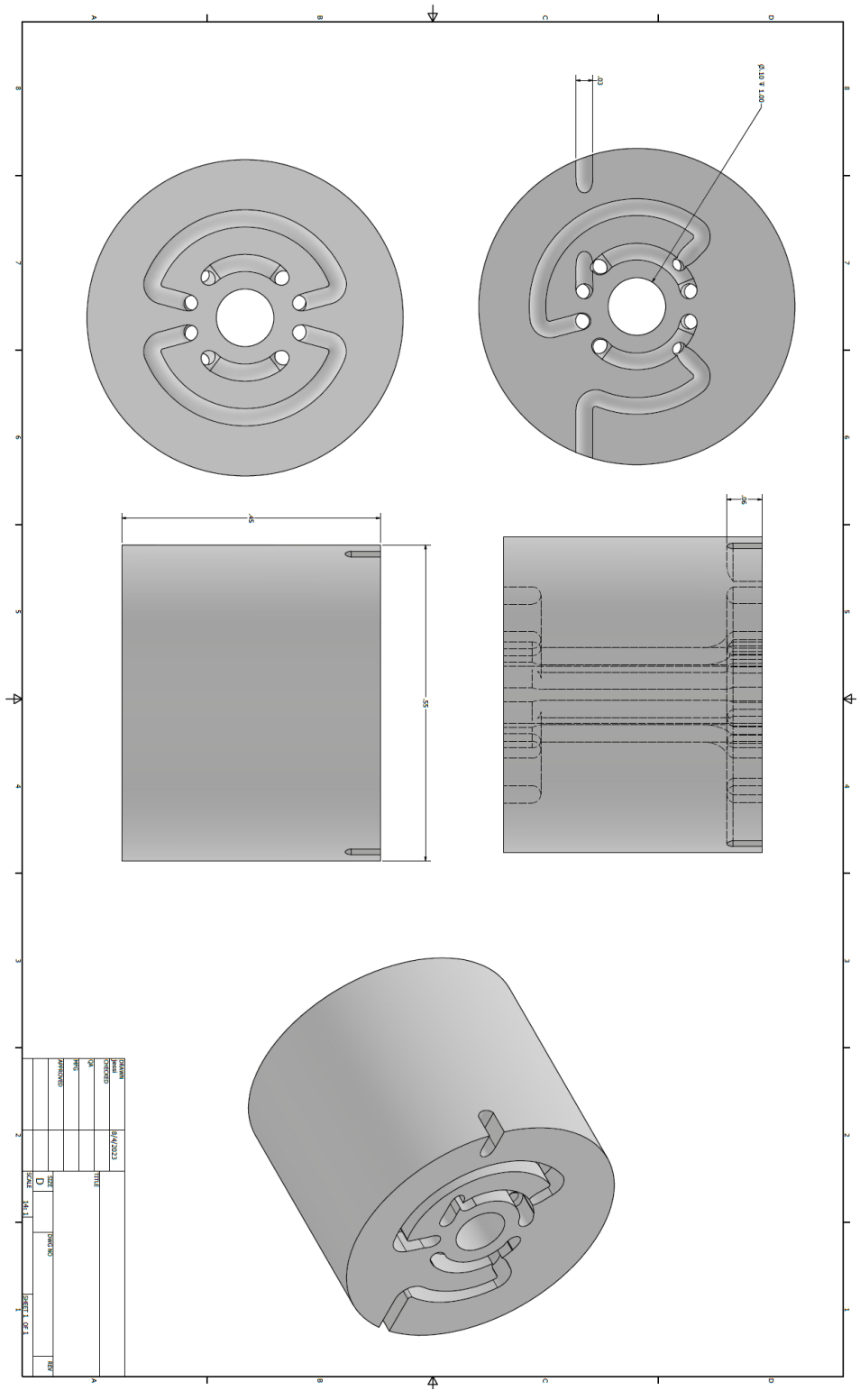

Figure A.15: Double-saddle coil template 0.027” diameter groove, 0.63” wall.

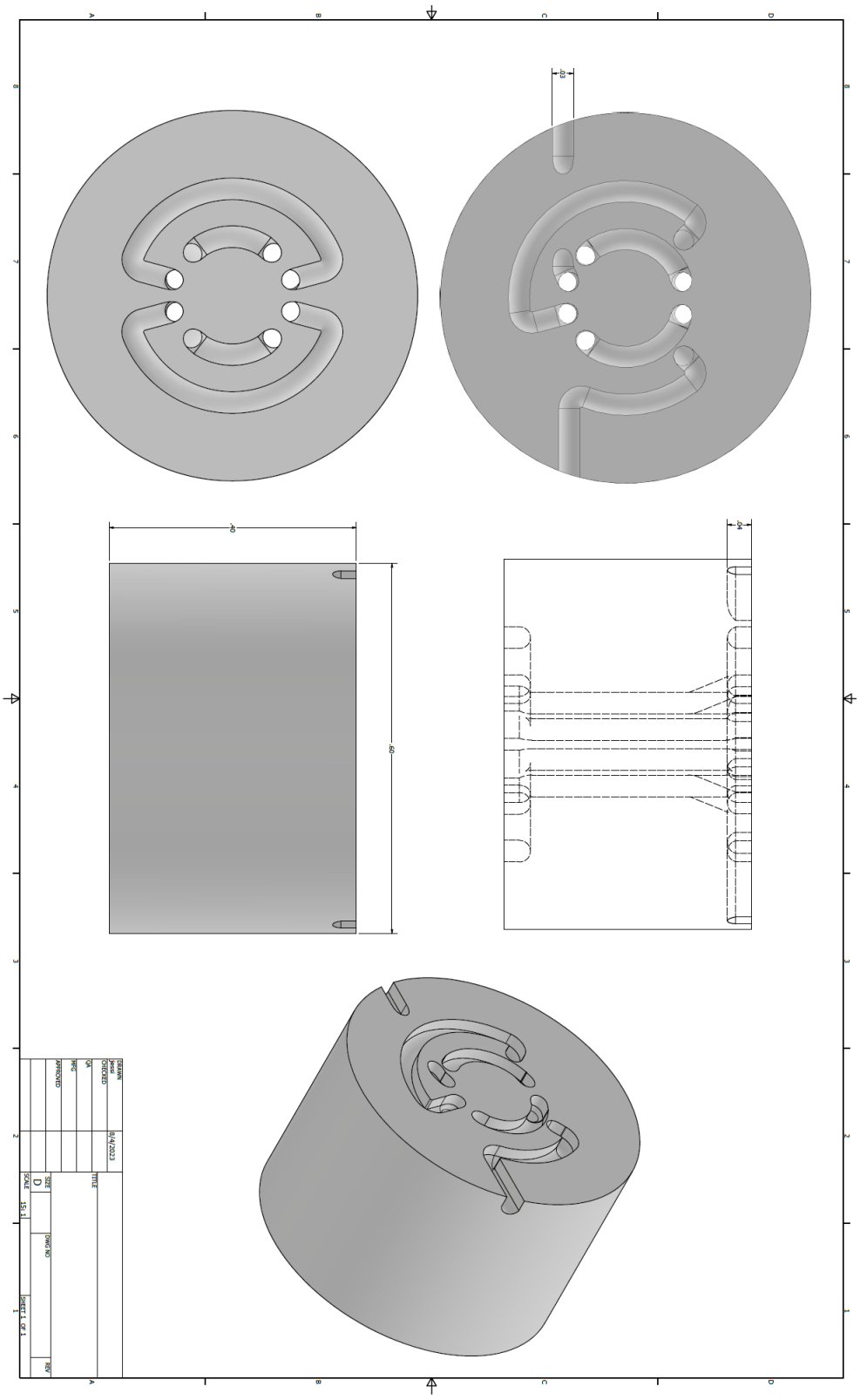

Figure A.16: Double-saddle coil template 0.035” diameter angled groove, 0.60” wall.

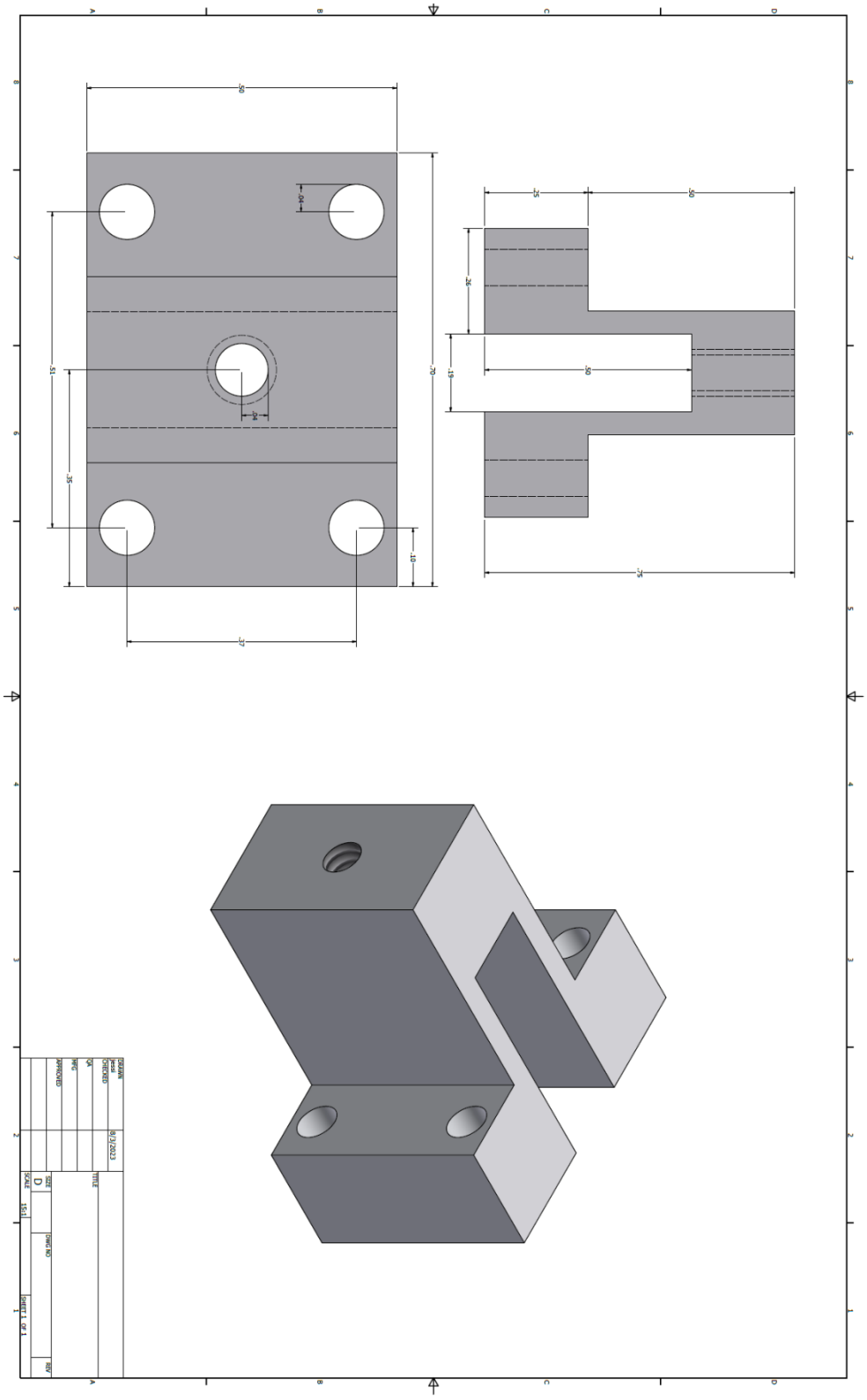

Figure A.17: Homogeneity test adapter for attachment to spinning assembly.

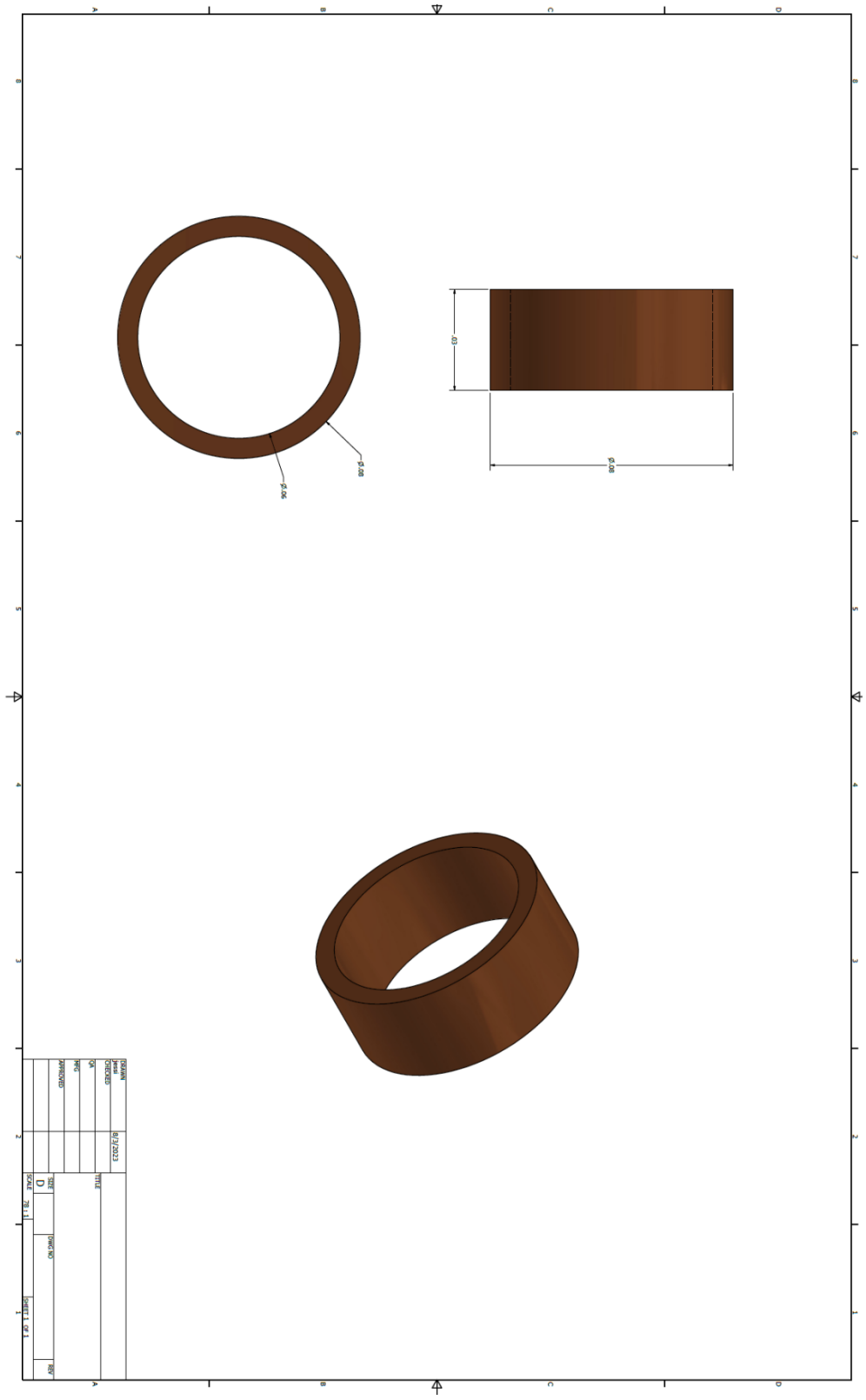

Figure A.18: Machined homogeneity probe conductive ring (copper).

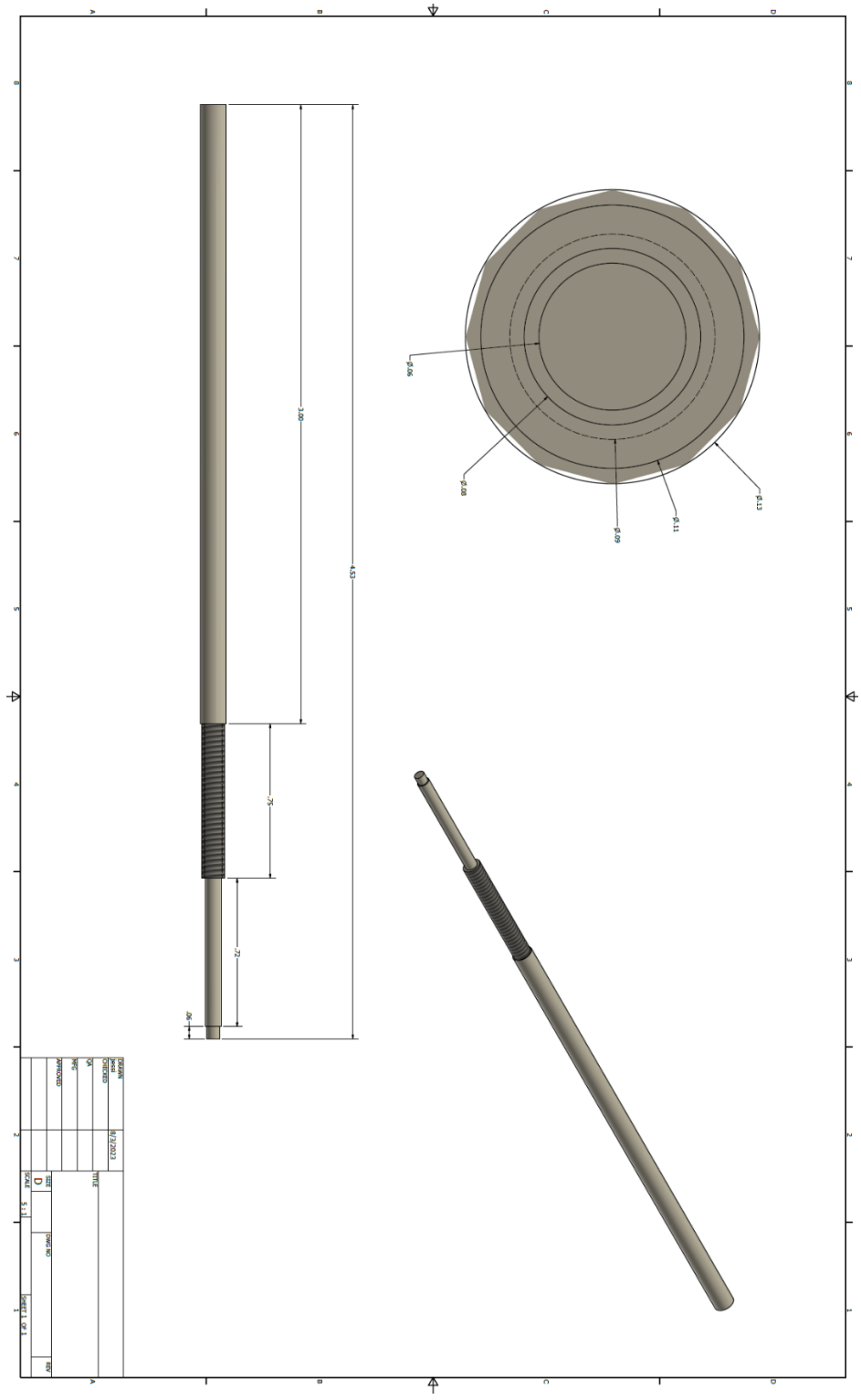

Figure A.19: Machined homogeneity probe rod (4-40 thread).

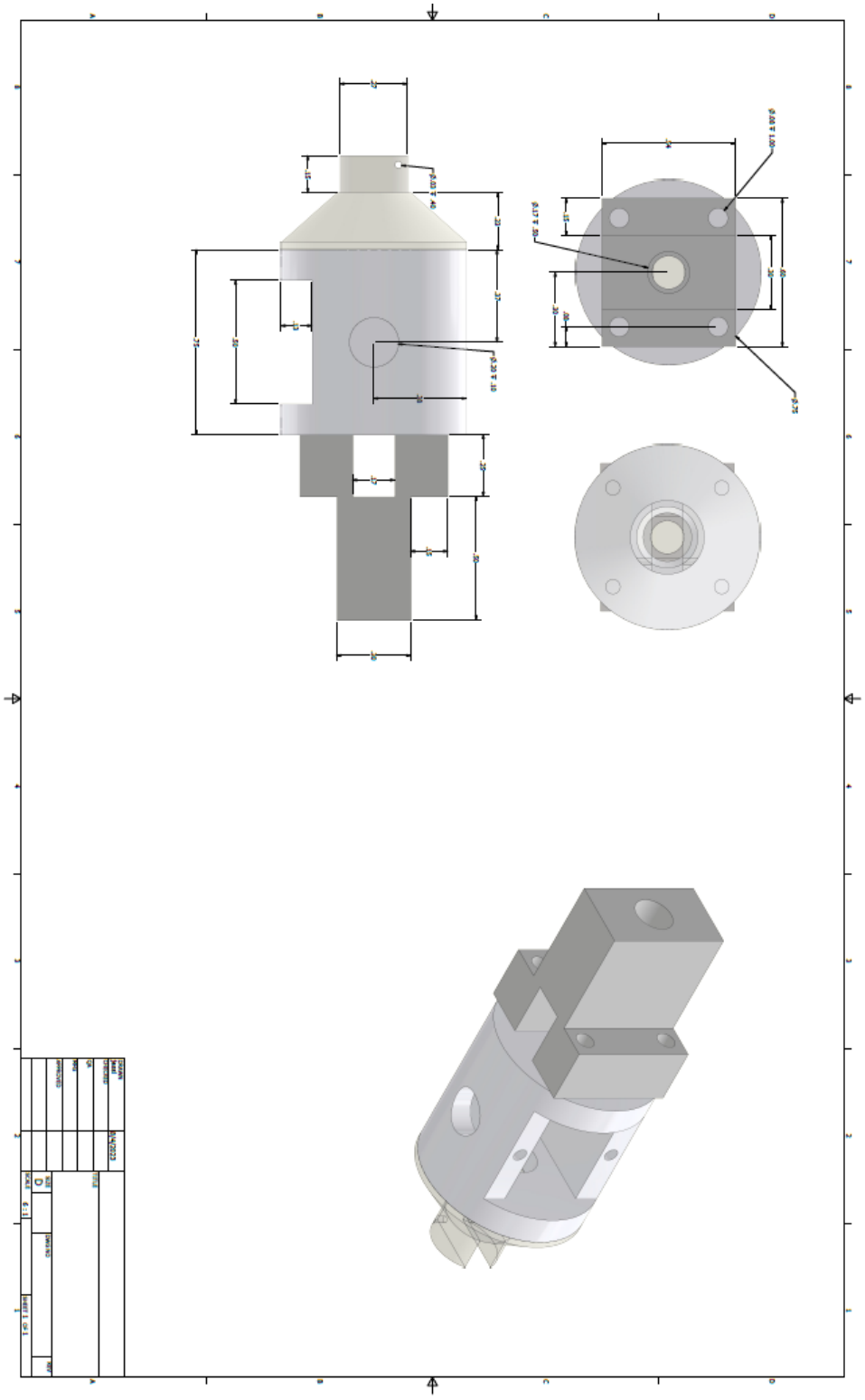

Figure A.20: Single piece 3.2mm spinning assembly and homogeneity probe adapter.

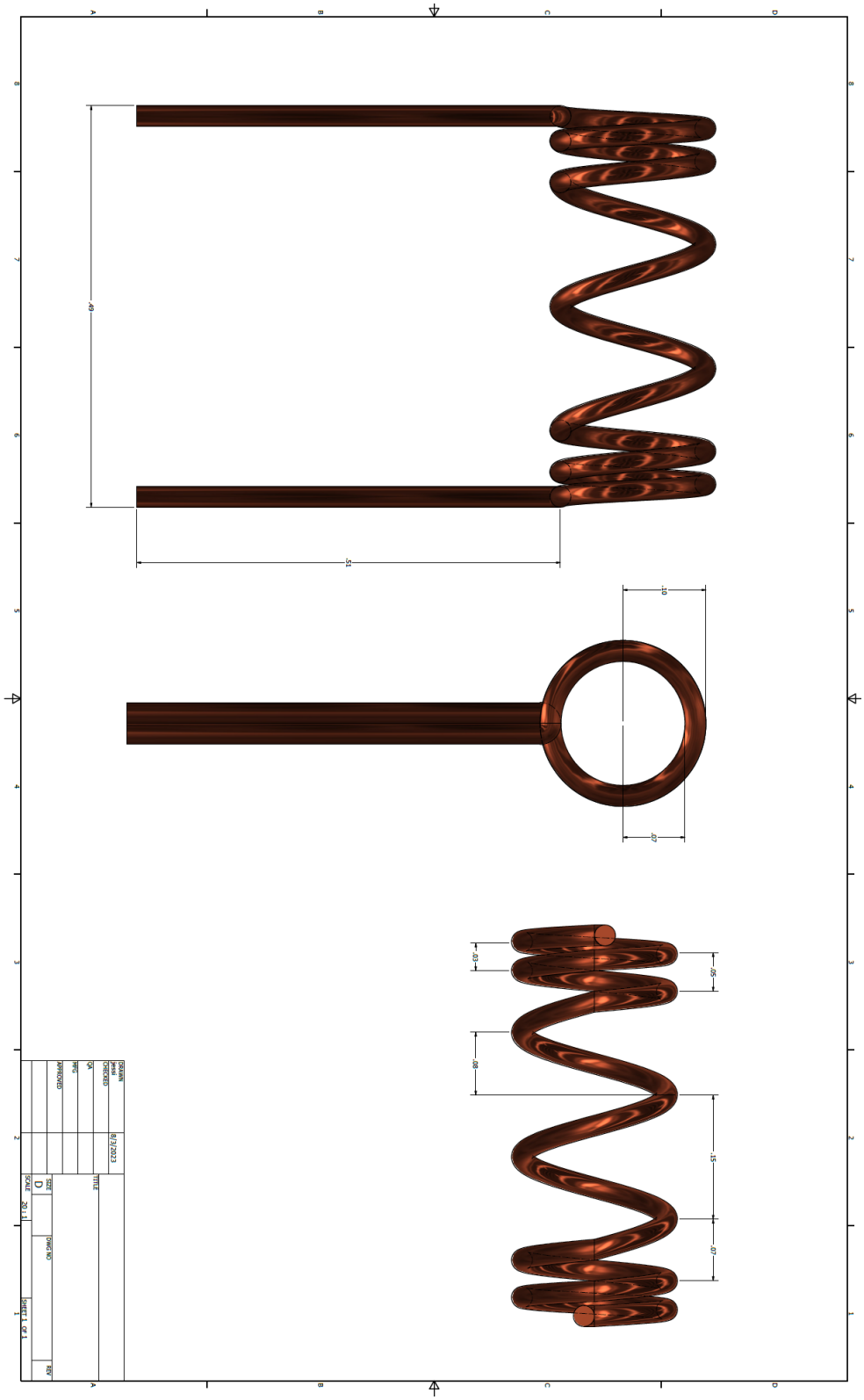

Figure A.21: Stretched variable pitch solenoid.

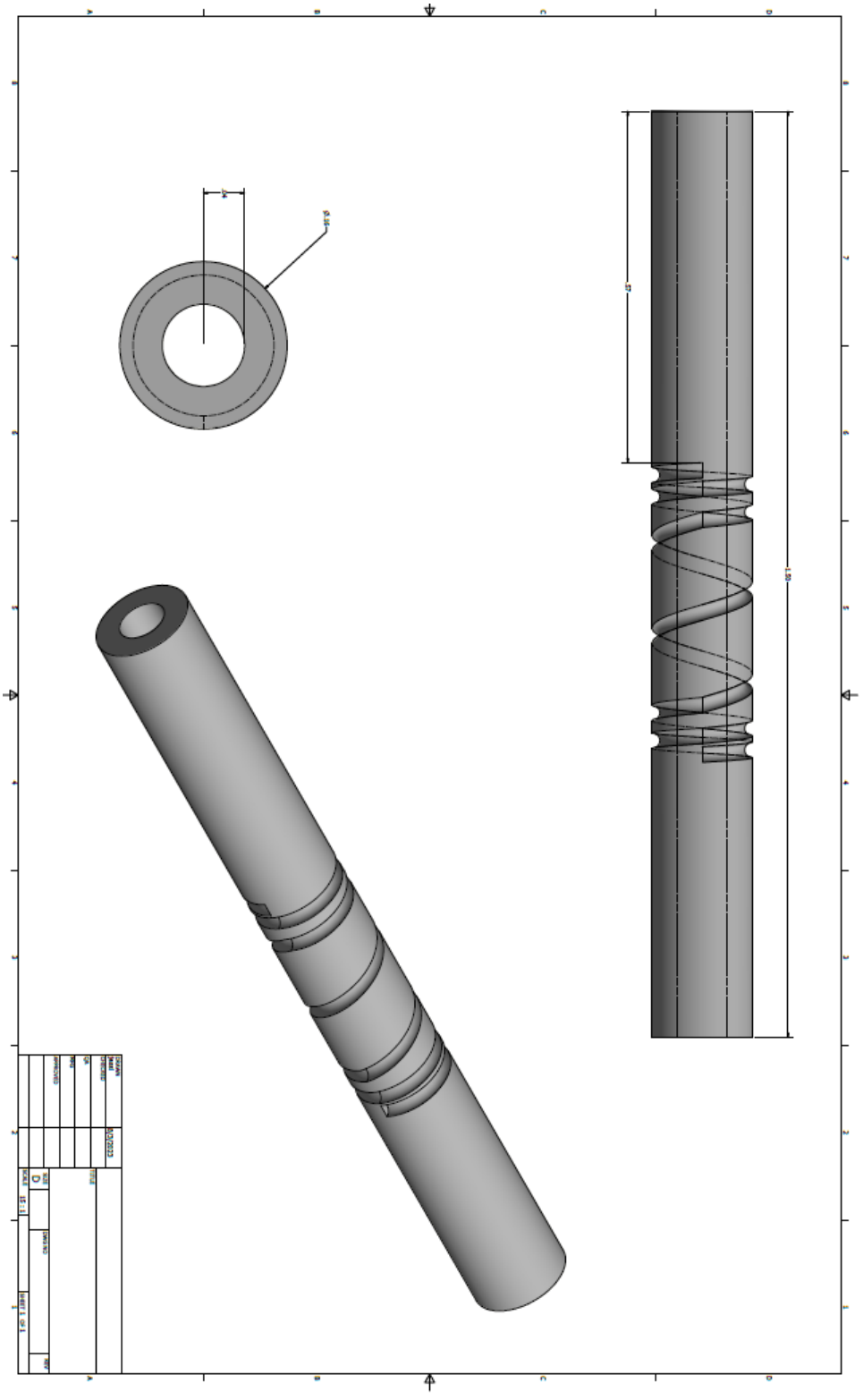

Figure A.22: Stretched variable pitch solenoid template.

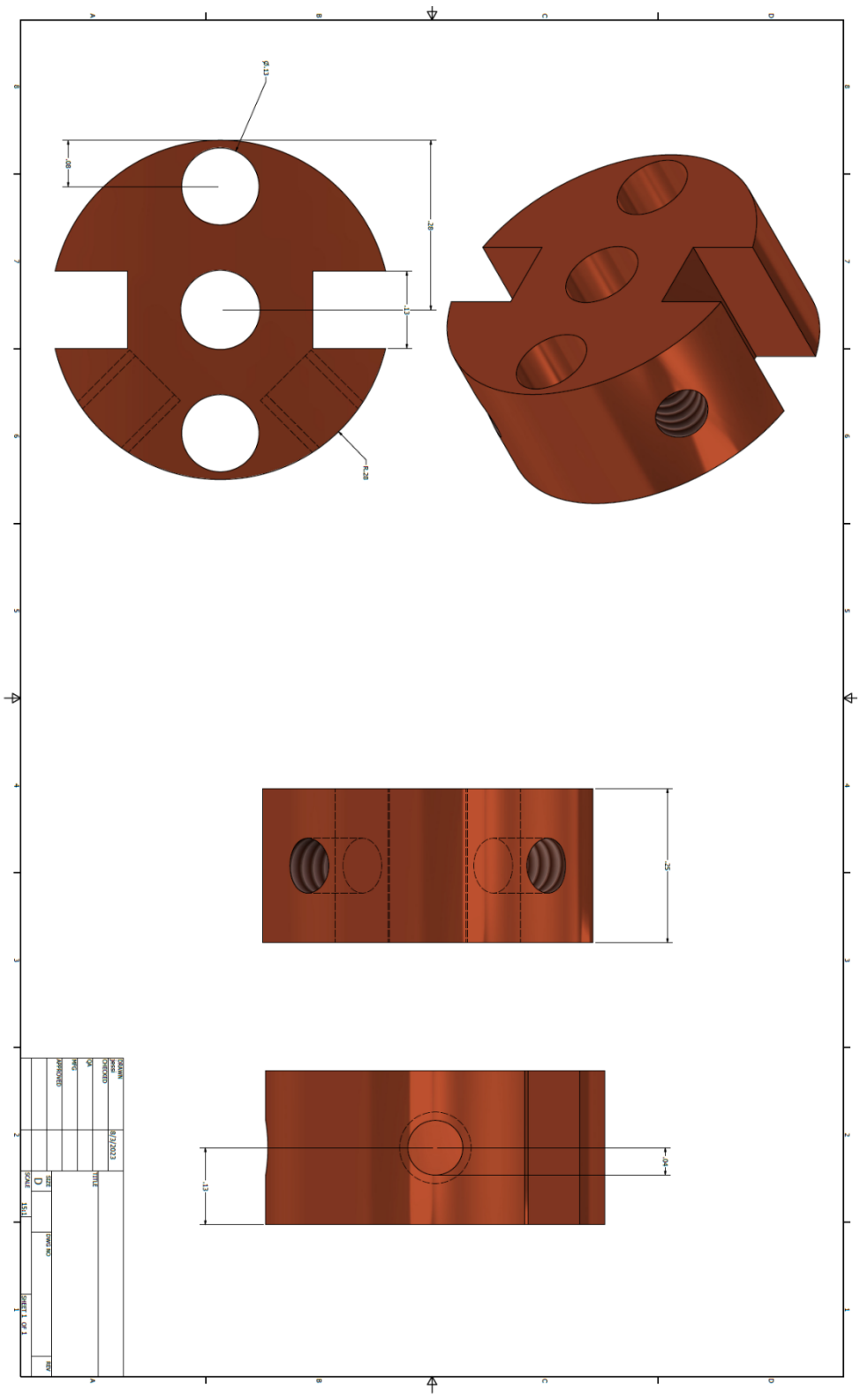

Figure A.23: Machined inductive stub (copper) for proton channel.

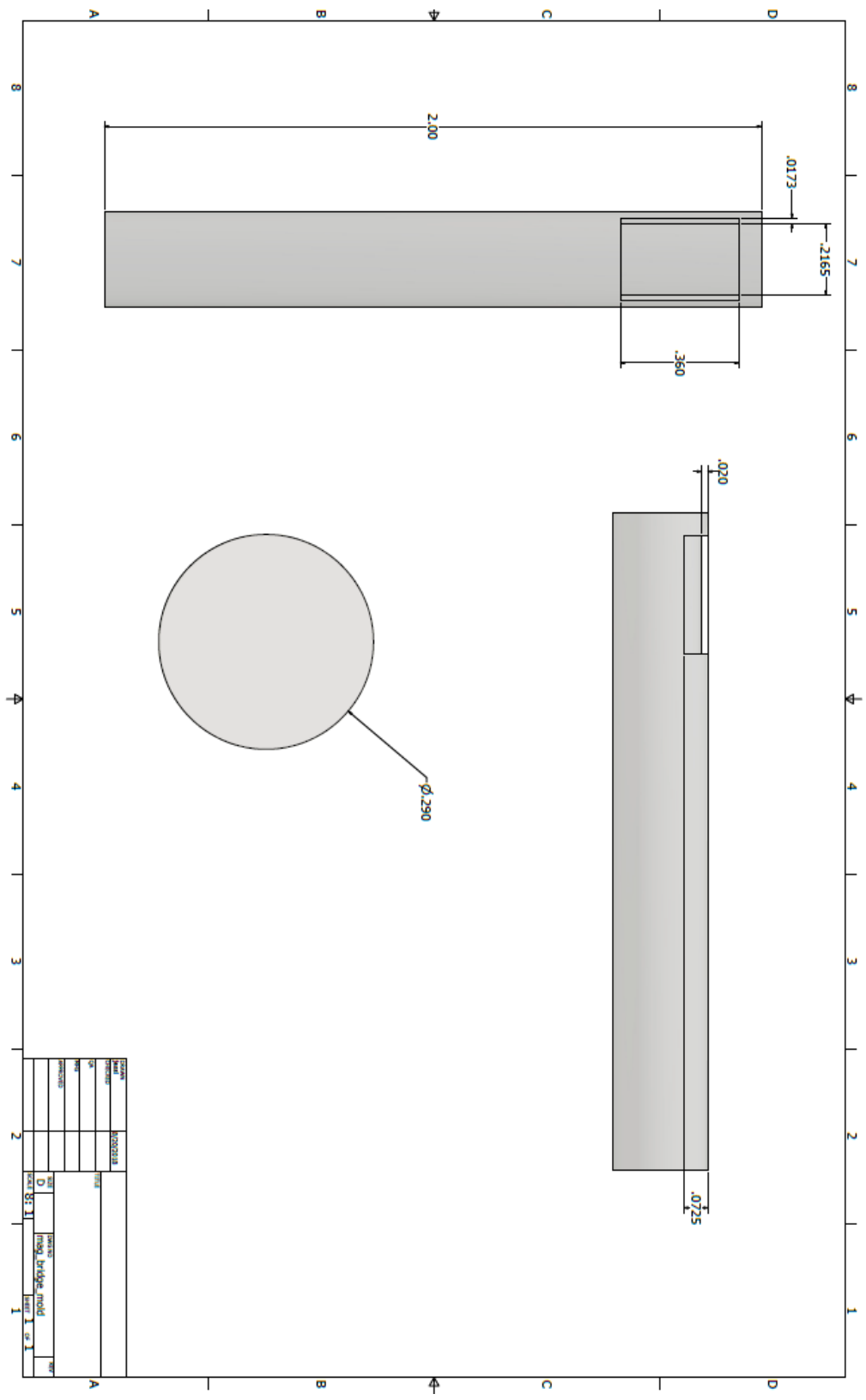

Figure A.24: Modified-Aldermann Grant coil capacitive bridge soldering tool.

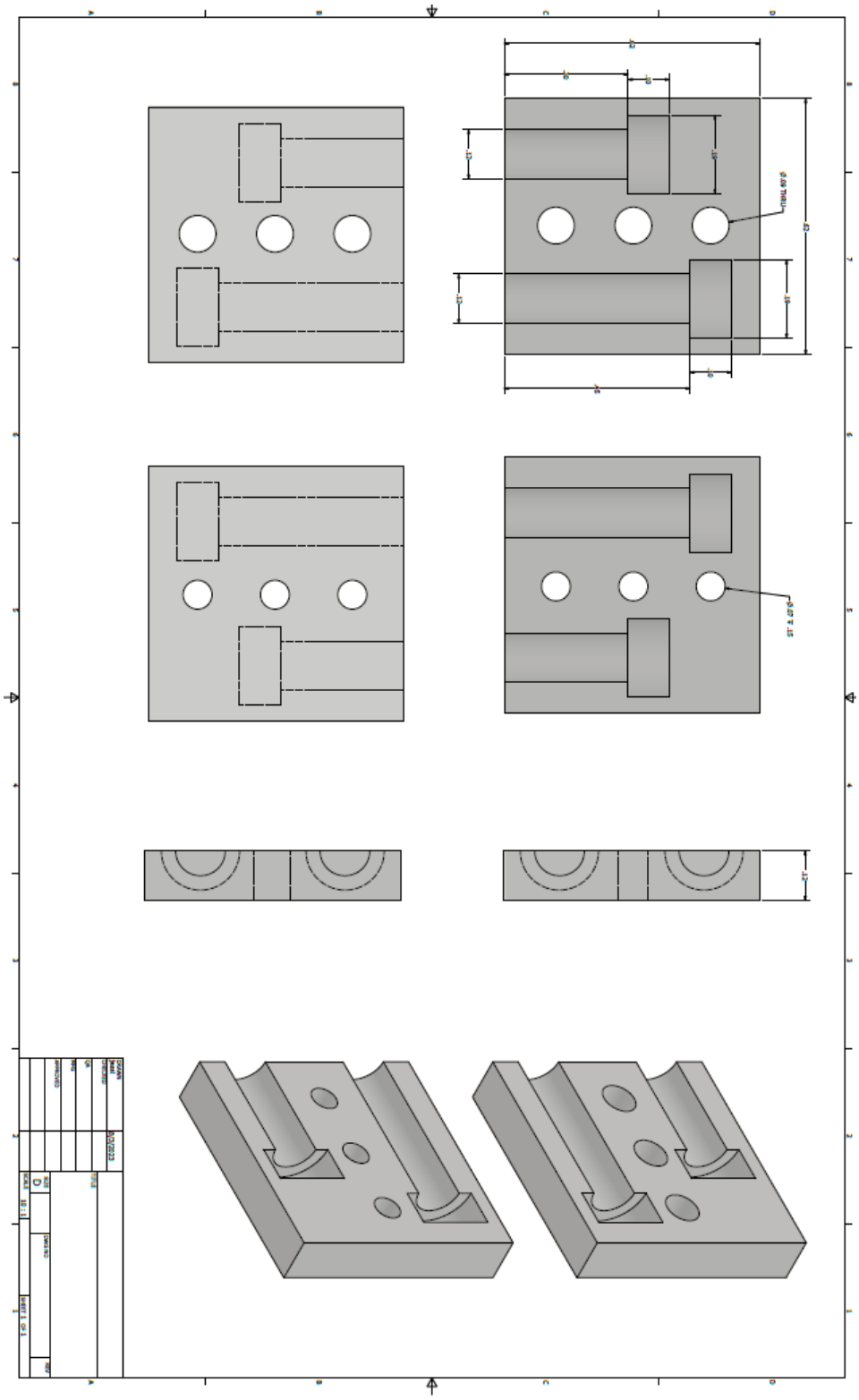

Figure A.25: Magic-angle adjust mechanism for cross-coil probe.

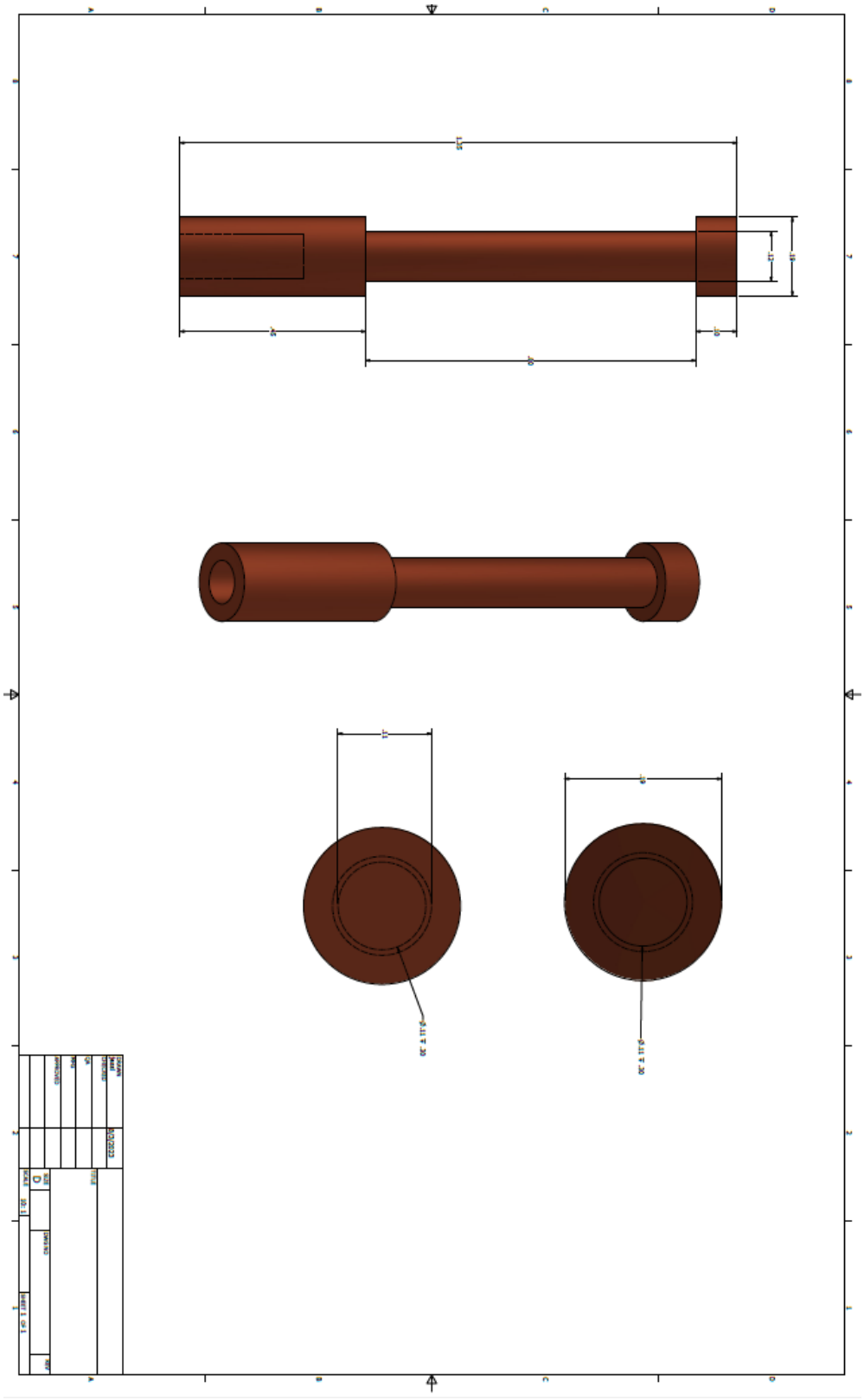

Figure A.26: Magic-angle adjust mechanism connector for cross-coil probe.

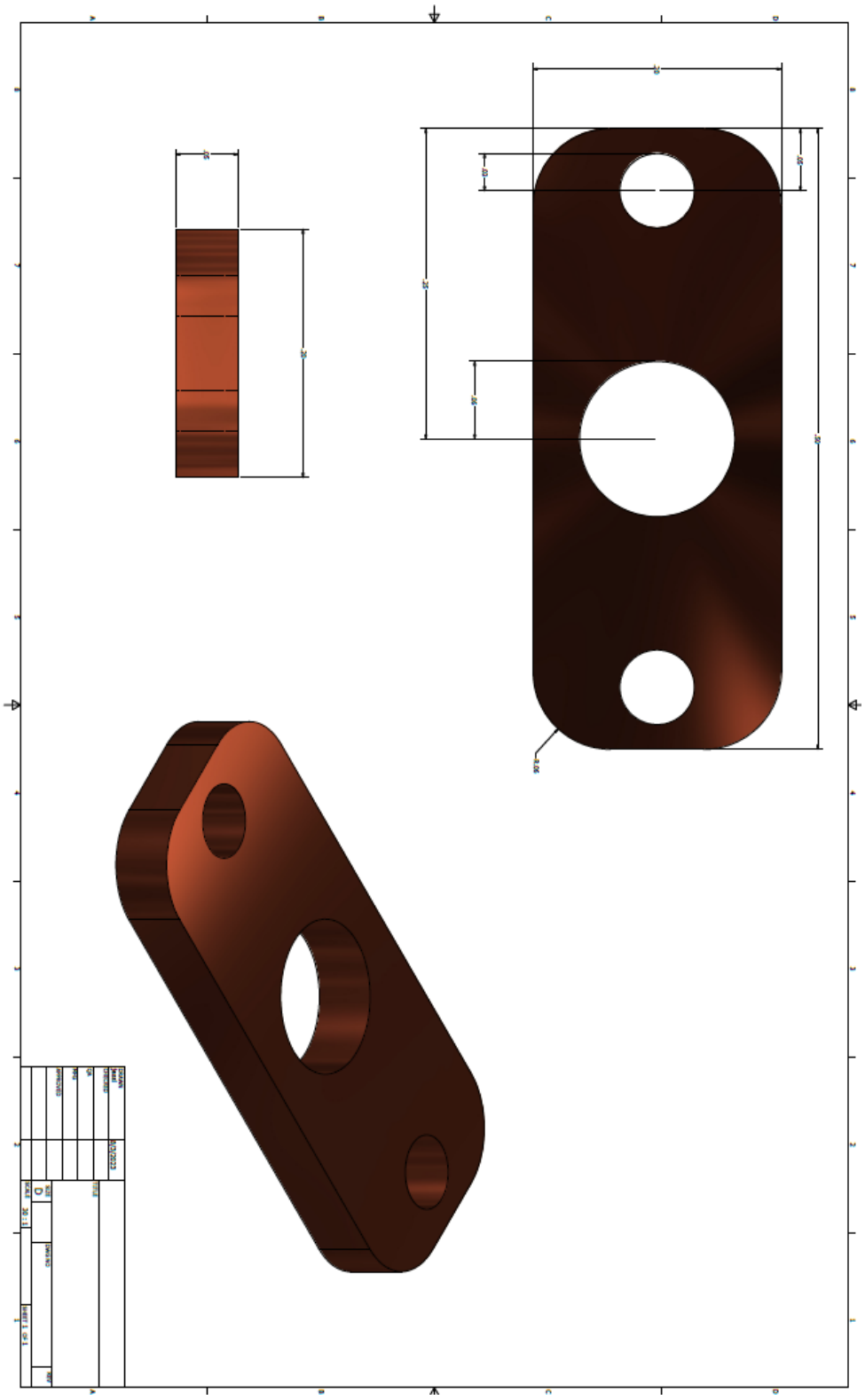

Figure A.27: Machined match plate (copper) for proton channel.

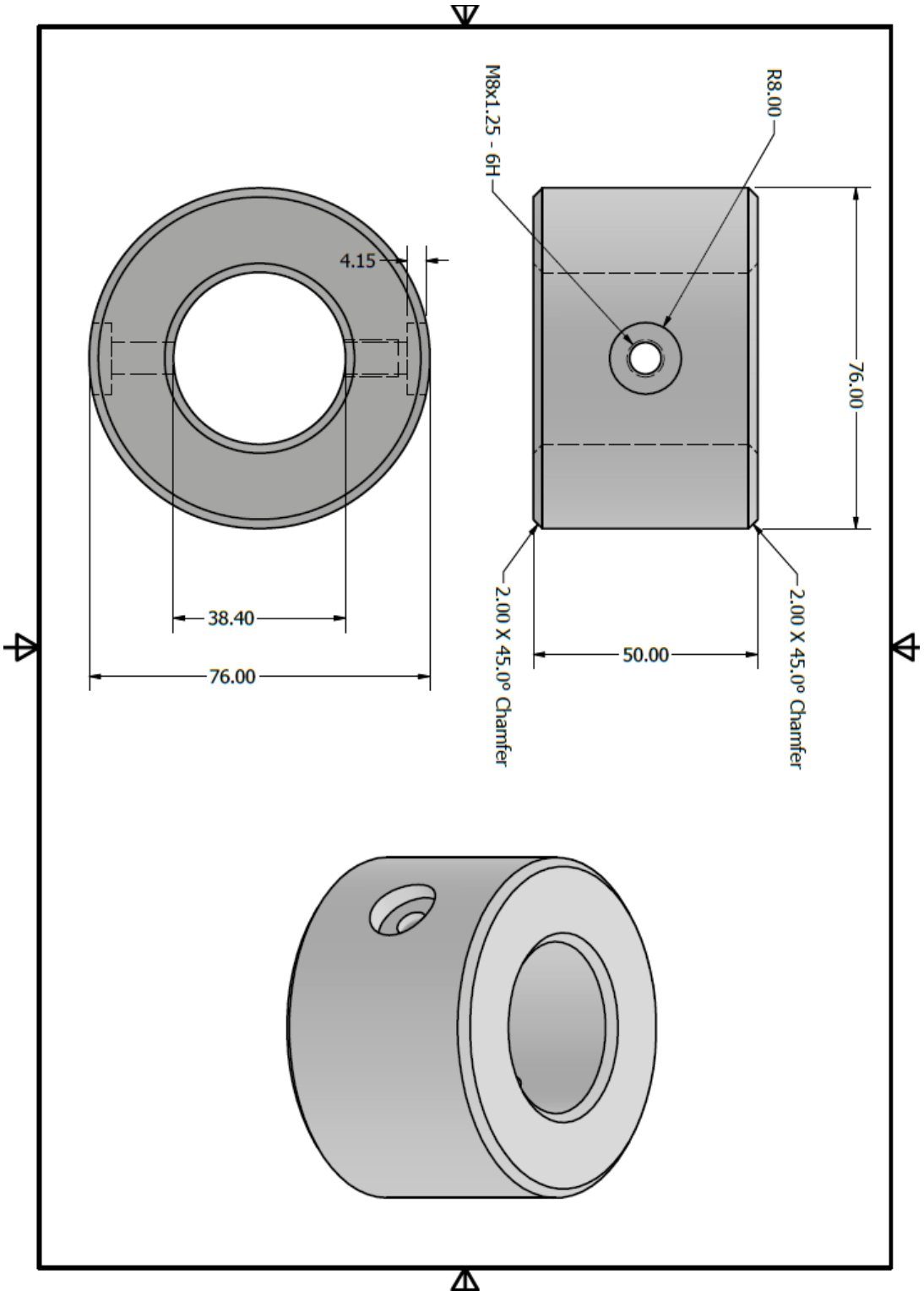

Figure A.28: Wide to narrow bore shim stack adapter.

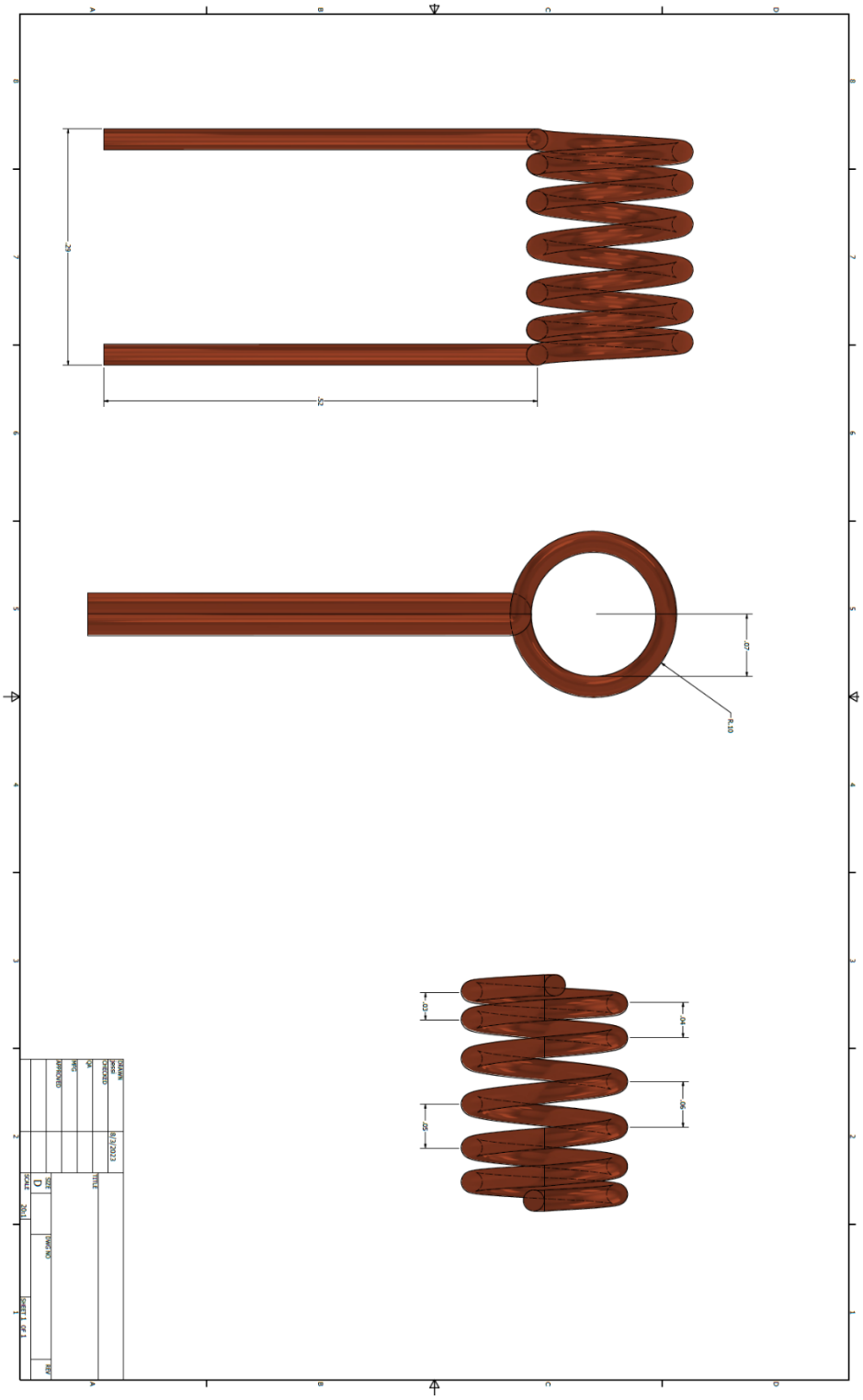

Figure A.29: Model variable pitch solenoid.

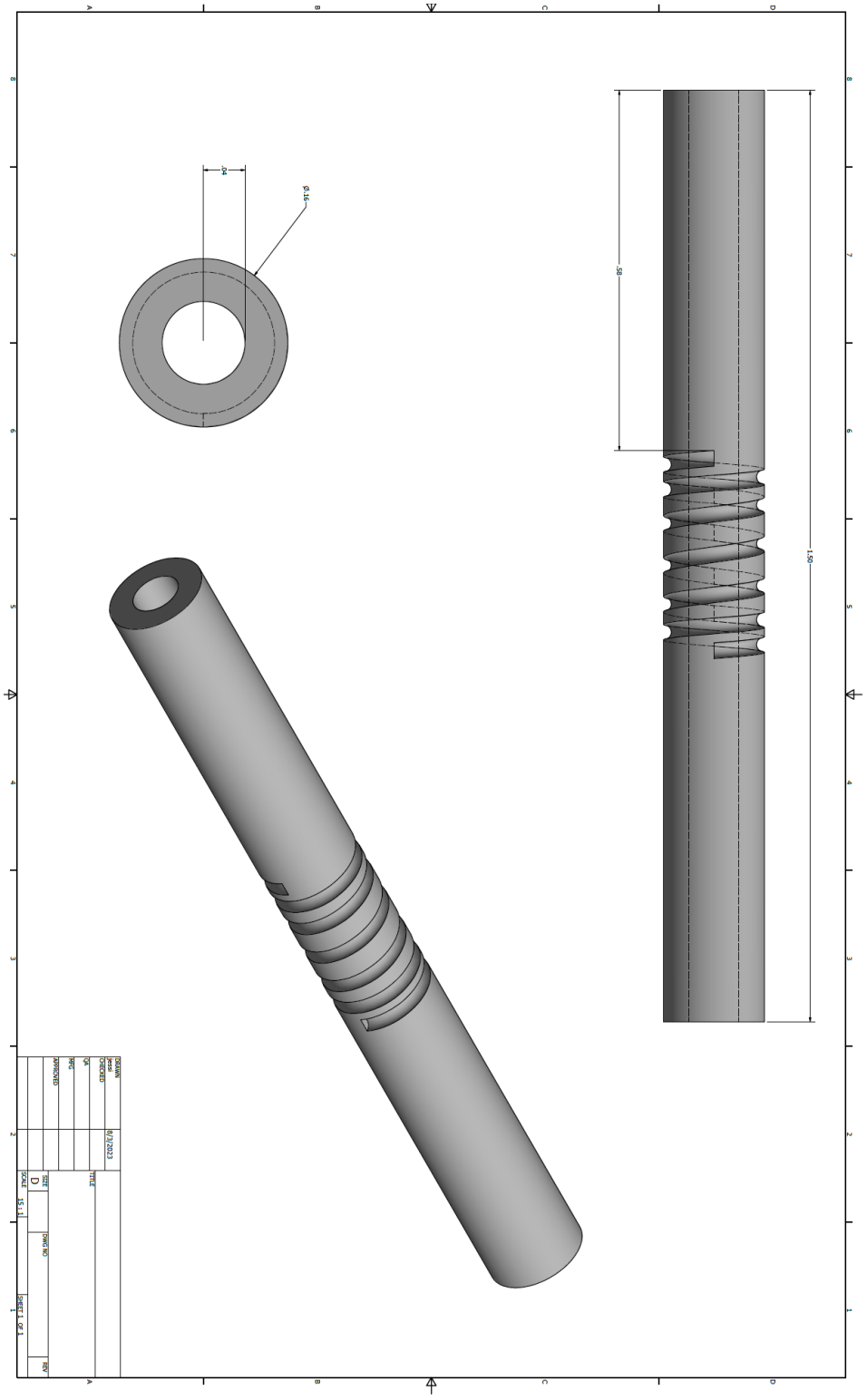

Figure A.30: Model variable pitch solenoid template.

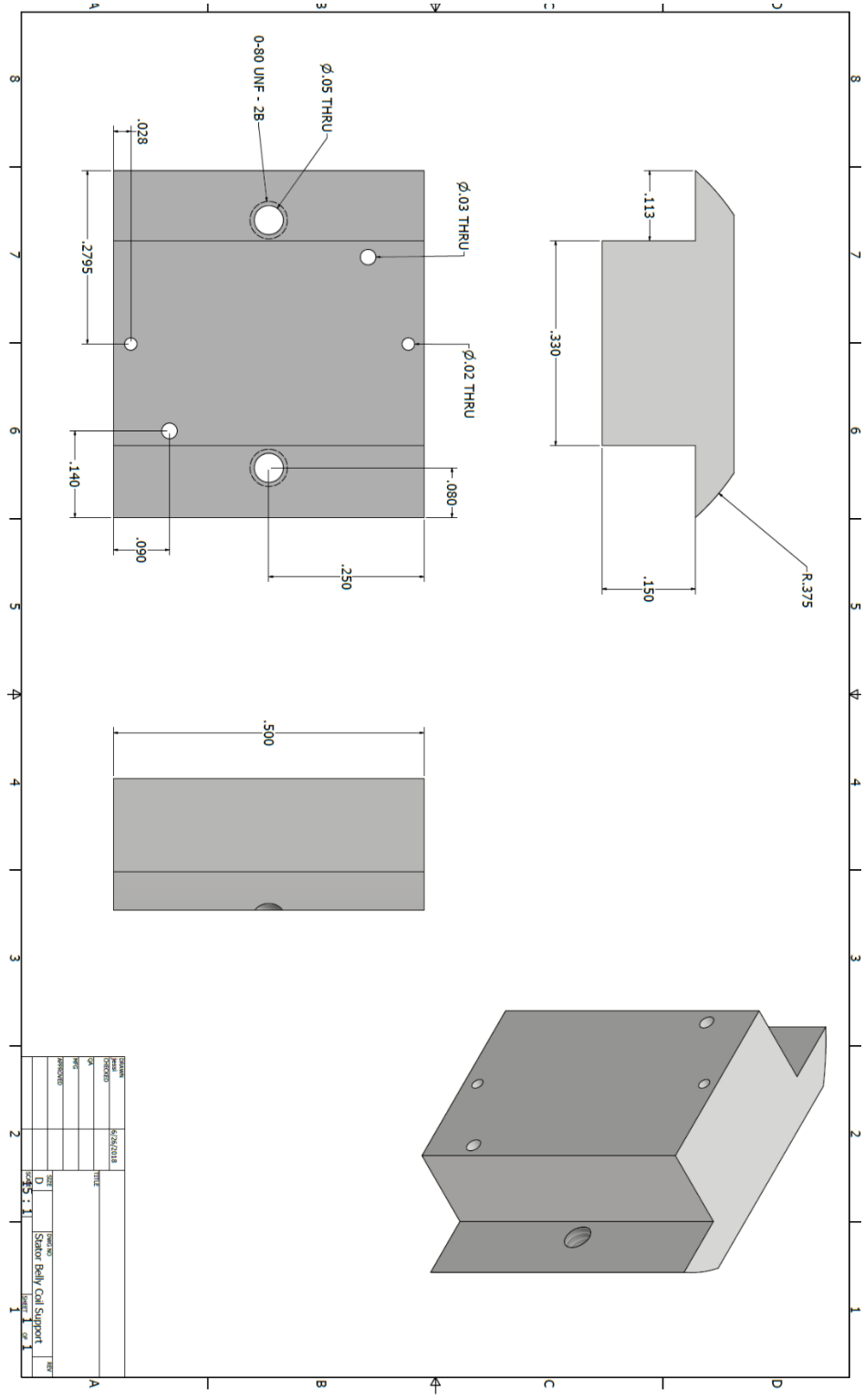

Figure A.31: Machined cross-coil platform for spinning assembly (PCTFE).

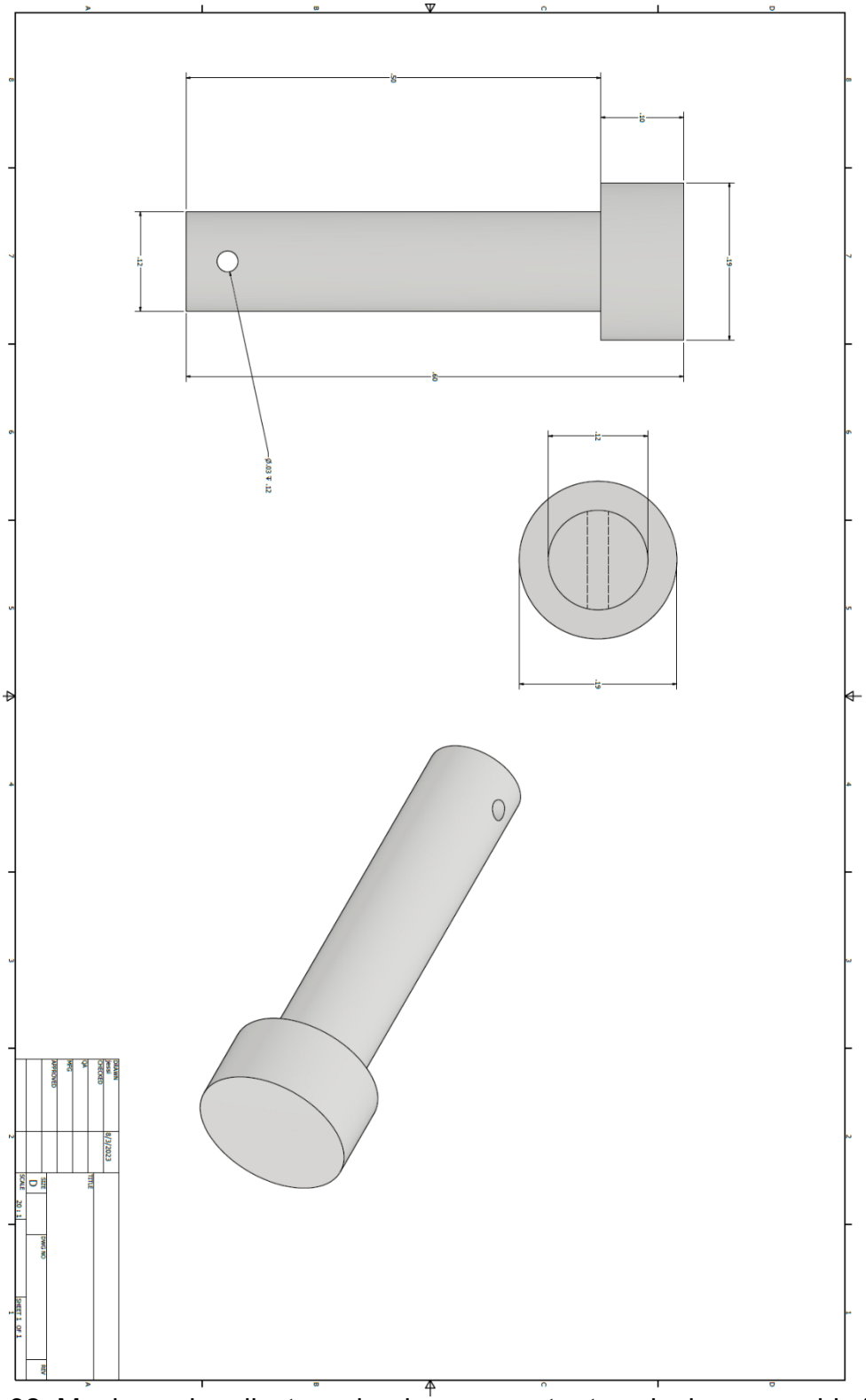

Figure A. 32: Magic-angle adjust mechanism connector to spinning assembly for cross-coil probe.

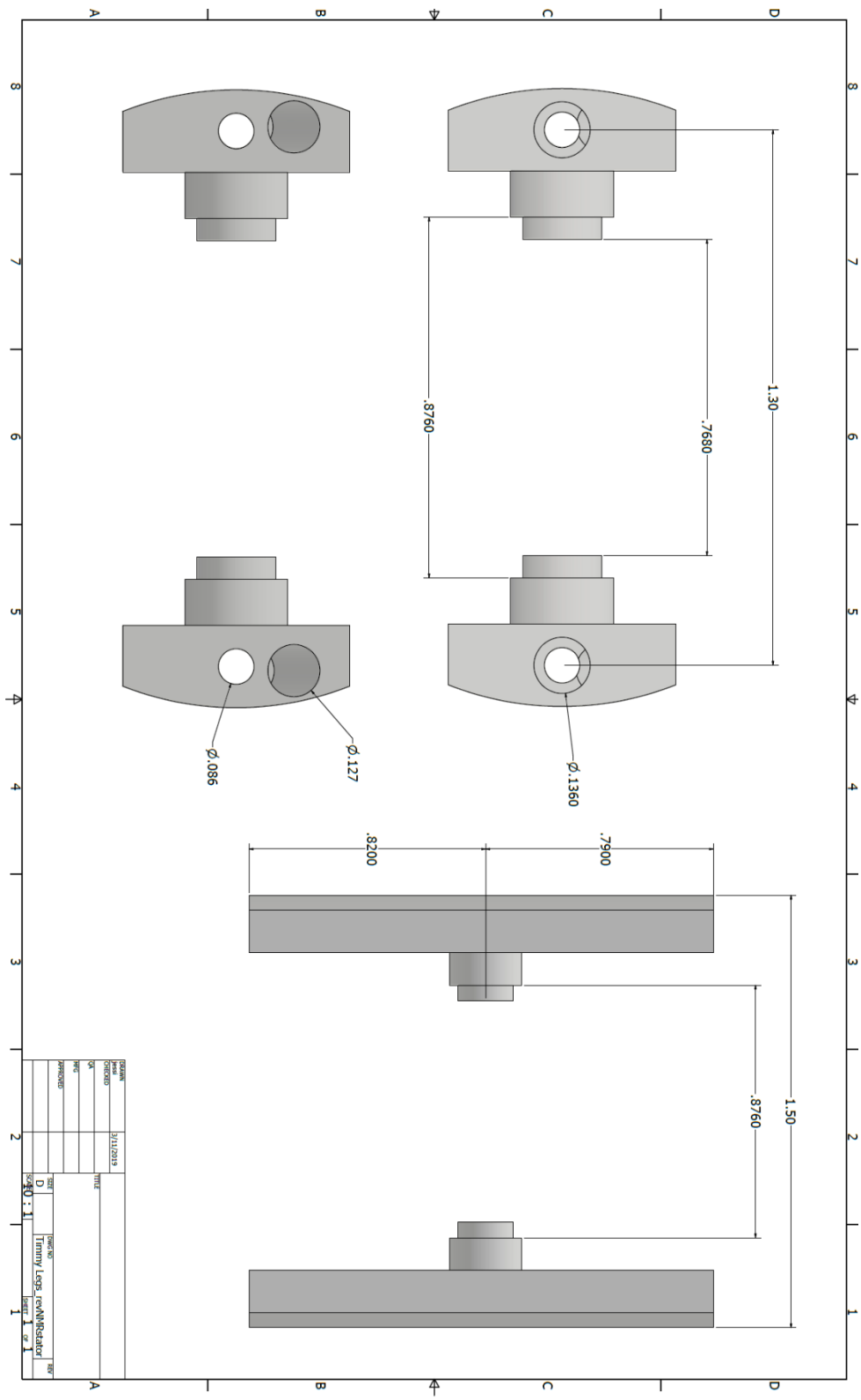

Figure A.33: Supports to enable use of a spinning assembly with different dimensions.

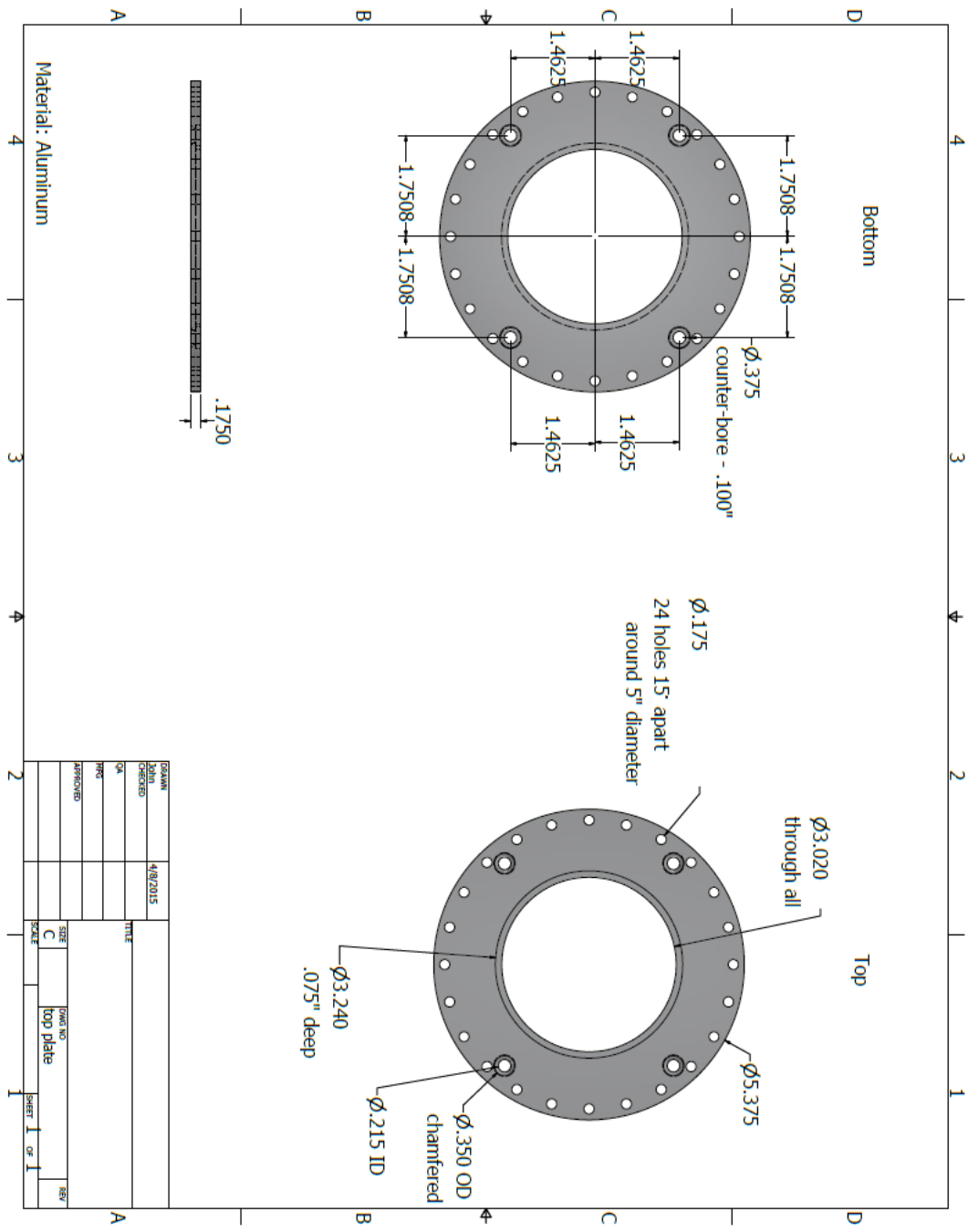

Figure A.34: Machined probe body top plate (aluminum).

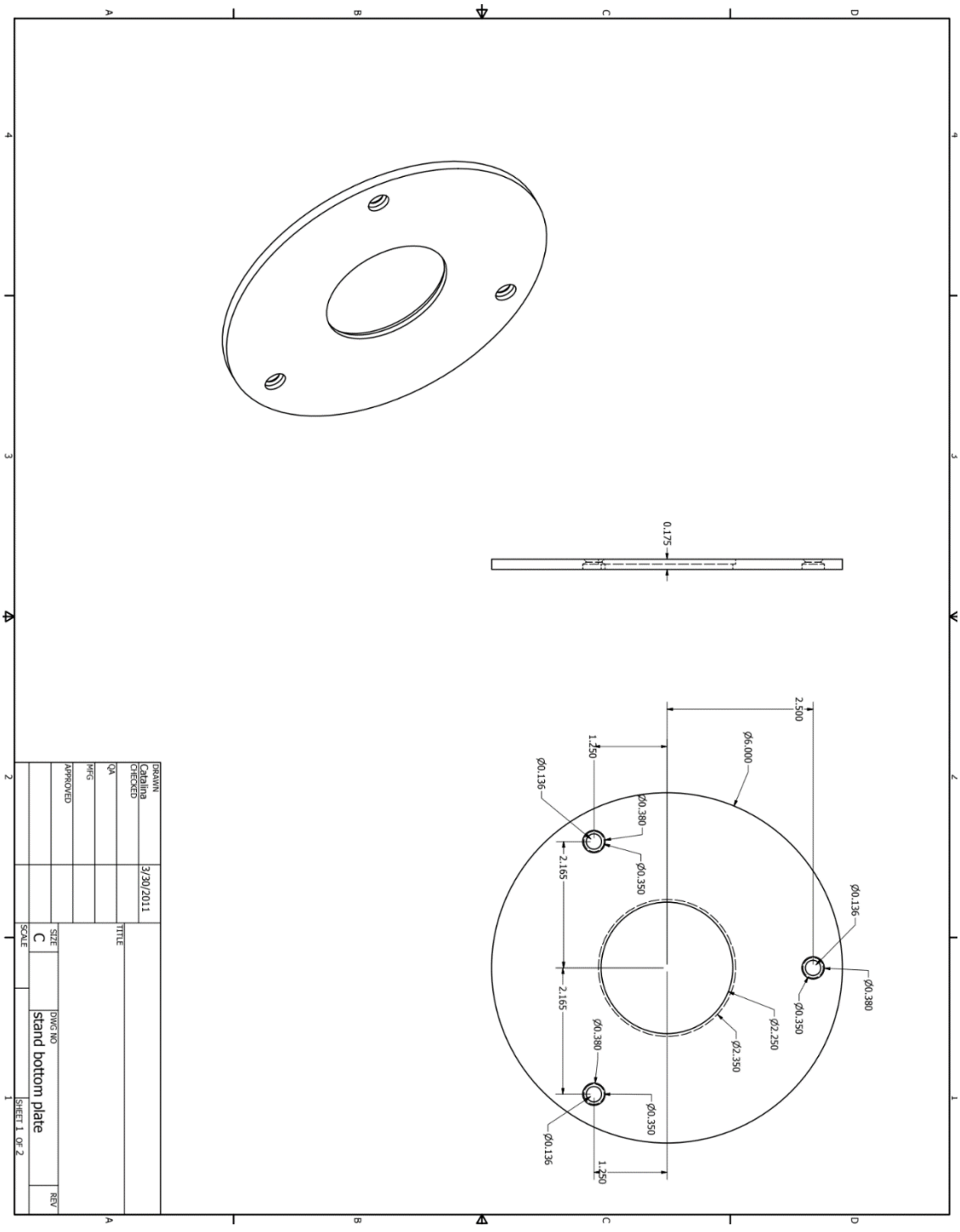

Figure A.35: Machined probe body bottom plate (aluminum).

APPENDIX B

MATLAB and Python Scripts

Figure B.1: MATLAB solenoid coil optimization script.

variablePitchNMR.m

```
clear;clc;
coil_IR = 1.905; %mm (0.075")
r=coil_IR;
wire_diam = 0.64262; %mm (0.0253" 22 gauge wire)
coil_length = 8.51916;%mm (0.3354")
max_coil_len = coil_length;

coil_OR = coil_IR+wire_diam;
minpitch = 0.762;%mm (0.03") minimum allowed pitch for the coil

%% variable pitch parameters
s = 1.8714;%pitch of const. pitch solenoid (max pitch of variable coil)
nu = -0.0001;%scalar factor
k = 3.8776;%exponential factor
nturns = 6;
tmin = -(nturns/2)*(2*pi);
tmax = (nturns/2)*(2*pi);

fx = @(t) r*cos(t);
fy = @(t) r*sin(t);
% fz = @(t) s/(2*pi)*t;
fz = @(t) s/(2*pi) * (t+nu*abs(t).^k.*sign(t));

%% plot parametric curve in 3d space
figure()
ezplot3(fx,fy,fz,[tmin,tmax])
view([1,0,0])%view plane normal to x (y-z plane)

%% plot pitch profile in z
figure()
fz1 = @(t) fz(t-pi);
fz2 = @(t) fz(t+pi);
pitch = @(t) fz2(t)-fz1(t);%difference in position between 2 turns at any point along
turn

t_plt = linspace(tmin,tmax,100);
z_plt = fz(t_plt);
pitch_plt = pitch(t_plt);
plot(z_plt, pitch_plt)
%need to fix ticks and axis limits here
xlabel('z-position (inches)')
ylabel('pitch (inches)')
grid on
title('Pitch vs Position')

%% plot contour of pitch >=0 vs log10(-nu), k. for fixed s, max t
%also put restrictions on nu and k
nx = 5000;
ny=nx;
nu_contour = -logspace(-10,0,nx);%nu is very small, use logspace
k_contour = linspace(0,10,ny);
```

```
[NU,K] = meshgrid(nu_contour,k_contour);
t_contour = tmax;
s_contour = s;

%dFz_dt = s_contour/(2*pi) + NU.*K.*t_contour.^(K-1);
pitch_contour = s_contour/(2*pi) * ((t_contour+pi) + NU.*(t_contour+pi).^K) -...
    s_contour/(2*pi) * ((t_contour-pi) + NU.*(t_contour-pi).^K);
figure()
%contourf(log10(-NU),K,dFz_dt)
maxlevel = max(pitch_contour(:));
minlevel = minpitch;
levelstep = (maxlevel-minlevel)/25;
levels = minlevel:levelstep:maxlevel;
contourf(log10(-NU),K,pitch_contour,levels, 'LineStyle', 'none')
%surf(log10(-NU),K,pitch_contour,'LineStyle', 'none')
xlabel('log10(-\nu)')
ylabel('k')
%title('df_z/dt vs nu and k')
title('Pitch vs nu and k (at edge of coil)(s=0.07in)')
colorbar()

%% 3D plot of S vs K and NU
npoints=50;
nu_3d = -logspace(-10,0,npoints);%nu is very small, use logspace
k_3d = linspace(0,10,npoints);
[NU,K] = meshgrid(nu_3d,k_3d);
t_3d = tmax;
nturns_3d = nturns;

% pitch_3d = S/(2*pi) .* (t_3d + NU.*t_3d.^K);
% coil_len = 2*S.*(nturns_3d/2 + (nturns_3d/2).^K .* ...
%                     NU.*(2*pi).^(K-1));

s_3d = zeros(npoints,npoints);
for i = 1:npoints
    for j = 1:npoints
        %minimum allowed s that still meets pitch requirements at ends for
        %fixed nu and k
        min_s = coil_length;
        for T=linspace(0,pi*nturns,50)
            min_s_new = minpitch*2*pi / (((T+pi) + NU(i,j)*(T+pi)^K(i,j)) - ...
                ((T-pi) + NU(i,j)*(T-pi)^K(i,j)));
            if min_s_new < min_s
               min_s = min_s_new;
            end
        end
        % s calculated to make coil length equal to fixed maximum
        s_3d(i,j) = (max_coil_len/2)/(nturns_3d/2 + (nturns_3d/2)^K(i,j) * ...
                    NU(i,j)*(2*pi)^(K(i,j)-1));
        % derivative of z-component must not cross zero to prevent overlap
        for T=linspace(0,pi*nturns,50)
           if  (s_3d(i,j)/(2*pi)*(1 + K(i,j)*NU(i,j)*(T)^(K(i,j)-1))) < 0
               s_3d(i,j) = NaN;
               break;
           end
```

```
        end
        % check that calculated s meets pitch requirements and is not
        % significantly large with respect to coil length
        %if s_3d(i,j) < min_s || s_3d(i,j) > max_coil_len/(nturns/2)

        % check that calculated s meets minimum pitch and derivative of z
        % does not cross zero and s is not significantly large w/respect to
        % coil length
        if isnan(s_3d(i,j))
           continue;
        end
        if (s_3d(i,j) < min_s) %minimum pitch not met
            s_3d(i,j) = NaN;%don't plot nonsensical values
        end
        if (s_3d(i,j) > max_coil_len/(nturns/2))%s value too high
            s_3d(i,j) = NaN;%don't plot nonsensical values
        end
    end
end
figure()
surf(log10(-NU),K,s_3d, 'LineStyle', 'none')
xlabel('log10(-\nu)')
ylabel('k')
zlabel('s')
titlestr = sprintf('%s%s%s%s%s','Map of values for coil of length '
,num2str(max_coil_len),...
    ' mm and minimum pitch ' , num2str(minpitch) , ' mm');
title(titlestr)

hold on;

%% calculate Bz curve flatness at each test point using 1-D biot savart
WaitBar = waitbar(0, 'calculating flatness, please wait...');
total_pts = npoints^2;
err_array = zeros(npoints,npoints);
width_array = zeros(npoints,npoints);
%iterate through each k,nu point
%evaluate error function only if s_3d ~= NaN
point_count = 0;
for i = 1:npoints
    for j = 1:npoints
        if isnan(s_3d(i,j))%skip point if NaN
            err_array(i,j) = NaN;
            width_array(i,j) = NaN;
        else
            [err_array(i,j),width_array(i,j)] = ...
                biotSavart_error_function(s_3d(i,j),NU(i,j),K(i,j));

        end
        waitbar(((i-1)*npoints+j) / total_pts, WaitBar)
    end
    percent_complete = ((i-1)*npoints+j) / total_pts * 100
end
close(WaitBar);
```

```
figure()
surf(log10(-NU),K,err_array, 'LineStyle', 'none')
xlabel('log10(-\nu)')
ylabel('k')
zlabel('stddev_{90%}')
titlestr = sprintf('%s%s%s%s%s','peak flatness for coil of length '
,num2str(max_coil_len),...
    ' mm and minimum pitch ' , num2str(minpitch) , ' mm');
title(titlestr)

% width_pt_stepsize = (fz(tmax)-fz(tmin))/100;% mm
width_pt_stepsize = 0.062;%mm
figure()
surf(log10(-NU),K,width_array*width_pt_stepsize, 'LineStyle', 'none')
xlabel('log10(-\nu)')
ylabel('k')
zlabel('peak-width_{90%} (mm)')
titlestr = sprintf('%s%s%s%s%s','peak width for coil of length '
,num2str(max_coil_len),...
    ' mm and minimum pitch ' , num2str(minpitch) , ' mm');
title(titlestr)
```

biotSavartTest.m

```
clear;clc;
mu0 = 4*pi*1e-7;
%% Dimensional inputs
coil_IR = 1.905; %mm (0.075")
r=coil_IR;
% s = 1.42;%pitch of const. pitch solenoid (max pitch of variable coil)
% nu = -10^(-10);%scalar factor
% k = 1;%exponential factor

s = 1450;
c = 28.68;

nturns = 6;
tmin = -(nturns/2)*(2*pi);
tmax = (nturns/2)*(2*pi);


I = 1;%driving coil with 1A

%% define parametric curve
fx = @(t) r*cos(t);
fy = @(t) r*sin(t);
% fz = @(t) s/(2*pi)*t;
% fz = @(t) s/(2*pi) * (t+nu*abs(t).^k.*sign(t));
fz = @(t) s/(2*pi) * (t/(c^2) .* exp(-(t.^2)/(2*(c^2))));%from derivative of (1-
gaussian)

%% Biot Savart law to find on-axis magnetic field components at each observer point
on-axis
delta_t = 0.05;% step size of parametric variable
delta_z = 0.1; %step size of axial observation points (mm)
```

```
zmin = fz(tmin);
zmax = fz(tmax);


t_pts = tmin:delta_t:tmax;
z_pts = zmin:delta_z:zmax;
num_zpts = numel(z_pts);
num_tpts = numel(t_pts);

%generate vector points in [x_arr;y_arr;z_arr] format
%on-axis observation points
zero_vec = squeeze(zeros(num_zpts,1))';
r_vec = [zero_vec;zero_vec;z_pts]*1e-3;%CONVERTING TO METERS HERE
% points along curve
l_vec = [fx(t_pts);fy(t_pts);fz(t_pts)]*1e-3;%CONVERTING TO METERS HERE
%differential length vector along curve
dl_vec = zeros(size(l_vec));
for t_idx = 1:(num_tpts-1)
    dl_vec(:,t_idx) = l_vec(:,t_idx+1)-l_vec(:,t_idx);
end
%get the last differential element by subtracting l_vec(tmax+delta_t)-l_vec(tmax)
%(be sure it is in meters too!)
% dl_vec(:,num_tpts) = ([fx(tmax+delta_t);fy(tmax+delta_t);fz(tmax+delta_t)]*1e-3)-
...
%     l_vec(:,num_tpts);

% take off final point of each vector
l_vec(:,num_tpts) = [];
dl_vec(:,num_tpts) = [];
num_tpts = num_tpts - 1;



% find B-field at each observation point on-axis, using rectangular
% numerical integration
B_vec = zeros(3,num_zpts);
for r_idx = 1:num_zpts
    r_prime_vec = r_vec(:,r_idx)*ones(1,num_tpts)-l_vec;

    %rectangular integration
    B = zeros(3,1);
    for t_idx = 1:num_tpts
        B = B + (cross(dl_vec(:,t_idx),r_prime_vec(:,t_idx)) /...
            norm(r_prime_vec(:,t_idx))^3);
    end
    B_vec(:,r_idx) = B*mu0*I/(4*pi);
end

%% plot Bz vs z on axis
figure()
plot(z_pts,B_vec(3,:))%Bz vs z on-axis
xlabel('z (mm)')
ylabel('B_z (T)')

%% plot Br vs z on axis
```

```
figure()
Br_vec = zeros(1,num_zpts);
for z_idx = 1:num_zpts
    Br_vec(z_idx) = norm(B_vec(1,z_idx),B_vec(2,z_idx));
end
plot(z_pts,Br_vec)%Br vs z on-axis
xlabel('z (mm)')
ylabel('B_r (T)')
```

biotSavart_1D.m

```
clear;clc;
mu0 = 4*pi*1e-7;
%% Dimensional inputs
coil_IR = 1.905; %mm (0.075")
r=coil_IR;
leg_length = 12.7;%mm
wire_diam = 0.64262;%mm (22AWG wire)

s = 1.7855523185281361;%pitch of const. pitch solenoid (max pitch of variable coil)
nu = -1.4802691267395071e-05;%scalar factor
k = 4.248496993987976 ;%exponential factor

% s = 1450;
% c = 28.68;
% s = 966700;
% c = 825;
nturns = 6;
t_coil_min = -(nturns/2)*(2*pi);
t_coil_max = (nturns/2)*(2*pi);

t_bend_min = -pi/2;
t_bend_max = 0;

t_straight_min = -leg_length;
t_straight_max = 0;


I = 1;%driving coil with 1A


%% define parametric curves
%define coil
fx_coil = @(t) r*cos(t);
fy_coil = @(t) r*sin(t);
% fz_coil = @(t) s/(2*pi)*t;
fz_coil = @(t) s/(2*pi) * (t+nu*abs(t).^k.*sign(t));
% fz_coil = @(t) s/(2*pi) * (t/(c^2) .* exp(-(t.^2)/(2*(c^2))));%from derivative of
(1-gaussian)

%define bend at start of coil
coil_start_x = fx_coil(t_coil_min);
coil_start_y = fy_coil(t_coil_min);
coil_start_z = fz_coil(t_coil_min);
```

```
fx_bend1 = @(t) -wire_diam/2*(cos(t)-1) + coil_start_x;%bend radius is wire diameter
fy_bend1 = @(t) wire_diam/2*sin(t) + coil_start_y;
fz_bend1 = @(t) coil_start_z*ones(1,numel(t));%no change in z component, vectorized

%define bend at end of coil
coil_end_x = fx_coil(t_coil_max);
coil_end_y = fy_coil(t_coil_max);
coil_end_z = fz_coil(t_coil_max);

fx_bend2 = @(t) wire_diam/2*(sin(t)+1) + coil_end_x;%bend radius is wire diameter
fy_bend2 = @(t) wire_diam/2*(cos(t)) + coil_end_y;
fz_bend2 = @(t) coil_end_z*ones(1,numel(t));%no change in z component

%define straight section at start of coil
bend1_start_x = fx_bend1(t_bend_min);
bend1_start_y = fy_bend1(t_bend_min);
bend1_start_z = fz_bend1(t_bend_min);

fx_straight1 = @(t) bend1_start_x - t;
fy_straight1 = @(t) bend1_start_y*ones(1,numel(t));
fz_straight1 = @(t) bend1_start_z*ones(1,numel(t));

%define straight section at end of coil
bend2_end_x = fx_bend2(t_bend_max);
bend2_end_y = fy_bend2(t_bend_max);
bend2_end_z = fz_bend2(t_bend_max);

fx_straight2 = @(t) bend2_end_x + t - t_straight_min;
fy_straight2 = @(t) bend2_end_y*ones(1,numel(t));
fz_straight2 = @(t) bend2_end_z*ones(1,numel(t));

%% load curves and t-ranges into arrays
%use cell arrays to store function handles!
fx_arr = {fx_straight1, fx_bend1, fx_coil, fx_bend2, fx_straight2};
fy_arr = {fy_straight1, fy_bend1, fy_coil, fy_bend2, fy_straight2};
fz_arr = {fz_straight1, fz_bend1, fz_coil, fz_bend2, fz_straight2};
tmin_arr = [t_straight_min,t_bend_min,t_coil_min,t_bend_min,t_straight_min];
tmax_arr = [t_straight_max,t_bend_max,t_coil_max,t_bend_max,t_straight_max];

%% setup domain of computation
extraSpace = 0;
% xmin = -(r+extraSpace);
% xmax = fx_straight2(t_straight_max)+extraSpace;
% ymin = -(r+extraSpace);
% ymax = r+extraSpace;
zmin = coil_start_z - extraSpace;
zmax = coil_end_z + extraSpace;

num_axis_pts = 100;
% x_vec = linspace(xmin,xmax,num_axis_pts);
% y_vec = linspace(ymin,ymax,num_axis_pts);
z_vec = linspace(zmin,zmax,num_axis_pts);

num_t_pts_per_segment = 1000;
scaling_factor = 1e-3;%mm to m
```

```
[l_vec, dl_vec] = get_l_vec(num_t_pts_per_segment, scaling_factor, fx_arr,...
    fy_arr, fz_arr, tmin_arr, tmax_arr);
num_t_pts = size(l_vec,2);
%% Biot Savart law to find on-axis magnetic field components at each observer point
on-axis

% line of observation points
zero_vec = squeeze(zeros(num_axis_pts,1))';
r_vec = [zero_vec;zero_vec;z_vec]*1e-3;%CONVERTING TO METERS HERE

% find B-field at each observation point, using rectangular
% numerical integration
B_vec = zeros(3,num_axis_pts);
for r_idx = 1:num_axis_pts
    r_prime_vec = r_vec(:,r_idx)*ones(1,num_t_pts)-l_vec;

    %rectangular integration
    B = zeros(3,1);
    for t_idx = 1:num_t_pts
        B = B + (cross(dl_vec(:,t_idx),r_prime_vec(:,t_idx)) /...
            norm(r_prime_vec(:,t_idx))^3);
    end
    B_vec(:,r_idx) = B*mu0*I/(4*pi);
end

%% plot Bz vs z on axis
figure()
bz_max = max(B_vec(3,:));
plot(z_vec,B_vec(3,:)/bz_max)%Bz vs z on-axis
xlabel('z (mm)')
ylabel('B_z/B_{z,max}')
% titlestr = sprintf('B_z vs z with s = %0.0f, c = %0.1f',s,c);
titlestr = sprintf('B_z vs z with s = %0.0f, k = %0.1f, v=%0.1e',s,k,nu);
title(titlestr)
grid on
axis([zmin,zmax,0, 1.2])
%% plot Br vs z on axis
figure()
Br_vec = zeros(1,num_axis_pts);
for z_idx = 1:num_axis_pts
    Br_vec(z_idx) = norm(B_vec(1,z_idx),B_vec(2,z_idx));
end
Br_max = max(Br_vec);
plot(z_vec,Br_vec/Br_max)%Br vs z on-axis
xlabel('z (mm)')
ylabel('B_r/B_{r,max}')
% titlestr = sprintf('|B_r| vs z with s = %0.0f, c = %0.1f',s,c);
titlestr = sprintf('|B_r| vs z with s = %0.0f, k = %0.1f, v=%0.1e',s,k,nu);
title(titlestr)
grid on
axis([zmin,zmax,0, 1.2])
%% compute length of wire used in coil

wire_length = 0;
```

```
for t_idx = 1:num_t_pts
    wire_length = wire_length + norm(dl_vec(:,t_idx));
end
sprintf('Wire length: %f mm',wire_length*1000)

%% compute standard deviation of Bz over top 90% of Bz vs z curve
% using stddev as a measure of flatness
% stddev is square root of variance, which is already quite small
% stddev is larger and easier to compare

Bz_normalized_vec = B_vec(3,:)/bz_max;
thresh = 0.9;
%locate first crossing of 90% Bz_max line
first_crossing_idx = 1;
last_crossing_idx = 1;
point_count = 0;
for Bz_idx = 1:num_axis_pts
    if Bz_normalized_vec(Bz_idx) > thresh
        point_count = point_count + 1;
        if point_count == 1 %first point found above 90% line
            first_crossing_idx = Bz_idx;
        else
           last_crossing_idx =  Bz_idx;% locate last point above 90% Bz_max line
        end
    end
end

% compute stddev over this range
stddev_90percent = std(Bz_normalized_vec(first_crossing_idx:last_crossing_idx))
```

Figure B.2: Python solenoid coil optimization script.

```
#!/usr/bin/env python
# coding: utf-8

# In[2]:


#Use the following code to install the required libraries for this script to function
#pip install numpy
#pip install matplotlib
#pip install tqdm
#pip install scipy
#%matplotlib notebook before import matplotlib
#pip install plotly


# In[3]:


# Setup
import numpy as np
import matplotlib.pyplot as plt
import plotly.graph_objects as go
from scipy.optimize import newton
from scipy.integrate import quad, simps
from scipy.spatial import distance
from tqdm import tqdm
from mpl_toolkits.mplot3d import Axes3D
from matplotlib.tri import Triangulation


# In[4]:


# User defined constraints
coil_IR = 1.905  # mm
wire_diam = 0.64262  # mm
coil_length = 8.51  # mm
nturns = 6
minpitch = 0.762  # mm


# In[5]:


# Constants
r = coil_IR
max_coil_len = coil_length
coil_OR = coil_IR + wire_diam
```

```
# In[6]:


# Exponential modulation of pitch
tmin = -(nturns/2)*(2*np.pi)
tmax = (nturns/2)*(2*np.pi)

fx = lambda t: r*np.cos(t)
fy = lambda t: r*np.sin(t)
fz = lambda t: s/(2*np.pi) * (t+nu*abs(t)**k*np.sign(t))


# In[7]:


# Selected variable pitch parameters s, nu, k for analysis
s = 1.903  # pitch of const. pitch solenoid (max pitch of variable coil)
nu = -10**(-2.285)  # scalar factor
k = 2.352  # exponential factor


# In[8]:


# Plot coil path in 3d space
fig = plt.figure()
ax = fig.add_subplot(111, projection='3d')
t = np.linspace(tmin, tmax, 100)
ax.plot(fx(t), fy(t), fz(t))
ax.view_init(elev=0., azim=-90)
plt.show()


# In[9]:


# Plot pitch vs axial position
fz1 = lambda t: fz(t-np.pi)
fz2 = lambda t: fz(t+np.pi)
pitch = lambda t: fz2(t)-fz1(t)
t_plt = np.linspace(tmin, tmax, 100)
z_plt = fz(t_plt)
pitch_plt = pitch(t_plt)
plt.figure()
plt.plot(z_plt, pitch_plt)
plt.xlabel('z-position (inches)')
plt.ylabel('pitch (inches)')
plt.title('Pitch vs Position')
plt.grid(True)
plt.show()
```

```
# In[9]:


#Plot contour of pitch >=0 vs log10(-nu), k for fixed s, max t
#also put restirctions on nu and k

nx = 50
ny = nx
nu_contour = -np.logspace(-10, 0, nx)  # nu is very small, use logspace
k_contour = np.linspace(0, 10, ny)
NU, K = np.meshgrid(nu_contour, k_contour)
t_contour = tmax
s_contour = s

pitch_contour = (
    s_contour / (2 * np.pi)
    * ((t_contour + np.pi) + NU * (t_contour + np.pi) ** K)
    - s_contour / (2 * np.pi) * ((t_contour - np.pi) + NU * (t_contour - np.pi) ** K)
)

plt.figure()
maxlevel = np.max(pitch_contour)
minlevel = minpitch
levelstep = (maxlevel - minlevel) / 25
levels = np.arange(minlevel, maxlevel + levelstep, levelstep)
plt.contourf(np.log10(-NU), K, pitch_contour, levels, linestyle='none')
plt.xlabel('log10(-nu)')
plt.ylabel('k')
plt.title('Pitch vs nu and k (at edge of coil)(s=0.07in)')
plt.colorbar()

plt.show()


# In[11]:


import plotly.graph_objects as go

# 3D plot of S vs K and NU
npoints = 500
nu_3d = -np.logspace(-10, 0, npoints)
k_3d = np.linspace(0, 10, npoints)
NU, K = np.meshgrid(nu_3d, k_3d)
t_3d = tmax
nturns_3d = nturns

s_3d = np.zeros((npoints, npoints))
valid_points = []
```

```
for i in range(npoints):
    for j in range(npoints):
        min_s = coil_length
        for T in np.linspace(0, np.pi*nturns, 50):
            min_s_new = minpitch*2*np.pi / (((T+np.pi) + NU[i, j]*(T+np.pi)**K[i, j])
- ((T-np.pi) + NU[i, j]*(T-np.pi)**K[i, j]))
            if min_s_new < min_s:
                min_s = min_s_new
        #s calculated to make coil length equal to fixed maximum
        s_3d[i, j] = (max_coil_len/2)/(nturns_3d/2 + (nturns_3d/2)**K[i, j] * NU[i,
j]*(2*np.pi)**(K[i, j]-1))
        #derivative of z-component must not cross zero to prevent overlap
        for T in np.linspace(0, np.pi*nturns, 50):
            if (s_3d[i, j]/(2*np.pi)*(1 + K[i, j]*NU[i, j]*T**(K[i, j]-1))) < 0:
                s_3d[i, j] = np.nan
                break
        #check that calculated s meets pitch requiremens and is not significantly
large with respect to coil length
        #check that calculated s meets minimum pitch and deritivative of z, does not
cross zero
        if np.isnan(s_3d[i, j]):
            continue
        if s_3d[i, j] < min_s or s_3d[i, j] > max_coil_len/(nturns/2): #minimum pitch
not met or value too high
            s_3d[i, j] = np.nan #don't plot nonsensical values
        # Check if the point is valid (not NaN)
        if not np.isnan(s_3d[i, j]):
            valid_points.append((s_3d[i, j], K[i, j], NU[i, j]))

# Filter out the NaN (invalid) values and extract valid data points
valid_indices = ~np.isnan(s_3d)
s_valid = s_3d[valid_indices]
k_valid = K[valid_indices]
nu_valid = NU[valid_indices]

# Store the valid points (s, k, nu) in a list
valid_points = list(zip(s_valid, k_valid, nu_valid))

# Create the plotly 3D scatter plot for valid data points
fig = go.Figure()

fig.add_trace(go.Scatter3d(x=np.log10(-nu_valid), y=k_valid, z=s_valid,
mode='markers',
                           marker=dict(size=5, color=s_valid, colorscale='Viridis'),
                           customdata=nu_valid,
                           hovertemplate='s: %{z:.20f}<br>k: %{y:.20f}<br>nu:
%{customdata:.20f}<extra></extra>'))

# Configure the layout
fig.update_layout(
```

```
    scene=dict(
        xaxis=dict(title='log10(-nu)'),
        yaxis=dict(title='k'),
        zaxis=dict(title='s'),
    ),
    title='Map of values for coil of length {} mm and minimum pitch {} mm'.format(
        max_coil_len, minpitch
    ),
    showlegend=True,
)

# Show the plot
fig.show()


# In[11]:


# Calculate the number of valid points
num_valid_points = len(valid_points)

print(f"Number of valid points: {num_valid_points}")


# In[12]:


#Define functions for BioSavart
#get_1_vec
def get_l_vec(t_pts_per_segment, scaling_factor, fx_arr, fy_arr, fz_arr, tmin_arr,
tmax_arr):
    num_curves = len(fx_arr)
    l_vec = np.zeros((3, num_curves*t_pts_per_segment))

    # build length vector from each segment (MUST BE IN METERS FIRST!)
    for curve_idx in range(num_curves):
        t_arr_segment = np.linspace(tmin_arr[curve_idx], tmax_arr[curve_idx],
t_pts_per_segment)
        segment_start_idx = curve_idx * t_pts_per_segment
        segment_end_idx = (curve_idx + 1) * t_pts_per_segment
        fx = fx_arr[curve_idx]
        fy = fy_arr[curve_idx]
        fz = fz_arr[curve_idx]
        l_vec[:, segment_start_idx:segment_end_idx] = np.array([fx(t_arr_segment),
fy(t_arr_segment), fz(t_arr_segment)]) * scaling_factor

    # compute differential length vector
    num_t_pts = l_vec.shape[1]
    dl_vec = np.zeros(l_vec.shape)
    for t_idx in range(num_t_pts - 1):
        dl_vec[:, t_idx] = l_vec[:, t_idx + 1] - l_vec[:, t_idx]
```

```
    # remove last (empty) point of dl and l vector due to how dl vector is computed
    dl_vec = dl_vec[:, :-1]
    l_vec = l_vec[:, :-1]

    return l_vec, dl_vec

#get_1vec_v2
def get_l_vec_v2(step_resolution_mm, scaling_factor, fx_arr, fy_arr, fz_arr,
tmin_arr, tmax_arr):
    num_curves = len(fx_arr)

    # compute approximate path length of each section
    npoints = 500  # number of points per section to calculate path lengths
    l_vec_pathlength = np.zeros((num_curves, 3, npoints))
    dl_vec_pathlength = np.zeros(l_vec_pathlength.shape)

    # get l and dl vector from each segment (MUST BE IN METERS FIRST!)
    for curve_idx in range(num_curves):
        t_arr_segment = np.linspace(tmin_arr[curve_idx], tmax_arr[curve_idx],
npoints)
        fx = fx_arr[curve_idx]
        fy = fy_arr[curve_idx]
        fz = fz_arr[curve_idx]
        # compute l vector for each segment
        l_vec_pathlength[curve_idx] = np.array([fx(t_arr_segment), fy(t_arr_segment),
fz(t_arr_segment)]) * scaling_factor
        # compute dl vector for each segment
        for t_idx in range(npoints - 1):
            dl_vec_pathlength[curve_idx, :, t_idx] = l_vec_pathlength[curve_idx, :,
t_idx + 1] - l_vec_pathlength[curve_idx, :, t_idx]

    # remove last (empty) point of dl vector due to how dl vector is computed
    dl_vec_pathlength = dl_vec_pathlength[:, :, :-1]

    # compute path length of each segment
    pathlength_per_segment = np.zeros(num_curves)
    for curve_idx in range(num_curves):
        for t_idx in range(npoints - 1):
            pathlength_per_segment[curve_idx] +=
np.linalg.norm(dl_vec_pathlength[curve_idx, :, t_idx])

    # compute l_vec and dl_vec using same step size for all segments
    step_resolution_m = step_resolution_mm / 1000
    npoints_per_segment = np.round(pathlength_per_segment /
step_resolution_m).astype(int)
    l_vec = np.zeros((3, np.sum(npoints_per_segment)))

    # build length vector from each segment (MUST BE IN METERS FIRST!)
    segment_start_idx = 0
    segment_end_idx = 0
```

```
    for curve_idx in range(num_curves):
        t_arr_segment = np.linspace(tmin_arr[curve_idx], tmax_arr[curve_idx],
npoints_per_segment[curve_idx])
        segment_end_idx += npoints_per_segment[curve_idx]
        fx = fx_arr[curve_idx]
        fy = fy_arr[curve_idx]
        fz = fz_arr[curve_idx]
        l_vec[:, segment_start_idx:segment_end_idx] = np.array([fx(t_arr_segment),
fy(t_arr_segment), fz(t_arr_segment)]) * scaling_factor
        segment_start_idx = segment_end_idx

    # compute differential length vector
    num_t_pts = l_vec.shape[1]
    dl_vec = np.zeros(l_vec.shape)
    for t_idx in range(num_t_pts - 1):
        dl_vec[:, t_idx] = l_vec[:, t_idx + 1] - l_vec[:, t_idx]

    # remove last (empty) point of dl and l vector due to how dl vector is computed
    dl_vec = dl_vec[:, :-1]
    l_vec = l_vec[:, :-1]

    return l_vec, dl_vec


# In[13]:


#BiotSavart error function

import numpy as np

def biotSavart_error_function(s, nu, k):
    if np.isnan(s) or np.isnan(nu) or np.isnan(k):
        return np.nan, np.nan

    # Dimensional inputs
    mu0 = 4 * np.pi * 1e-7
    coil_IR = 1.905  # mm (0.075")
    r = coil_IR
    leg_length = 12.7  # mm
    wire_diam = 0.64262  # mm (22AWG wire)

    # nturns = 6
    t_coil_min = -(6 / 2) * (2 * np.pi)
    t_coil_max = (6 / 2) * (2 * np.pi)

    t_bend_min = -np.pi / 2
    t_bend_max = 0

    t_straight_min = -leg_length
    t_straight_max = 0
```

```
    I = 1  # driving coil with 1A

    # define parametric curves
    # define coil
    fx_coil = lambda t: r * np.cos(t)
    fy_coil = lambda t: r * np.sin(t)
    fz_coil = lambda t: s / (2 * np.pi) * (t + nu * np.abs(t) ** k * np.sign(t))

    # define bend at start of coil
    coil_start_x = fx_coil(t_coil_min)
    coil_start_y = fy_coil(t_coil_min)
    coil_start_z = fz_coil(t_coil_min)

    fx_bend1 = lambda t: -wire_diam / 2 * (np.cos(t) - 1) + coil_start_x
    fy_bend1 = lambda t: wire_diam / 2 * np.sin(t) + coil_start_y
    fz_bend1 = lambda t: coil_start_z * np.ones_like(t)  # no change in z component,
vectorized

    # define bend at end of coil
    coil_end_x = fx_coil(t_coil_max)
    coil_end_y = fy_coil(t_coil_max)
    coil_end_z = fz_coil(t_coil_max)

    fx_bend2 = lambda t: wire_diam / 2 * (np.sin(t) + 1) + coil_end_x
    fy_bend2 = lambda t: wire_diam / 2 * np.cos(t) + coil_end_y
    fz_bend2 = lambda t: coil_end_z * np.ones_like(t)  # no change in z component

    # define straight section at start of coil
    bend1_start_x = fx_bend1(t_bend_min)
    bend1_start_y = fy_bend1(t_bend_min)
    bend1_start_z = fz_bend1(t_bend_min)

    fx_straight1 = lambda t: bend1_start_x - t
    fy_straight1 = lambda t: bend1_start_y * np.ones_like(t)
    fz_straight1 = lambda t: bend1_start_z * np.ones_like(t)

    # define straight section at end of coil
    bend2_end_x = fx_bend2
    bend2_end_y = fy_bend2
    bend2_end_z = fz_bend2

    fx_straight2 = lambda t: bend2_end_x(t) + t - t_straight_min
    fy_straight2 = lambda t: bend2_end_y(t) * np.ones_like(t)
    fz_straight2 = lambda t: bend2_end_z(t) * np.ones_like(t)

    # load curves and t-ranges into arrays
    fx_arr = [fx_straight1, fx_bend1, fx_coil, fx_bend2, fx_straight2]
    fy_arr = [fy_straight1, fy_bend1, fy_coil, fy_bend2, fy_straight2]
    fz_arr = [fz_straight1, fz_bend1, fz_coil, fz_bend2, fz_straight2]
    tmin_arr = [t_straight_min, t_bend_min, t_coil_min, t_bend_min, t_straight_min]
```

```
    tmax_arr = [t_straight_max, t_bend_max, t_coil_max, t_bend_max, t_straight_max]

    # setup domain of computation
    extraSpace = 0
    zmin = coil_start_z - extraSpace
    zmax = coil_end_z + extraSpace

    # compute needed number of axis observer points from resolution and computation
domain
    printer_resolution = 0.062  # mm
    num_axis_pts = round((zmax - zmin) / printer_resolution)
    z_vec = np.linspace(zmin, zmax, num_axis_pts)

    dl_stepsize_mm = 0.062
    scaling_factor = 1e-3  # mm to m
    l_vec, dl_vec = get_l_vec_v2(dl_stepsize_mm, scaling_factor, fx_arr,
                                 fy_arr, fz_arr, tmin_arr, tmax_arr)
    num_t_pts = l_vec.shape[1]

    # Biot Savart law to find on-axis magnetic field components at each observer
point on-axis
    zero_vec = np.zeros(num_axis_pts)
    r_vec = np.vstack((zero_vec, zero_vec, z_vec * 1e-3))  # CONVERTING TO METERS
HERE

    B_vec = np.zeros((3, num_axis_pts))
    for r_idx in range(num_axis_pts):
        r_prime_vec = np.tile(r_vec[:, r_idx, np.newaxis], (1, num_t_pts)) - l_vec

        B = np.zeros(3)
        for t_idx in range(num_t_pts):
            B += np.cross(dl_vec[:, t_idx], r_prime_vec[:, t_idx]) /
np.linalg.norm(r_prime_vec[:, t_idx]) ** 3
        B_vec[:, r_idx] = B * mu0 * I / (4 * np.pi)

    # compute standard deviation of Bz over top 90% of Bz vs z curve
    bz_max = np.max(B_vec[2, :])
    Bz_normalized_vec = B_vec[2, :] / bz_max
    thresh = 0.9
    first_crossing_idx = np.nonzero(Bz_normalized_vec > thresh)[0][0]
    last_crossing_idx = np.nonzero(Bz_normalized_vec > thresh)[0][-1]
    err = np.std(Bz_normalized_vec[first_crossing_idx:last_crossing_idx])
    width = last_crossing_idx - first_crossing_idx

    # Exclusion script
    crossings = np.nonzero(np.diff(np.where(Bz_normalized_vec > thresh, 1, 0)))[0]
    if len(crossings) > 2:
        return np.nan, np.nan

    return err, width
```

```
# In[14]:


#1D Biot Savart

# constants
mu0 = 4*np.pi*1e-7

# dimensional inputs
leg_length = 12.7  # mm
s = 1.42 #pitch of const. pitch solenoid (max pitch of variable coil)
nu = -10^(-10) #scalar factor
k = 1 #exponential factor

t_coil_min = -(nturns/2)*(2*np.pi)
t_coil_max = (nturns/2)*(2*np.pi)

t_bend_min = -np.pi/2
t_bend_max = 0

t_straight_min = -leg_length
t_straight_max = 0

I = 1  # driving coil with 1A

# define coil
fx_coil = lambda t: r*np.cos(t)
fy_coil = lambda t: r*np.sin(t)
fz_coil = lambda t: s/(2*np.pi) * (t+nu*np.abs(t)**k*np.sign(t))

# define bend at start of coil
coil_start_x = fx_coil(t_coil_min)
coil_start_y = fy_coil(t_coil_min)
coil_start_z = fz_coil(t_coil_min)

fx_bend1 = lambda t: -wire_diam/2*(np.cos(t)-1) + coil_start_x
fy_bend1 = lambda t: wire_diam/2*np.sin(t) + coil_start_y
fz_bend1 = lambda t: coil_start_z*np.ones(np.size(t))

# define bend at end of coil
coil_end_x = fx_coil(t_coil_max)
coil_end_y = fy_coil(t_coil_max)
coil_end_z = fz_coil(t_coil_max)

fx_bend2 = lambda t: wire_diam/2*(np.sin(t)+1) + coil_end_x
fy_bend2 = lambda t: wire_diam/2*(np.cos(t)) + coil_end_y
fz_bend2 = lambda t: coil_end_z*np.ones(np.size(t))

# define straight section at start of coil
bend1_start_x = fx_bend1(t_bend_min)
```

```
bend1_start_y = fy_bend1(t_bend_min)
bend1_start_z = fz_bend1(t_bend_min)

fx_straight1 = lambda t: bend1_start_x - t
fy_straight1 = lambda t: bend1_start_y*np.ones(np.size(t))
fz_straight1 = lambda t: bend1_start_z*np.ones(np.size(t))

# define straight section at end of coil
bend2_end_x = fx_bend2(t_bend_max)
bend2_end_y = fy_bend2(t_bend_max)
bend2_end_z = fz_bend2(t_bend_max)

fx_straight2 = lambda t: bend2_end_x + t - t_straight_min
fy_straight2 = lambda t: bend2_end_y*np.ones(np.size(t))
fz_straight2 = lambda t: bend2_end_z*np.ones(np.size(t))

# Load curves and t-ranges into arrays
fx_arr = [fx_straight1, fx_bend1, fx_coil, fx_bend2, fx_straight2]
fy_arr = [fy_straight1, fy_bend1, fy_coil, fy_bend2, fy_straight2]
fz_arr = [fz_straight1, fz_bend1, fz_coil, fz_bend2, fz_straight2]
tmin_arr = [t_straight_min,t_bend_min,t_coil_min,t_bend_min,t_straight_min]
tmax_arr = [t_straight_max,t_bend_max,t_coil_max,t_bend_max,t_straight_max]

# Setup domain of computation
extraSpace = 0
zmin = coil_start_z - extraSpace
zmax = coil_end_z + extraSpace

num_axis_pts = 100
step_size = (zmax - zmin) / (num_axis_pts - 1)  # if desire to tailor step size to
resolution
z_vec = np.linspace(zmin,zmax,num_axis_pts)

num_t_pts_per_segment = 1000
scaling_factor = 1e-3  # mm to m
# Apply the scaling_factor to l_vec and dl_vec
l_vec, dl_vec = get_l_vec(num_t_pts_per_segment, scaling_factor, fx_arr, fy_arr,
fz_arr, tmin_arr, tmax_arr)
num_t_pts = l_vec.shape[1]

# Biot Savart law to find on-axis magnetic field components at each observer point
on-axis
zero_vec = np.zeros(num_axis_pts)
r_vec = np.array([zero_vec, zero_vec, z_vec]) * 1e-3  # CONVERTING TO METERS HERE

# Find B-field at each observation point, using rectangular numerical integration
B_vec = np.zeros((3,num_axis_pts))
mu0 = 4 * np.pi * 1e-7  # vacuum permeability
I = 1  # current, replace with your actual current value

for r_idx in range(num_axis_pts):
```

```
    r_prime_vec = r_vec[:, r_idx].reshape(-1,1) - l_vec
    B = np.zeros(3)
    for t_idx in range(num_t_pts):
        B += np.cross(dl_vec[:,t_idx],r_prime_vec[:,t_idx]) /
np.linalg.norm(r_prime_vec[:,t_idx]) ** 3
    B_vec[:,r_idx] = B * mu0 * I / (4 * np.pi)

# Plot Bz vs z on axis
plt.figure()
bz_max = np.max(B_vec[2,:])
plt.plot(z_vec, B_vec[2,:] / bz_max)  # Bz vs z on-axis
plt.xlabel('z (mm)')
plt.ylabel('B_z/B_{z,max}')
plt.title(f'B_z vs z with s = {s}, k = {k}, v={nu:e}')
plt.grid(True)
plt.axis([zmin, zmax, 0, 1.2])
plt.show()

# Plot Br vs z on axis
plt.figure()
Br_vec = np.sqrt(B_vec[0,:]**2 + B_vec[1,:]**2)
Br_max = np.max(Br_vec)
plt.plot(z_vec, Br_vec / Br_max)  # Br vs z on-axis
plt.xlabel('z (mm)')
plt.ylabel('B_r/B_{r,max}')
plt.title(f'|B_r| vs z with s = {s}, k = {k}, v={nu:e}')
plt.grid(True)
plt.axis([zmin, zmax, 0, 1.2])
plt.show()

# Compute length of wire used in coil
wire_length = np.sum(np.linalg.norm(dl_vec, axis=0))
print(f'Wire length: {wire_length * 1000} mm')

# Compute standard deviation of Bz over top 90% of Bz vs z curve
Bz_normalized_vec = B_vec[2,:] / bz_max
thresh = 0.9

# Locate first crossing of 90% Bz_max line
first_crossing_idx = 0
last_crossing_idx = 0
point_count = 0
has_crossed = False  # Flag to check if has crossed 90% threshold

for Bz_idx in range(num_axis_pts):
    if Bz_normalized_vec[Bz_idx] > thresh:
        point_count += 1
        if point_count == 1:  # First point found above 90% line
            first_crossing_idx = Bz_idx
            has_crossed = True
        elif has_crossed:  # If it has crossed once before
```

```
            last_crossing_idx = Bz_idx  # Update last_crossing_idx with each point
above threshold

    elif has_crossed:  # If it has crossed and encounters a point below the threshold
        break  # Exit the loop

# Compute stddev over this range
thresh_data = Bz_normalized_vec[first_crossing_idx:last_crossing_idx + 1]

std_dev = np.std(thresh_data, ddof=1)  # Use ddof=1 for sample standard deviation


# In[ ]:


import plotly.graph_objects as go
from tqdm import tqdm

# Calculate Bz curve flatness at each test point using 1-D Biot Savart
total_pts = npoints ** 2
err_array = np.zeros((npoints, npoints))
width_array = np.zeros((npoints, npoints))
width_pt_stepsize = 0.062  # mm

# Iterate through each k, nu point
for i in tqdm(range(npoints)):
    for j in range(npoints):
        if np.isnan(s_3d[i, j]) or np.isnan(NU[i, j]) or np.isnan(K[i, j]):
            err_array[i, j] = np.nan
            width_array[i, j] = np.nan
        else:
            err, width = biotSavart_error_function(s_3d[i, j], NU[i, j], K[i, j])
            err_array[i, j] = err
            width_array[i, j] = width

# Enable interactive mode
fig1 = go.Figure(data=[go.Surface(x=np.log10(-NU), y=K, z=err_array,
colorscale='viridis')])
fig1.update_layout(
    title=f"Peak Flatness for coil of length {max_coil_len} mm and minimum pitch
{minpitch} mm",
    scene=dict(
        xaxis_title="log10(-v)",
        yaxis_title="k",
        zaxis_title="stddev_{90%}"
    )
)

# Enable interactive mode
fig2 = go.Figure(data=[go.Surface(x=np.log10(-NU), y=K, z=width_array *
width_pt_stepsize, colorscale='viridis')])
```

```
fig2.update_layout(
    title=f"Peak Width for coil of length {max_coil_len} mm and minimum pitch
{minpitch} mm",
    scene=dict(
        xaxis_title="log10(-v)",
        yaxis_title="k",
        zaxis_title="peak-width_{90%} (mm)"
    )
)

# Find the indices of the minimum error and maximum width
min_err_idx = np.unravel_index(np.nanargmin(err_array), err_array.shape)
max_width_idx = np.unravel_index(np.nanargmax(width_array), width_array.shape)

# Retrieve the corresponding S, K, and NU values
min_err_s = s_3d[min_err_idx]
min_err_k = K[min_err_idx]
min_err_nu = NU[min_err_idx]
min_err_z = err_array[min_err_idx]

max_width_s = s_3d[max_width_idx]
max_width_k = K[max_width_idx]
max_width_nu = NU[max_width_idx]
max_width_z = width_array[max_width_idx] * width_pt_stepsize

# Enable interactive mode
fig1 = go.Figure(data=[go.Surface(x=np.log10(-NU), y=K, z=err_array,
colorscale='viridis')])

# Add scatter trace for minimum error point
fig1.add_trace(go.Scatter3d(
    x=[np.log10(-min_err_nu)],
    y=[min_err_k],
    z=[min_err_z],
    mode='markers',
    marker=dict(
        color='red',
        size=5,
        symbol='circle'
    ),
    name='Minimum Error'
))

# Update layout
fig1.update_layout(
    title=f"Peak Flatness for coil of length {max_coil_len} mm and minimum pitch
{minpitch} mm",
    scene=dict(
        xaxis_title="log10(-v)",
        yaxis_title="k",
        zaxis_title="stddev_{90%}"
```

```
    )
)

# Show the interactive plot
fig1.show()

# Enable interactive mode
fig2 = go.Figure(data=[go.Surface(x=np.log10(-NU), y=K, z=width_array *
width_pt_stepsize, colorscale='viridis')])

# Add scatter trace for maximum width point
fig2.add_trace(go.Scatter3d(
    x=[np.log10(-max_width_nu)],
    y=[max_width_k],
    z=[max_width_z],
    mode='markers',
    marker=dict(
        color='blue',
        size=5,
        symbol='circle'
    ),
    name='Maximum Width'
))

# Update layout
fig2.update_layout(
    title=f"Peak Width for coil of length {max_coil_len} mm and minimum pitch
{minpitch} mm",
    scene=dict(
        xaxis_title="log10(-v)",
        yaxis_title="k",
        zaxis_title="peak-width_{90%} (mm)"
    )
)

# Show the interactive plot
fig2.show()

# Print the values
print(f"Minimum Error:")
print(f"S: {min_err_s:.4f}")
print(f"K: {min_err_k:.4f}")
print(f"NU: {min_err_nu:.4f}")
print(f"Z: {min_err_z:.4f}")

print(f"\nMaximum Width:")
print(f"S: {max_width_s:.4f}")
print(f"K: {max_width_k:.4f}")
print(f"NU: {max_width_nu:.4f}")
print(f"Z: {max_width_z:.4f} mm")
```

APPENDIX C

Specifications Grading Course Documents

Token Trade-In List Chem 128

To earn the first 1 token, you must complete the first discussion worksheet on specifications grading (available on Canvas week of Jan. 3rd, due Jan. 7th). You must complete this worksheet to earn any tokens. There will be other opportunities to earn additional tokens throughout the quarter. You can earn 2 for completing the initial course survey and 2 for completing the final course survey. This means 6 total tokens can be earned throughout the quarter.
To use tokens for resubmissions, a complete assignment must be submitted initially in order to receive feedback. If a complete assignment cannot be submitted then a token must be used for a late submission.
Deadline for you to use tokens: Friday March 4, 2022
You may use tokens in the following ways:

Trade in **1 Token** to:

- Reattempt and resubmit a **research paper** (2 first paper max, 1 second paper max)
    - Once you receive your graded assignment through Canvas, you have 1 week to resubmit.
    - A brief reflection outlining the corrections / edits made in the revision based on the rubric and feedback must be submitted to use the token.
- Reattempt and resubmit a **problem set** (2 max)
    - Once you receive your graded assignment through Canvas, you have 1 week to resubmit.
    - A brief reflection explaining the corrections made must be submitted to use the token.
- Revise one **quiz question** (1 per quiz, max 4)
    - Revise one quiz question if required to move from *needs revision* to a *low pass* OR from a *low pass* to a *high pass.*
        - A brief reflection explaining the corrections made must be submitted to use the token.
        - Once you receive your graded assignment through Canvas, you have 1 week to resubmit.

- Take final to replace a quiz score (1 per quiz, max 4)
- Miss a **discussion section** and worksheet, in addition to the free one everyone gets (1 max)
- Late submission on graded assignment (**not a quiz**) (3 per assignment)
    - One token will allow a 24-hour extension to the assignment deadline.
    - Up to three tokens may be used in succession for a maximum 72-hour extension.

Token Trade-Ins	**Tokens Used (check off as you go to keep track)**
Discussion Section Worksheets *(1 max)*	**Missed: ❑**
Problem Sets	**Reattempt: ❑ ❑ ❑ ❑ ❑**
Quizzes *(1 per quiz)*	**Revise one question: ❑ ❑ ❑ ❑** **Full reattempt: ❑ ❑ ❑ ❑**
Late submission (6 max)	**24-hour pass: ❑ ❑ ❑ ❑ ❑ ❑**
Research Paper *(2 max first paper, 1 max second paper)*	**Resubmit first paper: ❑ ❑** **Resubmit second paper: ❑**

Grade Criteria

C

- Remember facts (basic definitions, abbreviations for amino acids and nucleic acids, chemical properties of each amino acid, steps in a method flow chart, base pairs, families of molecules, sequence coding, enzyme classifications)
- Recognize important parts of a structure (N and C termini, amide bond, H-bond donors and acceptor, side chains, 5’ and 3’ ends, Watson-Crick face of nucleotide)
- Recognize important parts of a provided mechanism (transition states, stereochemistry)
- Identify key parts of a paper (controls, hypotheses, background info, etc.)
- Perform simple calculations (usually given in context or discussed in lecture)

B

- Make connections among different topics
- Apply principles to a new (but similar) situation
- Draw structures (DNA, RNA, amino acids, carbonyl/amino groups) from memory
- Draw mechanisms (arrow pushing notation or crosslinking) from memory or intuition of chemical/biological principles
- Describe how a hypothesis was tested in a paper; what methods were used and how those support the results
- Deduce the correct equations to use and their significance to a problem

A

- Explain methods in terms of how or why they were used or what they could be used for in the future
- Justify use of methods or controls by assessing their impact on the results or findings
- Capable of communicating concepts in concise language, especially in open-ended questions
- Generate hypotheses and describe how you would test them
- Make predictions or estimates (most acidic hydrogen, most basic heteroatom, basicity, pKa, stability, how reagents effect progression)
- Design primers or other experimental approaches and predict possible outcomes

Self-Efficacy Survey Chem 128

What is your name? (This will only be used for the purpose of credit to receive tokens. All identifying information will be deleted prior to any analysis of the survey results.)

1 How confident are you that you could critique an experiment described in a journal article (i.e., list the strengths and weaknesses)?

- ○ TOTALLY confident
- ○ VERY confident
- ○ FAIRLY confident
- ○ ONLY A LITTLE confident
- ○ NOT AT ALL confident

2 How confident are you that you will be successful in this chemical biology course?

- ○ TOTALLY confident
- ○ VERY confident
- ○ FAIRLY confident
- ○ ONLY A LITTLE confident
- ○ NOT AT ALL confident

3 How confident are you that you will be successful in a molecular biology course?

- ○ TOTALLY confident
- ○ VERY confident
- ○ FAIRLY confident
- ○ ONLY A LITTLE confident
- ○ NOT AT ALL confident

4 How confident are you that you would be successful in an analytical chemistry course?

- ○ TOTALLY confident
- ○ VERY confident
- ○ FAIRLY confident
- ○ ONLY A LITTLE confident
- ○ NOT AT ALL confident

5 How confident are you that you could analyze a set of data (i.e., look at the relationships between variables)?

- ○ TOTALLY confident
- ○ VERY confident
- ○ FAIRLY confident
- ○ ONLY A LITTLE confident
- ○ NOT AT ALL confident

6 How confident are you that you could analyze a set of data (i.e., look at the relationships between variables)?

- ○ TOTALLY confident
- ○ VERY confident
- ○ FAIRLY confident
- ○ ONLY A LITTLE confident
- ○ NOT AT ALL confident

7 How confident are you that you could analyze a set of data (i.e., look at the relationships between variables)?

- ○ TOTALLY confident
- ○ VERY confident
- ○ FAIRLY confident
- ○ ONLY A LITTLE confident
- ○ NOT AT ALL confident

8 How confident are you that you could analyze a set of data (i.e., look at the relationships between variables)?

- ○ TOTALLY confident
- ○ VERY confident
- ○ FAIRLY confident
- ○ ONLY A LITTLE confident
- ○ NOT AT ALL confident

9 How confident are you that you could ask a meaningful question that could be answered experimentally?

- ○ TOTALLY confident
- ○ VERY confident
- ○ FAIRLY confident
- ○ ONLY A LITTLE confident
- ○ NOT AT ALL confident

10 How confident are you that you could explain something that you learned in this chemical biology course to another person?

- ○ TOTALLY confident
- ○ VERY confident
- ○ FAIRLY confident
- ○ ONLY A LITTLE confident
- ○ NOT AT ALL confident

11 How confident are you that after reading an article about a chemical biology experiment, you could write a summary of its main points?

- ○ TOTALLY confident
- ○ VERY confident
- ○ FAIRLY confident
- ○ ONLY A LITTLE confident
- ○ NOT AT ALL confident

12 How confident are you that after reading an article about a chemical biology experiment, you could explain its main ideas to another person?

- ○ TOTALLY confident
- ○ VERY confident
- ○ FAIRLY confident
- ○ ONLY A LITTLE confident
- ○ NOT AT ALL confident

13 How confident are you that after watching a television documentary dealing with some aspect of chemical biology, you could write a summary of its main points?

- ○ TOTALLY confident
- ○ VERY confident
- ○ FAIRLY confident
- ○ ONLY A LITTLE confident
- ○ NOT AT ALL confident

14 How confident are you that after watching a television documentary dealing with some aspect of chemical biology, you could explain its main ideas to another person?

- ○ TOTALLY confident
- ○ VERY confident
- ○ FAIRLY confident
- ○ ONLY A LITTLE confident
- ○ NOT AT ALL confident

15 How confident are you that after listening to a public lecture regarding some chemical biology topic, you could write a summary of its main points?

- ○ TOTALLY confident
- ○ VERY confident
- ○ FAIRLY confident
- ○ ONLY A LITTLE confident
- ○ NOT AT ALL confident

16 How confident are you that after listening to a public lecture regarding some chemical biology topic, you could explain its main ideas to another person?

- ○ TOTALLY confident
- ○ VERY confident
- ○ FAIRLY confident
- ○ ONLY A LITTLE confident
- ○ NOT AT ALL confident

17 How confident are you that you could apply concepts learned in this chemical biology course to a research project?

- ○ TOTALLY confident
- ○ VERY confident
- ○ FAIRLY confident
- ○ ONLY A LITTLE confident
- ○ NOT AT ALL confident

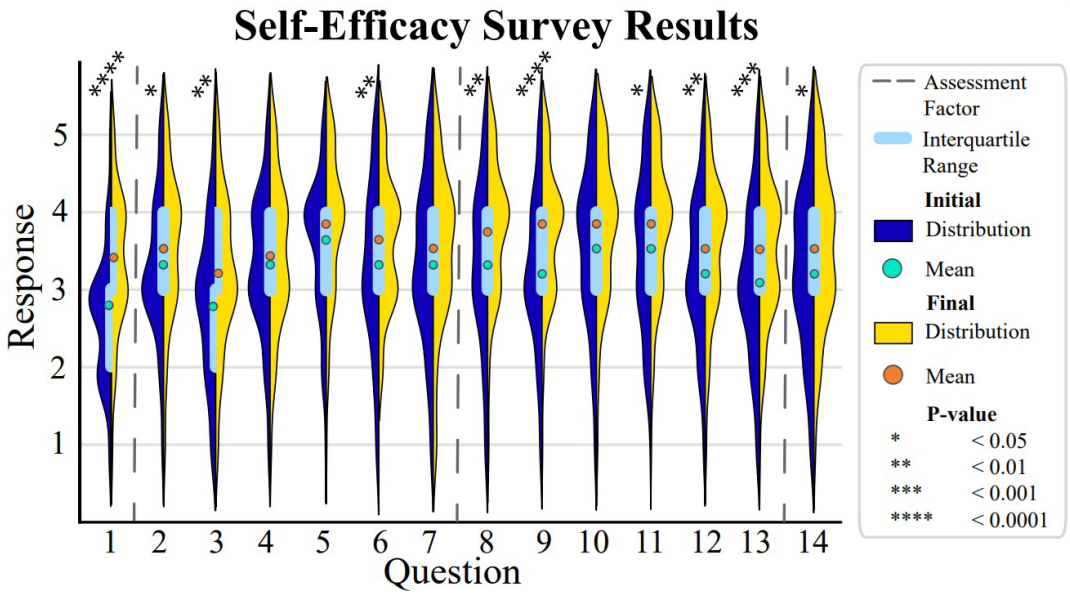

Figure C.1: Results of student self-efficacy survey recorded in week 2 (initial) and week 8 (final) of the Winter 22 quarter (n=77). Responses range from (1) NOT AT ALL confident to (5) TOTALLY confident. Question responses with statistically significant change in the mean from the initial to final survey based on assessment of the p-value from a t-test are shown using asterisks. Across all assessment factors, most questions had a significant and positive change in the mean.

Further analysis of the results for individual questions, shown in SM Figure 2, yielded no negative trends in student perceptions for the questions asked. The violin plots depict a probability density for the student answers and are split to intuitively compare changes from the initial and final surveys. Means and results of paired t-tests for each question are provided in Supplemental Materials Table 2. Four questions (4, 5, 7, 10) had initial and final means that were not statistically distinct, indicating no change over the duration of the course in the students' confidence to be successful in an analytical chemistry course, to analyze a set of data, explain something learned in this chemical biology course, or write a summary of a television documentary on some aspect of chemical biology respectively. The other ten questions yielded statistically significant positive trends, with the largest shifts observed for questions 1, 9, and 13. These

questions probed confidence in critiquing experiments described in a journal article, explaining the main ideas after reading a journal article about a chemical biology experiment, and explaining the main ideas after listening to a public lecture regarding a chemical biology topic.

Evaluation of Self-Efficacy Survey Data

Table C.1: Initial survey was conducted in week 1 and final survey was conducted in week 8 of the 10-week quarter. Means are provided for the 77 paired initial and final surveys evaluated (n=77) out of a total class size of 99 students. P-values are the results of paired t-test. Values shaded in green are statistically significant (p<0.05).

Question	Mean	P-Value	Question	Mean	P-Value
1	Initial: 2.8 Final: 3.4	<0.001	8	Initial: 3.3 Final: 3.7	0.001
2	Initial: 3.3 Final: 3.5	0.029	9	Initial: 3.2 Final: 3.7	<0.001
3	Initial: 2.8 Final: 3.2	0.002	10	Initial: 3.5 Final: 3.8	0.077
4	Initial: 3.3 Final: 3.4	0.199	11	Initial: 3.5 Final: 3.8	0.014
5	Initial: 3.6 Final: 3.8	0.059	12	Initial: 3.2 Final: 3.5	0.010
6	Initial: 3.3 Final 3.6	0.009	13	Initial: 3.1 Final: 3.5	<0.001
7	Initial: 3.3 Final: 3.5	0.230	14	Initial: 3.2 Final: 3.5	0.012